Theoretical Studies of Low Energy Positron-Atom and Atom-Antiatom Collisions

Joel T. Dunn

Thesis submitted for the

degree of Doctor of Philosophy

of the University of London

University College London, 2002

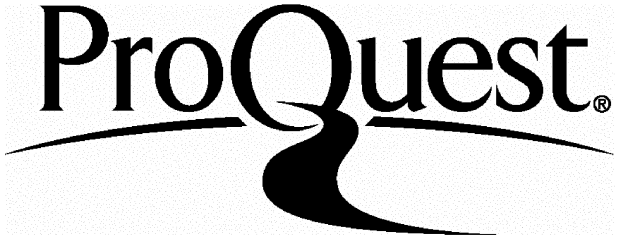

Abstract

Theoretical studies of low-energy positron collisions with various one-electron models of the helium atom have been made using the Kohn variational method in order to find out if such a model atom is capable of yielding accurate cross sections for elastic scattering, positronium (Ps) formation and annihilation.

For positron-helium scattering, comparisons are made with the accurate results obtained from the *ab initio* variational calculations of Van Reeth and Humberston. All the models provide qualitatively accurate results over some energy intervals. Although one model gives excellent values for the elastic scattering cross section up to the Ps formation threshold, it is affected by a resonance near the threshold. None of the models yields very accurate results for the annihilation cross section, although a comparatively crude model reproduces the accurate distribution function for the Doppler broadening of the annihilation γ-ray energy spectrum.

A correlation has been found by Van Reeth *et al* between the Ps formation cross section and the associated threshold energy for the noble gas atoms. A parameter in the correlation equation has been interpreted as the Ps formation cross section for an atom with a zero threshold energy, so Ps formation cross sections have been calculated for such a model atom. The results obtained compare reasonably favourably with the energy dependence of this parameter obtained from experimental data.

An adiabatic model has also been used to study hydrogen-antihydrogen collisions, and further studies may involve a model one-electron atom in the study of helium-antihydrogen collisions. The results are satisfactory, but further investigations are needed to include the rearrangement of the atom-antiatom system into positronium and protonium.

Acknowledgements

I would like to express my most sincere gratitude to my supervisor, Prof. J. W. Humberston, who has shared his expertise in positron physics and scattering theory. I am most grateful to his patient support and clear explanations which he has given to my physics training and to this work.

I would like to extend my thanks to Dr. P. Van Reeth of University College London for his continuous help with the development of this work as well as his patient support with the computational aspects of this study, all of which have proved invaluable.

I am very grateful to Dr. G. Peach of University College London for providing the one-electron models of helium and the many useful discussions regarding these and atomic physics generally, and to Prof. E. A. G. Armour of the University of Nottingham for the helpful discussions on hydrogen-antihydrogen collisions.

I would also like to acknowledge Dr. P. T. O'Neil, Mr. S. R. Colley, Dr. P. Dando, Mr. O. Pribyl, Mr. P. G. Donnelly and Dr. R. Bannocks, all of University College London, for their patient support and advice on various computational aspects of this study. I wish to give my thanks for the support provided by Group C and the whole of the Department of Physics and Astronomy at UCL.

Financial support has been gratefully received from the Engineering Physical and Sciences Research Council, and I thank the Department of Physics and Astronomy at UCL, and the Graduate School, UCL, for financial support allowing me to attend national and international conferences.

Contents

Chapter 1

Introduction

1.1 Background

The experimental discovery of the positron by Anderson (1932) provided verification of one of the most important predictions arising from relativistic quantum mechanics. Dirac's (1928) relativistic theory of the electron, predicted solutions corresponding to both positive and negative values of the total energy of the electron. The total energy of an electron, E, is given by

$$E^2 = p^2c^2 + m^2c^4, \tag{1.1}$$

where p is the momentum of the particle, m the rest mass and c is the speed of light in a vacuum. The positive root of this equation represents the total energy of an electron in everyday matter, between mc^2 and $+\infty$. But Dirac could not justify ignoring the negative root solution corresponding to energies in the range $-mc^2$ and $-\infty$. Dirac's relativistic wave equation for an electron in an external electromagnetic field predicted the usual bispinor, representing two spin states of the electron (spin-up and spin-down), but also two others with *negative* energies.

Fundamental physics states that particles will naturally relax to the lowest available energy state. Therefore, if negative energy states are possible, why do we not see electrons making transitions down to such states? This question led Dirac to postulate that all the

states in the "sea" of negative energy electrons, with energies between $-mc^2$ and $-\infty$, are full so that, because of the Pauli exclusion principle, there are no empty negative energy states available into which a positive energy electron can fall.

In Dirac's negative energy "sea" picture, it should be possible to excite a negative energy electron to a positive energy, leaving a negative energy "hole". This "hole" in a sea of negatively charged particles should behave like a positively charged particle, the positron, moving in a vacuum. The promotion of an electron from a negative energy state to one of positive energy, leaving a hole in the sea of negative energy states, is the process of pair-production, which requires an input energy of at least $2mc^2$. The reverse process, in which a positive energy electron drops into an available hole, releasing energy of at least $2mc^2$, is electron-positron annihilation.

Subsequent theories have used different pictures to describe antiparticles such as the positron; for example, Feynman's representation of antimatter involves reversing the direction of the particle through time.

1.2 Positrons and Antimatter

Theoretically, the positron has the same spin, mass, magnitude of charge (but opposite sign) and gyromagnetic ratio as the electron, as a consequence of the CPT symmetry theorem; under the operations of charge conjugation (C), parity exchange (P) and time reversal (T) together, the laws of physics are invariant. The gyromagnetic ratio of the positron, for instance, has been found to be equal to that of the electron to within 2 parts in 10^{12} (Van Dyck *et al* 1987).

Since Anderson's discovery of the positron, much theoretical and experimental work has been done to discover its properties. Initially most of the work was carried out to test the fundamental theories of antimatter, but recently positrons have been used as a tool in their own right, as a probe in atomic and molecular physics, and in solid state physics. They are also used in *positron emission tomography*, to map out the areas of the brain.

A significant consequence of the discovery of antimatter is the idea of the annihilation

of electrons and positrons in a vacuum, without violating any conservation laws. When annihilating in a vacuum, the electron and positron leave behind two or more γ-rays, the number being dependent on the total spin of the annihilating pair. The most rapid decay channel is into two γ-rays, when the electron and positron are in the spin singlet state.

The bound state of an electron and a positron was first predicted by Mohorovičić (1934), (although the details of his ideas about the system were incorrect) and this became known as *positronium* (Ps) (Ruark 1945). Although the positron is stable, the bound state of a positron with an electron is not, and positronium can annihilate with lifetimes of the order of 10^{-7}s or less, so their detection is by their subsequent annihilation.

Neglecting the hyperfine corrections and effects due to the finite mass of the proton, positronium has energy levels half those of the hydrogen atom. However, the hyperfine separations of the energy levels are very different from hydrogen due to the large magnetic moment of the positron compared to that of the proton and the contribution from QED effects.

The total spin state of positronium also has a very small effect on the separation of the energy levels. Positronium exists in two total spin states, $S = 0$ (singlet state) where the spins are antiparallel, denoted para-positronium (para-Ps), and $S = 1$ (triplet state) where the spins are parallel, denoted ortho-positronium (ortho-Ps). These spin states also have a dramatic effect on the lifetime of the positronium. In order to conserve spin and parity, the annihilation route of (singlet) para-Ps has to be through an even number of γ-rays, and for (triplet) ortho-Ps, an odd number, where the lower order processes, two and three γ-rays respectively, are overwhelmingly the most common. The lifetimes of these species in their ground states are 142 ns for ortho-Ps but only 125 ps for para-Ps (Charlton and Humberston 2001). From simple spin statistics, the ratio of creation of ortho-Ps to para-Ps is expected to be 3:1, which means that the ratio of annihilation rates of para-Ps to ortho-Ps is approximately 370:1.

Further bound states involving positronium exist, such as electron-positronium, denoted Ps^- (and its charge conjugate Ps^+), predicted in 1946 by Wheeler (1946) but not

discovered until 1981 (Mills 1981). The positronium "atom" can also form a bound system with another positronium, to form molecular positronium, Ps_2, as well as with hydrogen to form positronium hydride, PsH, and with other atoms (e.g. Ryzhikh and Mitroy 1997). Perhaps the most significant bound state involving a positron is antihydrogen, a positron bound to an antiproton. Experiments at CERN in Geneva (Baur *et al* 1996) and Fermilab near Chicago (Blanford *et al* 1998) have recently created the first antihydrogen atoms, however at high energies, approximately 90% the speed of light. If the antihydrogen can be created at low enough energies to allow an examination of its properties, the energy spectrum may be studied. It would provide an excellent test of CPT symmetry. If CPT symmetry holds then the antihydrogen atom should have exactly the same energy spectrum as does the hydrogen atom. The availability of this antiatom will also enable tests to made of the interaction of antimatter with gravity and thus test the weak equivalence principle (WEP).

1.3 Positron-Matter Interaction

Electron-atom scattering has been studied in great detail for many years but only quite recently has it been possible to perform comparable experiments with positrons. One of the main problems holding back positron-atom scattering has been the creation and manipulation of slow positron beams.

At high collision energies the total cross sections for positron-atom and electron-atom scattering merge. Figure 1.1 shows the total cross-sections of electron-helium and positron-helium scattering, from 0 eV to 600 eV, from Kauppila *et al* (1981), where it can be seen that the differences are most pronounced at low energies. Positrons can be created in two main ways, either through pair production by sufficiently high energy photons or by the radioactive "β^+-decay" of certain radioisotopes. The most common isotope used in scattering experiments is ^{22}Na, where the branching ratio of the β^+-decay is 91% and the half-life is 2.6 years (Charlton and Humberston 2001). The positrons, or β^+ particles, are ejected with a wide range of energies, approximately 0.5 MeV, and so the positrons need

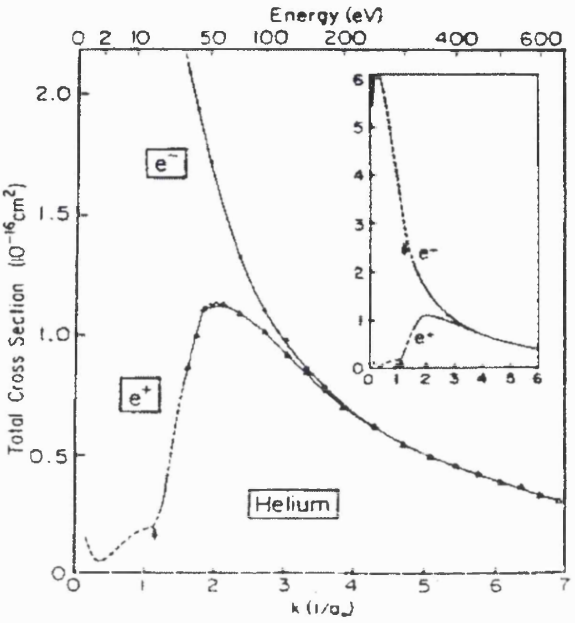

Figure 1.1: Total cross-sections for electron-helium and positron-helium impact with respect to different electron or positron wavenumber, k($1/a_0$) and energy (eV). From Kauppila *et al* (1981)

to be slowed down to energies of a few electron-volts in order to study the more interesting aspects of positron-atom scattering.

During the 1970s and 1980s great advances were made in increasing the positron beam current, reducing the energy spread and improving the counting techniques. Combined with the general increase in computer power, this allowed more accurate investigations, both experimentally and theoretically, into the interaction of matter and slow positrons.

In *ab initio* calculations, which can only be made for relatively simple systems, e. g. positron-hydrogen and positron-helium scattering, the calculations assume a system similar to electron-atom scattering but reverse the sign of the charge on the incident particle. This alone has a dramatic effect on the calculations. Electron-atom scattering has to take account of exchange between the incident projectile and the atomic electrons since they are identical. The positron and electron are not identical, however, so there is no exchange between the incident positron and atomic electrons. Another difference is the interaction potential between the incident particle and the polarizable target. The interaction between an electron and an atom has an attractive static part, which assumes an undistorted tar-

Table 1.1: A summary of the differences between the interactions and processes involved in electron-atom and positron-atom scattering.

Interaction/ Collision Process	**Incident Particle**	
	positron	**electron**
Static	Repulsive	Attractive
Polarization	Attractive	Attractive
Exchange	×	√
Positronium formation	√	×
Annihilation	√	×

get, and an attractive polarization potential which takes into account the distortion of the target: in the semi-classical picture the atomic electrons are repelled by the negative electron and so the positive nucleus is less well shielded, making the electron-atom potential more attractive. In the positron-atom system, the static potential is repulsive, since the sign of the charge is reversed, but the polarization potential is also attractive, since, in the semi-classical picture, the positron attracts the electrons around the atom, shielding the positive nucleus and thereby making the positron-atom interaction potential more attractive. The interactions and possible collision processes involved in electron-atom and positron-atom scattering are summarized in table 1.1.

There is also a difference in the convergence of the numerical methods used to study electron- and positron-atom collisions, which can be mainly attributed to the strong correlation between the atomic electrons and the incident positron. In electron-atom scattering the incident electron is repelled by the atomic electrons, but an incident positron is attracted to the atomic electrons, so the positron-electron correlations have to be particularly well represented in any scattering calculation if accurate results are to be obtained.

This effect is most noticeable when considering the formation of positronium in positron-atom scattering, when the electron and positron can form a bound state and move away

from the remaining atomic ion. Positronium formation is very much dependent on the type of target atom considered and the incident positron energy. For positronium to be formed, conservation of energy considerations mean that the incident positron energy, E_{e+}, must be greater than the difference between the binding energy of one electron to the target atom, E_i (the single ionization energy threshold), and the binding energy of positronium, $E_{Ps} = 6.8$ eV, so

$$E_{e+} \geq E_i - E_{Ps}. \tag{1.2}$$

Certain atoms, for example the alkalis, such as lithium or sodium, have outer electrons bound so weakly that positronium can be formed even when the incident positron energy is zero, so that $E_{Ps} \geq E_i$. In this situation the positronium formation process is *exothermic*, so the positronium is "kicked out" with more energy than that of the incoming positron.

Other atoms, such as the noble gas atoms like helium and neon, have tightly bound outer electrons so the incoming positron must have a positive amount of energy in order to liberate an electron from the target. In this situation $E_i \geq E_{Ps}$ and the process is *endothermic*, so the positron loses energy as it picks up an electron. The amount of energy that the positron needs in order to form positronium is denoted by the positronium formation threshold energy, E_{th}. At incident energies above E_{th} positronium formation is possible, below it is not.

In this study the energy region in positron-atom collisions where we have considered positronium formation is between the positronium formation threshold and the next inelastic threshold, which is the first excited state of the target. This region is called the *Ore gap*.

The final major process considered here, with no comparable process in electron-atom scattering, is the annihilation of a positron and an electron. All positronium eventually annihilates and direct annihilation of an electron and a positron can occur at any energy. The total cross-section for this process is usually negligible relative to the elastic scattering and positronium formation cross-sections, so it is not considered as an explicit open channel in the collision process.

1.4 Present Work

The aspects of positron collisions studies here are broken into two main areas: positron-atom scattering using one-electron models of atoms, and hydrogen-antihydrogen collisions.

The first system studied is low energy positron-helium scattering using a one-electron model of helium. One-electron models of atoms can be considered advantageous because a many electron atom is then reduced to two bodies: an electron orbiting an atomic ion core, so positron-atom scattering using one-electron models of atoms are automatically reduced to three body problems, where only three interparticle coordinates need be considered. As the number of electrons, N, in the target atom is increased, the number of interparticle coordinates which need to be considered increases as $N(N+1)/2$, so it is easy to see how the calculations for positron-helium and positron-lithium scattering, for example, become much more complicated than the positron-hydrogen scattering system.

One-electron models of helium have been used to investigate positron-helium collisions before, for example Hewitt *et al*, (1992), but this earlier work investigated the excitation of helium using incident positron energies between approximately 30 eV and 200 eV and the formation of excited states of positronium. We are interested in the low energy region between 0 eV and the first excitation threshold, 20.61 eV for positron-helium scattering, where annihilation and positronium formation are considered to be most important. Note that the first excitation threshold for electron-helium scattering is lower, 19.79 eV, because spin interactions cannot be ignored and exchange can take place between the incident and atomic electrons, and the 2^3S excitation of the helium target is accessible. The general positron-atom scattering theory is described in Chapter 2. Three one-electron models of helium have been developed by Peach (1982 and 1998) and the author, the first of which has independently provided accurate spectroscopic data for the helium atom, the third of which has no empirically fitted parameters but is based on physical assumptions of the helium atom, and the second of which takes elements of each. These are described in full in Chapter 3.

Detailed *ab initio* calculations have been made of positron-helium scattering by Van

Reeth and Humberston (1999) with which the results obtained here are compared in Chapters 4 and 5. If the models successfully yield accurate results for positron-atom scattering, then it may be appropriate to use these and similar one-electron models to look at more complicated systems where *ab initio* calculations are very complicated, for example, positron-neon scattering or helium-antihydrogen collisions (see below).

In Chapter 8 a model one-electron atom with a binding energy of 6.8 eV has been developed in order that positronium formulation can be investigated in positron collisions with an atom having a zero positronium formation threshold energy. Interest in this process arose from the empirical observation that in positron collisions with the noble gases the cross-section for positronium formation in single ionization, $\sigma_{\rm Ps}$, was strongly correlated with the threshold energy for the process, $E_{\rm th}$, in the following way:

$$\sigma_{\rm Ps} = Ae^{-BE_{\rm th}}, \tag{1.3}$$

where A and B are atom-independent functions of the energy of the positron in excess of the threshold (Humberston and Van Reeth 2000). Thus A can be interpreted as the positronium formation cross section for an atom with $E_{\rm th} = 0$, i. e. a binding energy of 6.8. eV.

Chapter 9 describes the final system investigated, that of hydrogen interacting with antihydrogen. A model has been used in which the relatively heavy nuclei are assumed to be fixed, and a total interaction potential energy is calculated variationally using a flexible trial wave function. Using this interaction potential, a two body scattering calculation can then be carried out to provide approximate hydrogen-antihydrogen scattering data. Other accurate and rigorous methods have been implemented, for example, Jonsell *et al* (2001), Armour *et al* (1998) and Chamberlain and Armour (2000), but our method should allow the modification of including the one-electron models of helium to provide preliminary results for helium-antihydrogen collisions, which along with hydrogen- and molecular hydrogen-antihydrogen scattering, is one of the most important processes when considering the trapping of antihydrogen.

In this work we have mainly used atomic units, a.u., where wavenumbers are given

in the reciprocal of Bohr radii, a_0^{-1}, and the conversion of energy from atomic units to electron-volts is 1 a.u.=27.2 eV.

Chapter 2

Theory

2.1 Introduction

In low-energy positron-atom collisions three processes are possible just below the first excitation threshold of the target; that is, there are three *open* channels:

$$e^+ + A \longrightarrow e^+ + A \quad \text{(elastic scattering)} \tag{2.1}$$

$$e^+ + A \longrightarrow A^+ + 2 \text{ or } 3\gamma\text{-rays} \quad \text{(annihilation)} \tag{2.2}$$

$$e^+ + A \longrightarrow Ps + A^+ \quad \text{(positronium formation)} \tag{2.3}$$

The first two channels, elastic scattering and positron-electron annihilation respectively, are open at all incident positron energies. The third, positronium formation, is only open when the incident positron has an energy in excess of E_{th}, the threshold energy for positronium formation, where

$$E_{\text{th}} = E_{\text{i}} - E_{\text{Ps}} \tag{2.4}$$

and E_{i} is the ionization energy of the target atom and E_{Ps} is the binding energy of positronium ($E_{\text{Ps}} = 6.8\,\text{eV}$ or $0.25\,\text{a.u.}$). Annihilation has a negligible cross-section and is therefore considered to be a minor perturbation to elastic scattering. To begin with we will consider only single channel elastic scattering.

2.2 Single Channel Elastic Scattering Theory

We are considering a beam of low energy positrons incident on a target atom in its ground state. The time-independent Schrödinger equation is

$$H_{\mathrm{T}}\Psi(\boldsymbol{r}_1, \boldsymbol{R}) = E_{\mathrm{T}}\Psi(\boldsymbol{r}_1, \boldsymbol{R}) \tag{2.5}$$

where $\boldsymbol{r}_1$ is the position vector of the positron and the variable $\boldsymbol{R}$ represents the coordinates of all the electrons on the target. In atomic units, the total Hamiltonian is

$$H_{\mathrm{T}} = -\frac{1}{2}\boldsymbol{\nabla}^2_{r_1} - \frac{1}{2}\boldsymbol{\nabla}^2_{R} + V(\boldsymbol{r}_1, \boldsymbol{R}), \tag{2.6}$$

where V is the total interaction potential between all the particles and E_T is the total energy of the system, the sum of the positron energy and that of the target atom,

$$E_{\mathrm{T}} = E(\mathrm{e}^+) + E(\mathrm{A}) = \frac{k^2}{2} + E_{\mathrm{A}}, \tag{2.7}$$

where k is the wave number of the positron.

2.2.1 Deriving the Total Cross Section

Asymptotically, when the positron is a large distance away from the scattering centre, the total wave function is a product of the scattering function, ψ_{sc}, and the target wave function, Φ_{A},

$$\Psi(\boldsymbol{r}_1, \boldsymbol{R}) \underset{r_1\to\infty}{\sim} \psi_{\mathrm{sc}}(\boldsymbol{r}_1)\Phi_{\mathrm{A}}(\boldsymbol{R}). \tag{2.8}$$

The asymptotic form of the scattering wave function is

$$\psi_{\mathrm{sc}}(\boldsymbol{r}_1) \underset{r_1\to\infty}{\sim} e^{i\boldsymbol{k}.\boldsymbol{r}_1} + f_{\mathrm{el}}(\theta, \phi)\frac{e^{ikr_1}}{r_1}, \tag{2.9}$$

where the first term on the right represents the incident positron plane wave, with wavenumber k, and the second, is the spherical outgoing wave with amplitude $f_{\mathrm{el}}(\theta, \phi)$.

Working in polar coordinates with $\boldsymbol{k}$ as the z-axis and assuming a spherically symmetric potential, the scattering amplitude can be expanded into Legendre polynomials so that

$$f_{\mathrm{el}}(\theta) = \sum_{l=0}^{\infty} f_l\, P_l(\cos\theta), \tag{2.10}$$

where f_l is the partial wave scattering amplitude, and the (axially symmetric) incident plane wave can be represented as

$$e^{i\boldsymbol{k}.\boldsymbol{r}_1} = e^{ikz} = \sum_{l=0}^{\infty} A_l \, P_l(\cos\theta) \, j_l(kr_1) \tag{2.11}$$

where A_l=$(2l + 1)i^l$ and $j_l(kr_1)$ is the spherical Bessel function, which is the regular solution of

$$\left(\frac{1}{r_1^2}\frac{d}{dr_1}\left(r_1^2\frac{d}{dr_1}\right) + k^2 - \frac{l(l+1)}{r_1^2}\right) j_l(kr_1) = 0, \tag{2.12}$$

where

$$j_l(kr_1) \underset{r_1\to\infty}{\sim} \frac{\sin(kr_1 - \frac{l\pi}{2})}{kr_1}. \tag{2.13}$$

Similarly, the scattering wave function can be represented as a sum over all angular momentum state, denoted by l, as,

$$\psi_{\rm sc} = \sum_{l=0}^{\infty} B_l \, P_l(\cos\theta) \, G_l(kr_1), \tag{2.14}$$

where B_l are arbitrary constants and $G_l(kr_1)$ is the regular solution to the radial Schrödinger equation of a particle in the field of the atom, that is

$$\left(\frac{1}{r_1^2}\frac{d}{dr_1}\left(r_1^2\frac{d}{dr_1}\right) + k^2 - \frac{l(l+1)}{r_1^2} - V(r_1)\right) G_l(kr_1) = 0. \tag{2.15}$$

Here $V(r_1)$ is short range, so that G_l satisfies the boundary conditions

$$G_l(kr_1) \underset{r_1\to 0}{\sim} r_1^l, \tag{2.16}$$

$$G_l(kr_1) \underset{r_1\to\infty}{\sim} \frac{\sin(kr_1 - \frac{l\pi}{2} + \eta_l)}{kr_1}, \tag{2.17}$$

where η_l is the *phase shift*. Substituting the equations (2.11) and (2.14) into (2.9), the scattering amplitude can be expressed as

$$f_{\rm el}(\theta) = \frac{1}{2ik}\sum_{l=0}^{\infty}(2l+1)\left(e^{2i\eta_l} - 1\right) P_l(\cos\theta). \tag{2.18}$$

For simplicity later on, it is useful to introduce the *scattering matrix*, or S-matrix, which for elastic scattering has only one element,

$$S_l = e^{2i\eta_l} = \frac{1 + i\tan\eta_l}{1 - i\tan\eta_l} \tag{2.19}$$

The total single channel elastic scattering cross-section, σ_{el}, is given by

$$\sigma_{\rm el} = \int_{\Omega} |f_{\rm el}(\theta)|^2 \, d\Omega \tag{2.20}$$

$$= \frac{4\pi}{k^2} \sum_{l=0}^{\infty} (2l+1) \sin^2 \eta_l \tag{2.21}$$

$$= \frac{\pi}{k^2} \sum_{l=0}^{\infty} (2l+1) \left| S_l - 1 \right|^2 . \tag{2.22}$$

2.2.2 Calculating the Phase Shift

Experimentally, it is the cross-section that can be measured. In order to calculate this from theoretical considerations it is necessary to evaluate the phase shift. The powerful mathematical methods which are used for this task throughout this work are *Variational Methods.*

The variational method relies on the fact that an appropriately chosen functional, F, of the wave function, is stationary with respect to small changes in the wave function. So if a flexible trial wave function, Ψ^t, is dependent on a finite set of parameters, for example $c_1, c_2, c_3, ..., c_i, ..., c_N$, then the functional is stationary when

$$\frac{\partial F}{\partial c_i} = 0, \qquad i = 1, 2, 3, ..., N \tag{2.23}$$

and an approximate wave function, Ψ^v, may be found. The stationary value of the functional found using Ψ^v is correct to first order errors in the wave function.

Another useful feature of the variational method is that frequently the value found using the approximation constitutes a bound on the exact value. In the case of the ground state energy (described in the next chapter), *any* approximation to the exact wave function will result in a ground state energy more positive than the exact one, so the better the approximation, the lower the calculated energy, and a very good approximation to the exact value may then be obtained by extrapolation.

The Kohn variational method which we have used here, usually provides a lower bound on the phase shift, so that the more positive the phase shift the method provides, the more accurate it is.

In the Kohn method, we start with the following functional I of the exact wave function Ψ,

$$I[\Psi] = \langle \Psi \mid L \mid \Psi \rangle = \langle \Psi \mid 2(H_{\mathrm{T}} - E_{\mathrm{T}}) \mid \Psi \rangle = 0. \tag{2.24}$$

The exact wave function is not known but we can relate it to a trial wave function, Ψ^t, which differs slightly from Ψ by the value $\delta\Psi$,

$$\Psi^t = \Psi + \delta\Psi. \tag{2.25}$$

The application of the variational method means that the functional $I[\Psi^t]$ becomes stationary as $\delta\Psi$ becomes negligible, i.e. $\delta I = 0$ to first order. Expanding δI we see that

$$\begin{aligned} \delta I[\Psi^t] &= I[\Psi + \delta\Psi] - I[\Psi] && (2.26) \\ &= \langle \Psi \mid L \mid \Psi \rangle + \langle \Psi \mid L \mid \delta\Psi \rangle + \langle \delta\Psi \mid L \mid \Psi \rangle \\ &\quad + \langle \delta\Psi \mid L \mid \delta\Psi \rangle - \langle \Psi \mid L \mid \Psi \rangle. && (2.27) \end{aligned}$$

From equation (2.5), the first, third and fifth terms of equation (2.27) are zero, so we are left with

$$\delta I[\Psi^t] = \langle \Psi \mid L \mid \delta\Psi \rangle + \langle \delta\Psi \mid L \mid \delta\Psi \rangle. \tag{2.28}$$

The second term is of second order in the error in the wave function and, in keeping with the spirit of variational methods, can be assumed to be negligible. Using $L \mid \Psi >= 0$, we can also write

$$\delta I[\Psi^t] = \langle \Psi \mid L \mid \delta\Psi \rangle - \langle \delta\Psi \mid L \mid \Psi \rangle. \tag{2.29}$$

Green's theorem states that

$$\int_\tau \left[f\nabla^2 g - g\nabla^2 f \right] d\tau = \int_\sigma \left[f\boldsymbol{\nabla} g - g\boldsymbol{\nabla} f \right] . d\boldsymbol{\sigma} \tag{2.30}$$

where τ is the volume enclosed by the surface σ. In polar coordinates, the volume elements are given by

$$d\tau = r^2\, dr\, \sin\theta\, d\theta\, d\phi \tag{2.31}$$

$$d\boldsymbol{\sigma} = r^2\, \sin\theta\, d\theta\, d\phi\, \hat{\boldsymbol{r}}, \tag{2.32}$$

and using Green's theorem

$$\delta I[\Psi^t] = \int_\sigma [\Psi \boldsymbol{\nabla}(\delta\Psi) - (\delta\Psi)\boldsymbol{\nabla}\Psi] .d\boldsymbol{\sigma}. \tag{2.33}$$

From equations (2.8) and (2.17) we know that the asymptotic form of the total scattering wave function is

$$\Psi \underset{r_1\to\infty}{\sim} Y_{l,0}(\theta_1,\phi_1)A\left(\frac{\sin(kr_1 - \frac{l\pi}{2} + \eta_l)}{kr_1}\right)\Phi_{\mathrm{T}}(\boldsymbol{R}) \tag{2.34}$$

where $Y_{l,0}(\theta_1,\phi_1)$ is the relevant spherical harmonic and $\Phi_{\mathrm{T}}(\boldsymbol{R})$ is the target wave function. The parameter A is a normalizing factor which can be chosen to be a constant or any function of η. A case of special interest is $A = \sqrt{k}\sec\eta$, so the trial wave function is

$$\Psi^t \underset{r_1\to\infty}{\sim} Y_{l,0}(\theta_1,\phi_1)\sqrt{k}\left(\frac{\sin(kr_1 - \frac{l\pi}{2})}{kr_1} + \tan\eta^t\frac{\cos(kr_1 - \frac{l\pi}{2})}{kr_1}\right)\Phi_{\mathrm{T}}(\boldsymbol{R}). \tag{2.35}$$

Using (2.25), $\delta\Psi$ is

$$\delta\Psi \underset{r_1\to\infty}{\sim} Y_{l,0}(\theta_1,\phi_1)\sqrt{k}\left(\tan\eta^t - \tan\eta\right)\frac{\cos(kr_1 - \frac{l\pi}{2})}{kr_1}, \tag{2.36}$$

and, using Green theorem described above, we have finally,

$$\delta I[\Psi^t] = \tan\eta^t - \tan\eta. \tag{2.37}$$

Expressing the asymptotic functions in (2.35) in terms of the spherical Bessel and Neumann functions, the trial wave function is

$$\begin{aligned}\Psi^t &\underset{r_1\to\infty}{\sim} Y_{l,0}(\theta_1,\phi_1)\sqrt{k}\left[j_l(kr_1) - \tan\eta_l^t\, n_l(kr_1)\right]\Phi_{\mathrm{T}}(\boldsymbol{R}) \\ &\underset{r_1\to\infty}{\sim} Y_{l,0}(\theta_1,\phi_1)\sqrt{k}\left[j_l(kr_1) - K^t\, n_l(kr_1)\right]\Phi_{\mathrm{T}}(\boldsymbol{R}),\end{aligned} \tag{2.38}$$

and the *variational* estimate of the phase shift, η^v, becomes

$$\tan\eta^v = \tan\eta^t - \langle\, \Psi^t \mid L \mid \Psi^t \,\rangle, \tag{2.39}$$

or

$$K^v = K^t - I^t. \tag{2.40}$$

The wave functions described above represent the scattering function at long range. In order to represent the wave functions when the positron is close to the target atom, we use

Hylleraas functions to represent the various interparticle correlations. These offer great flexibility and are also mainly dependent on linear variational parameters. So the full trial wave function is chosen to be

$$\Psi^t = S + K^t C + \sum_{i=1}^{N} c_i \phi_i, \tag{2.41}$$

where

$$S = Y_{l,0}(\theta_1, \phi_1)\sqrt{k}\, j_l(kr_1)\Phi_{\mathrm{T}}(\boldsymbol{R}), \tag{2.42}$$

$$C = -Y_{l,0}(\theta_1, \phi_1)\sqrt{k}\, n_l(kr_1)\Phi_{\mathrm{T}}(\boldsymbol{R}), \tag{2.43}$$

and ϕ_i are Hylleraas functions, which for a three-body system such as positron-hydrogen, have the form

$$\phi_i = e^{-(\alpha r_1 + \beta r_2 + \gamma r_{12})}\, r_1^{k_i}\, r_2^{l_i}\, r_{12}^{m_i} \tag{2.44}$$

and the indices k_i, l_i and m_i take non-negative integer values related to a given positive integer, ω, in such a way that

$$k_i + l_i + m_i \leq \omega. \tag{2.45}$$

By expanding (2.24) and differentiating with respect to the linear parameters K^t, c_i ($i = 1, ..., N$) (see equation 2.23), we get a set of N+1 simultaneous equations which can be set out in matrix form such that,

$$\begin{bmatrix} (C,LC) & \dots & (C,L\phi_j) & \dots \\ \vdots & & \vdots & \\ (\phi_i,LC) & \dots & (\phi_i,L\phi_j) & \dots \\ \vdots & & \vdots & \end{bmatrix} \begin{bmatrix} K^t \\ \vdots \\ c_i \\ \vdots \end{bmatrix} = - \begin{bmatrix} (C,LS) \\ \vdots \\ (\phi_i,LS) \\ \vdots \end{bmatrix}, \tag{2.46}$$

or

$$\boldsymbol{A}\,\boldsymbol{X} = -\boldsymbol{B}. \tag{2.47}$$

where a term such as (C, LS) means $\langle C \mid L \mid S \rangle$ etc... The variational, or stationary, value of K^v can be found from (2.40) and (2.47) by,

$$K^v = -\begin{bmatrix} \boldsymbol{X}^T & 1 \end{bmatrix} \begin{bmatrix} \boldsymbol{A} & \boldsymbol{B} \\ \boldsymbol{B}^T & (S,LS) \end{bmatrix} \begin{bmatrix} \boldsymbol{X} \\ 1 \end{bmatrix}, \tag{2.48}$$

$$= -\boldsymbol{B}^T\boldsymbol{X} - (S,LS). \tag{2.49}$$

2.3 Schwartz Singularities

The Kohn method described above is a very useful method of calculating the phase shifts, and furthermore, it usually provides a lower bound. However, this bound is not rigorous but empirical, because for particular values of the non-linear parameters in the trial wave function, the phase shift may display an *anomalous singularity.*

The first analysis of this phenomenon was made by Schwartz (1961a), studying the phase shifts for electron and positron-hydrogen scattering. He found that at particular values of the non-linear parameter in the short range terms in the trial wave function, the tangent of the phase shift went through spurious jumps over ranges of energy. He also found that if the number of terms in the short range part of the trial wave function was increased, then the number of singularities would also increase but they would be narrower in the range of the non-linear parameter, so the range over which the results would be reliable would be greater.

Schwartz concluded that these singularities arose from the inversion of the $\boldsymbol{\phi L \phi}$ matrix. If there are N short range terms, this matrix will have N eigenvalues of the operator L, one of which may vary continuously through zero as the energy is varied. In numerical calculations it is sufficient for one of these eigenvalues to be close to zero to create problems when inverting the matrix.

Further investigations (Nesbet 1980) established that the long range terms in the trial wave function were also important in contributing to the existence of these singularities. In the case of the Kohn method described above, singularities can arise from the inversion of the $\boldsymbol{A}$ matrix (see equation 2.47). Various methods have been developed to deal with this problem, but in this study three variants of the Kohn method have been used (described below), and a comparison is then made between the results of the three methods. A singularity arising in the results obtained using all three methods at the same energy for the same values of non-linear parameters is *extremely* unlikely, unless it is a genuine feature of the system, e.g. a resonance.

2.4 Variants of the Variational Methods

In addition to the standard Kohn variation method outlined above two variants of the Kohn method have been used in this work which provide a useful check on the accuracy of the results and identify Schwartz singularities. Both these methods have the advantage that they use the same matrix elements as those calculated in the standard Kohn method, but different matrix manipulations are needed to create the variational phase shifts.

2.4.1 Inverse Kohn Method

In this case another value of the normalization parameter, A, given in (2.34), is chosen, $A = \sqrt{k}\,\mathrm{cosec}\,\eta_l$, so the single-channel trial wave function for the inverse Kohn method is,

$$\Psi^t = \overline{K}^t S + C + \sum_{i=1}^{N} c_i \phi_i \tag{2.50}$$

where

$$\overline{K} = \cot \eta_l. \tag{2.51}$$

This changes the functional and also the matrix structure in (2.46).

2.4.2 Complex Kohn Method

This method uses the same functional as in the Kohn method but the form of the wave function is changed. Instead of expressing the asymptotic form of the wave function in terms of spherical Bessel and Neumann functions, it is now expressed in terms of two *irregular* solutions to the differential equation (2.12). These are known as Hankel functions, $h_l^{(\pm)}$, and are the complex sums of the spherical Bessel and Neumann functions, so

$$h_l^{(\pm)}(kr) = j_l(kr) \pm i\, n_l(kr). \tag{2.52}$$

The Neumann function in the C terms is replaced with $i\, h_l^{(-)}$, and so the matrix $\boldsymbol{A}$ becomes complex. It was originally considered (McCurdy *et al* 1987) that the complex symmetric $\boldsymbol{A}$-matrix would never have a zero determinant, but Luchesse (1989) has shown that although unlikely, it is still possible. If the determinant is to be zero then the real

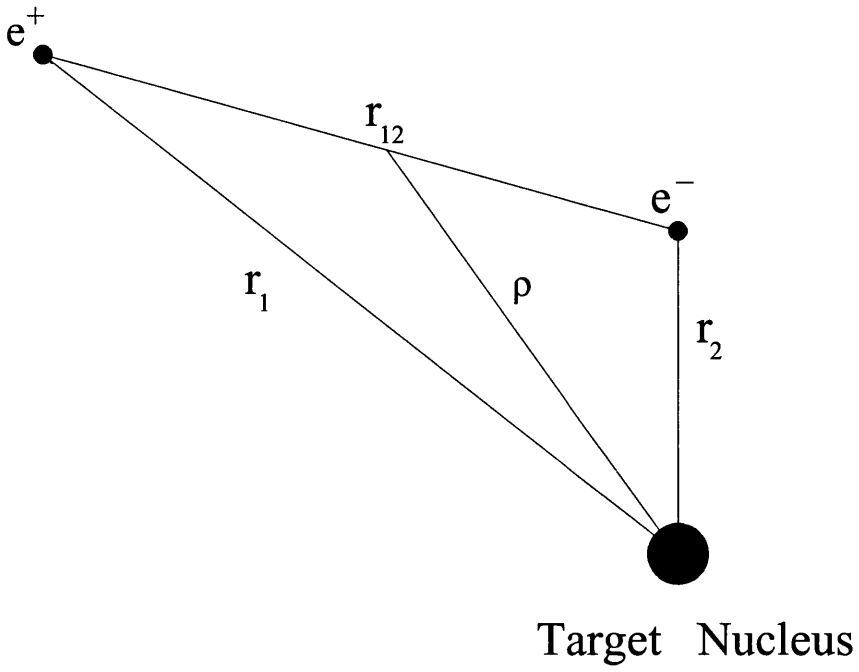

Figure 2.1: The coordinates of the positron-one electron atom system.

and imaginary parts have to be zero simultaneously, which is possible when there is more than one non-linear parameter to consider.

2.5 Two Channel Scattering Theory

When the incident positron has an energy in excess of the threshold energy, $E_{\mathrm{Ps}} = E_{\mathrm{i}} - 6.8$ eV, for positronium formation, there are two open channels to consider (see 1.1 and 1.3).

The two channel scattering formalism can be derived in a similar manner to that described previously for single-channel scattering but using a two component scattering wave function.

To begin with let us consider the Schrödinger equation (2.5) and, for convenience, a one-electron target, as shown in figure 2.1.

The Hamiltonian can be represented in terms of the positron-atom coordinates, $\boldsymbol{r}_1$ and

$\boldsymbol{r}_2$, so that the Hamiltonian is

$$H_{\mathrm{T}} = -\frac{1}{2}\boldsymbol{\nabla}^2_{\boldsymbol{r}_1} - \frac{1}{2}\boldsymbol{\nabla}^2_{\boldsymbol{r}_2} + V(r_1, r_2, r_{12}), \tag{2.53}$$

or in terms of the positronium-ion coordinates,

$$H_{\mathrm{T}} = -\frac{1}{4}\boldsymbol{\nabla}^2_{\boldsymbol{\rho}} - \boldsymbol{\nabla}^2_{\boldsymbol{r}_{12}} + V(r_1, r_2, r_{12}), \tag{2.54}$$

where $\boldsymbol{\rho} = \frac{1}{2}(\boldsymbol{r}_1 + \boldsymbol{r}_2)$ is the position of the centre of mass of the positronium relative to the target nucleus.

From conservation of energy,

$$E_{\mathrm{T}} = \frac{k^2}{2} - E_{\mathrm{i}} = \frac{\kappa^2}{4} - E_{\mathrm{Ps}} \tag{2.55}$$

where κ is the positronium wavenumber, and E_{i} and E_{Ps} are the single ionization energy of the atom and the positronium binding energy (= 6.8 eV), respectively.

The asymptotic form of the scattering wave function given by (2.8) and (2.9) is modified such that, when positronium is formed, the scattering wave function as $\rho \to \infty$ is

$$\Psi(\boldsymbol{r}_1, \boldsymbol{r}_2) \underset{\rho\to\infty}{\sim} \psi_{\mathrm{sc}}(\boldsymbol{\rho})\Phi_{\mathrm{Ps}}(\boldsymbol{r}_{12}), \tag{2.56}$$

where $\Phi_{\mathrm{Ps}} = \frac{1}{\sqrt{8\pi}}e^{-\frac{1}{2}r_{12}}$ is the exact positronium wave function, and the scattering wave function now has no incoming positronium plane wave, so

$$\psi_{sc}(\boldsymbol{\rho}) \underset{\rho\to\infty}{\sim} f_{\mathrm{Ps}}(\theta_\rho)\frac{e^{ik\rho}}{\rho}. \tag{2.57}$$

In order to indicate which processes are being described, a numerical subscript is used; positron-atom elastic scattering is denoted "11", (or el), and positronium formation "12" (or Ps). The two asymptotic forms of the first component of the scattering wave function Ψ_1 are then,

$$\Psi_1 \underset{r_1\to\infty}{\sim} \left(e^{i\boldsymbol{k}.\boldsymbol{r}_1} + f_{11}(\theta_1)\frac{e^{ikr_1}}{r_1}\right)\Phi_{\mathrm{T}}(\boldsymbol{r}_2) \tag{2.58}$$

$$\underset{\rho\to\infty}{\sim} f_{12}(\theta_\rho)\frac{e^{ik\rho}}{\rho}\,\Phi_{\mathrm{Ps}}(\boldsymbol{\rho}). \tag{2.59}$$

The complete picture needs to take into consideration the time-reverse processes, i.e. positronium-ion elastic scattering ("22") and atom formation, i. e. capture by the ion

of the electron in the positronium ("21") with the release of the positron, so the second component of the wave function, Ψ_2, has the asymptotic forms

$$\Psi_2 \underset{\rho\to\infty}{\sim} \left(e^{i\boldsymbol{\kappa}.\boldsymbol{\rho}} + f_{22}(\theta_\rho)\frac{e^{ik\rho}}{\rho}\right)\Phi_{\rm Ps}(\boldsymbol{\rho}) \tag{2.60}$$

$$\underset{r_1\to\infty}{\sim} f_{21}(\theta_1)\frac{e^{ikr_1}}{r_1}\Phi_{\rm T}(\boldsymbol{r}_2). \tag{2.61}$$

A similar analysis to that given from (2.11) onward provides us with a two component real wave function with the asymptotic forms,

$$\Psi_1 \underset{r_1\to\infty}{\sim} Y_{l,0}(\theta_1,\phi_1)\sqrt{k}\,[j_l(kr_1) - K_{11}\,n_l(kr_1)]\,\Phi_{\rm T}(\boldsymbol{r}_2), \tag{2.62}$$

$$\underset{\rho\to\infty}{\sim} -Y_{l,0}(\theta_\rho,\phi_\rho)\sqrt{2\kappa}K_{12}n_l(\kappa\rho)\Phi_{\rm Ps}(\boldsymbol{r}_{12}), \tag{2.63}$$

$$\Psi_2 \underset{\rho\to\infty}{\sim} Y_{l,0}(\theta_\rho,\phi_\rho)\sqrt{2\kappa}\,[j_l(\kappa\rho) - K_{22}\,n_l(\kappa\rho)]\,\Phi_{\rm Ps}(\boldsymbol{r}_{12}), \tag{2.64}$$

$$\underset{r_1\to\infty}{\sim} -Y_{l,0}(\theta_1,\phi_1)\sqrt{k}K_{21}n_l(kr_1)\Phi_{\rm T}(\boldsymbol{r}_2). \tag{2.65}$$

Extending the $\boldsymbol{S}$ matrix (see equations 2.19 and 2.22) to include the two channels, the $\boldsymbol{K}$ and $\boldsymbol{S}$ matrix elements are related by

$$\boldsymbol{S} = \frac{\mathbf{1} + i\boldsymbol{K}}{\mathbf{1} - i\boldsymbol{K}}, \tag{2.66}$$

where $\mathbf{1}$ is the 2×2 identity matrix. The partial wave cross sections for each process are then

$$\sigma_{pq} = \frac{\pi(2l+1)}{k_p^2}\,|\boldsymbol{S} - \mathbf{1}|^2 \tag{2.67}$$

$$= \frac{4\pi(2l+1)}{k_p^2}\left|\left(\frac{\boldsymbol{K}}{\mathbf{1} - i\boldsymbol{K}}\right)_{pq}\right|^2; \qquad p\,,q = 1,\,2, \tag{2.68}$$

where $k_1 = k$ and $k_2 = \kappa$. The positron elastic scattering cross section and the positronium formation cross section are denoted by σ_{11} and σ_{12} respectively and are dependent on a coupling between the $\boldsymbol{K}$ matrix elements.

The subsequent variational calculations are much like those for single-channel scattering except there are now four functionals to consider,

$$I_{pq} = \langle\,\Psi_p \mid L \mid \Psi_q\,\rangle, \tag{2.69}$$

and the variational $\boldsymbol{K}^v$ matrix is then found as an extension of (2.40) so that

$$\delta I_{pq} = K^t_{pq} - K_{pq} + \langle\, \delta\Psi_p \mid L \mid \delta\Psi_q \,\rangle \tag{2.70}$$

and therefore

$$\boldsymbol{K}^v = \boldsymbol{K}^t - \boldsymbol{I}^t, \tag{2.71}$$

or

$$\begin{bmatrix} K^v_{11} & K^v_{12} \\ K^v_{21} & K^v_{22} \end{bmatrix} = \begin{bmatrix} K^t_{11} & K^t_{12} \\ K^t_{21} & K^t_{22} \end{bmatrix} - \begin{bmatrix} (\Psi_1, L\Psi_1) & (\Psi_1, L\Psi_2) \\ (\Psi_2, L\Psi_1) & (\Psi_2, L\Psi_2) \end{bmatrix}. \tag{2.72}$$

Suitable choices for the two components of the wave function are

$$\Psi^t_1 = S_1 + K^t_{11}\, C_1 + K^t_{21}\, C_2 + \sum_{i=1}^{N} c_i\, \phi_i, \tag{2.73}$$

$$\Psi^t_2 = S_2 + K^t_{22}\, C_2 + K^t_{12}\, C_1 + \sum_{j=1}^{N} d_j\, \phi_j, \tag{2.74}$$

where

$$S_1 = Y_{l,0}(\theta_1, \phi_1)\sqrt{k}\, j_l(kr_1)\Phi_{\rm T}(\boldsymbol{r}_2), \tag{2.75}$$

$$C_1 = -Y_{l,0}(\theta_1, \phi_1)\sqrt{k}\, n_l(kr_1)\, f_1(r_1)\, \Phi_{\rm T}(\boldsymbol{r}_2), \tag{2.76}$$

$$S_2 = Y_{l,0}(\theta_\rho, \phi_\rho)\sqrt{2\kappa}\, j_l(\kappa\rho)\Phi_{\rm Ps}(\boldsymbol{r}_{12}), \tag{2.77}$$

$$C_2 = -Y_{l,0}(\theta_\rho, \phi_\rho)\sqrt{2\kappa}\, n_l(\kappa\rho)\, f_2(\rho)\, \Phi_{\rm Ps}(\boldsymbol{r}_{12}), \tag{2.78}$$

and ϕ_i are Hylleraas-type short range correlation functions of the form given in equation (2.44). The functions $f_1(r_1)$ and $f_2(\rho)$ shield the singularities in $n_l(kr_1)$ and $n_l(\kappa\rho)$ at their respective origins. It is noticeable that the subscripts on the $\boldsymbol{K}^t$ matrix elements in (2.73) and (2.74) differ from those in (2.62)-(2.65). This is because had the notation given in the asymptotic form been kept we would have arrived at a transpose of the variational $\boldsymbol{K}$ matrix. This change is valid because of the symmetry of the exact *and* the variational $\boldsymbol{K}$ matrix, that is, $K_{12} = K_{21}$, but not of $\boldsymbol{K}^t$.

The calculation of the $\boldsymbol{K}^v$ matrix is similar to that given in (2.46) except that now the single column matrix becomes two columns and the elements (C, LC) etc. are 2×2

matrices, so that

$$\begin{bmatrix} (C_1,LC_1) & (C_1,LC_2) & \dots & (C_1,L\phi_j) & \dots \\ (C_2,LC_1) & (C_2,LC_2) & \dots & (C_2,L\phi_j) & \dots \\ \vdots & \vdots & & \vdots & \\ (\phi_i,LC_1) & (\phi_i,LC_2) & \dots & (\phi_i,L\phi_j) & \dots \\ \vdots & \vdots & & \vdots & \end{bmatrix} \begin{bmatrix} K_{11}^t & K_{12}^t \\ K_{21}^t & K_{22}^t \\ \vdots & \vdots \\ c_i & d_i \\ \vdots & \vdots \end{bmatrix} = - \begin{bmatrix} (C_1,LS_1) & (C_1,LS_2) \\ (C_2,LS_1) & (C_2,LS_2) \\ \vdots & \vdots \\ (\phi_i,LS_1) & (\phi_i,LS_2) \\ \vdots & \vdots \end{bmatrix} \tag{2.79}$$

or, with new notation,

$$\boldsymbol{A}\,\boldsymbol{X} = -\boldsymbol{B}. \tag{2.80}$$

Now,

$$\boldsymbol{K}^v = -\begin{bmatrix} \boldsymbol{X}^T & \mathbf{1} \end{bmatrix} \begin{bmatrix} \boldsymbol{A} & \boldsymbol{B} \\ \boldsymbol{B}^T & \boldsymbol{SLS} \end{bmatrix} \begin{bmatrix} \boldsymbol{X} \\ \mathbf{1} \end{bmatrix} \tag{2.81}$$

$$= -\boldsymbol{B}^T\boldsymbol{X} - \boldsymbol{SLS}, \tag{2.82}$$

where $\mathbf{1}$ is the 2×2 identity matrix and the matrices $\boldsymbol{CLC}$, $\boldsymbol{CLS}$ and $\boldsymbol{SLS}$ are of the form,

$$\boldsymbol{SLS} = \begin{bmatrix} (S_1,LS_1) & (S_1,LS_2) \\ (S_2,LS_1) & (S_2,LS_2) \end{bmatrix} \quad \text{etc....} \tag{2.83}$$

2.5.1 Singularities

The two-channel scattering calculations are subject to similar anomalous singularities as described by Schwartz (1961a) (see Section 2.3) in the single-channel case. Singularities in the variational $\boldsymbol{K}$ matrix elements can be pinpointed by comparing the results yielded by the inverse and the complex Kohn methods described in Section 2.4 applied to a two-channel scattering formalism.

The complex Kohn method is useful not only because Schwartz singularities rarely occur but also because, in the two channel case it provides a measure of its own reliability. Luchesse (1989) showed that the unitarity of the calculated $\boldsymbol{S}$ matrix is a good measure

of the reliability of the results of the complex Kohn method. If $\boldsymbol{S}$ is unitary, then

$$\overline{\boldsymbol{S}}^T \boldsymbol{S} = \mathbf{1} \tag{2.84}$$

and this relation is broken as a singularity is approached.

Chapter 3

Model Potentials

3.1 Introduction

The first scattering system under investigation in this work is that of positron-helium scattering. *Ab initio* investigations of this system have four particles to consider (the positron, two electrons and the atomic nucleus). This means that, taking the nucleus as being infinitely massive, three particle vectors, or six interparticle coordinates and three Euler angles, are required to specify the configuration. Integration over the three Euler angles is straight-forward and consequently the various matrix elements that need to be evaluated involve six-dimensional integration which requires a large amount of computational time for a relatively simple system. Such calculations have been done with excellent results (Van Reeth and Humberston 1999) but they used a lot of computational time. Since the number of interparticle coordinates for an N-body system is $N(N-1)/2$, detailed *ab initio* studies of the collisions of positrons with heavier atoms are not realistic.

A possible way around this difficulty is to use a model in which the neutral target atom is represented as one electron orbiting an ion core. This turns the positron-atom scattering system into a three body problem, with only three interparticle coordinates and a great reduction in calculating time. The disadvantage with this method is that it is only a model so there may be real aspects of the system that a specific model cannot represent. Whether these are important or not in this case will be revealed by the current

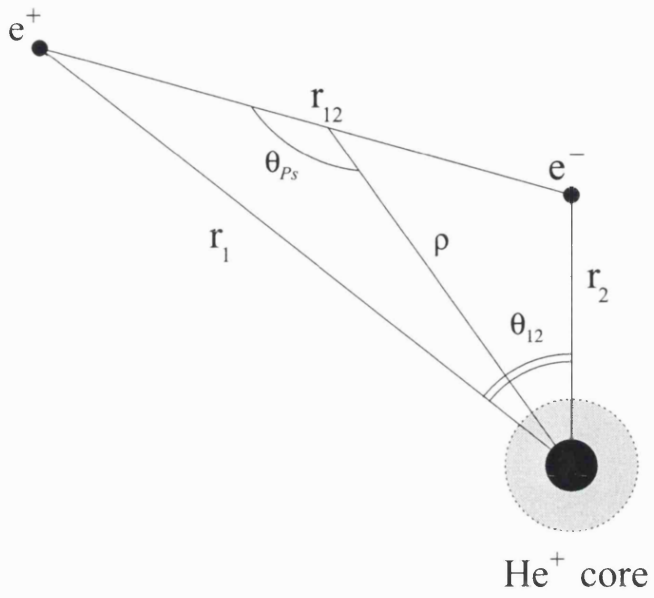

Figure 3.1: The coordinates of the positron-helium system.

investigations.

Helium is arguably the worst choice of atom to represent as a one-electron model. It has two equivalent electrons which should not allow either one to be treated as special. One electron models of alkali atoms have been successful, for example lithium (Watts 1994 and Watts and Humberston 1994), since such an atom consists of one relatively loosely bound electron orbiting a core of tightly bound inner shell electrons, and so the system is physically similar to a hydrogenic atom. Noble gases on the other hand have filled outer shells, so the outer electrons are equivalent. Studies of one-electron models of helium are therefore a useful test of the validity of the models, and perhaps an extension to positron collisions with heavier noble gases can be made.

3.2 Calculating Model Potentials

3.2.1 Hydrogenic Static Potentials

The simplest construction of a one-electron model of helium is to create a 'hydrogenic static' potential. Taking the full three body system of the helium atom, where the nucleus is taken to be of infinite mass at the origin, the electron-nucleus coordinates are denoted $\boldsymbol{r}_a$ and $\boldsymbol{r}_b$ and the electron-electron coordinate is $\boldsymbol{r}_{ab}$. Let electron a be the 'one-electron' for which we want to find an interaction potential between it and the *core* (the nucleus and the other electron) that is dependent only on r_a. The potential felt by a, V_a, and the helium-ion wave function, Φ_{He^+} are both known exactly,

$$V_a = -\frac{2}{r_a} + \frac{1}{r_{ab}}, \qquad \Phi_{\mathrm{He}^+} = \sqrt{\frac{8}{\pi}} e^{2r_b}, \tag{3.1}$$

and the static potential, $V(r_a)$, is given by

$$V(r_a) = \int_{\phi=0}^{2\pi} \int_{\theta=0}^{\pi} \int_{r_b=0}^{\infty} V_a \mid \Phi_{\mathrm{He}^+}(r_b) \mid^2 r_b^2 \, dr_b \, \sin\theta \, d\theta \, d\phi. \tag{3.2}$$

Evaluating this integral fully gives the *static* interaction potential between the electron and helium-ion core,

$$V(r_a) = -\frac{1}{r_a} - e^{-4r_a}\left(\frac{1}{r_a} + 2\right). \tag{3.3}$$

As $r_a \rightarrow 0$, the electron feels only the attraction of the doubly charged nucleus, and as $r_a \rightarrow \infty$ only the Coulomb attraction of the singly charged ion core.

3.2.2 Accurate Model Potentials

The problem with the static potential is that it represents a rigid helium ion core. The potential takes no account of distortion of the core by the bound electron and the low energy positron, and no account of exchange between the two physically equivalent electrons in the atom. An accurate electron-helium ion potential which does take account of some of these factors has been found by Peach (1998) with the form

$$\begin{aligned} V(r) = & -\frac{1}{r} - \frac{Z'}{r}\left(1 + \delta r + \delta' r^2\right) e^{-\gamma r} - \frac{\alpha_d}{2r^4}\omega_2(\beta r) \\ & - \frac{\alpha_q}{2r^6}\chi_3(\beta' r)\,\chi_4(\beta' r) + \frac{3\beta_d}{r^6}\omega_2(\beta_1 r) + \frac{24\gamma_d}{r^6} f(E_{\mathrm{i}})\,\omega_2(\beta_2 r), \end{aligned} \tag{3.4}$$

where the functions ω_n and χ_n shield the singularities as $r \rightarrow 0$, so

$$\omega_n(x) = [\chi_n(x)]^2 \tag{3.5}$$

and

$$\chi_n(x) = 1 - e^{-x} \sum_{m=0}^{n} \frac{x^m}{m!}. \tag{3.6}$$

The potential given in equation (3.4) has been chosen to reproduce spectroscopic data accurately. The first term in the potential function is the long range Coulomb attraction, the second term represents a static-type interaction with the core, with $Z' = 1$ (in general $Z' = Z - 1$, where Z is the total number of electrons in the atom). The third and fourth terms represent the dipole, α_d, and quadrapole, α_q, polarizabilities of the core respectively, and the the last two terms are dynamical corrections to the dipole polarizability potential (β_d and γ_d), where E_i is the ionization energy of the atom corresponding to the potential, and the function $f(E_\mathrm{i})$ is given by

$$f(E_\mathrm{i}) = \frac{\gamma_E}{\pi} \tan^{-1}\left(-\frac{\pi}{\gamma_E} E_\mathrm{i}\right). \tag{3.7}$$

Although only the parameters Z, α_d, α_q, β_d, γ_d and E_i represent known physical properties of the ion, the others are found empirically by fitting the potential to spectroscopic and electron scattering data, so exchange effects and distortions of the atom are all taken into account in the potential as a whole.

3.3 Properties of Model Potentials

Model potentials have been used to reproduce accurate spectroscopic results for the excited states of sodium. This is an alkali atom and therefore the excitation energy of the valence electron is much smaller than that of the inner shell electrons, so a one-electron model is quite appropriate. But although it reproduces these results very well, the model potential may also support other bound states which are not present in the physical system. For example, in sodium the valence electron is in a $3s$ orbital and the $1s$, $2s$ and $2p$ shells are filled by the other electrons. A good model sodium potential reproduces the real states

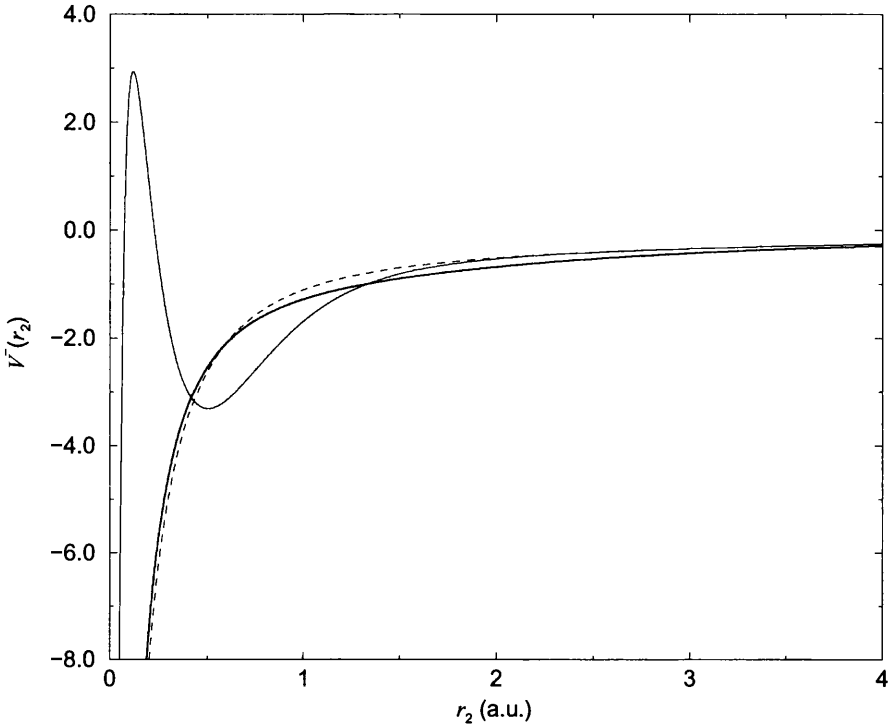

Figure 3.2: Variation of electron-core model potentials with electron coordinate, r_2 for helium. Thick line, V_1^-; thin line, V_2^-; dashed line, V_3^-.

of the $3s$ electron to more than 99.9% accuracy but it also supports three bound states representing the $1s$, $2s$ and $2p$ electrons, lying at energies well below the physically real ground-state.

Therefore, although a model potential may provide very accurate spectroscopic results, it may also produce unphysical properties as well. Later we shall see the effect these can have.

3.4 Properties of Helium Potentials

In this work, three model helium potentials will be used, each with the same form as that given in equation (3.4). The three models are plotted in figure 3.2. The first, V_1^-, is the one provided by Dr Peach which reproduces spectroscopic data very well; the second, V_2^- (also provided by Dr Peach), only contains the first three terms of equation (3.4), but the parameter γ in the static part of the potential is closer to the value of the exponent in the hydrogenic static (see equation 3.3). It also reproduces the energy of the first excited

state of helium more accurately. The third potential, V_3^-, is the exact hydrogenic static potential with the core dipole polarizability term added; thus

$$\begin{aligned} V_1^-(r) &= -\frac{1}{r} - \frac{1}{r}\left(1+\delta_{(1)}r+\delta'_{(1)}r^2\right)e^{-\gamma_{(1)}r} - \frac{\alpha_d}{2r^4}\omega_2(\beta r) \\ &\quad - \frac{\alpha_q}{2r^6}\chi_3(\beta' r)\,\chi_4(\beta' r) + \frac{3\beta_d}{r^6}\omega_2(\beta_1 r) + \frac{24\gamma_d}{r^6}f(E_i)\,\omega_2(\beta_2 r), \quad (3.8) \\ V_2^-(r) &= -\frac{1}{r} - \frac{1}{r}\left(1+\delta_{(2)}r+\delta'_{(2)}r^2\right)e^{-\gamma_{(2)}r} - \frac{\alpha_d}{2r^4}\omega_2(\beta r), \quad (3.9) \\ V_3^-(r) &= -\frac{1}{r} - \left(\frac{1}{r}+2\right)e^{-4r} - \frac{\alpha_d}{2r^4}\omega_2(\beta r). \quad (3.10) \end{aligned}$$

The values of the parameters are listed in the appendix.

In order to use these potentials in the scattering calculations we need to determine the target wave function representing the model atom in addition to its ground-state energy. We can also calculate other properties of the model atom, in particular, the dipole polarizability and the first excitation energy of the electron.

It should be noted that there are differences between the descriptions of the energy levels when referring to one-electron model atoms or to real many-electron atoms. In helium, for instance, the ground state energy of the real atom is $E_0 = -2.9077$ a.u., i.e. the energy threshold for double (or total) ionization is 2.9077 a.u. However, a one-electron model can only be singly ionized by definition, so the ground state energy of our one-electron model helium atom should be the negative of the energy required to singly ionize the helium atom, -0.9069 a.u., and similarly for the excited states. In general, then, a real atom with ground state energy E_A, and its positive ion ground state energy E_{A+}, will be represented by a one-electron model with a ground state energy E_0 where,

$$E_0 = E_A - E_{A+}. \quad (3.11)$$

and similarly the first excited state of the model, E_1, is related to the first excited state of helium, E_{A^*}, by

$$E_1 = E_{A^*} - E_{A+}. \quad (3.12)$$

In this work, we are only interested in positron scattering up to the first excitation threshold, so these are also calculated but only in order to know up to which point the results are valid.

3.4.1 Rayleigh Ritz Method

A convenient method of finding the ground state energy of an electron in a model potential is the *Rayleigh Ritz* variational method. This provides a rigorous upper bound on the ground state energy E_0. We start with the functional E of the wave function Φ,

$$E[\Phi] = \frac{\langle \Phi \mid H \mid \Phi \rangle}{\langle \Phi \mid \Phi \rangle} \tag{3.13}$$

which yields the exact E_0 for the Hamiltonian, H, for the model when Φ is the exact ground state wave function, Φ_0. As with the Kohn functional, E is stationary with respect to small variations in the wave function away from the exact wave function Φ. Taking the exact wave function to be equal to the ground state wave function, i.e. $\Phi = \Phi_0$, a trial function, Φ^t can be defined as

$$\Phi^t = \Phi + \delta\Phi, \tag{3.14}$$

and

$$\delta E = E[\Phi] - E[\Phi^t] = E_0 - E_0^v. \tag{3.15}$$

and we shall show that $\delta E = 0$ to first order in the error in the wave function.

We know that $H \mid \Phi \rangle = E_0 \mid \Phi \rangle$, and taking into account the fact that the Hamiltonian is a Hermitian operator,

$$E[\Phi^t] = \frac{\langle \Phi + \delta\Phi \mid H \mid \Phi + \delta\Phi \rangle}{\langle \Phi + \delta\Phi \mid \Phi + \delta\Phi \rangle} \tag{3.16}$$

$$= \frac{\langle \Phi \mid H \mid \Phi \rangle + 2\langle \delta\Phi \mid H \mid \Phi \rangle + \langle \delta\Phi \mid H \mid \delta\Phi \rangle}{\langle \Phi \mid \Phi \rangle + 2\langle \delta\Phi \mid \Phi \rangle + \langle \delta\Phi \mid \delta\Phi \rangle}, \tag{3.17}$$

$$= \frac{E_0\langle \Phi \mid \Phi \rangle + 2E_0\langle \delta\Phi \mid \Phi \rangle + \langle \delta\Phi \mid H \mid \delta\Phi \rangle}{\langle \Phi \mid \Phi \rangle + 2\langle \delta\Phi \mid \Phi \rangle + \langle \delta\Phi \mid \delta\Phi \rangle}. \tag{3.18}$$

But

$$E_0 = E_0\frac{\langle \Phi^t \mid \Phi^t \rangle}{\langle \Phi^t \mid \Phi^t \rangle} \tag{3.19}$$

$$= \frac{E_0\langle \Phi \mid \Phi \rangle + 2E_0\langle \delta\Phi \mid \Phi \rangle + E_0\langle \delta\Phi \mid \delta\Phi \rangle}{\langle \Phi \mid \Phi \rangle + 2\langle \delta\Phi \mid \Phi \rangle + \langle \delta\Phi \mid \delta\Phi \rangle}. \tag{3.20}$$

Substituting (3.18) and (3.20) into (3.15), we find the stationary condition,

$$\delta E = \frac{\langle \delta\Phi \mid H \mid \delta\Phi \rangle - E_0 \langle \delta\Phi \mid \delta\Phi \rangle}{\langle \Phi^t \mid \Phi^t \rangle}, \tag{3.21}$$

so $\delta E \sim 0$ to first order in $\delta\Phi$.

The fact that E_0^v is a rigorous upper bound on E_0 can be proved by expanding the trial wave function into a complete set of orthonormal eigenfunctions, Φ_i, of H, so

$$\Phi_n^t = \sum_{i=0}^{\infty} c_i \Phi_i \tag{3.22}$$

and since $H\Phi_i = E_i\Phi_i$ $(i = 0, 1, ...)$ then

$$E_n^v = \frac{\left\langle \sum_{i=0}^{\infty} c_i\Phi_i \middle| H \middle| \sum_{j=0}^{\infty} c_j\Phi_j \right\rangle}{\left\langle \sum_{i=0}^{\infty} c_i\Phi_i \middle| \sum_{j=0}^{\infty} c_j\Phi_j \right\rangle} \tag{3.23}$$

$$= \frac{\sum_{i,j=0}^{\infty} c_i^* c_j \langle \Phi_i \mid \Phi_j \rangle E_j}{\sum_{i,j=0}^{\infty} c_i^* c_j \langle \Phi_i \mid \Phi_j \rangle} \tag{3.24}$$

$$= \frac{\sum_{j=0}^{\infty} \mid c_j \mid^2 E_j}{\sum_{j=0}^{\infty} \mid c_j \mid^2} \tag{3.25}$$

so

$$E_n^v - E_0 = \frac{\sum_{j=0}^{\infty} \mid c_j \mid^2 (E_j - E_0)}{\sum_{j=0}^{\infty} \mid c_j \mid^2} \tag{3.26}$$

but since E_j is an eigenvalue of H, it follows that for all j $E_j \geq E_0$ and therefore all $E_n^v \geq E_0$.

In order to calculate the ground state energy of the model a Hylleraas-type trial wave function is used so that

$$\Phi^t(r) = \sum_{i=0}^{N} c_i\phi_i = e^{-\beta r} \sum_{i=0}^{N} c_i r^i. \tag{3.27}$$

The functional E_0^v is stationary with respect to small changes in the wave function so that

$$\frac{\partial E_0^v}{\partial c_i} = 0 \tag{3.28}$$

which leads to a set of N simultaneous linear homogeneous equations which can be expressed as a matrix eigenvalue equation,

$$(\boldsymbol{H} - E_0^v \boldsymbol{A})\, \boldsymbol{c} = 0, \tag{3.29}$$

where the matrix elements of $\boldsymbol{H}$ and $\boldsymbol{A}$ are given by

$$H_{ij} = \langle \phi_i \mid H \mid \phi_j \rangle\,, \tag{3.30}$$

$$A_{ij} = \langle \phi_i \mid \phi_j \rangle\,, \tag{3.31}$$

and $\boldsymbol{c}$ is a column matrix listing the optimum values of the linear coefficients in the variational wave function. Equation (3.29) is a standard matrix eigenvalue equation and many computational routines exist to solve it, giving us the optimized values of the coefficients (for a particular value of non-linear parameter, β) and the eigenvalues, E_n^v $(n = 0, 1...N)$.

Since the calculated value of E_0^v is an upper bound on the exact value of the energy of the ground state, we can vary the non-linear parameter, β, and the number of terms, N, in the trial wave function to obtain the lowest value of E_0^v. For a given value of β, E_0^v decreases (becomes more negative) as N is increased. The minimum in E_0^v with respect to variations in β is then found by repeating the calculation for different values of β. It is noticeable that as N is increased, if E_0^v is well converged in the range over which β provides an accurate value of E_0^v, the minimum in figure (3.3) is broadened out.

There are N solutions to the eigenvalue equation (3.29), each representing an approximation to a state of the model atom, either the ground states or an excited state. The subsequent eigenvalues, denoted E_1^v, $E_2^v, ...E_N^v$, also follow the same bound rules as the ground state eigenvalue.

Since we are only considering positron collisions up to the first excitation threshold, it is necessary to consider only the energy of the first excited state, which can be determined reasonably accurately as the second eigenvalue, E_1^v, of the above eigenvalue equation.

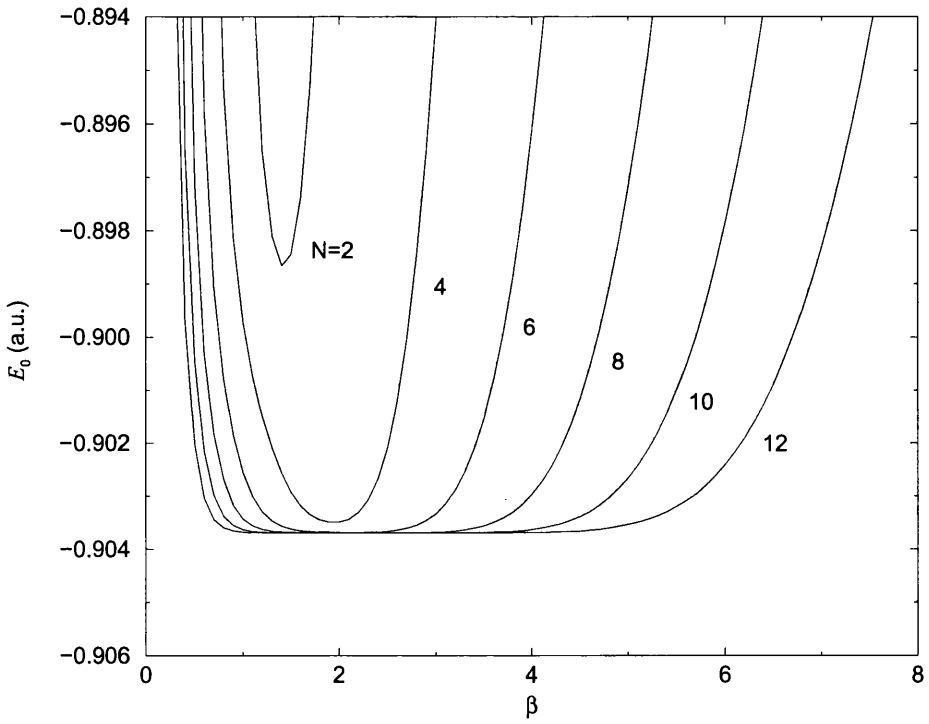

Figure 3.3: Variation of the lowest eigenvalue, E_0^v, using model V_1^-, with respect to the non-linear parameter β in the trial wave function (see equation 3.27). As the number of terms, N in equation (3.27), is increased the minimum value of E_0^v decreases, providing an improved upper bound on the exact ground state energy E_0. Also the minimum becomes flatter.

3.4.2 Dipole Polarizability

The dipole polarizability, α, is a measure of how easily the atom can be distorted by an applied electric field. If the atom is in a small uniform electric field of strength, ϵ, then the dipole polarizability is defined by the difference between the perturbed ground state energy, E_0', and the unperturbed energy, E_0, as follows

$$\alpha = \frac{2\left(E_0 - E_0'\right)}{\epsilon^2}. \tag{3.32}$$

The perturbation produced by the applied electric field, is $\epsilon r\cos\theta$, where θ is the angle between the direction of the electric field and the position vector of the electron. The perturbed Hamiltonian for this system also has to take account of the polarization of the core by the electron so the perturbed Hamiltonian is

$$H' = H + \epsilon\left(r - \frac{\alpha_d}{r^2}\chi_2\left(\beta_3 r\right)\right)\cos\theta, \tag{3.33}$$

where α_d is the dipole polarizability of the core. The trial wave function has to be able to represent this dipole or p-type distortion so our new trial function can take one of two forms

$$\Phi_1' = e^{-\beta' r}\left[\sum_{i=0}^{N} a_i r^i + \sum_{j=0}^{M} b_j r^{j+1}\cos\theta\right], \tag{3.34}$$

or, since Φ_{He} is nodeless,

$$\Phi_2' = \Phi_{\mathrm{He}}\left[1 + \sum_{j=0}^{M} d_j r^{j+1}\cos\theta\right] \tag{3.35}$$

where Φ_{He} is the wave function using the optimized linear parameters. The perturbed ground state energy, E_0', is also obtained using the Rayleigh-Ritz variational method with functional

$$E_0' = \frac{\langle\Phi_i' \mid H \mid \Phi_i'\rangle}{\langle\Phi_i' \mid \Phi_i'\rangle}; \qquad i = 1, 2. \tag{3.36}$$

There is no bound on the dipole polarizability because it involves the difference of two energies, each of which is an upper bound on the corresponding exact energy. However, α is found to be stationary over a range of values of β', and as M and/or N, are increased the region of stability increases.

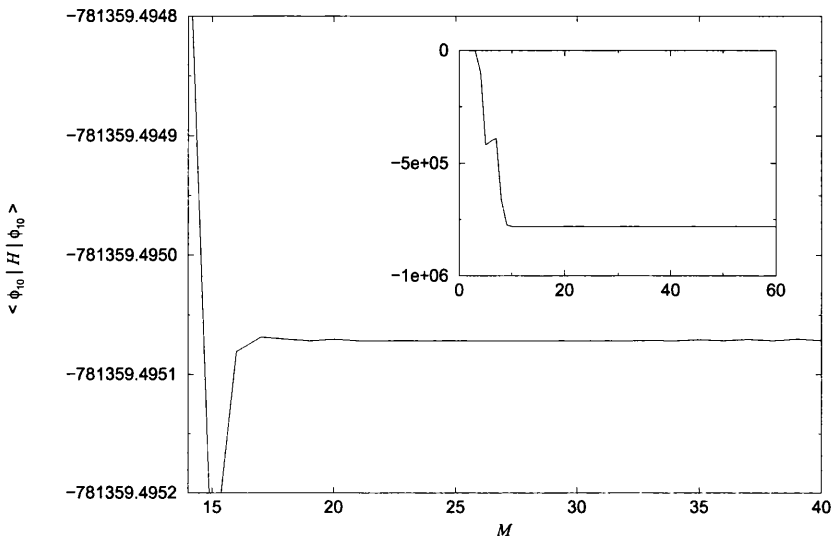

Figure 3.4: Convergence of the matrix element $H_{10,10}$ with respect to increasing the number of points, M, in the numerical integration with model V_1^-. The inset shows the same results on a smaller scale.

It must be noted that the method described above yields the polarizability of the electron-core system only and the total dipole polarizability is equal to the sum of that calculated here and that of the helium ion core, the parameter α_d in equations (3.4) and (3.33), where $\alpha_d = 0.28125\ a_0^3$ for helium.

3.4.3 Integration Techniques

The matrix elements of $\boldsymbol{H}$ and $\boldsymbol{A}$ are calculated using a numerical integration procedure called *Gauss-Laguerre* quadrature. The integral of the product of an exponential and a function, $F(x)$, which can be approximated by a polynomial expressed as

$$\int_0^\infty e^{-\alpha x} F(x) dx \approx \frac{1}{\alpha} \sum_{i=1}^{M} w_i F\left(\frac{x_i}{\alpha}\right), \tag{3.37}$$

where α is a constant and w_i are weights dependent on i and M. This procedure is exact if $F(x)$ is a polynomial of degree $2M-1$ or less. This procedure works well, even for the potential energy component of each matrix elements, as can be seen in figure (3.4) where the value of the matrix elements $\boldsymbol{H}_{10,10}$ converges rapidly with respect to the number of

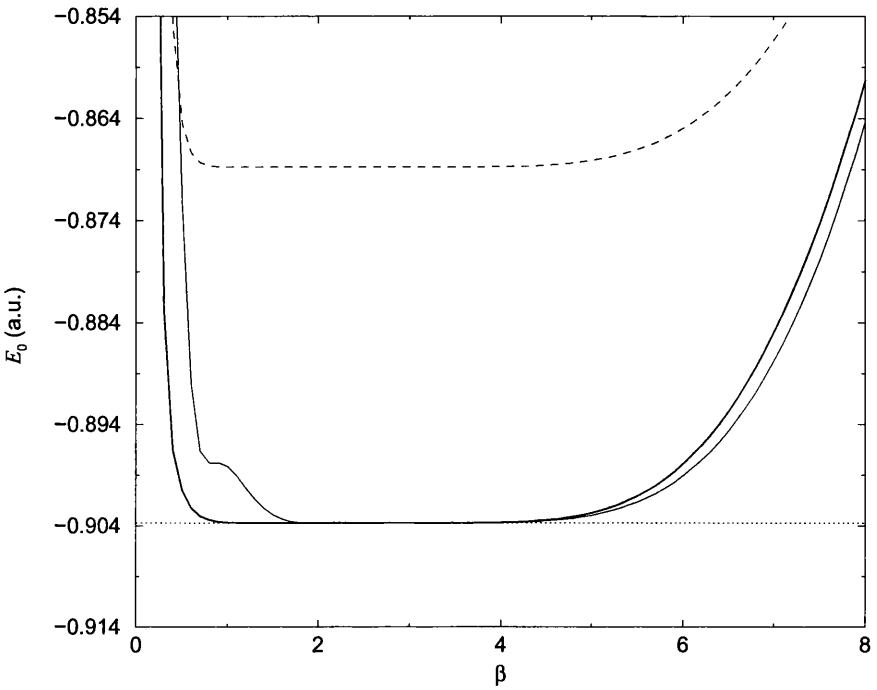

Figure 3.5: Variation of the ground state energy E_0 with respect to the non-linear parameter β, for the three electron-core model potentials. Thick line, V_1^-; thin line, V_2^-; dashed line, V_3^-; dotted line parallel to the abscissa, exact value of E_0 for the helium atom. N=10 in equation (3.27) for all models.

integration points, M.

3.5 Energy, Polarizability and Target Wave Functions

The accuracy of the representation of each model can be appreciated by looking at the energy levels and the model wave functions it provides. The results in figure (3.3) clearly show the rapid convergence of the lowest eigenvalue. These values are upper bounds but it seems highly likely that additional terms would only cause E_0 to decrease by a negligible amount. Figures (3.5) and (3.6) show how the three models compare in terms of the ground state energy they provide using the most accurate 10-term trial wave functions. Models V_1 and V_2 both provide upper bounds which are extremely close to the exact value for helium, to at least 5 decimal places (see table 3.1).

The stable value of the dipole polarizability, α, for these two models also coincides

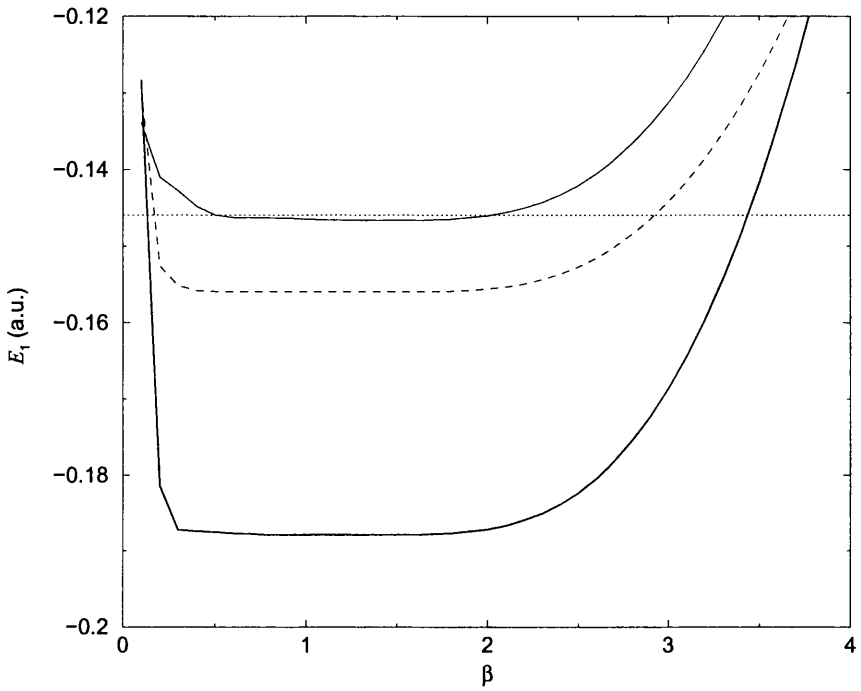

Figure 3.6: Variation of the second lowest eigenvalue, E_1, with respect to the non-linear parameter β, for the three electron-core model potentials. Thick line, V_1^-; thin line, V_2^-; dashed line, V_3^-; dotted line parallel to the abscissa, exact value of E_1 for helium. N=10 in equation (3.27) for all models.

with the exact value for helium. Model V_3 does not provide such good agreement with the known properties of the helium atom, but this might be expected due to the relatively simple nature of this model.

Whether the good agreement with the binding energy and dipole polarizability provided by models V_1^- and V_2^- is sufficient to yield accurate positron scattering data can only be shown in the scattering calculations.

The target atom wave functions, Φ_{He}, used in the scattering calculations are defined by the coefficients that constitute the eigenvector corresponding to the lowest eigenvalue, obtained by solving the matrix equation (3.29). Ideally, the value of the non-linear parameter β should be that which yields the minimum *and* the stationary variational values for the properties of the target. For a small number of terms in the trial wave function, the value of β which provides the lowest value E_0 may not be the same as that which provides a stationary value of α. However, if there are sufficient terms in the trial wave

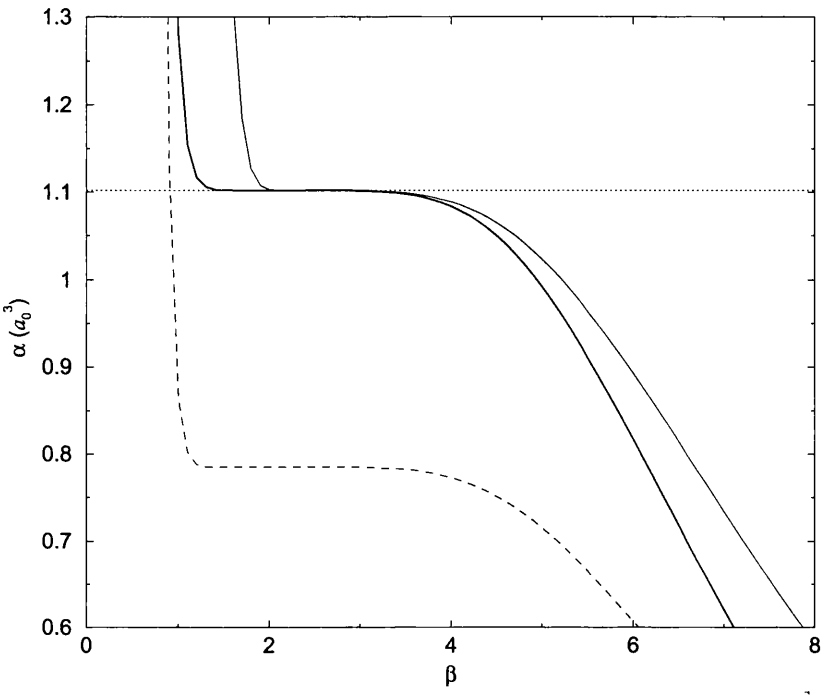

Figure 3.7: Variation of the dipole polarizability of the electron-core system, α, with respect to the non-linear parameter β in equation (3.35), for the three electron-core model potentials. Thick line, V_1^-; thin line, V_2^-; dashed line, V_3^-; dotted line parallel to the abscissa, exact value of α which is the full dipole polarizability of helium minus the contribution from the He^+ core. N=M=10 in equation (3.35) for all models.

function, the precise value of β becomes less important both in terms of the energies and polarizabilities calculated and the form of the wave function itself.

The electron density functions for each of the three models with β=2.0 and N=10 (see equation 3.27 and 3.29) are shown in figure (3.8). This reveals differences in the electron cloud density around the atom for the different models. Since we are considering low energy positron-atom scattering, where the positron has time to interact with the electron cloud, this may have an effect on the scattering results. However, all these results are derived from the model potentials so the sensitivity of the scattering results to the accuracy of target wave functions may or may not be important. This is investigated in the scattering calculations.

The electron densities corresponding to the various models cannot be directly compared with that of a two electron model of helium, but one of the electrons can be specified by

Table 3.1: Properties of the model atoms (minimum or stabilized values): ground state energy (E_0), first excited state energy (E_1), full dipole polarizability of the model atom (α_{He}), dipole polarizability of the model neglecting the core dipole polarizability(α) and the expectation value of the electron coordinate ($\langle r \rangle$). N.B. The total dipole polarizability of the model helium atom is the sum of the polarizability of the single electron and the core polarizability.

Model	E_0(a.u.)	E_1(a.u.)	$\alpha_{\mathrm{He}}(a_0^3)$	$\alpha(a_0^3)$	$\langle r \rangle$(a.u.)
V_1^-	-0.90369424	-0.18785	1.38327	1.10202	1.0813
V_2^-	-0.90369322	-0.14658	1.38375	1.10250	1.1320
V_3^-	-0.86873648	-0.15599	1.06659	0.78534	0.9658
exact	-0.90369424[a]	-0.14597[b]	1.38324[c]	-	-

[a]Moore (1970)

[b]Martin (1960)

[c]Bhatia *et al* (1997)

integrating over the coordinates of the other. The accurate helium wave function created by Van Reeth and Humberston (1999), Φ_{VR}, is a function of the two electron coordinates $\boldsymbol{r}_2$, and $\boldsymbol{r}_3$,

$$\Phi_{\mathrm{VR}}(r_2, r_3) = e^{-\gamma(r_2+r_3)} \sum_{j=0}^{N} b_j (r_2 + r_3)^{k_j} (r_2 - r_3)^{m_j} r_{23}^{n_j} \tag{3.38}$$

where r_{23} is the inter-electron coordinate. A comparable one-electron cloud density can be calculated by integrating over either one of the electron coordinates, in this case $\boldsymbol{r}_3$

$$|\Phi_{\mathrm{VR}}(r_2)|^2 = \int |\Phi_{\mathrm{VR}}(r_2, r_3)|^2 d\boldsymbol{r}_3. \tag{3.39}$$

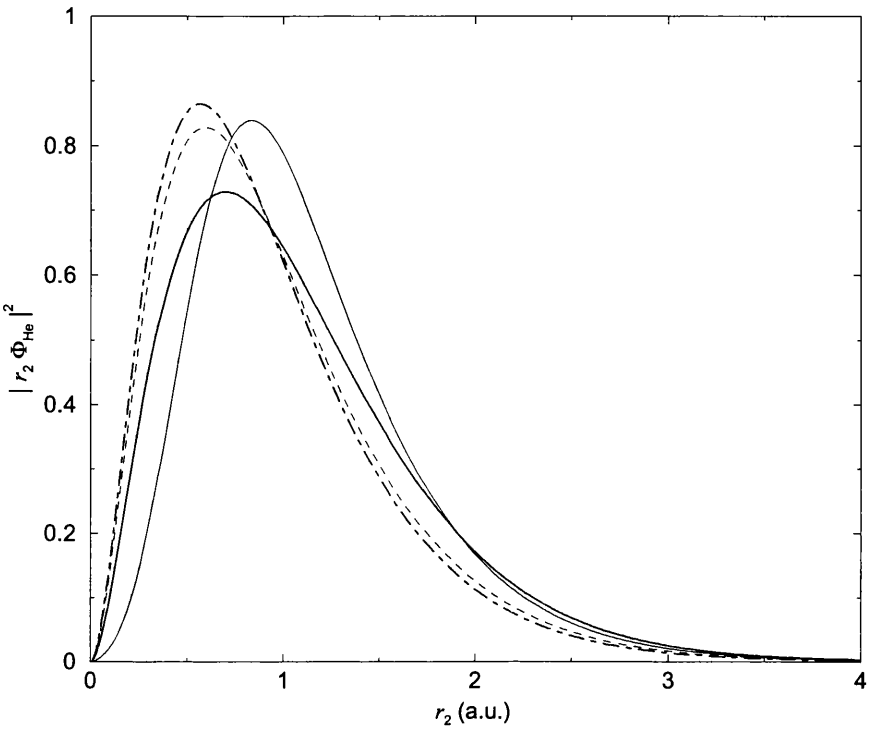

Figure 3.8: Variation of the electron density with electron-core coordinate r_2 for the *ab initio* work of Van Reeth and Humberston (see text and equation 3.39) and the three models, using 10 terms in the trial function (see equation 3.27 with β=2.0) and calculating the coefficients from equation (3.29). Thick line, V_1^-; thin line, V_2^-; dashed line, V_3^-; chain curve, Van Reeth and Humberston (see equation 3.39).

3.6 Positron-Core and Electron-Core Potentials

The full potential function for the positron-target system, $V(\boldsymbol{r}_1, \boldsymbol{r}_2)$, is the sum of the three interparticle potentials. The electron-helium ion core potential, $V^-(r_2)$, has been discussed above (see equation 3.4). The positron-core potential, $V^+(r_1)$, is taken to be the exact hydrogenic static interaction between the positron and the helium ion, which is the negative of that calculated for the electron-helium ion (see equation 3.3) with a dipole polarizability term added,

$$V^+(r_1) = \frac{1}{r_1} + \left(\frac{1}{r1} + 2\right) e^{-4r_1} - \frac{\alpha_d}{2r_1^4}\omega_2(\beta r_1)\,. \tag{3.40}$$

It is not valid to create a positron-core potential simply by taking the negative of the electron-core potential, i.e. $V^+(r_1) = -V_1^-(r_1)$, because V_1^- the dipole polarizability

terms are attractive in each and also the electron-core potential includes electron exchange contributions which are absent from the positron-core interaction.

Since the polarization potentials are attractive, independent of the sign of the charge of the particle, an additional 'three-body' potential term, V_θ, must be included in the overall interaction potential to account for a reduced polarizing effect on the core when the two leptons are close to one another, and an increased effect when the leptons are on opposite sides of the helium ion. This three-body term is of the form

$$V_\theta\left(r_1, r_2, \theta_{12}\right) = \frac{\alpha_d}{r_1^2 r_2^2} \cos\theta_{12}\, \chi_2\left(\beta_3 r_1\right) \chi_2\left(\beta_3 r_2\right). \tag{3.41}$$

Including the electron-positron Coulomb attraction,

$$V_{e^-e^+}(r_{12}) = -\frac{1}{r_{12}}, \tag{3.42}$$

the total interaction potential in the positron-target system is

$$V(\boldsymbol{r}_1, \boldsymbol{r}_2) = V^-(r_2) + V^+(r_1) + V_{e^-e^+}(r_{12}) + V_\theta\left(r_1, r_2, \theta_{12}\right). \tag{3.43}$$

The positron-atom scattering calculations will depend on the total interaction potential and not just the electron-core model potentials, hence from now on the three complete model potentials will be labelled V_1, V_2 and V_3.

Chapter 4

Positron-Helium Scattering

4.1 Introduction

This chapter deals with how the methods described in Chapter 2 were applied to positron-helium scattering and how the results were obtained. There are details to consider, such as the numerical integration techniques used and the analytical forms of the Hamiltonian operating on the scattering wave functions. We also consider the extension to higher partial waves.

4.2 Calculating the S-Wave Matrix Elements

4.2.1 Integration Techniques

In order to calculate the various matrix elements that arise in equations (2.46) and (2.79), the six dimensional integration needs to be reduced to integration over three interparticle coordinates and three external angles. The full six dimensional volume element including external coordinates is

$$d\tau_1 d\tau_2 = d\boldsymbol{r}_1 d\boldsymbol{r}_2 \tag{4.1}$$

$$= r_1^2 dr_1 \sin\theta_1 d\theta_1 d\phi_1 r_2^2 dr_2 \sin\theta_2 d\theta_2 d\phi_2, \tag{4.2}$$

which, when integrated over the external Euler angles, becomes

$$d\tau = 8\pi^2 r_1 dr_1 r_2 dr_2 r_{12} dr_{12}, \tag{4.3}$$

or

$$d\tau = 8\pi^2 r_1^2 dr_1 r_2^2 dr_2 \sin\theta_{12} d\theta_{12}, \tag{4.4}$$

using the nomenclature of figure 3.1. Certain terms in the $(\phi_i, L\phi_j)$ matrix elements, for example, take the form

$$\int_0^\infty \int_0^\infty \int_{|r_1-r_2|}^{r_1+r_2} e^{-2(\alpha r_1+\beta r_2+\gamma r_{12})} P_n(r_1, r_2, r_{12})\, r_1 dr_1 r_2 dr_2 r_{12} dr_{12}, \tag{4.5}$$

where P_n is a polynomial of finite degree n in r_1, r_2, r_{12}. The r_{12} integral is complicated as is stands, so *perimetric* coordinates are used, defined by

$$x = r_1 + r_2 - r_{12}, \qquad y = r_2 + r_{12} - r_1, \qquad z = r_{12} + r_1 - r_2, \tag{4.6}$$

the integral (4.5) then becoming

$$\int_0^\infty \int_0^\infty \int_0^\infty e^{-(Ax+By+Cz)} Q_n(x, y, z)\, dxdydz. \tag{4.7}$$

This integral can be readily computed using the Gauss-Laguerre procedure described in the Section 3.4.3,

$$\int_0^\infty e^{-\alpha x} F(x) dx \approx \frac{1}{\alpha} \sum_{i=1}^{M} w_i F\left(\frac{x_i}{\alpha}\right). \tag{4.8}$$

4.2.2 Scattering Wave Function

Since the single channel matrix elements in equation (2.46) are included in the two-channel formulation (see equation 2.79), we will consider a derivation of the forms of the two channel matrix elements. The full form of the two-channel wave function is

$$\Psi_1^t = S_1 + K_{11}^t C_1 + K_{21}^t C_2 + \sum_{i=1}^{N} c_i \phi_i, \tag{4.9}$$

$$\Psi_2^t = S_2 + K_{22}^t C_2 + K_{12}^t C_1 + \sum_{j=1}^{N} d_j \phi_j, \tag{4.10}$$

where

$$S_1 = Y_{0,0}(\theta,\phi)\sqrt{k}\, j_0(kr_1)\Phi_{\mathrm{He}}(\boldsymbol{r}_2) \tag{4.11}$$

$$C_1 = -Y_{0,0}(\theta,\phi)\sqrt{k}\, n_0(kr_1) f_1 \Phi_{\mathrm{He}}(\boldsymbol{r}_2) \tag{4.12}$$

$$S_2 = Y_{0,0}(\theta,\phi)\sqrt{2\kappa}\, j_0(\kappa\rho)\Phi_{\mathrm{Ps}}(\boldsymbol{r}_{12}) \tag{4.13}$$

$$C_2 = -Y_{0,0}(\theta,\phi)\sqrt{2\kappa}\, n_0(\kappa\rho) f_2 \Phi_{\mathrm{Ps}}(\boldsymbol{r}_{12}) \tag{4.14}$$

$$\phi_i = Y_{0,0}(\theta,\phi) e^{-(\alpha r_1+\beta r_2+\gamma r_{12})}\, r_1^{k_i}\, r_2^{l_i}\, r_{12}^{m_i} \tag{4.15}$$

where f_1 and f_2 are functions which shield the singularities in the Neumann functions as $r_1 \to 0$ and $\rho \to 0$, and

$$Y_{0,0}(\theta,\phi) = \frac{1}{\sqrt{4\pi}}. \tag{4.16}$$

These shielding functions have to ensure that the following boundary conditions are satisfied,

$$\Psi \underset{r_1\to 0}{\sim} r_1^l, \tag{4.17}$$

$$\Psi \underset{\rho\to 0}{\sim} \rho^l, \tag{4.18}$$

so a suitable choice of f_1 is

$$f_1 = 1 - e^{-\lambda r_1}. \tag{4.19}$$

The function f_2 also has to take into account that as $\rho \to 0$ there is no particle at $\rho = 0$. Considering the situation in positron-hydrogen scattering when $\rho \to 0$, then $r_1 \to r_2$ so in this limit, the total interaction potential reduces to

$$V = -\frac{1}{r_{12}} \tag{4.20}$$

with no $1/\rho$ singularity in the potential function at $\rho = 0$ as there is in the r_1 coordinate. The Schrödinger equation (equation 2.54) provides us with the condition that, in the limit as $\rho \to 0$

$$\nabla_\rho^2 C_2 = -\kappa^2 C_2 \tag{4.21}$$

and so the choice of f_2 is limited by

$$C_2 \underset{\rho\to 0}{\propto} \rho^l \tag{4.22}$$

and

$$\nabla_\rho^2 C_2 \underset{\rho \to 0}{\propto} \rho^l. \tag{4.23}$$

A suitable form of f_2 for s-wave scattering is

$$f_2 = 1 - e^{-\mu\rho}\left(1 + \frac{\mu\rho}{2}\right). \tag{4.24}$$

4.2.3 Matrix Symmetry

The total Hamiltonian,

$$\begin{aligned} H_T &= -\frac{1}{2}\boldsymbol{\nabla}_{\boldsymbol{r}_1}^2 - \frac{1}{2}\boldsymbol{\nabla}_{\boldsymbol{r}_2}^2 + V^-(r_2) + V^+(r_1) + V^{e^-e^+}(r_{12}) + V_\theta\left(r_1, r_2, \theta_{12}\right) && (4.25)\\ &= -\frac{1}{4}\boldsymbol{\nabla}_{\boldsymbol{\rho}}^2 - \boldsymbol{\nabla}_{\boldsymbol{r}_{12}}^2 + V^-(r_2) + V^+(r_1) + V^{e^-e^+}(r_{12}) + V_\theta\left(r_1, r_2, \theta_{12}\right), && (4.26) \end{aligned}$$

produces a symmetric square matrix in equation (2.79) and so it is not necessary to calculate all the elements explicitly. The following symmetry rules can be exploited,

$$(S_1, LS_2) = (S_2, LS_1) \tag{4.27}$$

$$(C_1, LS_2) = (S_2, LC_1) \tag{4.28}$$

$$(S_1, LC_2) = (C_2, LS_1) \tag{4.29}$$

$$(C_1, LC_2) = (C_2, LC_1) \tag{4.30}$$

$$(S_1, LC_1) = (C_1, LS_1) + 1 \tag{4.31}$$

$$(S_2, LC_2) = (C_2, LS_2) + 1 \tag{4.32}$$

$$(\phi_i, LS_1) = (S_1, L\phi_i) \tag{4.33}$$

$$(\phi_i, LC_1) = (C_1, L\phi_i) \tag{4.34}$$

$$(\phi_i, LS_2) = (S_2, L\phi_i) \tag{4.35}$$

$$(\phi_i, LC_2) = (C_2, L\phi_i) \tag{4.36}$$

$$(\phi_i, L\phi_j) = (\phi_j, L\phi_i) \tag{4.37}$$

which can all be proved by applying Green's theorem with the appropriate boundary conditions at infinity.

4.2.4 Long-range Terms

Although not all of the terms in the matrices $\boldsymbol{SLS}$, $\boldsymbol{SLC}$, $\boldsymbol{CLS}$ and $\boldsymbol{CLC}$ have explicit exponential fall-offs in all three coordinates, these terms can nevertheless be evaluated using the Gauss-Laguerre procedure with perimetric coordinates by introducing an exponential fall-off in the appropriate coordinate which must then be compensated for by multiplying by the corresponding positive exponential factor. Thus, in comparison with equation (3.37),

$$\int_0^\infty F(x)dx = \int_0^\infty e^{-\alpha x}F(x)e^{+\alpha x}dx \approx \frac{1}{\alpha}\sum_{i=1}^{M} w_i F\left(\frac{x_i}{\alpha}\right)e^{+\alpha x}. \tag{4.38}$$

If the value of α is chosen appropriately, and the function $F(x)$ is finite everywhere and decreases faster than $1/x$, as we have here, this approximation still provides sufficiently accurate results. For example, this technique is used when calculating part of the (S_1, LS_1) term which contains no exponential term explicitly (see equation 4.46),

$$2k\int_0^\infty j_0^2(kr_1)\left(-\frac{\alpha_d\omega_2}{2r_1^4}\right)r_1^2\,dr_1. \tag{4.39}$$

In deriving the analytic forms of the integrands which include the ∇^2 operator, some explicit terms cancel, since the spherical harmonics and the Bessel and Neumann functions are eigenfunctions of the ∇^2 operator. Using the full radial and angular parts of ∇^2,

$$\nabla^2 Y_{l,0}(\theta)\, j_l(kr) = -k^2 Y_{l,0}(\theta)\, j_l(kr) \tag{4.40}$$

$$\nabla^2 Y_{l,0}(\theta)\, n_l(kr) = -k^2 Y_{l,0}(\theta)\, n_l(kr). \tag{4.41}$$

The calculations can be further simplified by reducing some three-dimensional integrations to one-dimensional integration. This reduces the computational time needed for the single-channel elastic scattering calculations. The (S_1, LS_1), (C_1, LS_1), (S_1, LC_1) and (C_1, LC_1) matrix elements can all be reduced by making use of the fact the the target wave function

created from the model potential is a very good approximation to an eigenfunction of the target Hamiltonian. Furthermore,

$$\int_0^\infty \Phi_{\rm He}\left(\nabla_{r_2}^2 + 2V^- - 2E_0\right)\Phi_{\rm He}\, r_2^2\, dr_2 \;=\; 0, \tag{4.42}$$

even for an inexact wave function for the model potential, since equation (4.42) is satisfied because E_0 is the expectation value of the model Hamiltonian, i. e.

$$E_0 = \frac{\langle \Phi_{\rm He}\,|H|\,\Phi_{\rm He}\rangle}{\langle \Phi_{\rm He}\,|\,\Phi_{\rm He}\rangle} \tag{4.43}$$

and $\Phi_{\rm He}$ is normalized so that

$$4\pi \int_0^\infty |\Phi_{\rm He}|^2\, r_2^2\, dr_2 \;=\; 1. \tag{4.44}$$

The (S_1, LS_1) matrix element, for example, can be reduced by substituting from equation (4.40), and the remaining terms in (S_1, LS_1) are

$$(Y_{0,0})^2\, k\, 8\pi^2 \int_0^\infty \int_0^\infty \int_0^\pi |\Phi_{\rm He}|^2\, j_0^2\, (2V^+ + 2V^\pm)\, r_1^2\, dr_1\, r_2^2\, dr_2\, \sin\theta_{12}\, d\theta_{12}. \tag{4.45}$$

Then, using equation (4.44),

$$\begin{aligned}(S_1, LS_1) &= 2k \int_0^\infty j_0^2(kr_1)\left(e^{-4r_1}\left(\frac{1}{r_1}+2\right) - \frac{\alpha_d \omega_2}{2r_1^4}\right) r_1^2\, dr_1 \\ &+ 4\pi k \int_0^\infty \int_0^\infty \int_0^\pi |\Phi_{\rm He}(r_2)|^2\, j_0^2(kr_1)\left(\frac{1}{r_1} - \frac{1}{r_{12}}\right) r_1^2\, dr_1\, r_2^2\, dr_2\, \sin\theta_{12}\, d\theta_{12}.\end{aligned} \tag{4.46}$$

The first term can be readily calculated using the Gauss-Laguerre procedure and equation (4.38). The second term can be reduced by exploiting the relationships relating to the Legendre polynomials, $P_l(\cos\theta)$,

$$\frac{1}{|\boldsymbol{r}_1 - \boldsymbol{r}_2|} = \frac{1}{r_{12}} = \frac{1}{r_>} \sum_{l=0}^{\infty} \left(\frac{r_<}{r_>}\right)^l P_l(\cos\theta), \tag{4.47}$$

$$\int_0^\pi P_l\, P_{l'} \sin\theta\, d\theta = \frac{2}{2l+1}\,\delta_{l\,l'}, \tag{4.48}$$

where $r_<$ and $r_>$ are the lesser or greater values, respectively, of r_1 and r_2. The second term in equation (4.46) becomes

$$\begin{aligned}8\pi k \Bigg[&\int_0^\infty \int_0^{r_1} j_0^2(kr_1)\,|\Phi_{\rm He}(r_2)|^2 \left(\frac{1}{r_1} - \frac{1}{r_1}\right) r_1^2\, dr_1\, r_2^2\, dr_2 \\ &+ \int_0^\infty \int_{r_1}^\infty j_0^2(kr_1)\,|\Phi_{\rm He}(r_2)|^2 \left(\frac{1}{r_1} - \frac{1}{r_2}\right) r_1^2\, dr_1\, r_2^2\, dr_2\Bigg]\end{aligned} \tag{4.49}$$

$$= 8\pi k \int_0^\infty j_0^2(kr_1) \left[\int_{r_1}^\infty |\Phi_{\rm He}(r_2)|^2 \, r_2^2 \, dr_2 - r_1 \int_{r_1}^\infty |\Phi_{\rm He}(r_2)|^2 \, r_2 \, dr_2 \right] r_1 \, dr_1. \qquad (4.50)$$

Since $\Phi_{\rm He}(r_2)$ is a product of an exponential term and a polynomial in r_2, this term can be reduced to an integral involving r_1 by using the relation

$$\int_{r_1}^\infty e^{-\alpha r_2} \, r_2^n \, dr_2 \; = \; e^{-\alpha r_1} \sum_{k=0}^{n} \frac{n!}{k!} \frac{r_1^k}{\alpha^{n-k+1}}, \qquad (4.51)$$

so equation (4.46) is reduced entirely to a one-dimensional integral. A similar method can analytically reduce the other remaining single-channel long-range - long-range terms to one-dimensional integrals.

The long-range - long-range matrix elements relating solely to the two-channel case need three dimensional integration since the terms are too complicated to reduce analytically. However the eigenvalue relations in equations (4.40) and (4.42) can still be used to simplify these matrix elements.

The calculation of the long-range - short-range matrix elements (e. g. $(S_1, L\phi_j)$, $(C_1, L\phi_j)$, etc.) makes use of the symmetry relations in equations (4.33) - (4.36). Only the matrix elements on the left hand side of equations (4.33) - (4.36) need to be evaluated.

4.2.5 Short-range - Short-range Matrix Elements

The matrix elements $(\phi_i, L\phi_j)$ are evaluated by first using Green's theorem, so the full matrix element is

$$\begin{aligned} (\phi_i, L\phi_j) &= \int_{\boldsymbol{r}_1, \boldsymbol{r}_2} \phi_i \left(-\nabla^2_{\boldsymbol{r}_1} - \nabla^2_{\boldsymbol{r}_2} + 2V(\boldsymbol{r}_1, \boldsymbol{r}_2) - k^2 - 2E_0 \right) \phi_j \, d\boldsymbol{r}_1 \, d\boldsymbol{r}_2 \qquad (4.52) \\ &= \int_{\boldsymbol{r}_1, \boldsymbol{r}_2} [\boldsymbol{\nabla}_1 \phi_i \cdot \boldsymbol{\nabla}_1 \phi_j + \boldsymbol{\nabla}_2 \phi_i \cdot \boldsymbol{\nabla}_2 \phi_j \\ &\quad + \phi_i \phi_j \left(2V(\boldsymbol{r}_1, \boldsymbol{r}_2) - k^2 - 2E_0 \right)] \, d\boldsymbol{r}_1 \, d\boldsymbol{r}_2. \qquad (4.53) \end{aligned}$$

Noting that $\boldsymbol{\nabla}$ is a vector operator, which in polar coordinates is

$$\boldsymbol{\nabla}_i = \hat{\boldsymbol{r}}_i \frac{\partial}{\partial r_i} + \hat{\boldsymbol{\theta}}_i \frac{1}{r_i} \frac{\partial}{\partial \theta_i} + \hat{\boldsymbol{\phi}}_i \frac{1}{r_i \sin\theta_i} \frac{\partial}{\partial \phi_i}, \qquad i = 1, 2 \qquad (4.54)$$

where $\hat{\boldsymbol{r}}_i$, $\hat{\boldsymbol{\theta}}_i$ and $\hat{\boldsymbol{\phi}}_i$ are the radial, polar angle and azimuthal angle unit vectors respectively, and

$$r_{12}^2 = r_1^2 + r_2^2 - 2 r_1 r_2 \cos\theta_{12}, \qquad (4.55)$$

then

$$\begin{aligned}\boldsymbol{\nabla}_1\phi_i\cdot\boldsymbol{\nabla}_1\phi_j+\boldsymbol{\nabla}_2\phi_i\cdot\boldsymbol{\nabla}_2\phi_j &= \Big\{\Big(-\alpha+\tfrac{k_i}{r_1}\Big)\Big[\Big(-\alpha+\tfrac{k_j}{r_1}\Big)+\cos\theta_{1,12}\Big(-\gamma+\tfrac{m_j}{r_{12}}\Big)\Big]\\ &\quad+\Big(-\beta+\tfrac{l_i}{r_2}\Big)\Big[\Big(-\beta+\tfrac{l_j}{r_2}\Big)+\cos\theta_{2,12}\Big(-\gamma+\tfrac{m_j}{r_{12}}\Big)\Big]\\ &\quad+\Big(-\gamma+\tfrac{m_i}{r_{12}}\Big)\Big[2\Big(-\gamma+\tfrac{m_j}{r_{12}}\Big)+\cos\theta_{1,12}\Big(-\alpha+\tfrac{k_j}{r_1}\Big)\\ &\quad+\cos\theta_{2,12}\Big(-\beta+\tfrac{l_j}{r_2}\Big)\Big]\Big\}\phi_i\phi_j, \qquad (4.56)\\ &= C_{ij}\phi_i\phi_j, \qquad (4.57)\end{aligned}$$

where $\theta_{1,12}$ and $\theta_{2,12}$ are the internal angles between r_1 and r_{12}, and r_2 and r_{12} respectively.

4.3 Convergence and Optimizing Non-linear Parameters

The wave function in the single channel case has four non-linear parameters, α, β, γ and λ, which need to be optimized. Theoretically all four parameters should be varied for each incident positron energy, and for a particular number of terms in the short-range part of the wave function. The values which give the most positive value of the phase shift, η, are chosen, whilst neglecting those that correspond to Schwartz singularities. Figures 4.1-4.3 show the phase shifts in two dimensional parameter space. The choice of parameter should usually be the one which provides the most positive η, however, figure 4.2 shows a singularity at $\gamma \sim 0.7$, $\lambda \sim 0.02$ in the complex Kohn calculations. Although a singularity in the complex Kohn is highly unlikely, the choices of parameters also need to fit the physics of the problem since the lower bound on η is not rigorous. For example, below E_{th} the positron cannot bind with the electron to form positronium so the exponent associated with the r_{12} coordinate should be smaller than that for positronium, $\phi_{\text{Ps}} \propto \exp(-0.5r_{12})$, since the correlation between the two leptons is quite extended. Consequently $\gamma \sim 0.7$ is too high to be considered a realistic choice of parameter. Similarly, choosing $\lambda \sim 0.02$ would shield the Neumann function in the scattering wave function for too large values of r_1, so this is also not a suitable choice of parameter. Looking at the parameter space within reasonable limits shows a less dramatic maximum in the phase shift (see figure 4.3). However, the convergence of the phase shift with respect to increasing the number

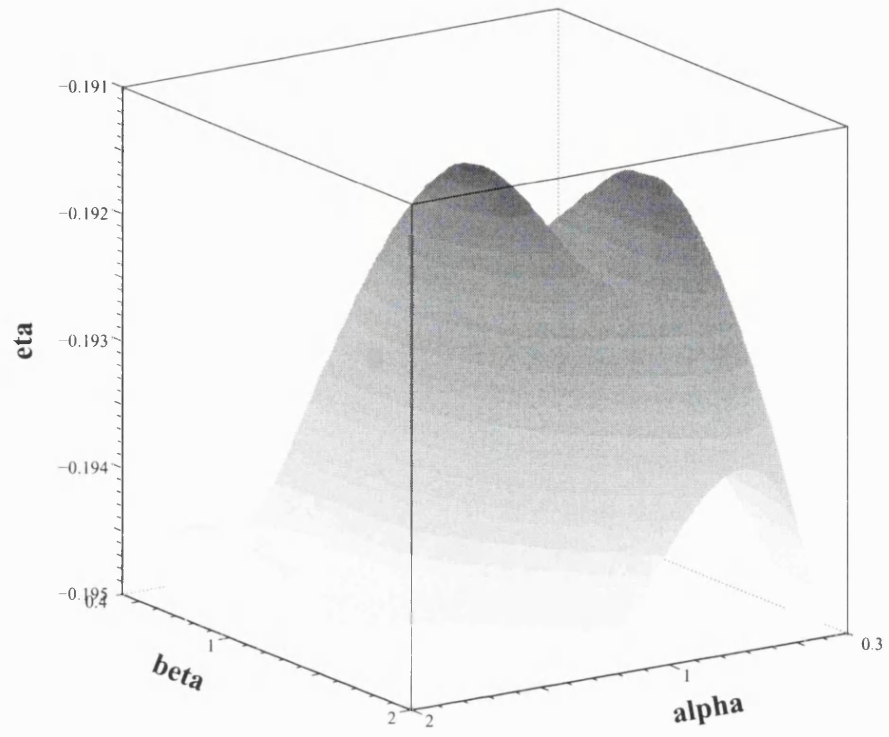

Figure 4.1: Variation of the s-wave phase shift, η, with respect to variations in the choice of non-linear parameters α and β with fixed $\gamma = 0.3$, $\lambda = 1.0$ and $k = 1.0$ with $\omega = 4$. Notice there are two peaks in the phase shift corresponding to optimal choices of α and β.

of short-range terms is generally good enough for one set of non-linear parameters to be chosen for all energies.

The optimization of the two channel scattering calculations is complicated, not only by an extra parameter, μ, but also because the two channel Kohn method provides empirical lower bounds on K_{11}^v *and* K_{22}^v. One set of non-linear parameters may be an optimal set for one of the diagonal $\boldsymbol{K}$ matrix elements but not necessarily, and usually not, for both.

Because of the empirical lower bound on K_{11}^v and K_{22}^v, the calculated values converge on to the exact ones as the non-linear parameters are optimized, and also as the number of short-range terms in the wave function, expressed in terms of the parameter ω in equation (2.45), is increased. It is most likely that above a small number of short-range terms in the wave function, any subsequent terms will make increasingly smaller corrections to the calculated variational $\boldsymbol{K}$-matrix element.

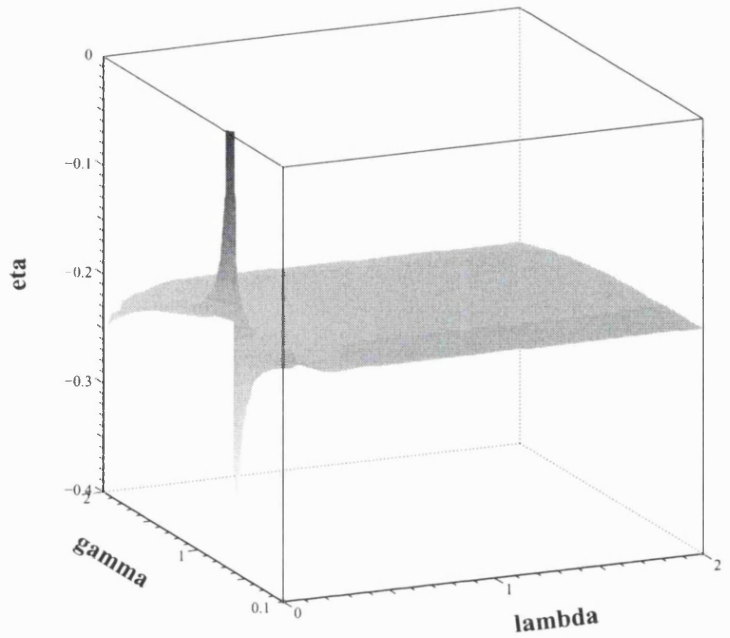

Figure 4.2: Variation of the s-wave phase shift, η, with respect to variations in the choice of non-linear parameters γ and λ with fixed $\alpha = 0.6$, $\beta = 1.2$ and $k = 1.0$ with $\omega = 4$. The singularity in parameter space exists in the complex Kohn method, however, at choices of γ and λ which seem unphysical.

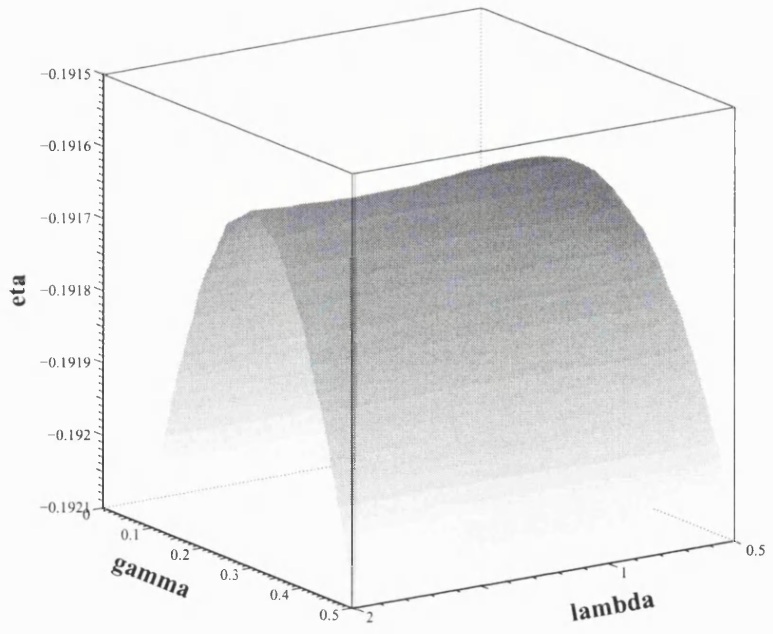

Figure 4.3: Variation of the s-wave phase shift, η, with respect to variations in the choice of non-linear parameters γ and λ. Same as figure 4.2 but a smaller region of parameter space is chosen. Notice the peak in the phase shift is almost independent of λ.

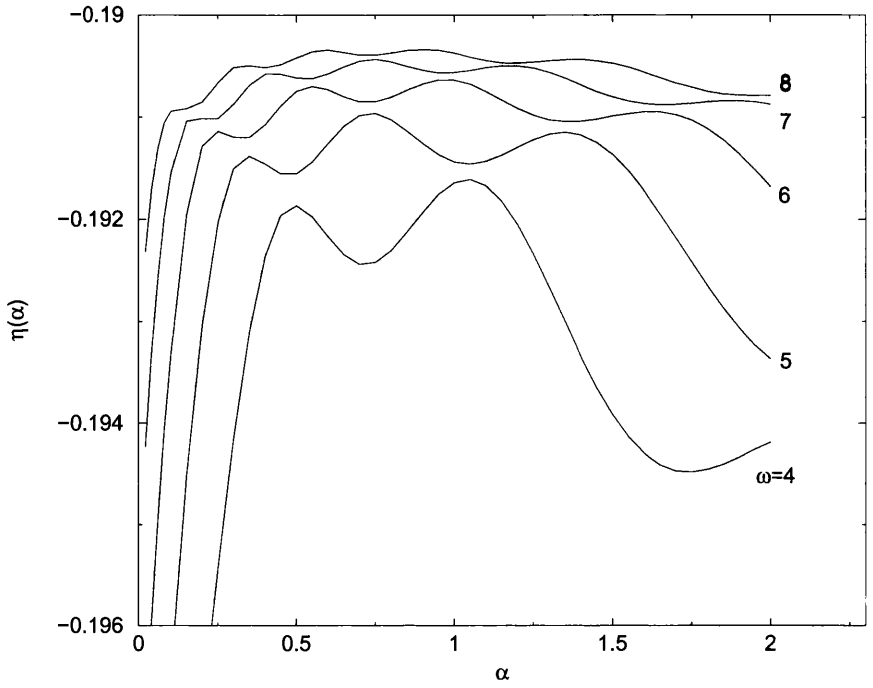

Figure 4.4: Variation of the s-wave phase shift, η, with respect to α and ω, with fixed $\beta = 1.2$, $\gamma = 0.3$, $\lambda = 1.0$ and $k = 1.0\ a_0^{-1}$. Notice, the $\omega = 4$ curve has the same double peak structure shown in figure 4.1. As ω is increased the number of peaks increases but it flattens out over parameter space.

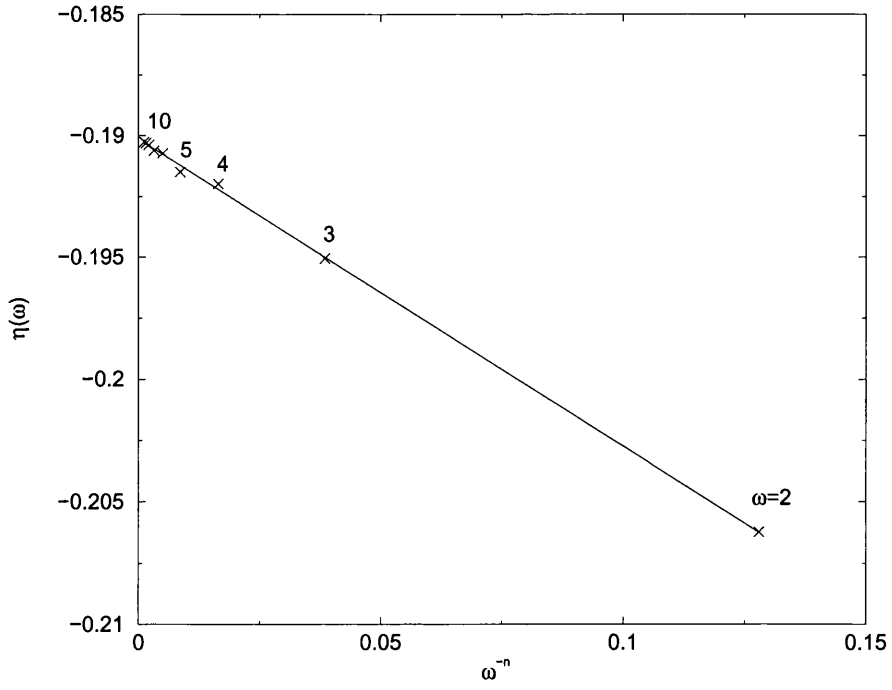

Figure 4.5: Convergence of the s-wave phase shifts for increasing ω at $k = 1.0\ a_0^{-1}$. The straight line is the line of best fit when $n = 2.97$.

A useful, empirical method of finding the value on to which the results with higher values of ω converge is to plot the variational values of the phase shift η (or K_{11}^v or K_{22}^v) for different values of ω, against $1/\omega^n$. A fit to the curve has the form

$$K_{ii}^v(\omega) = K_{ii}^v(\omega = \infty) + \frac{A}{\omega^n}, \tag{4.58}$$

or

$$\eta^v(\omega) = \eta^v(\omega = \infty) + \frac{B}{\omega^n}, \tag{4.59}$$

where A and B a parameters to be determined by fitting to a straight line. The parameter n can be found using curve fitting algorithms as that value which gives the best straight line fit to the values of $\eta(\omega)$, and the intercept of this line with the $1/\omega^n = 0$ axis corresponds to $\eta(\omega = \infty)$, the fully converged phase shift (see figure 4.5).

In these investigations we are not creating results for a previously uninvestigated system, but we are comparing the results obtained in this work with the previous accurate data of Van Reeth and Humberston (1999). The variations between the three models vary more than any subtle optimization or convergence calculations, so the above methods need only be used to check the accuracy of the calculations rather than rigorously to extract the exact data from these models.

4.4 Results - S-Wave

The s-wave elastic scattering phase shifts are shown in figure 4.6. These results are for $\omega = 8$ for each of the three models. Figure 4.5 shows the convergence of the phase shifts with respect to ω. The line of best fit through the points provides an approximation to the converged value of $\eta(\omega = \infty)$. The error in the intercept is about $5{\times}10^{-5}$. Table 4.1 shows how well these results are converged for model V_1 at $k = 1.0\ a_0^{-1}$, and similar convergence patterns exist for the other two models. The value of $\eta(\omega = 8)$ only differs from $\eta(\infty)$ by a factor of 0.1%.

The s-wave elastic phase shifts for model V_1 show excellent agreement with the results of Van Reeth and Humberston (1999), except for a a slight anomaly at $k = 1.13\ a_0^{-1}$

Table 4.1: Convergence of the s-wave phase shifts for model V_1 with respect to the number of terms in the trial wave function at $k = 1.0\ a_0^{-1}$. The value of $\eta(\infty)$ is taken from the intercept in figure 4.5.

$\omega(N)$	$\eta(\omega)$
2(10)	-0.20623
3(20)	-0.19504
4(35)	-0.19197
5(56)	-0.19150
6(84)	-0.19072
7(120)	-0.19061
8(165)	-0.19038
9(220)	-0.19030
10(286)	-0.19026
$\omega = \infty$	-0.19018

as can be seen in figure 4.6. This is discussed in greater detail in Chapter 6. All the models show a similar energy dependence to that of the accurate data. and contain the important feature of passing through $\eta = 0$ as the attractive dipole polarizability becomes less dominant at higher positron energies.

The resonant feature in the s-wave phase shift for model V_1 is not a Schwartz singularity, because the feature appears in all three variants of the Kohn method. The precise nature of this resonant feature is discussed in full in Chapter 6, but we shall see that it will affect the cross sections for the higher partial waves above and below the positronium formation. Models V_2 and V_3 do not reveal a similar resonant structure but the phase

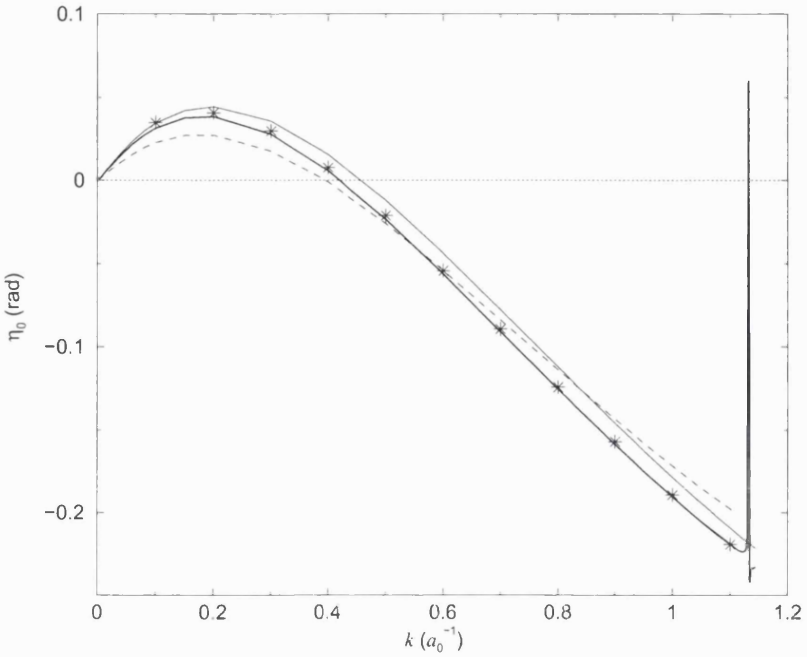

Figure 4.6: The variation of the s-wave elastic scattering phase shift with respect to the positron wavenumber, k for $\omega = 8$. Thick line, V_1; thin line, V_2; dashed line, V_3; $*$, accurate results of Van Reeth and Humberston (1999). Note: the results are only plotted up to the positronium threshold, $k_{\rm th}$, for each model.

shifts, although following a similar energy dependence, do not fit the accurate *ab initio* data as well as do those of model V_1.

4.4.1 Virtual Positronium

When the incident positron energy is close to, but less than, the positronium formation threshold, positronium cannot be formed but the positron and electron become *highly correlated* as if positronium was trying to be formed, but cannot quite succeed. This structure has been called *virtual positronium*, as it does not relate to an open channel of positronium formation.

The work of Humberston *et al* (1997) used this picture to explain a feature in the single-channel s-wave elastic scattering cross section very close to $E_{\rm th}$. The single-channel elastic scattering cross section, $\sigma_{\rm el}$, falls very slightly to match the two-channel elastic scattering cross section at the $E_{\rm th}$ boundary.

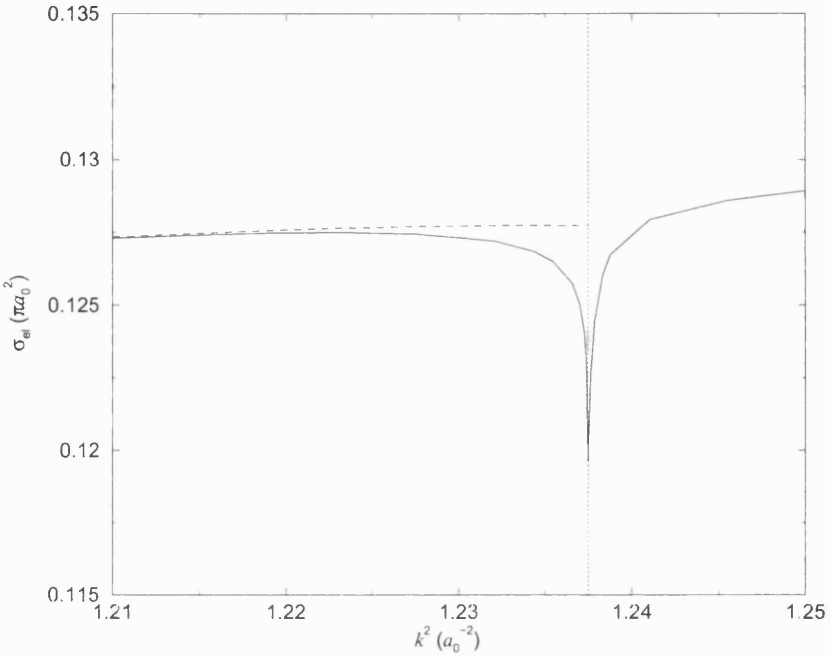

Figure 4.7: The variation of the s-wave elastic scattering cross section with respect to k^2 for model V_3 and $\omega = 8$. The dotted line parallel to the ordinate marks the positronium formation threshold, $E_{\rm th}$; solid line below $E_{\rm th}$, single channel elastic scattering cross section, with $\phi_{\rm vps}$ term included; solid line above $E_{\rm th}$, two channel $\sigma_{\rm el}$; dashed line, single channel $\sigma_{\rm el}$ without $\phi_{\rm vps}$ term included.

In the work of Humberston *et al* (1997), an extra term, $\phi_{\rm vps}$, was added to the trial wave function to provide an explicit representation of virtual positronium. For s-wave scattering this is of the form

$$\phi_{\rm vps} = c_0 Y_{0,0}(\boldsymbol{\rho}) \phi_{\rm Ps}(r_{12}) \frac{e^{-\kappa\rho}}{\rho} \left(1 - e^{-\delta\rho}\right)^3, \tag{4.60}$$

where c_0 is the associated linear parameter and κ is the wavenumber of positronium for the equivalent incident energy above $E_{\rm th}$, i.e.

$$\kappa = \sqrt{4\left|E_0 - E_{\rm Ps} + \frac{k^2}{2}\right|}. \tag{4.61}$$

As an example of the effect of including this term, figure 4.7 shows the improvement in the s-wave $\sigma_{\rm el}$ above and below $E_{\rm th}$, in model V_3, as the elastic cross section below $E_{\rm th}$ matches that above when the $\phi_{\rm vps}$ term is included. A similar feature was noted in the *ab initio* work of Van Reeth and Humberston (1999) and (1998) both for positron-

helium and positron-hydrogen scattering. This term produces a very narrow feature in the elastic scattering cross-section but it is important very close to the positronium formation threshold. We will also see its importance in calculating the positron-electron annihilation rate in Chapter 5, and its effect on the resonance supported by model V_1, in Chapter 6

4.4.2 Two Channel S-Wave Scattering Results

The two-channel scattering cross section results shown in figures 4.8-4.12 do not reveal such good agreement between any of the three models and the accurate results of Van Reeth and Humberston (1999). As with the single channel elastic scattering phase shifts, the results which are shown are well converged, and they are plotted against positronium wavenumber κ so that the different positronium formation thresholds for the different models all correspond to $\kappa = 0$. Also, the results are only plotted as far as the first excitation threshold for each model, beyond which the excitation of the target needs to be taken into account, which is a three-channel scattering problem.

The results for models V_2 and V_3 follow the energy dependence of the accurate *ab initio* results of Van Reeth and Humberston (1999) satisfactorily, with only very slight differences in magnitudes as may be seen in figures 4.8 and 4.9. The threshold features in the elastic and positronium formation cross sections ($\sigma_{\rm el}$ and $\sigma_{\rm Ps}$ respectively) are well represented. The sharp rise in $\sigma_{\rm Ps}$ for all three models is apparent at $\kappa = 0$, followed by the abrupt change of slope. The rise is a consequence of Wigner's threshold theory (Wigner 1948) which predicts that, for the $l^{\rm th}$ partial wave, $K_{12} \propto \kappa^{l+1/2}$ as can be seen in figure 4.10. Since, at low energies $\sigma_{\rm Ps} \propto \mid K_{12} \mid^2 /k^2$, then $\sigma_{\rm Ps} \propto \kappa^{2l+1}/k^2$. As $\kappa \rightarrow 0$, k tends to a finite constant and then $\sigma_{\rm Ps} \rightarrow 0$ as $\kappa \rightarrow 0$. However, the slope of $\sigma_{\rm Ps}$ is infinite at $\kappa = 0$ as can be established by the following derivation:

$$\frac{d\sigma_{\rm Ps}}{d\kappa} = (2l+1)\frac{\kappa^{2l}}{k^2}, \tag{4.62}$$

and

$$\frac{d\sigma_{\rm Ps}}{dk} = \frac{d\sigma_{\rm Ps}}{d\kappa}\frac{d\kappa}{dk}, \tag{4.63}$$

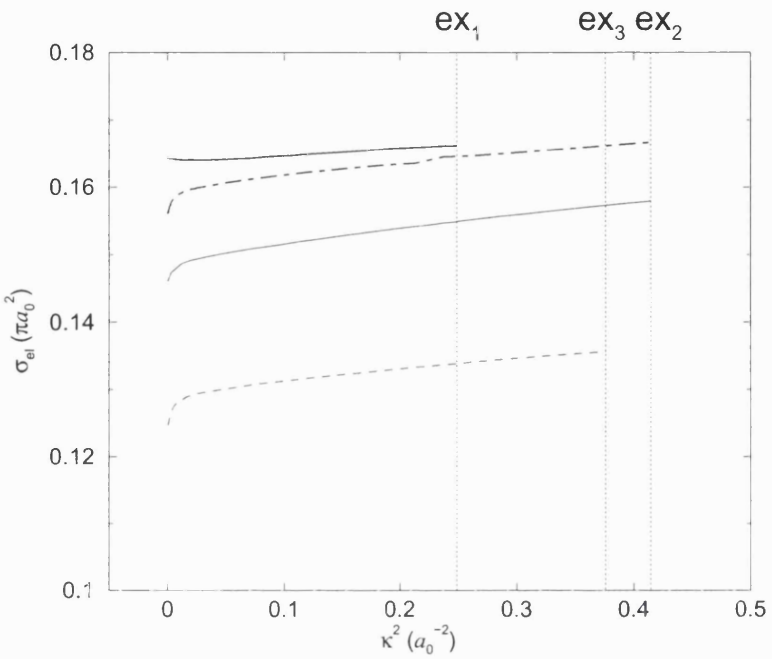

Figure 4.8: The variation of the s-wave elastic scattering cross section with respect to κ^2 for $\omega = 8$. Thick line, V_1; thin line, V_2; dashed line, V_3; chain curve, accurate results of Van Reeth and Humberston (1999). Note: the results are only plotted up to the excitation threshold, ex, for each model.

since

$$E_0 + \frac{k^2}{2} = \frac{\kappa^2}{4} - E_{\mathrm{Ps}}, \tag{4.64}$$

then

$$\frac{d\kappa}{dk} \propto \frac{k}{\kappa} \tag{4.65}$$

and therefore

$$\frac{d\sigma_{\mathrm{Ps}}}{dk} \propto \frac{\kappa^{2l-1}}{k}. \tag{4.66}$$

For s-wave scattering ($l = 0$) and when $\kappa = 0$, k is finite and non-zero, $\frac{d\sigma_{\mathrm{Ps}}}{dk} \propto 1/\kappa$ so the slope is infinite at the threshold.

This feature was noted both in the positronium formation cross section for positron-helium and positron-hydrogen scattering in the *ab initio* work of Van Reeth and Humberston (1998).

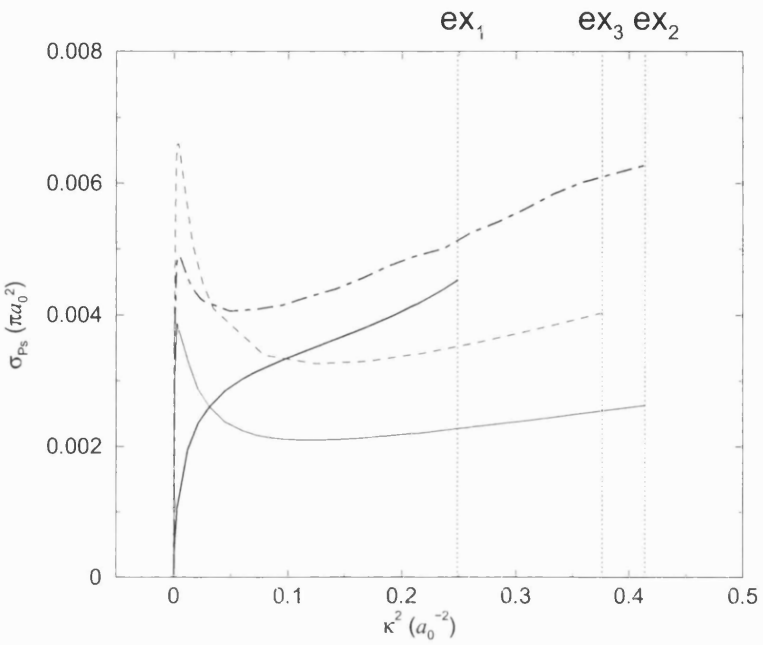

Figure 4.9: The variation of the s-wave positronium formation cross section with respect to κ^2 for $\omega = 8$. See caption to figure 4.8 for legend.

Model V_1 does not reproduce these features in such detail, despite quantitatively being very good; in fact $\sigma_{\rm el}$ seems to have a slight fall at the threshold. The lack of the threshold features in this model is believed to be caused by the resonance feature below $E_{\rm th}$.

The $\boldsymbol{K}$ matrix elements plotted in figures 4.10 to 4.12 show the similarity between the results for models V_2 and V_3 despite the difference in the potentials and the properties of the model atoms. In the expression for the full trial scattering wave function in equation (4.10), K_{22} plays a somewhat similar role to the tangent of the phase shift in the single channel scattering wave function, but is associated with the elastic scattering of positronium by a helium ion target. Figure 4.12 shows how K_{22} has a similar energy dependence to the elastic scattering phase shift below the threshold. However for model V_1 there is another resonance feature above the positronium formation threshold at $\kappa \approx 0.2\ a_0^{-1}$.

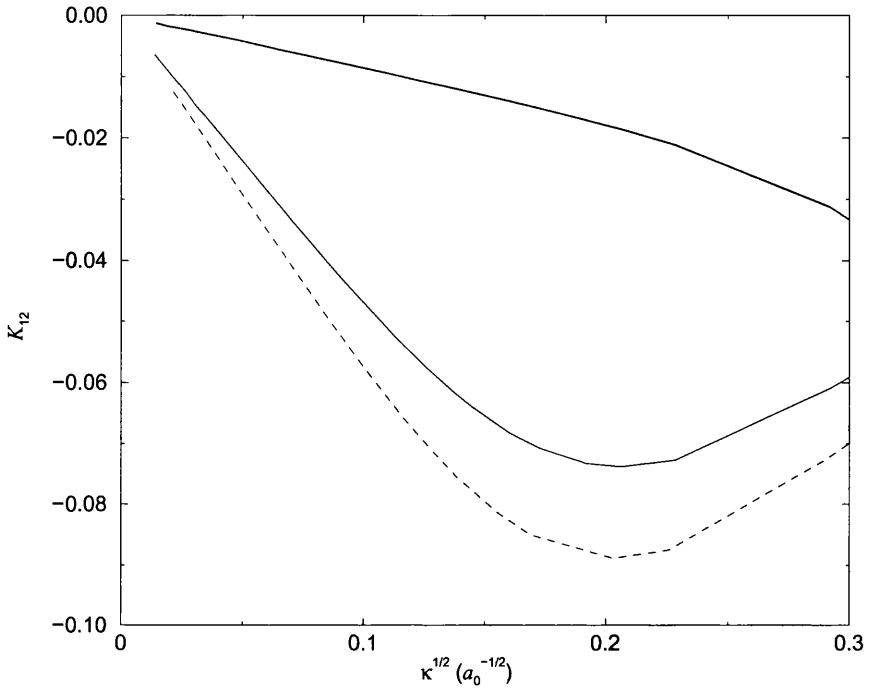

Figure 4.10: The variation of the s-wave K_{12} matrix element with respect to $\kappa^{1/2}$ for $\omega = 8$. See caption to figure 4.8 for legend.

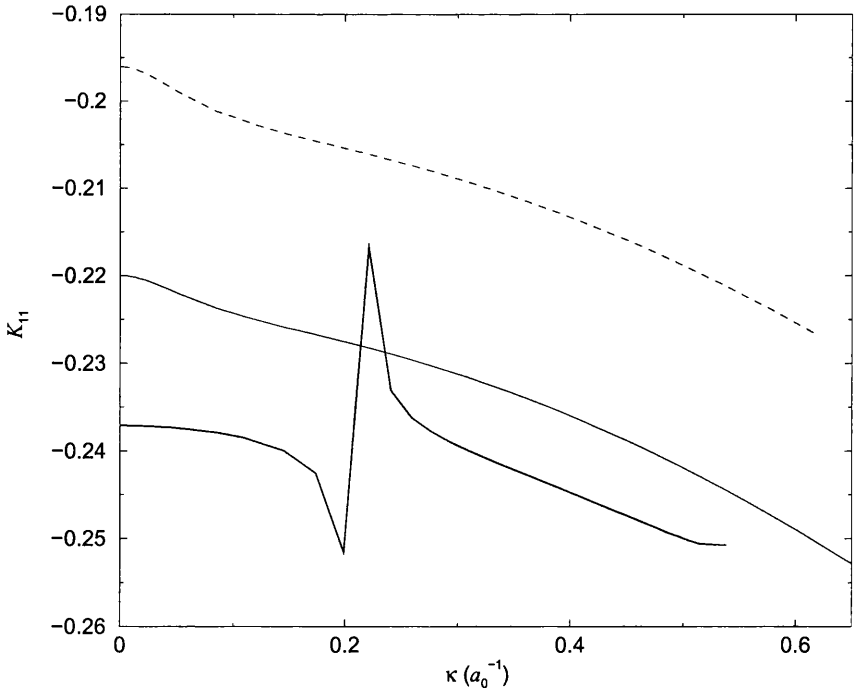

Figure 4.11: The variation of the s-wave K_{11} matrix element with respect to κ for $\omega = 8$. See caption to figure 4.8 for legend.

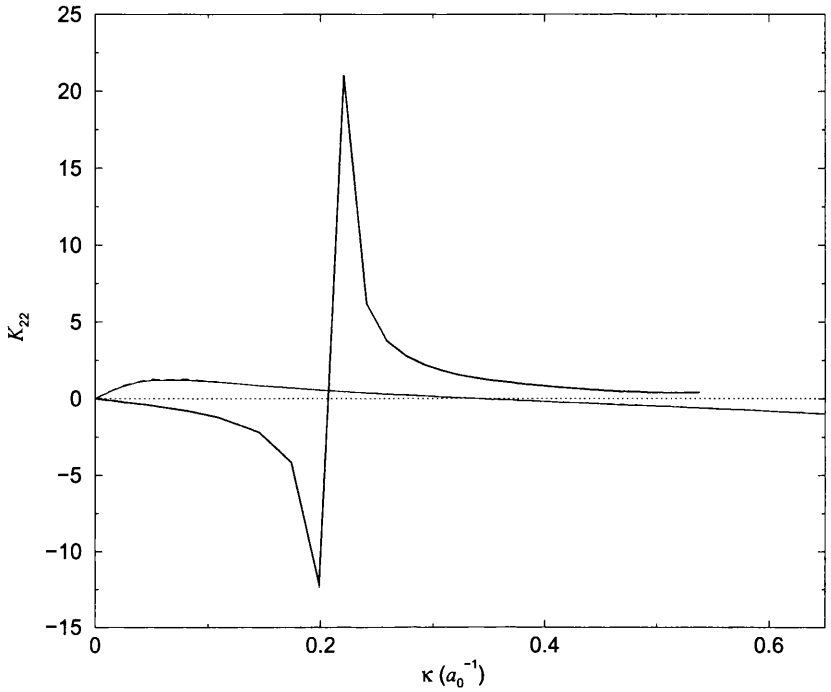

Figure 4.12: The variation of the s-wave K_{22} matrix element with respect to κ for $\omega = 8$. See caption to figure 4.8 for legend. Note that the results for models V_2 and V_3 are very similar to each other on the scale used.

4.5 Higher Partial Waves

In order to calculate the scattering parameters for higher partial waves, changes need to be made to the scattering wave function. Since, at low energies, the positron cannot impart a change of angular momentum to the target atom, the long-range parts of the wave function representing the incoming positron and outgoing positron or positronium must have all the spherical harmonics, Bessel and Neumann functions, and the appropriate shielding functions, appropriate to the same angular momentum, l. The short-range parts need to represent all the necessary couplings of the angular momentum of the positron with the electron, where the angular momentum is shared between the two particles at close range, although overall the total angular momentum must also be l.

There are, in theory, an infinite number of combinations of positron and electron angular momenta which result in a total angular momentum l, but Schwartz (1961b) showed that the number of terms needed to represent this coupled state can be significantly

reduced by introducing the vector-coupled state $\psi(l_1, l_2; l, m)$, where

$$\psi(l_1, m_1, l_2, m_2; l, m) = \sum_{m_1, m_2} Y_{l_1 m_1}(\theta_1, \phi_1) Y_{l_2 m_2}(\theta_2, \phi_2) \langle l_1, m_1, l_2, m_2 \mid l, m \rangle. \quad (4.67)$$

The terms $\langle l_1, m_1, l_2, m_2 \mid l, m \rangle$ are the Clebsch-Gordon coefficients, and the sum is constrained by

$$m_1 + m_2 = m, \quad (4.68)$$

and

$$\mid m_i \mid \leq l_i, \qquad i = 1, 2. \quad (4.69)$$

The eigenstate of *total* angular momentum, $\Psi(\boldsymbol{r}_1, \boldsymbol{r}_2, l, m)$, is expressed as an expansion in ψ, so that

$$\Psi(\boldsymbol{r}_1, \boldsymbol{r}_2, l, m) = \sum_{l_1, l_2} \psi(l_1, l_2; l, m) F_{l_1, l_2}(r_1, r_2, r_{12}), \quad (4.70)$$

where F_{l_1, l_2} represents the short-range spherically symmetric terms in r_1, r_2 and r_{12}, each corresponding to a combination of l_1 and l_2 called a *symmetry*. This summation can be restricted so that

$$l_1 + l_2 = l, \quad (4.71)$$

and

$$\mid l_1 - l_2 \mid \leq l. \quad (4.72)$$

For each value of l there are $l + 1$ symmetries of a given parity. The short-range terms must also satisfy the boundary conditions

$$\Psi(\boldsymbol{r}_1, \boldsymbol{r}_2, l, m) \underset{r_1 \to 0}{\sim} r_1^l, \quad (4.73)$$

$$\Psi(\boldsymbol{r}_1, \boldsymbol{r}_2, l, m) \underset{r_2 \to 0}{\sim} r_2^l. \quad (4.74)$$

4.5.1 P-Wave Wave Function and Matrix Elements

For p-wave scattering, $l = l_1 + l_2 = 1$ and exploiting the axial symmetry so that we can take $m = 0$, we have the vector-coupled states $\psi(l_1, m_1, l_2, m_2)$

$$\psi(1, 0, 0, 0) = Y_{1,0}(\theta_1, \phi_1) Y_{0,0}(\theta_2, \phi_2) \langle 1, 0, 0, 0 \mid 1, 0 \rangle, \quad (4.75)$$

$$\psi(0, 0, 1, 0) = Y_{0,0}(\theta_1, \phi_1) Y_{1,0}(\theta_2, \phi_2) \langle 0, 0, 1, 0 \mid 1, 0 \rangle. \quad (4.76)$$

The two components of the two-channel p-wave scattering wave function therefore have the forms

$$\begin{aligned}\Psi_1^t = Y_{1,0}(\theta_1)\sqrt{k}\,\left[j_1(kr_1) - K_{11}^t\, n_1(kr_1) f_1^3\right]\Phi_{\rm He}(\boldsymbol{r}_2) \\ + K_{21}^t\, Y_{1,0}(\theta_\rho)\sqrt{2\kappa}\, n_1(\kappa\rho) f_2^5 \Phi_{\rm Ps}(\boldsymbol{r}_{12}) \\ + Y_{1,0}(\theta_1) r_1 \sum_{i=1}^{N} c_i\,\phi_i + Y_{1,0}(\theta_2) r_2 \sum_{i=1}^{M} c_i'\,\phi_i,\end{aligned} \tag{4.77}$$

$$\begin{aligned}\Psi_2^t = Y_{1,0}(\theta_\rho)\sqrt{2\kappa}\,\left[j_1(\kappa\rho) - K_{22}^t\, n_1(\kappa\rho) f_2^5\right]\Phi_{\rm Ps}(\boldsymbol{r}_{12}) \\ + K_{12}^t\, Y_{1,0}(\theta_1)\sqrt{k}\, n_1(kr_1) f_1^3 \Phi_{\rm He}(\boldsymbol{r}_2) \\ + Y_{1,0}(\theta_1) r_1 \sum_{j=1}^{N} d_j\,\phi_j + Y_{1,0}(\theta_2) r_2 \sum_{j=1}^{M} d_j'\,\phi_j,\end{aligned} \tag{4.78}$$

where

$$\phi_i = e^{-(\alpha r_1 + \beta r_2 + \gamma r_{12})}\, r_1^{k_i}\, r_2^{l_i}\, r_{12}^{m_i}, \tag{4.79}$$

and the Clebsch-Gordon coefficients have been absorbed into the linear coefficients. The shielding functions f_1 and f_2 given in equations (4.19) and (4.24) are raised to the power 3 and 5, respectively.

The matrix elements are calculated as for s-wave scattering, but the new matrix elements are ordered by the following notation,

$$\Psi_1^t = S_1 + K_{11}^t\, C_1 + K_{21}^t\, C_2 + Y_{1,0}(\theta_1) r_1 \sum_{i=1}^{N} c_i\,\phi_i + Y_{1,0}(\theta_2) r_2 \sum_{i=1}^{M} c_i'\,\phi_i, \tag{4.80}$$

$$\Psi_2^t = S_2 + K_{22}^t\, C_2 + K_{12}^t\, C_1 + Y_{1,0}(\theta_1) r_1 \sum_{i=1}^{N} d_i\,\phi_i + Y_{1,0}(\theta_2) r_2 \sum_{i=1}^{M} d_i'\,\phi_i, \tag{4.81}$$

where

$$S_1 = Y_{1,0}(\theta_1)\sqrt{k}\, j_1(kr_1)\Phi_{\rm He}(\boldsymbol{r}_2) \tag{4.82}$$

$$C_1 = -Y_{1,0}(\theta_1)\sqrt{k}\, n_1(kr_1) f_1^3 \Phi_{\rm He}(\boldsymbol{r}_2) \tag{4.83}$$

$$S_2 = Y_{1,0}(\theta_\rho)\sqrt{2\kappa}\, j_1(\kappa\rho)\Phi_{\rm Ps}(\boldsymbol{r}_{12}) \tag{4.84}$$

$$C_2 = -Y_{1,0}(\theta_\rho)\sqrt{2\kappa}\, n_1(\kappa\rho) f_2^5 \Phi_{\rm Ps}(\boldsymbol{r}_{12}) \tag{4.85}$$

The p-wave spherical harmonic is

$$Y_{1,0}(\theta) = \sqrt{\frac{3}{4\pi}}\cos\theta, \tag{4.86}$$

and the first order Bessel and Neumann functions are

$$j_1(kr) = \frac{\sin kr}{(kr)^2} - \frac{\cos kr}{kr}, \tag{4.87}$$

$$n_1(kr) = -\frac{\cos kr}{(kr)^2} - \frac{\sin kr}{kr}. \tag{4.88}$$

The analytical calculations are complicated by the powers of the shielding functions associated with the Neumann functions and the angular part of the wave function, which is a function of the external angles. The integration of the products of p-wave spherical harmonics over the external angles are,

$$\int_{\tau_{\text{ext}}} Y_{1,0}(\theta_1)\, Y_{1,0}(\theta_2)\, d\tau_{\text{ext}} = 2\pi \cos\theta_{12}, \tag{4.89}$$

$$\int_{\tau_{\text{ext}}} Y_{1,0}(\theta_1)\, Y_{1,0}(\theta_\rho)\, d\tau_{\text{ext}} = 2\pi \left(\frac{r_1 + r_2 \cos\theta_{12}}{2\rho}\right), \tag{4.90}$$

$$\int_{\tau_{\text{ext}}} Y_{1,0}(\theta_2)\, Y_{1,0}(\theta_\rho)\, d\tau_{\text{ext}} = 2\pi \left(\frac{r_2 + r_1 \cos\theta_{12}}{2\rho}\right), \tag{4.91}$$

$$\int_{\tau_{\text{ext}}} Y_{1,0}(\theta_i)\, Y_{1,0}(\theta_i)\, d\tau_{\text{ext}} = 2\pi, \qquad i = 1, 2, 3, \tag{4.92}$$

where $\theta_3 = \theta_\rho$.

The short-range - short-range square matrix can now be split into four matrices representing the different symmetries. Let

$$F_i = Y_{1,0}(\theta_1)\, r_1\, \phi_i, \tag{4.93}$$

$$G_i = Y_{1,0}(\theta_2)\, r_2\, \phi_i, \tag{4.94}$$

$$\Phi_i = F_i, \qquad 1 \le i \le N, \tag{4.95}$$

$$\Phi_{i+N} = G_i, \qquad 1 \le i \le M, \tag{4.96}$$

so the total square matrix $\boldsymbol{\Phi L \Phi}$, the square matrix with size $(N + M)$ and elements $(\Phi_i, L\Phi_j)$, becomes

$$\boldsymbol{\Phi L \Phi} = \begin{bmatrix} \boldsymbol{FLF} & \boldsymbol{FLG} \\ \boldsymbol{GLF} & \boldsymbol{GLG} \end{bmatrix}. \tag{4.97}$$

Although the matrices $\boldsymbol{\Phi L \Phi}$, $\boldsymbol{FLF}$ and $\boldsymbol{GLG}$ are symmetric, $\boldsymbol{FLG}$ and $\boldsymbol{GLF}$ are not. The matrices $\boldsymbol{FLF}$ and $\boldsymbol{GLG}$ are similar to the $(\phi_i, L\phi_j)$ matrix elements in the s-wave

calculations, the main difference being the inclusion of the repulsive centrifugal potential barrier, $l(l+1)/r^2$. The $\mathbf{\Phi L \Phi}$ matrix elements can be expressed in terms of C_{ij} (see equation 4.57) as,

$$F_i L F_j = \left(C_{ij} + \frac{2}{r_1^2} - k^2 - 2E_0\right) F_i F_j, \tag{4.98}$$

$$G_i L G_j = \left(C_{ij} + \frac{2}{r_2^2} - k^2 - 2E_0\right) G_i G_j, \tag{4.99}$$

$$\begin{aligned} F_i L G_j &= \left\{\left(C_{ij} + \frac{2}{r_2^2} - k^2 - 2E_0\right)\cos\theta_{12}\right. \\ &\quad \left. - \left[\frac{r_1}{r_2 r_{12}}\left(-\gamma + \frac{m_i}{r_{12}}\right) + \frac{r_2}{r_1 r_{12}}\left(-\gamma + \frac{m_j}{r_{12}}\right)\right]\sin^2\theta_{12}\right\} F_i L G_j, \quad (4.100) \\ &= G_i L F_j. \quad (4.101) \end{aligned}$$

4.5.2 D-Wave Wave Function and Matrix Elements

The d-wave, $l = 2$, trial wave function has three symmetries corresponding to the combinations $\{l_1 = 2, l_2 = 0\}$, $\{l_1 = 0, l_2 = 2\}$ and $\{l_1 = 1, l_2 = 1\}$. As in the p-wave case, the z component of l can be chosen to be zero, so the first two symmetries listed here have $m_1 = m_2 = 0$. Using the same formalism as with the p-wave,

$$\psi(2,0,0,0) = Y_{2,0}(\theta_1,\phi_1) Y_{0,0}(\theta_2,\phi_2) \langle\, 2,0,0,0 \mid 2,0 \,\rangle, \tag{4.102}$$

$$\psi(0,0,2,0) = Y_{0,0}(\theta_1,\phi_1) Y_{2,0}(\theta_2,\phi_2) \langle\, 0,0,2,0 \mid 2,0 \,\rangle, \tag{4.103}$$

but the third combination, or *mixed* symmetry, is

$$\begin{aligned} \psi(1,1;2,0) &= Y_{1,-1}(\theta_1,\phi_1) Y_{1,+1}(\theta_2,\phi_2) \langle\, 1,-1,1,+1 \mid 2,0 \,\rangle \\ &+ Y_{1,0}(\theta_1,\phi_1) Y_{1,0}(\theta_2,\phi_2) \langle\, 1,0,1,0 \mid 2,0 \,\rangle \\ &+ Y_{1,+1}(\theta_1,\phi_1) Y_{1,-1}(\theta_2,\phi_2) \langle\, 1,+1,1,-1 \mid 2,0 \,\rangle. \end{aligned} \tag{4.104}$$

Using the spherical harmonics

$$Y_{2,0}(\theta,\phi) = \sqrt{\frac{5}{4\pi}}\left(\frac{3}{2}\cos^2\theta - \frac{1}{2}\right), \tag{4.105}$$

$$Y_{1,\pm 1}(\theta,\phi) = \mp\sqrt{\frac{3}{8\pi}}\sin\theta\, e^{\pm\phi}, \tag{4.106}$$

$$\tag{4.107}$$

and the Clebsch-Gordon coefficients, the mixed symmetry vector coupling is given by

$$\psi(1,1;2,0) = \frac{3}{4\pi}\frac{1}{\sqrt{6}}\left(3\cos\theta_1\cos\theta_2 - \cos\theta_{12}\right). \tag{4.108}$$

The full d-wave trial wave function is

$$\begin{aligned}\Psi_1^t = {} & Y_{2,0}(\theta_1)\sqrt{k}\left[j_2(kr_1) - K_{11}^t\, n_2(kr_1) f_1^5\right]\Phi_{\rm He}(\boldsymbol{r}_2) \\ & + K_{21}^t\, Y_{2,0}(\theta_\rho)\sqrt{2\kappa}\, n_2(\kappa\rho) f_2^7 \Phi_{\rm Ps}(\boldsymbol{r}_{12}) \\ & + Y_{2,0}(\theta_1) r_1^2 \sum_{i=1}^{N} c_i\,\phi_i + Y_{2,0}(\theta_2) r_2^2 \sum_{i=1}^{M} c_i'\,\phi_i + \psi(1,1;2,0) r_1 r_2 \sum_{i=1}^{N} c_i''\,\phi_i \end{aligned} \tag{4.109}$$

$$\begin{aligned}\Psi_2^t = {} & Y_{2,0}(\theta_\rho)\sqrt{2\kappa}\left[j_2(\kappa\rho) - K_{22}^t\, n_2(\kappa\rho) f_2^7\right]\Phi_{\rm Ps}(\boldsymbol{r}_{12}) \\ & + K_{12}^t\, Y_{2,0}(\theta_1)\sqrt{k}\, n_2(kr_1) f_1^5 \Phi_{\rm He}(\boldsymbol{r}_2) \\ & + Y_{2,0}(\theta_1) r_1^2 \sum_{j=1}^{N} d_j\,\phi_j + Y_{2,0}(\theta_2) r_2^2 \sum_{j=1}^{M} d_j'\,\phi_j + \psi(1,1;2,0) r_1 r_2 \sum_{j=1}^{M} d_j''\,\phi_j, \end{aligned} \tag{4.110}$$

where the Bessel and Neumann functions for $l = 2$ are

$$j_2(kr) = \left(\frac{3}{(kr)^3} - \frac{1}{kr}\right)\sin kr - \frac{3}{(kr)^2}\cos kr, \tag{4.111}$$

$$n_2(kr) = -\left(\frac{3}{(kr)^3} - \frac{1}{kr}\right)\cos kr - \frac{3}{(kr)^2}\sin kr, \tag{4.112}$$

As with the p-wave calculations, the matrix elements are complicated by the integration of the spherical harmonics over the external angles, and the high powers of the Neumann shielding functions. The integration of the spherical harmonics over the external angles are

$$\int_{\tau_{\rm ext}} Y_{2,0}(\theta_1)\, Y_{2,0}(\theta_2)\, d\tau_{\rm ext} = 2\pi\left(1 - \frac{3}{2}\sin^2\theta_{12}\right), \tag{4.113}$$

$$\int_{\tau_{\rm ext}} Y_{2,0}(\theta_1)\, Y_{2,0}(\theta_\rho)\, d\tau_{\rm ext} = 2\pi\left(1 - \frac{3r_2^2\sin^2\theta_{12}}{8\rho^2}\right), \tag{4.114}$$

$$\int_{\tau_{\rm ext}} Y_{2,0}(\theta_2)\, Y_{2,0}(\theta_\rho)\, d\tau_{\rm ext} = 2\pi\left(1 - \frac{3r_1^2\sin^2\theta_{12}}{8\rho^2}\right), \tag{4.115}$$

$$\int_{\tau_{\rm ext}} Y_{2,0}(\theta_1)\, \psi(1,1;2,0)\, d\tau_{\rm ext} = 2\pi\sqrt{\frac{9}{5\pi}}\cos\theta_{12}, \tag{4.116}$$

$$\int_{\tau_{\rm ext}} Y_{2,0}(\theta_2)\, \psi(1,1;2,0)\, d\tau_{\rm ext} = 2\pi\sqrt{\frac{9}{5\pi}}\cos\theta_{12}, \tag{4.117}$$

$$\int_{\tau_{\rm ext}} Y_{2,0}(\theta_i)\, Y_{2,0}(\theta_i)\, d\tau_{\rm ext} = 2\pi, \qquad i = 1,2,3, \tag{4.118}$$

where $\theta_3 = \theta_\rho$.

4.5.3 F-Wave and the Born Approximation

As the angular momentum is increased the centrifugal barrier term becomes more and more important in keeping the positron away from the core of the target atom, so the short-range terms become less and less important. This is useful in determining the contribution of higher partial waves to the total scattering cross sections. In the single channel case, s-wave scattering is the dominant contribution at low energies, and higher partial waves are successively less important as a proportion of the total elastic scattering cross-section. As the projectile energy is increased, however, the higher partial wave contributions become more important.

The f-wave contribution is calculated in a similar way to the p- and d-wave contributions, with the appropriate spherical harmonics, Bessel, Neumann and shielding functions, except that the vector coupling terms in the short-range part of the wave function have not been calculated in full. There should be four symmetries, representing $(l_1 = 3, l_2 = 0)$, $(l_1 = 2, l_2 = 1)$, $(l_1 = 1, l_2 = 2)$ and $(l_1 = 0, l_2 = 3)$. The second and third are mixed symmetries, but the external integration and the Hamiltonian operations on these would be rather difficult compared with the increase in accuracy gained by their inclusion. So only the first and fourth symmetries are included, and the trial wave function looks like this;

$$\begin{aligned}\Psi_1^t = Y_{3,0}(\theta_1)\sqrt{k}\,\left[j_3(kr_1) - K_{11}^t\, n_3(kr_1) f_1^7\right]\Phi_{\mathrm{He}}(\boldsymbol{r}_2) \\ + K_{21}^t\, Y_{3,0}(\theta_\rho)\sqrt{2\kappa}\, n_3(\kappa\rho) f_2^9 \Phi_{\mathrm{Ps}}(\boldsymbol{r}_{12}) \\ + Y_{3,0}(\theta_1) r_1^3 \sum_{i=1}^{N} c_i\,\phi_i + Y_{3,0}(\theta_2) r_2^3 \sum_{i=1}^{M} c_i'\,\phi_i,\end{aligned} \tag{4.119}$$

$$\begin{aligned}\Psi_2^t = Y_{3,0}(\theta_\rho)\sqrt{2\kappa}\,\left[j_3(\kappa\rho) - K_{22}^t\, n_3(\kappa\rho) f_2^9\right]\Phi_{\mathrm{Ps}}(\boldsymbol{r}_{12}) \\ + K_{12}^t\, Y_{3,0}(\theta_1)\sqrt{k}\, n_3(kr_1) f_1^7 \Phi_{\mathrm{He}}(\boldsymbol{r}_2) \\ + Y_{3,0}(\theta_1) r_1^3 \sum_{j=1}^{N} d_j\,\phi_j + Y_{3,0}(\theta_2) r_2^3 \sum_{j=1}^{M} d_j'\,\phi_j,\end{aligned} \tag{4.120}$$

where the $l = 3$ Bessel and Neumann functions are

$$j_3(kr) = \left(\frac{15}{(kr)^4} - \frac{6}{(kr)^2}\right)\sin kr - \left(\frac{15}{(kr)^3} - \frac{1}{kr}\right)\cos kr, \tag{4.121}$$

$$n_3(kr) = -\left(\frac{15}{(kr)^4} - \frac{6}{(kr)^2}\right)\cos kr - \left(\frac{15}{(kr)^3} - \frac{1}{kr}\right)\sin kr, \tag{4.122}$$

and the spherical harmonic is,

$$Y_{3,0}(\theta) = \sqrt{\frac{7}{4\pi}}\left(\frac{5}{2}\cos^3\theta - \frac{3}{2}\cos\theta\right). \tag{4.123}$$

In order to calculate the $l > 3$ partial wave contributions to the cross sections, the Born approximation can be used. This assumes that the incident particle does not distort the target atom, and the positron wave function is a plane wave. Thus, the trial wave function in the Born approximation has no variational parameters, and the partial wave elastic scattering cross section is

$$\sigma_{\rm el}^B(l) = \frac{4\pi(2l+1)}{k^2} \mid (S_1, LS_1) \mid^2. \tag{4.124}$$

This approximation is rather poor even for higher partial waves but there is an analogous approximation for the positronium formation cross-section for the $l > 3$ partial wave contributions,

$$\sigma_{\rm Ps}^B(l) = \frac{4\pi(2l+1)}{k^2} \mid (S_1, LS_2) \mid^2. \tag{4.125}$$

A slightly more accurate approximation within the spirit of the Born approximation, which includes the coupling between the two open channels, uses the full two-channel cross section formula given in equation 2.68, but with the full $\boldsymbol{K}$ matrix is replaced by the $\boldsymbol{SLS}$ matrix so that,

$$\sigma_{pq} = \frac{4\pi(2l+1)}{k_p^2}\left|\left(\frac{\boldsymbol{SLS}}{\mathbf{1} - i\boldsymbol{SLS}}\right)_{pq}\right|^2, \tag{4.126}$$

The accuracy of these procedures can be measured by comparing the results of the Born approximations with those of the complete s-, p-, d- and f-wave calculations. As l increases, $\sigma_{\rm Ps}^B(l)$ should become a much better approximation to $\sigma_{\rm Ps}(l)$.

4.6 Results - P-Wave and Higher Partial Waves

The single channel elastic scattering phase shifts for the p-, d- and f-partial wave contributions can be seen in figures 4.13-4.15. As with the s-wave contribution, the results yielded by the three models are qualitatively good, and again, model V_1 agrees excellently with the accurate results of Van Reeth and Humberston (1999) except near the positronium formation threshold where the resonant feature again affects the results. One noticeable effect of the higher partial waves is that the resonance becomes broader and occurs at higher energies. This is consistent with the introduction of the centrifugal barrier for the higher partial waves which restricts the interaction of the positron close to the atom. For $l > 1$ partial waves the resonance does not actually occur below E_{th}, and the small rise just below is not obviously part of a resonance unless the behaviour above is noted. Although the phase shifts are calculated for single-channel scattering, the results above the threshold clearly define the presence of the resonance.

As $k \rightarrow 0$, $\eta \rightarrow 0$ for all three models. The behaviours at low energies closely follows O'Malley's formula (from O'Malley *et al* 1962) relating the dipole polarizability of the atoms to the low energy phase shift,

$$\eta_l = \frac{\pi \alpha_{\text{He}} k^2}{(2l-1)(2l+1)(2l+3)} + \mathcal{O}(k^3). \tag{4.127}$$

Figures 4.13-4.15 clearly show the low energy phase shifts following the O'Malley formula, which remains accurate over a larger energy range for progressively higher partial waves. The results for model V_3 appear not to fit the formula so well, but this is because the dipole polarizability for this model is significantly different from the other two. The V_3 results are consistent with the formula if the dipole polarizability for V_3 is substituted into equation (4.127).

The elastic scattering and positronium formation cross sections for the higher partial waves are shown in figures 4.16-4.20. The first noticeable feature in both cross sections for p-wave scattering is the enormous resonant feature and the steep rise in σ_{el} and σ_{Ps} at the threshold for model V_1. This occurs because figure 4.13 shows the resonance sitting right

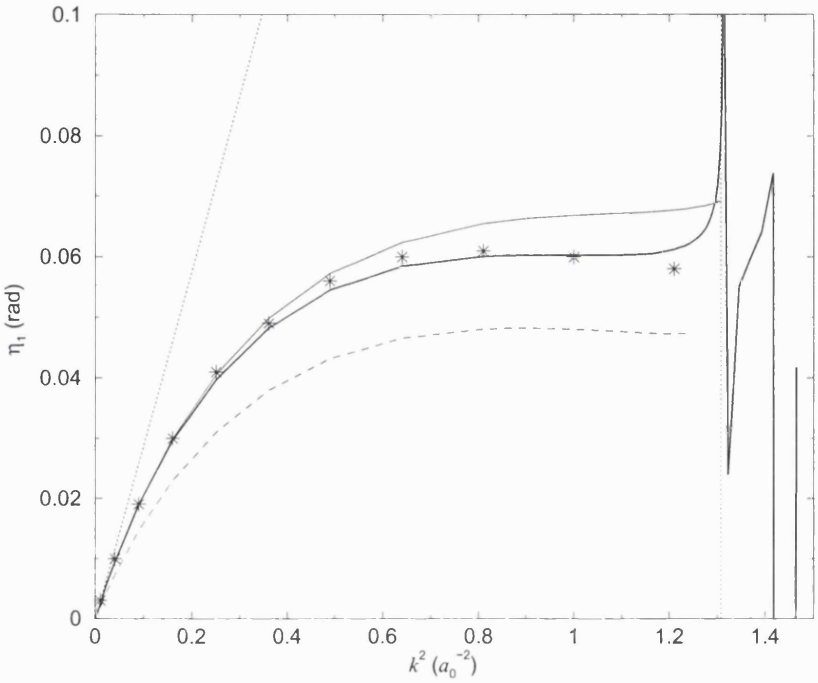

Figure 4.13: The variation of the p-wave elastic scattering phase shift with respect to k^2 for $\omega = 8$. Thick line, V_1; thin line, V_2; dashed line, V_3; $*$, accurate results of Van Reeth and Humberston (1999); dotted line parallel to the ordinate, marks $k_{\rm th}$; dotted curve, line fit to O'Malley formula (see equation 4.127). Note: the results are only plotted up to $k_{\rm th}$ for models V_2 and V_3.

at the threshold itself. In the d-wave cross section for model V_1 the cross section is still greatly affected by the resonance but at higher energies, and the effect of the resonance is significantly broader for the higher partial waves. F-wave contributions to the cross sections have not been calculated above the threshold for these three models because the matrix elements become very large and manipulation of the matrices becomes more susceptible to errors. This is especially noticeable in model V_1 where the effect of the resonance is expected to be broad enough to span a significant fraction of the range of the Ore gap.

Models V_2 and V_3 show excellent energy dependence for both the elastic scattering and positronium formation cross sections for all the higher partial waves. Figure 4.20 shows the sum of the partial wave positronium formation cross sections and there is a good agreement between the results for these two models and the accurate results of Van

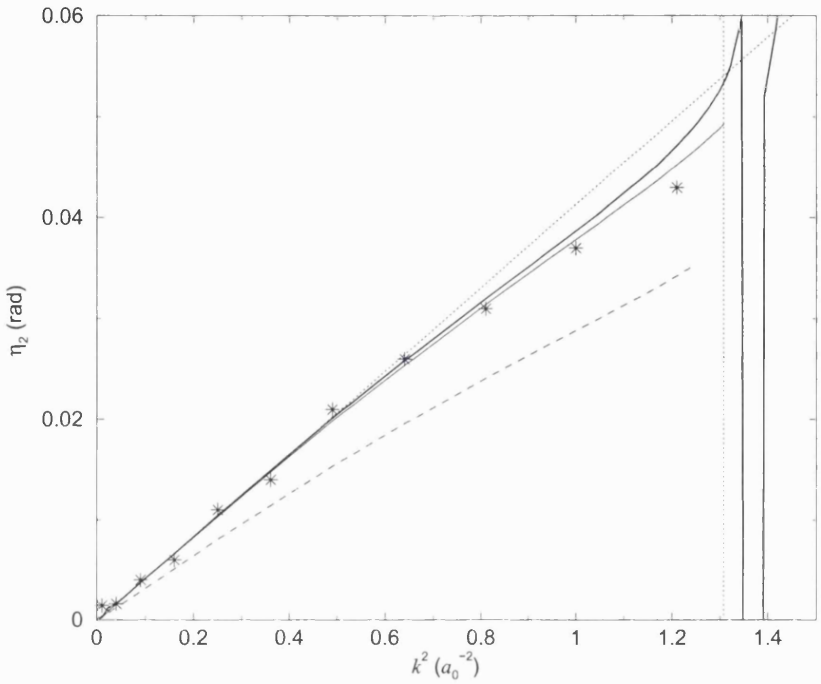

Figure 4.14: The variation of the d-wave elastic scattering phase shift with respect to k^2 for $\omega = 8$. See caption to figure 4.13 for legend.

Reeth and Humberston (1999).

Although we have only included s-, p- and d-wave contributions in the sum of the partial wave positronium formation cross sections, higher partial waves are believed to contribute a relatively small fraction of the sum (see Van Reeth and Humberston 1999) compared with the discrepancies between the different models. The model which fits best is, perhaps surprisingly, model V_3 which is comparatively crude and yields rather poor values of the ground state energy, the energy of the first excited state and the polarizability compared to the other two models. Despite its success in recreating the results for σ_{Ps} it cannot do the same for σ_{el} above or below the threshold, with the added difficulty of recreating the threshold at the wrong energy.

Not one of the three models reproduces the accurate cross section results of the *ab initio* calculation of Van Reeth and Humberston (1999) but all three do have elements of success. The results from this chapter are discussed in more detail in Chapter 7.

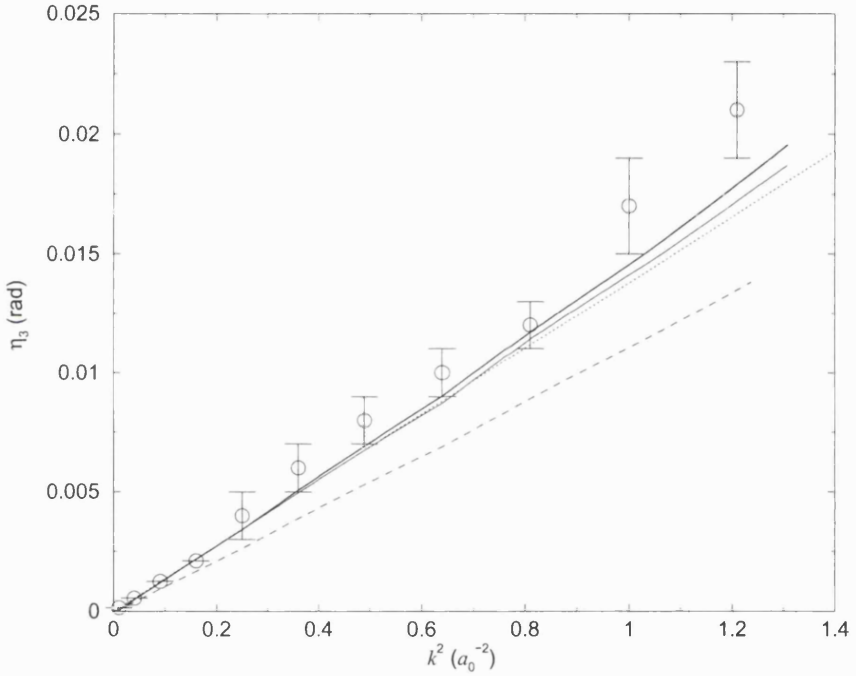

Figure 4.15: The variation of the f-wave elastic scattering phase shift with respect to k^2 for $\omega = 8$. Thick line, V_1; thin line, V_2; dashed line, V_3; $\circ$, accurate results of Van Reeth and Humberston (1999) including estimated errors; dotted curve, line fit to O'Malley formula (see equation 4.127). Note: the results are only plotted up to the positronium formation threshold, k_{th}, for models V_2 and V_3.

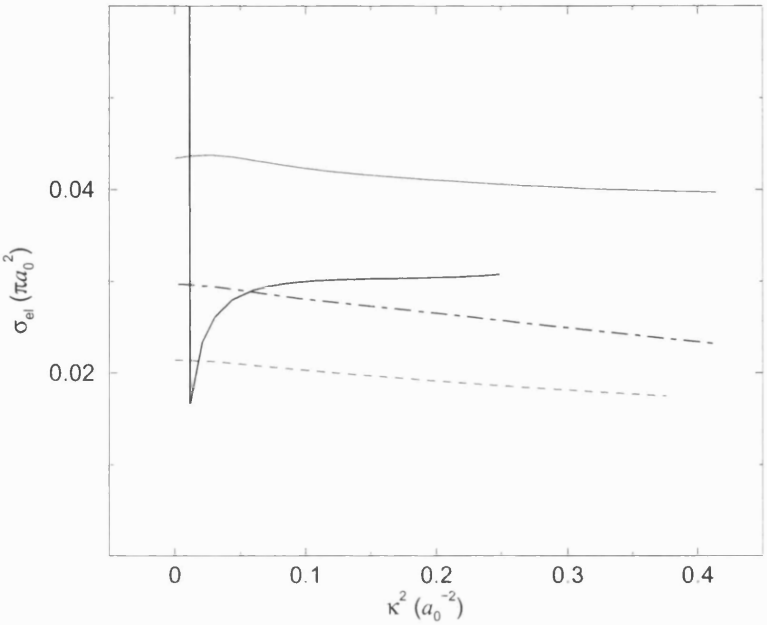

Figure 4.16: The variation of the p-wave elastic scattering cross section with respect to κ^2 for $\omega = 8$. Thick line, V_1^-; thin line, V_2^-; dashed line, V_3^-; chain curve, accurate results of Van Reeth and Humberston (1999). Note: the results are only plotted up to the first excitation threshold for each model.

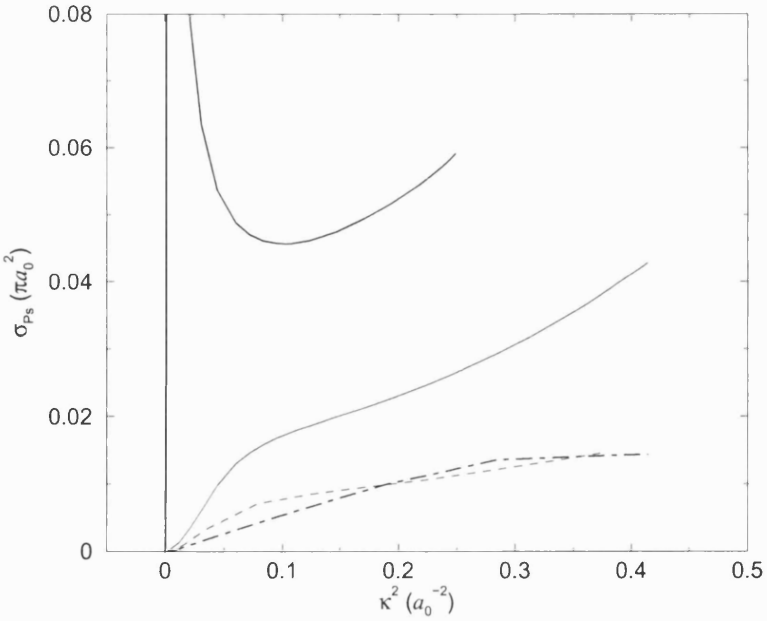

Figure 4.17: The variation of the p-wave positronium formation cross section with respect to κ^2 for $\omega = 8$. See caption to figure 4.16 for legend.

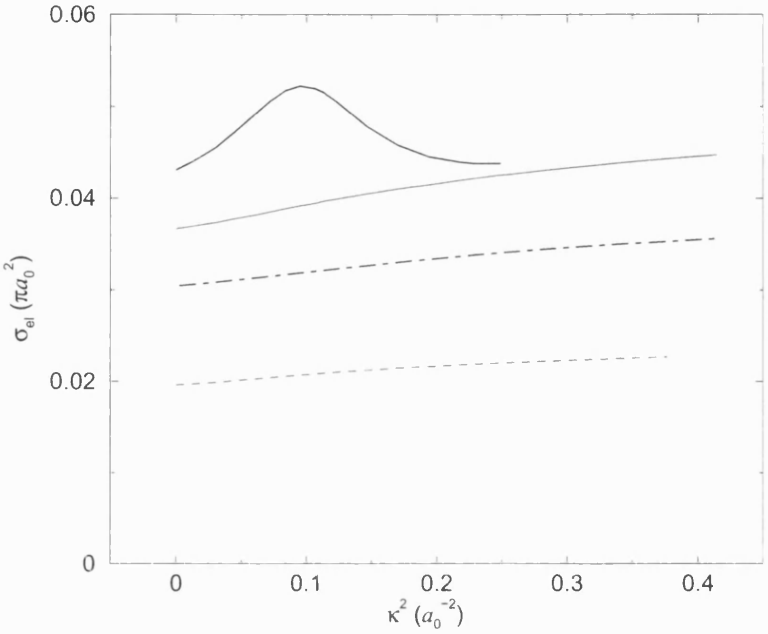

Figure 4.18: The variation of the d-wave elastic scattering cross section with respect to κ^2 for $\omega = 8$. See caption to figure 4.16 for legend.

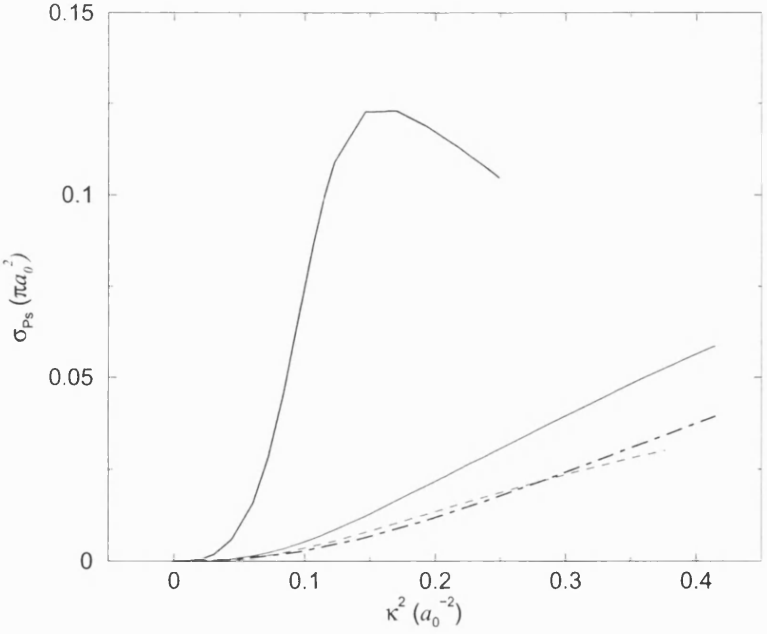

Figure 4.19: The variation of the d-wave positronium formation cross section with respect to κ^2 for $\omega = 8$. See caption to figure 4.16 for legend.

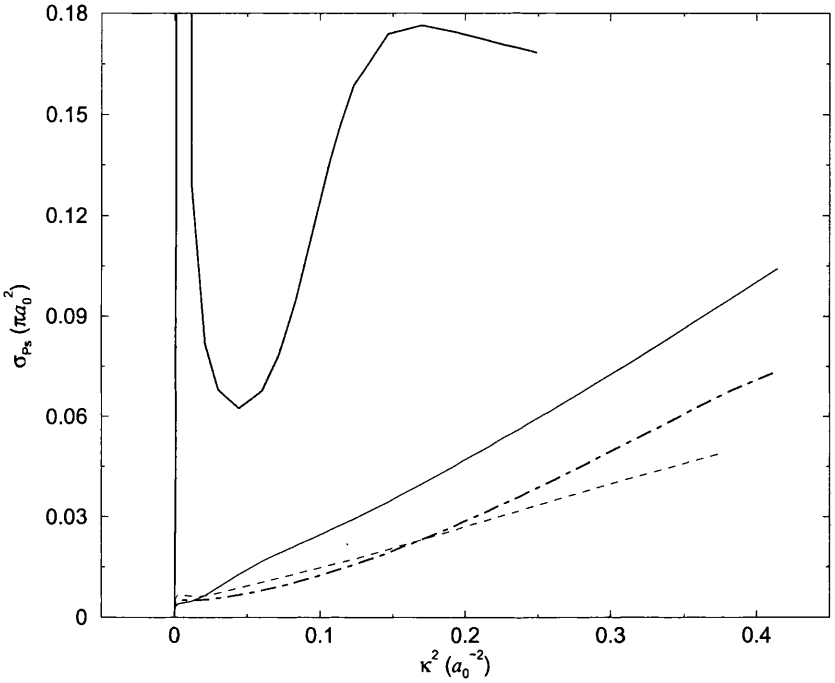

Figure 4.20: The variation of the sum of the s-, p- and d- partial wave positronium formation cross sections with respect to κ^2 for $\omega = 8$. Thick line, V_1; thin line, V_2; dashed line, V_3; chain curve, accurate results of Van Reeth and Humberston (1999) including $l \geq 3$ partial waves in sum. Note: the results are only plotted up to the first excitation threshold for each model.

Chapter 5

Annihilation in e^+-He Scattering

5.1 Introduction

One of the most interesting features of positron-atom scattering is the possibility of electron-positron annihilation. Many theoretical (e.g. Van Reeth *et al* 1996) and experimental (e.g. Coleman *et al* 1975) studies of positron-electron annihilation have been made, and the comparisons between experiment and theory have generally been favourable. Recent advances in experimental techniques, such as the use of Penning traps, have provided a source of positrons with sufficiently well defined energies to enable detailed comparisons to be made with theoretical calculations (Gilbert *et al* 2002, Gribakin 2001, Van Reeth *et al* 1996). The annihilation of positrons with atomic electrons can reveal a great deal about the electronic structure of the target system in general, and so a simple model of an atom which could be used to simulate annihilation in positron-atom scattering would be advantageous.

The annihilation process of positrons with electrons occurs mainly by the production of two or three γ-rays, with a combined energy of 1022 keV (in the rest frame of the positron-electron pair). Decay into four or more γ-rays is possible but highly unlikely. The positron-electron pair in a singlet spin state annihilates into two γ-rays and the triplet spin state into three. In positron-atom scattering, with an unpolarized positron beam, 25% of the annihilating positron-electron pairs are created in the singlet state and 75% in

the triplet state. However, annihilation into three γ-rays is much less likely than for two γ-rays. The ratio of the singlet to triplet annihilation rates is found to be approximately 370:1, taking into account the fact that there are three triplet states to one singlet state. Because of this, we shall only look at the contribution from singlet spin state annihilation.

Since the cross section for direct annihilation is negligible compared with the elastic scattering cross section, the present study has not treated annihilation as an open channel. We have extracted two pieces of information relating to annihilation from the scattering wave functions derived from the model potential, both of which involve the direct annihilation of positrons with electrons. The first is the annihilation rate and the second is the Doppler shift in the energy of the two γ-rays resulting from the motion of the electron-positron pair at the moment of annihilation. Because all positronium eventually annihilates, direct annihilation is difficult to measure above the positronium formation threshold, so our analysis will be confined to the single channel elastic scattering region.

5.2 Annihilation Rate and Z_{eff}

For a low-energy, unpolarized beam of electrons, the annihilation rate, λ_{a}, and the annihilation cross section, σ_{a}, for the production of two γ-rays, are

$$\lambda_a = \pi r_0^2 c N Z_{\text{eff}}, \tag{5.1}$$

$$\sigma_{\text{a}} = \frac{\lambda_{\text{a}}}{Nv} = \pi r_0^2 \frac{c}{v} Z_{\text{eff}}, \tag{5.2}$$

where N is the number density of target atoms, $r_0 (= e^2/mc^2)$ is the classical radius of the electron, v is the speed of the positrons, and the parameter Z_{eff} is the effective number of electrons per atom. Because the low energy positron distorts the target atom as it approaches it, the effective number of electrons with which the positron can annihilate is generally not equal to the actual number of electrons in the target atom, Z, and the value of Z_{eff} is dependent on the energy of the incident positron. All noble gases except neon have a value of Z_{eff} which is greater than Z.

Z_{eff} is a measure of the probability of the incident positron being at the same position

as one of the electrons, so for a general target with Z electrons, each with coordinate $\boldsymbol{r}_i$, $(i = 2, \cdots, Z+1)$, Z_{eff} is defined as

$$Z_{\text{eff}} = \sum_{i=2}^{Z+1} \int |\Psi(\boldsymbol{r}_1, \boldsymbol{r}_2, \cdots, \boldsymbol{r}_Z)|^2 \, \delta(\boldsymbol{r}_1 - \boldsymbol{r}_i) \, d\boldsymbol{r}_1 d\boldsymbol{r}_2 \cdots d\boldsymbol{r}_{Z+1}, \tag{5.3}$$

where Ψ is the scattering wave function for the positron-atom system which is normalized to unit positron density as $r_1 \to \infty$. It can be seen from equation (5.3) that this definition is only applicable in the single channel scattering formalism. Above the positronium formation threshold, that part of the scattering wave function which represents positronium formation has the asymptotic form given in equation (2.63)

$$\Psi \underset{\rho \to \infty}{\sim} -Y_{l,0}(\theta_\rho, \phi_\rho)\sqrt{2\kappa} K_{12} n_l(\kappa\rho) \Phi_{\text{Ps}}(\boldsymbol{r}_{12}), \tag{5.4}$$

and since we are looking at the condition when $r_{12} = 0$, it is clear that the integrand in equation (5.3) would remain finite as $r_1 \to \infty$, resulting in an infinite value of Z_{eff}. The conclusion from this result is not that there is an infinite electron density, but that the total annihilation cross section essentially becomes the cross section for positronium formation, which is very much larger than normal annihilation cross section.

For our one-electron model, the l^{th} partial wave contribution to Z_{eff} is

$$Z^l_{\text{eff}} = \int |\Psi_l(r_1, r_1 = r_2, r_{12} = 0)| \, d\boldsymbol{r}_1, \tag{5.5}$$

but since we are representing a two-electron atom as a one-electron model system, it is not clear how many electrons should be represented in our calculation of Z_{eff}. In the Born approximation, where the target atom is not distorted, the scattering wave function, Ψ^B, for our general Z-electron atom is

$$\Psi^B = e^{i\boldsymbol{k}.\boldsymbol{r}_1} \Phi_T(\boldsymbol{r}_2, \cdots, \boldsymbol{r}_{Z+1}), \tag{5.6}$$

where $e^{i\boldsymbol{k}.\boldsymbol{r}_1}$ is the incident plane wave and $\Phi_T(\boldsymbol{r}_2, \cdots, \boldsymbol{r}_{Z+1})$ is the Z-electron target wave function The Born approximation therefore yields the result $Z_{\text{eff}} = Z$. In our model system, which only contains one electron, the Born approximation to the value of Z_{eff} is therefore $Z^B_{\text{eff}} = 1$.

The determination of Z_{eff} provides a stringent test of the accuracy of the total wave function because the error in the expression for Z_{eff} is of first order in the error in the wave function, whereas the error in the Kohn phase shift is of second order, as was shown in the derivation of the Kohn method in Chapter 2. This means that any slight numerical errors that appear in the calculations of the phase shift are magnified in Z_{eff}; for example, a 1% error in the phase shift may appear as approximately a 10% error in Z_{eff}. Similarly, Schwartz singularities appear broader, and the convergence for Z_{eff} will be slower than for the phase shift.

5.3 Results for Z_{eff}

The results of the calculations of Z_{eff} are shown in figures 5.1-5.4. The three models display a similar energy dependence to that calculated by Van Reeth *et al* (1996) for the s-, p- and d-wave contributions. At the higher energies, close to the positronium formation threshold, models V_2 and V_3, which do not support resonances, reproduce the sharp rise in Z_{eff} very close to E_{th} found by Van Reeth *et al* (1996). This, however, is only apparent with the inclusion of the virtual positronium term (see Section 4.4.1) in the scattering wave function. If this is not included, there is no observable increase. As discussed above, Z_{eff} cannot be calculated above E_{th} since the integral in equation (5.3) becomes infinite. We would therefore expect Z_{eff} to approach infinity from below E_{th}, as the electron and positron do not quite form positronium but become increasingly highly correlated.

There are however significant discrepancies between the present calculated values of Z_{eff} and the accurate results of Van Reeth *et al* (1996), especially in the s-wave contribution which dominates Z_{eff} at low energies. The value of Z_{eff} at $k = 0$ is for most noble gas atoms (except neon) larger than the value of Z, and the most accurate experimental data, Coleman *et al* (1975), gives a value of $Z_{\text{eff}} = 3.94 \pm 0.02$ for helium, in good agreement with the accurate theoretical result $Z_{\text{eff}} = 3.93$ obtained by Van Reeth *et al* (1996). None of the three models reproduce this value. Although the error in Z_{eff} is only of first order of the error in the wave function, the discrepancy between the results of this work and

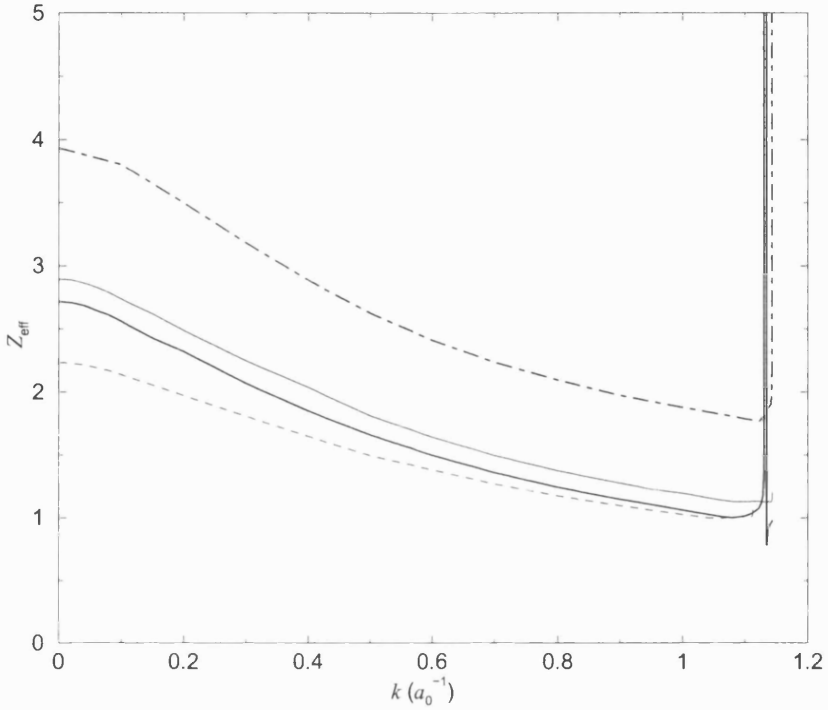

Figure 5.1: The variation of the s-wave contribution to $Z_{\rm eff}$ with respect to k for $\omega = 8$. Thick line, V_1; thin line, V_2; dashed line, V_3; chain curve, accurate results of Van Reeth *et al* (1996). Note: the results are only plotted up to the positronium formation threshold for each model.

those of Van Reeth and Humberston (1999) is too large to be explained by errors in the trial scattering wave function.

One immediate difference is that in the Born approximation the present calculations yield $Z_{\rm eff}^B = 1$, compared to the Born value of 2 for the real system. One might therefore think that the calculated result for $Z_{\rm eff}$ should be multiplied by 2 before comparing with the accurate value. However, because two of the one-electron models of helium used here have the correct value of the dipole polarizability, $\alpha_{He} = 1.383\ a_0^3$, and there is known to be a fairly good correlation between the dipole polarizability of a target atom and the value of $Z_{\rm eff}$ at low positron energies (Osman 1965; Davies *et al* 1989), one might expect a reasonably accurate value of $Z_{\rm eff}$ to be obtained without multiplication by a factor of 2. Using the most accurate elastic scattering wave function generated here, the value obtained for $Z_{\rm eff}$ at essentially zero energy (1.4×10^{-7} eV) is 2.56 (for model 1), which is

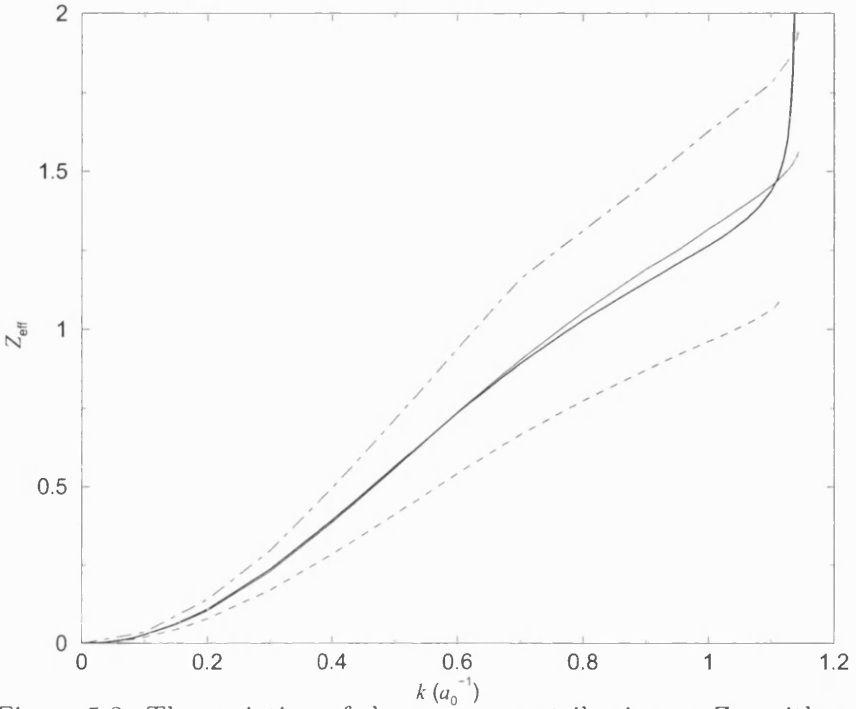

Figure 5.2: The variation of the p-wave contribution to Z_{eff} with respect to k for $\omega = 8$. See caption to figure 5.1 for legend.

significantly smaller than the accurate value of 3.93 obtained by Van Reeth *et al* (1996) at the same energy; however, multiplying by 2 gives $Z_{\text{eff}} = 5.12$ which is significantly larger than the accurate value. It would therefore seem that we are not justified in multiplying by 2.

Part of the discrepancy may be due to the fact that the polarizability of our single electron model differs from the exact value by the polarizability of the helium ion core, 0.28125 a_0^3. Accordingly, because of the above mentioned correlation between Z_{eff} and the dipole polarizability, we should probably expect the calculated value of Z_{eff} to be approximately 20% smaller than the correct total value, i.e. $Z_{\text{eff}} \sim 3.1$. On this basis the present value is only 18% smaller than it might be expected to be. Furthermore, in the real two-electron helium atom the total Z_{eff} is the sum of two (equal) contributions, each one corresponding to positron annihilation with a single electron. In our one-electron model of helium the 'second' electron is in a sense in the core, and therefore we should perhaps add a contribution arising from positron 'annihilation' with the core, i.e.

$$Z_{\text{eff}}^{+} = 4\pi \int |\Psi(r_1 = 0, r_2, r_{12} = r_2)|^2 \, r_2^2 dr_2. \tag{5.7}$$

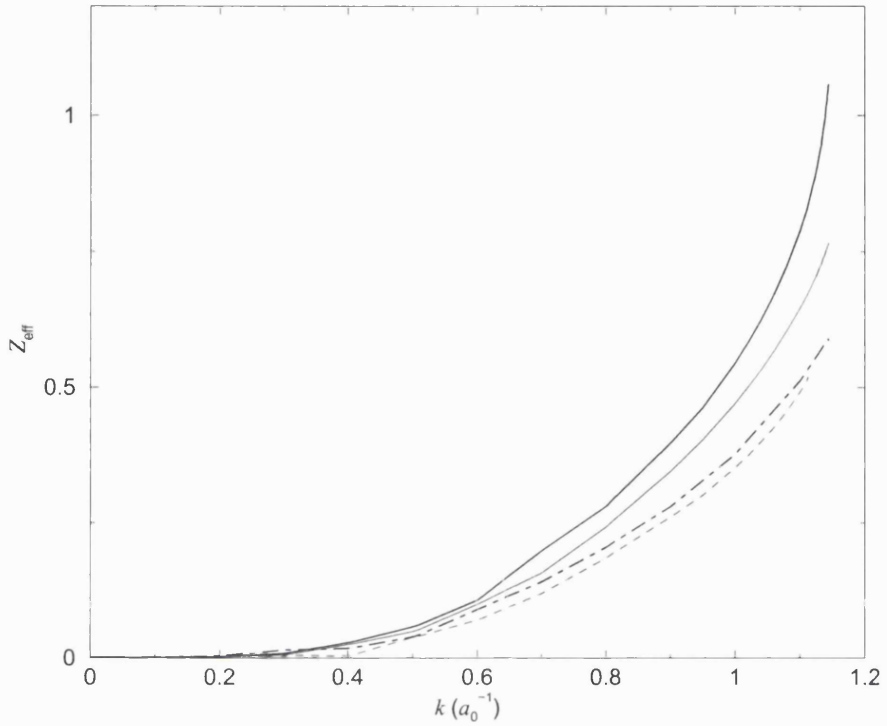

Figure 5.3: The variation of the d-wave contribution to Z_{eff} with respect to k for $\omega = 8$. See caption to figure 5.1 for legend.

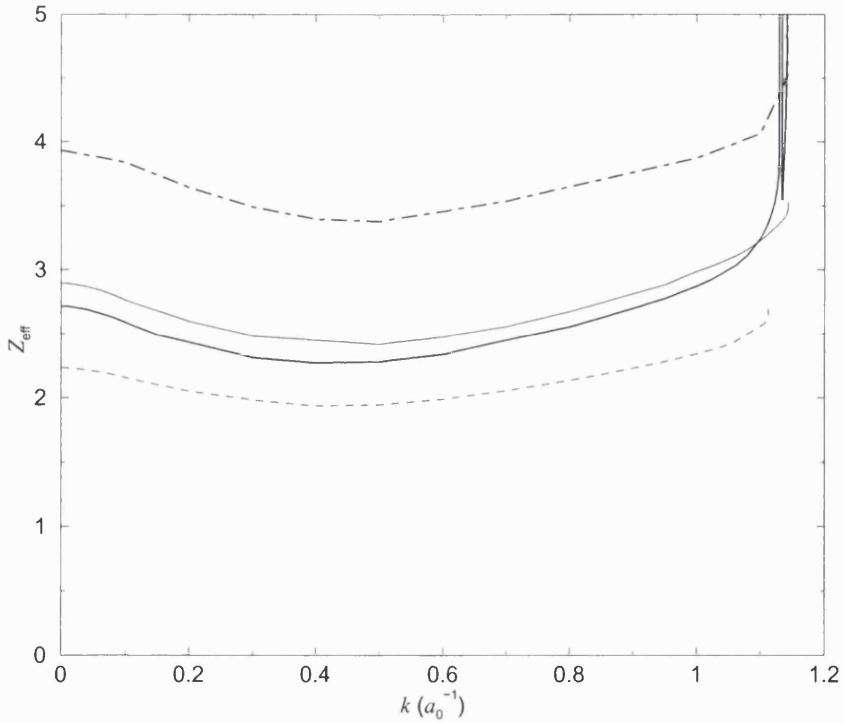

Figure 5.4: The variation of the sum of the s-, p- and d- wave contributions to Z_{eff} with respect to k for $\omega = 8$. See caption to figure 5.1 for legend.

This contribution to Z_{eff} is, however, zero at zero incident positron energy, and is small at all energies, having a maximum value of 0.12. It therefore has a negligible effect on the results and we must accept that the one-electron models used here do not provide as accurate a representation of annihilation as they do of elastic scattering

Despite the reasonable agreement between the accurate *ab initio* results and the present results with respect to the scattering phase shifts and cross sections, it seems that accurate calculations of Z_{eff} using a one-electron model of helium may not be possible and are a limitation of using a one-electron model.

5.4 Doppler Broadening of γ-Ray Spectrum

In the frame of reference in which the annihilating electron-positron spin singlet pair is at rest, the two γ-ray are emitted back-to-back (the angle between them is π radians) each with an energy of 511 keV. In the laboratory frame of reference, however, the centre of mass of the lepton pair is moving with a velocity $\boldsymbol{v}$ and the momentum of the pair is $\boldsymbol{p} = 2m\boldsymbol{v}$, so the two γ-rays detected in the experiment are Doppler shifted to energies depending on the velocity of the electron-positron pair and the orientation of the emitted photons.

Figure 5.5 shows a greatly exaggerated example of the kinematics of the annihilating positron-electron pair and the emitted γ-rays. The electron-positron pair has a momentum $\boldsymbol{p}$ in the laboratory frame shown at an angle α to the x-axis. The two γ-rays are shown emitted back-to-back in the centre-of-mass frame, traveling along the positive and negative y-axis each with a momentum $\boldsymbol{p}_0$. In the laboratory frame of reference the two Doppler shifted γ-rays have momenta $\boldsymbol{p}_1$ and $\boldsymbol{p}_2$ where

$$\boldsymbol{p}_1 = mc\hat{\boldsymbol{j}} + m\boldsymbol{v} \quad \text{and} \quad \boldsymbol{p}_2 = m\boldsymbol{v} - mc\hat{\boldsymbol{j}}, \tag{5.8}$$

where $\hat{\boldsymbol{j}}$ is the unit vector along the y-axis. At very low incident energies, the energy imparted to the lepton pair by the positron is negligible compared to that from the atomic

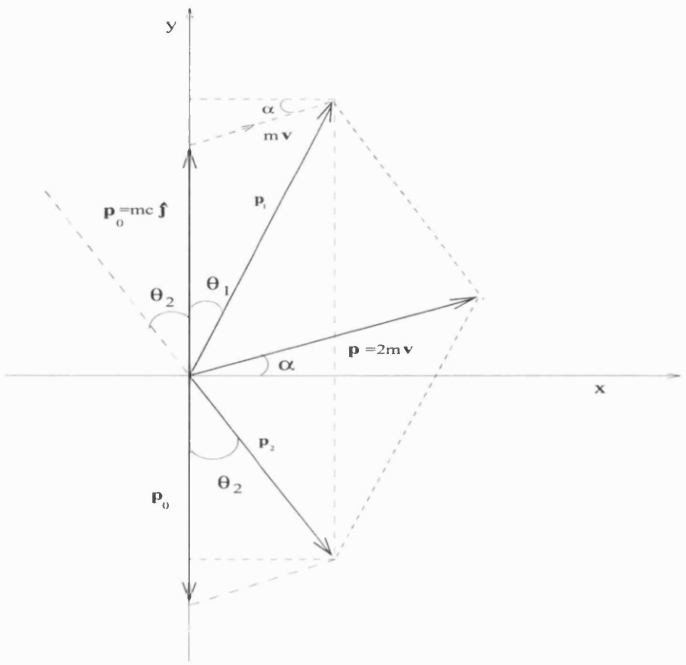

Figure 5.5: Illustration of the relationships between the momenta of the two annihilation γ-rays and the momentum of the positron-electron pair in the rest frame of the pair and in the laboratory frame of reference.

electron, so $v/c \ll 1$ and the magnitude of the γ-ray momenta, are

$$p_1 = p_0 + mv\sin\alpha \quad \text{and} \quad p_2 = p_0 - mv\sin\alpha. \tag{5.9}$$

Therefore, the Doppler shift in the energy of one of the γ-rays is

$$\Delta E = E_1 - E_0 = c(p_1 - mc) = \frac{c}{2}\,p_y, \tag{5.10}$$

where $p_y = 2mv\sin\alpha$ is the y component of the electron-positron pair momentum in the laboratory frame of reference.

As well as looking at the Doppler shift in the energy of the γ-rays, the same information can also be obtained by measuring the angle between the two γ-rays. In the rest frame of the electron-positron pair the angle is π, and in the laboratory it is $(\pi - \theta)$ where

$$\theta = \theta_1 + \theta_2 = \frac{2mv\cos\alpha}{mc} = \frac{p_x}{mc}, \tag{5.11}$$

p_x being the x-component of the electron-positron pair momentum in the laboratory frame of reference.

We have described the electron-positron annihilation occurring in the $x-y$ plane, but this is an isotropic system in which all directions of the momentum of the electron-positron pair are equally probable and each of the components of the momenta have the same distribution function, so the relationship between the Doppler shift in energy, ΔE, and the angle θ can be written as

$$\Delta E = mc^2\frac{\theta}{2} = \frac{c}{2}p_x. \tag{5.12}$$

Since the relationship between the energy shift and the angular shift is trivial, we shall choose to only look at the Doppler shift in energy.

The Doppler-broadened annihilation spectrum is given by the probability distribution function for one of the γ-rays being emitted with an energy shift ΔE,

$$F(\Delta E) \propto \int_{-\infty}^{\infty}\int_{-\infty}^{\infty} \Gamma\left(p_x = \frac{2\Delta E}{c}, p_y, p_z\right) dp_y dp_z, \tag{5.13}$$

where Γ is the momentum distribution function for the annihilating electron-positron pair, which for our model positron-helium scattering system is

$$\Gamma(\boldsymbol{p}) = \left|\int e^{-i\boldsymbol{p}\cdot\boldsymbol{\rho}}\Psi\left(\boldsymbol{r}_1,\boldsymbol{r}_2\right)\delta\left(\boldsymbol{r}_1-\boldsymbol{r}_2\right)d\boldsymbol{r}_1 d\boldsymbol{r}_2\right|^2, \tag{5.14}$$

where $\boldsymbol{\rho} = \frac{1}{2}(\boldsymbol{r}_1+\boldsymbol{r}_2)$ in the position of the centre of mass of the annihilating electron-positron pair. Thus,

$$\begin{aligned}
\Gamma(\boldsymbol{p}) &= \left|\int e^{-i\boldsymbol{p}\cdot\boldsymbol{r}_1}\Psi\left(r_1, r_2 = r_1, r_{12} = 0\right) r_1^2 dr_1 d\theta_1 d\phi_1\right|^2, &(5.15)\\
&= 2\pi\left|\int e^{-ipr_1\cos\theta_1}\Psi\left(r_1\right) r_1^2 dr_1 d\theta_1\right|^2, &(5.16)\\
&= 2\pi\left|\int \frac{2}{p}\sin\left(pr_1\right)\Psi\left(r_1\right) r_1^2 dr_1\right|^2. &(5.17)
\end{aligned}$$

We have arbitrarily chosen to fix p_x so we are restricted to the $p_y - p_z$ plane. To do the double integral in equation (5.13), we can change to polar coordinates,

$$p_y, p_z \longrightarrow p', \beta \tag{5.18}$$

and

$$dp_y dp_z = p' dp' d\beta. \tag{5.19}$$

Since $p' = \sqrt{p_y^2 + p_z^2}$, equation (5.13) can be rewritten as

$$F(p) \propto \int_0^{\infty} \int_0^{2\pi} \Gamma(p') p' dp' d\beta. \tag{5.20}$$

Integrating over the polar angle β and using the substitution

$$p^2 = p'^2 + p_x^2, \tag{5.21}$$

the probability distribution function of one of the γ-rays emerging with momentum p_x is

$$F(p_x) \propto 2\pi \int_{p_x}^{\infty} \Gamma(p) p dp. \tag{5.22}$$

Experimental measurements suffer from small inefficiencies in the γ-ray detectors, and in order to compare theory with experiment it is necessary to take account of the finite *response function* of the γ-ray detectors. Deconvoluting the experimental data in order to compare directly with theory is well known to provide spurious results, so it is easier and more reliable to convolute the theoretical data with the known response function, $g(E, E')$, of the detectors. In terms of the γ-ray energy, E, the response function is taken to be

$$g(E, E') = A \exp\left[-\frac{(E - E')^2}{\lambda^2}\right], \tag{5.23}$$

where A and λ are known constants, so the convoluted theoretical results are given by

$$G(E) = \int_0^{\infty} g(E, E') F(E') dE'. \tag{5.24}$$

The experimental Doppler-broadened annihilation spectrum is not normalized, but we are only interested in the width and the shape of our theoretical curves, which can be normalized to the experimental data of Surko *et al* (1989) and Greaves *et al* (1994) or to the accurate results of Van Reeth *et al* (1996). Hence any constants carried through the calculation of $G(E)$ can be ignored. The integrations in equations (5.13)-(5.24) can be carried out using the simple but effective trapezoidal rule.

The formulae given in equations (5.13)-(5.24) provide the momentum distribution functions $F(E)$ and $G(E)$ which are centred about $E = 0$ in atomic units. The energy and

momentum of a γ-ray are trivially related, so to convert from atomic units of momenta to the more usual units of energy, electron-volts,

$$1 \text{ a.u.} \equiv \frac{1}{2} c \hbar a_0^{-1} \text{ eV} = \frac{m_e e^2}{2 \epsilon_0 h} \text{ eV}, \tag{5.25}$$

$$\equiv 1.8645 \text{ keV}, \tag{5.26}$$

where a_0 is the Bohr radius of the hydrogen atom. The results of the calculations of $F(E)$ and $G(E)$ are shown in electron-volts and are shifted along the horizontal axis by 511 keV - the rest energy of an electron or positron - so what is plotted is the Doppler shifted energy spectrum of one of the γ-rays.

5.4.1 Doppler Shift Results

The annihilation γ-ray spectra for the three models are compared with the accurate *ab initio* results of Van Reeth *et al* (1996) in figures 5.7 and 5.8. The first two models, V_1 and V_2, which reproduce the spectroscopic properties of the helium atom most accurately, provide relatively poor spectra, yet the comparatively crude model, V_3, matches the accurate results best. Since at $k = 0$ the momentum of the electron-positron pair is mainly from the momentum of the orbiting electron, the width of the spectrum is, in the semi-classical picture, a measure of the speed of the electron within the atom. Some understanding of the differences between the annihilation γ-ray spectra for the various models can be obtained by examining the electron density functions for the respective atoms. Figure 5.6 shows the electron density functions for the three models compared with the corresponding functions obtained by Van Reeth and Humberston (1999). This clearly shows that the electron density of model V_2, and to a lesser extent that of model V_1, is peaked further out in r_2 than that of model V_3 and, perhaps more importantly, the tails of the electron density functions in V_1 and V_2 are more extended than those of V_3 and of the *ab initio* calculations. This corresponds to the electron in model V_3 spending more time closer to the atomic core and hence having a greater speed and contributing more momentum to the positron-electron pair in the annihilation. This similarity between the wave functions

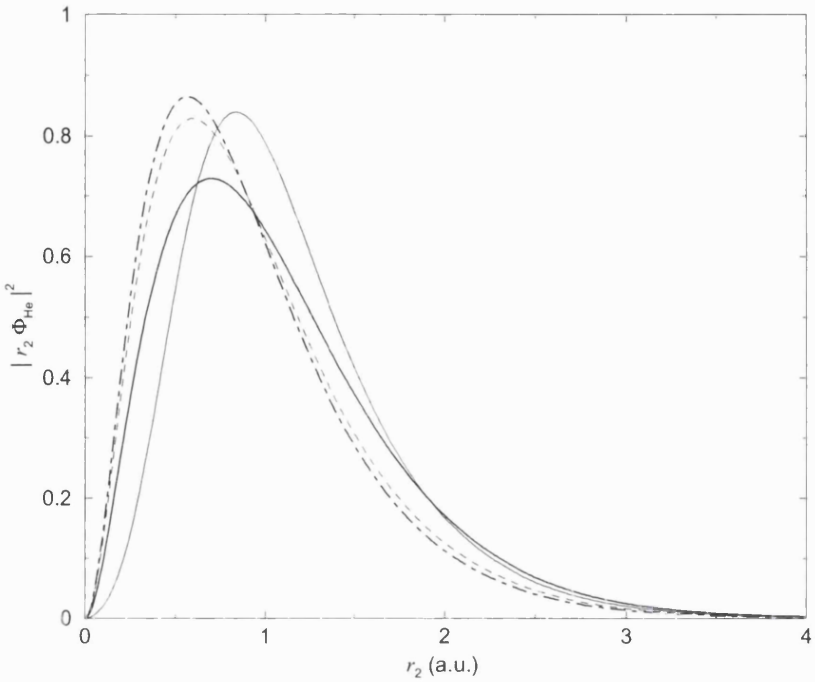

Figure 5.6: Variation of the electron density with electron-core coordinate r_2 for the *ab initio* work of Van Reeth and Humberston. This is a repeat of figure 3.8. Thick line, V_1; thin line, V_2; dashed line, V_3; chain curve, Van Reeth and Humberston (see equation 3.39).

of model V_3 and the results of Van Reeth and Humberston (1999) may also explain the success of this model when describing the positronium formation processes discussed in Chapter 4.

The present investigations of the annihilation phenomena have revealed some of the limitations and accuracies which can be expected from one-electron models of many electron atoms. In the real helium atom both electrons are equivalent, but in these models the positron can only interact with one electron. Annihilation involves such an extreme interaction between the positron and electron that a one-electron model may not be able to represent it accurately. The study of the Doppler-broadening has revealed the relevance of the electron density functions, but this has not led to more accurate results for Z_{eff}.

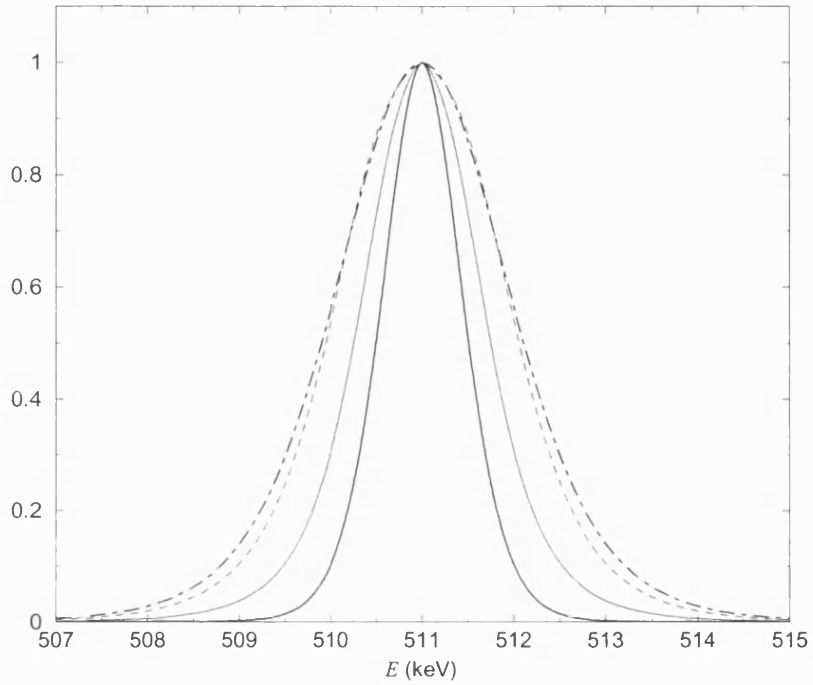

Figure 5.7: Annihilation γ-ray spectrum from the unconvoluted theory (see equation 5.13). Thick line, V_1; thin line, V_2; dashed line, V_3; chain curve, accurate results of Humberston and Van Reeth (1997).

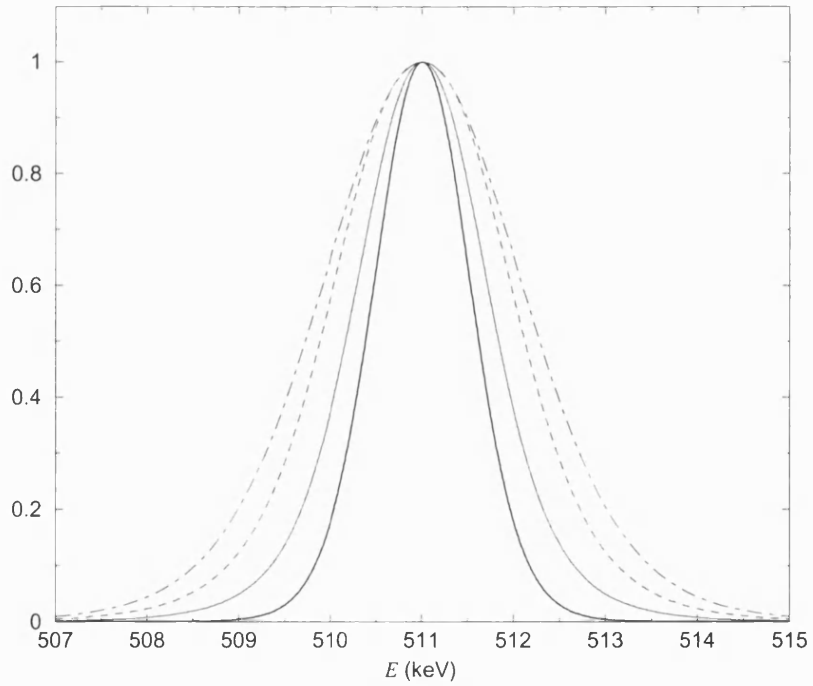

Figure 5.8: Annihilation γ-ray spectrum from the convoluted theory (see equation 5.24). See caption to figure 5.7 for legend.

Chapter 6

Resonance in Positron-Helium Scattering

6.1 Introduction

The results shown in figure 4.6 reveal a resonance-type structure in the s-wave elastic scattering phase shift at an energy just below E_{th} for the model potential V_1. As mentioned in Chapter 3, it is quite possible for a model potential representing a real atom to contain an unphysical feature in the cross section such as a resonance. However, it is necessary to test whether this resonance-type feature in the phase shift is indeed a resonance and not just a numerical anomaly such as a Schwartz singularity. As discussed in Section 4.4, the results yielded by the Kohn, complex Kohn and inverse Kohn variational methods all show this resonance-type feature. Although a Schwartz singularity in all three methods is highly unlikely, it is possible, but in this chapter we shall show that there are other tests that can be made on the wave function and the model potentials that support the case that the resonance is a true feature of the model, but not of the real positron-helium system. However, we shall see that this feature of the model verifies a mechanism believed to be responsible for the very high annihilation rates obtained in some positron-molecule scattering experiments.

6.2 Stabilization Method

This method, described by Bhatia and Drachman (1990), has been used quite successfully to study resonances in positron-atom and electron-positronium scattering.

The stabilization method provides a means of detecting resonances by looking at how the energy eigenvalues of a system on a square-integrable basis change as the number of terms in the trial wave function is changed. The energy eigenvalues are found by solving the matrix eigenvalue equation

$$(\boldsymbol{H}_{\mathrm{T}} - E_{\mathrm{T}}\boldsymbol{A})\,\boldsymbol{c} = 0 \tag{6.1}$$

where the matrix elements of $\boldsymbol{H}_{\mathrm{T}}$ and $\boldsymbol{A}$ are given by

$$H_{\mathrm{T},ij} = \langle \phi_i \mid H_{\mathrm{T}} \mid \phi_j \rangle\,, \tag{6.2}$$

$$A_{ij} = \langle \phi_i \mid \phi_j \rangle\,, \tag{6.3}$$

where H_{T} is the total Hamiltonian of the projectile-target system given in equation (4.25), ϕ_i are the short-range Hylleraas type terms in the trial wave function in equation (4.15),

$$\phi_i = Y_{0,0} e^{-(\alpha r_1 + \beta r_2 + \gamma r_{12})}\, r_1^{k_i}\, r_2^{l_i}\, r_{12}^{m_i}, \tag{6.4}$$

and $\boldsymbol{c}$ is a column matrix listing the optimum values of the linear coefficients in the variational wave function. All the matrix elements required for the stabilization method have already been calculated for use in the evaluation of the scattering parameters.

Figure 6.1 shows how the first several eigenvalues converge as the number of terms, N, in the trial wave function is increased. The lowest eigenvalue, E_0, is seen to converge to the ground state energy of the helium atom, with the wave function attempting to represent a zero energy positron interacting with the ground state helium atom. The higher energy eigenvalues also converge to the ground state energy of the helium atom, with the wave function representing a very low energy positron interacting with the helium ground state. The fifth energy eigenvalue for $N \approx 50$ does not change significantly from $E_5 \approx -0.25$ a.u. as more terms are added, until $N \approx 65$, where it starts to fall again, but the sixth energy

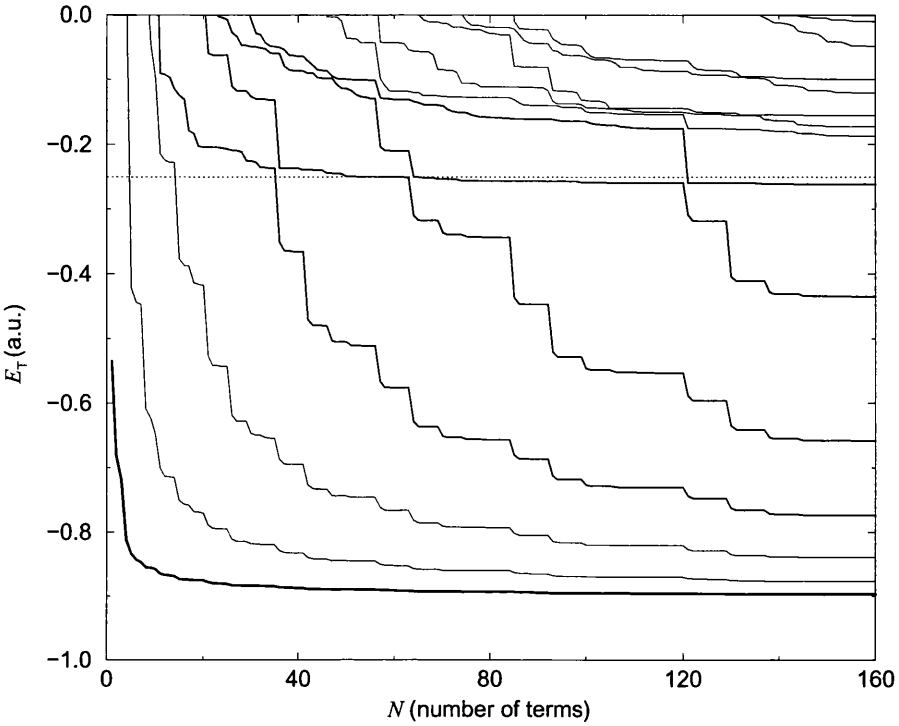

Figure 6.1: Variation of the lowest eigenvalues of the Hamiltonian of the model positron-helium system with respect to increasing N, the number of short-range correlation functions in the basis. Thick line, E_1; fine lines, E_2, E_3 and E_i $(i \geq 7)$; medium lines, E_4, E_5, E_6 and E_7; dotted line parallel to the abscissa is at the exact positronium formation threshold: $E_{\mathrm{T}} = -0.25$ a.u.$= -6.8$ eV.

eigenvalue then takes its place and holds the same value and is stable until $N \approx 120$ where the seventh energy eigenvalue takes its place, a succession of 'avoided crossings'. The stabilization method is revealing an energy region where the energy eigenvalues stabilize at a value just below -0.25 a.u., implying a structure for the system of positronium weakly bound to the residual ion. This is further evidence that the resonance in the scattering problem is a real feature of the model and not a numerical anomaly produced by the method used in the scattering calculation.

6.3 Virtual Positronium

When the incident positron energy is close to, but less than, the positronium formation threshold, positronium cannot be formed but the positron and the electron nevertheless

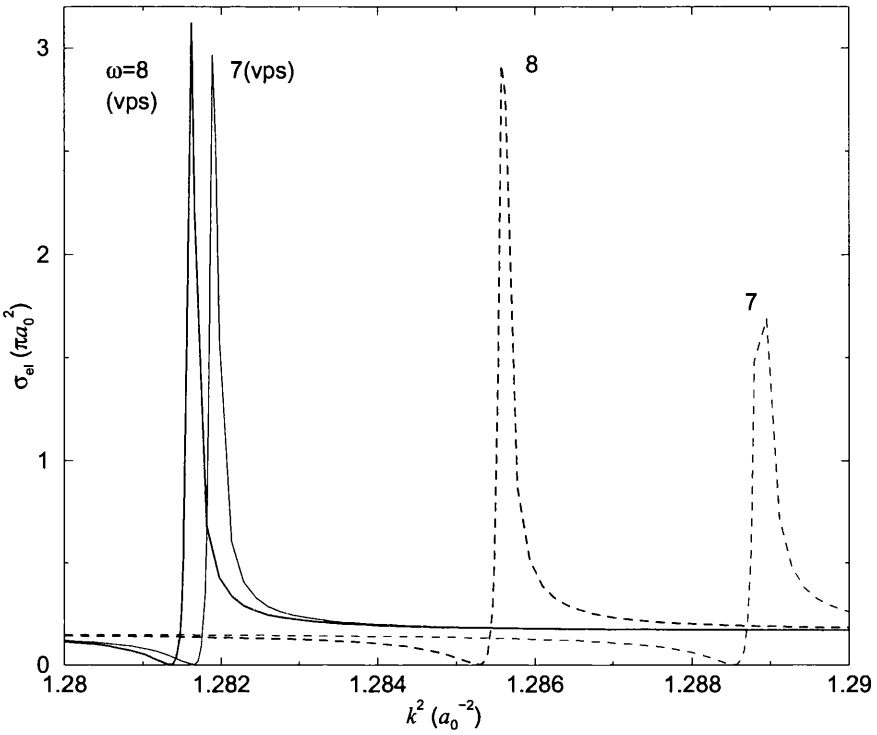

Figure 6.2: The variation of the s-wave elastic scattering cross section with respect to k^2 for different ω both with and without the virtual positronium term, $\phi_{\rm vps}$, included in the trial wave function. Thick line, $\omega = 8$ with $\phi_{\rm vps}$ term; thin line, $\omega = 7$ with $\phi_{\rm vps}$ term; thick dashed line, $\omega = 8$ without $\phi_{\rm vps}$ term; thin dashed line, $\omega = 7$ without $\phi_{\rm vps}$ term.

show a strong correlation as if positronium was trying to be formed, but cannot quite escape. This configuration has been called *virtual positronium*, as it does not constitute an open positronium formation channel. Virtual positronium formation is represented by the term

$$\phi_{\rm vps} = c_0 Y_{0,0}(\boldsymbol{\rho})\phi_{\rm Ps}(r_{12})\frac{e^{-\kappa\rho}}{\rho}\left(1 - e^{-\delta\rho}\right)^3 . \tag{6.5}$$

Adding such a term to the scattering calculations using model V_1 will show if such a term is required, and may possibly reveal information about the mechanism responsible for the resonance. If it is not required the Kohn variational method would yield a value of the coefficient c_0 close to zero.

Figure 6.2 shows that by adding the virtual positronium term to the trial wave function, the position of the resonance feature in k converges much faster with respect to ω than without this term. In addition, the resonance becomes narrower, although the coarse grid

of energy points in the figure may not make this obvious, so the term is useful. This supports the idea of the feature representing a Feshbach resonance with the configuration of positronium bound to the residual ion. Further evidence of this configuration being responsible for the resonance is given below.

6.4 Expectation Values of the Total Potential

Since the total interaction potential varies with respect to three variables, r_1, r_2 and r_{12}, it would be difficult to view any attractive potential wells in a straightforward way. Picking out specific configurations of the three particles and finding how the total potential varies with respect to one variable is possible but not very useful since it is would not provide any information about the likelihood of any particular configuration arising.

However, it is possible to view the expectation value of the total interaction potential with respect to the virtual positronium, for a given incident particle energy. This represents the interaction between the helium core and the 'positronium' in one dimension, for a less specific configuration of the three particles. The expectation potential, $\overline{V}_k$, with respect to the positronium coordinate ρ is calculated by fixing ρ and integrating the total scattering wave function and the potential between the 'positronium' and the core, $(V^-(r_2) + V^+(r_1))$, over the coordinates defining the positronium, r_3 and $\theta_{\rm Ps}$,

$$\overline{V}_k(\rho) = \int \Psi(\rho, r_{12}, \theta_{\rm Ps}) \left(V^+ + V^-\right) \Psi(\rho, r_{12}, \theta_{\rm Ps}) r_{12}^2 dr_{12} \sin\theta_{\rm Ps} d\theta_{\rm Ps}. \tag{6.6}$$

The integration was carried out using a Gauss-Laguerre procedure (described in Section 3.4.3) for the radial part, and a Gauss-Legendre procedure for the angular part, so that

$$\int_0^{\pi} P_n(\cos\theta)\sin\theta d\theta = \int_{-1}^{+1} P_n(t)dt \approx \sum_{i=1}^{N} P_n(t_i)w_i, \tag{6.7}$$

where P_n is a Legendre polynomial of degree n, and t_i and w_i are the abscissa and weights, respectively, readily provided by the Fortran NAG libraries.

We can similarly calculate expectation values of the potential with respect to the

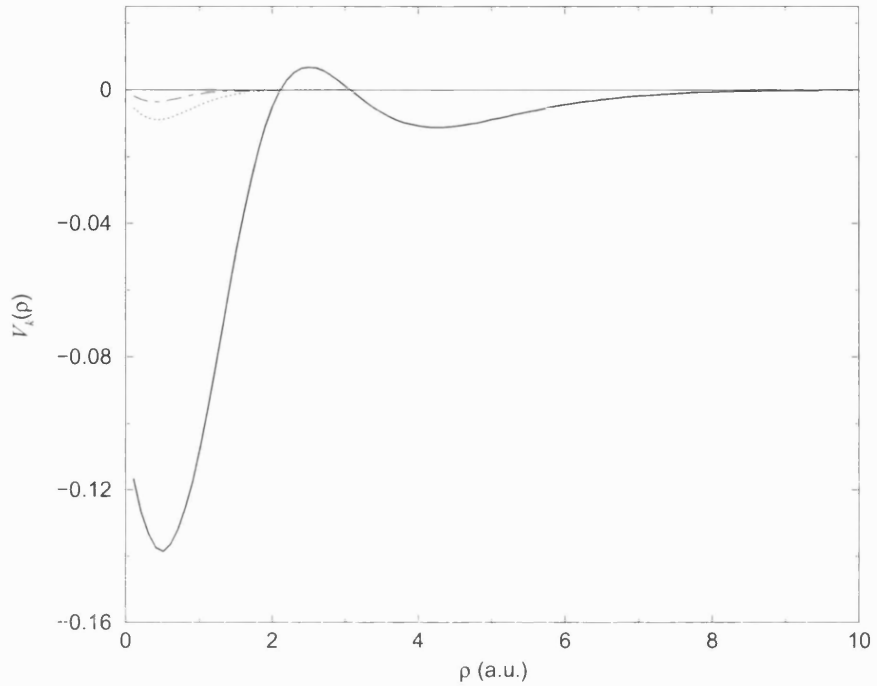

Figure 6.3: Variation of V_k with respect to ρ (see equation 6.6), with the virtual positronium term included, at three incident positron energies. Thick line, V_k at resonance ($k = 1.132\ a_0^{-1}$); dotted line, V_k just above resonance ($k = 1.133\ a_0^{-1}$); dashed line, V_k just below resonance ($k = 1.131\ a_0^{-1}$); solid line, V_k at $k = 10^{-4}\ a_0^{-1}$.

positron and electron coordinates, $\overline{V}_k(r_1)$ and $\overline{V}_k(r_2)$ respectively,

$$\overline{V}_k(r_1) = \int \Psi(\rho, r_{12}, \theta_{\rm Ps})\,(V^+ + V_{12})\,\Psi(\rho, r_{12}, \theta_{\rm Ps}) r_2^2 dr_2 \sin\theta_{12} d\theta_{12}, \tag{6.8}$$

$$\overline{V}_k(r_2) = \int \Psi(\rho, r_{12}, \theta_{\rm Ps})\,(V^- + V_{12})\,\Psi(\rho, r_{12}, \theta_{\rm Ps}) r_1^2 dr_1 \sin\theta_{12} d\theta_{12}. \tag{6.9}$$

The integral in equation (6.9) is complicated slightly by the fact that there is no explicit exponent in r_1, but the Gauss-Laguerre procedure can still be used by including a false exponent in the integration as described in equation (4.38).

It can be seen in figures 6.3-6.5 that at energies very close to the resonance, deep potential wells are apparent. Figure 6.3 shows that $\overline{V}_k(\rho)$ has two local minima, at $\rho \sim 0.5$ a.u. and a shallower one at $\rho \sim 4$ a.u. Figure 6.4 shows a similar potential curve in $\overline{V}_k(r_1)$, but the deepest minimum is at $r_1 \sim 2.5$ a.u and a shallower one at $\rho \sim 7$ a.u. These minima show that the positron is likely to be trapped in this complicated potential structure at the energy of the resonance found in the elastic scattering phase shift.

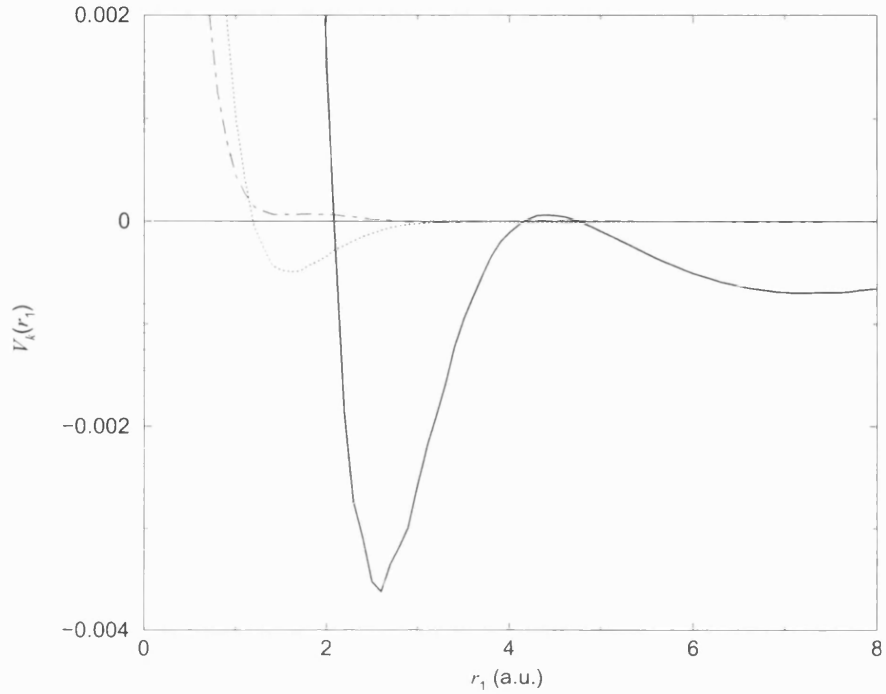

Figure 6.4: Variation of V_k with respect to r_1 (see equation 6.8), with the virtual positronium term included. See caption to figure 6.3 for legend.

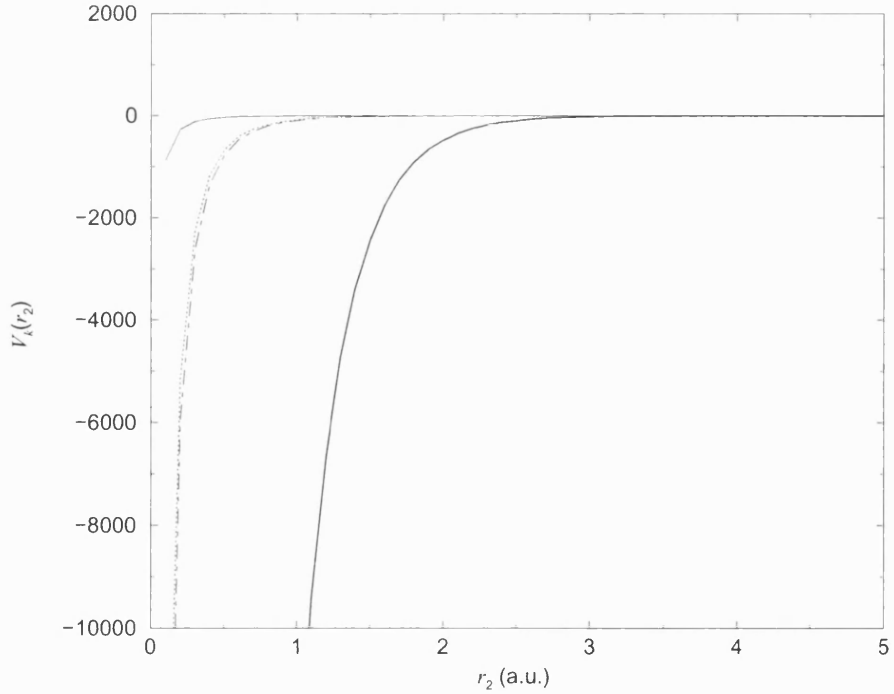

Figure 6.5: Variation of V_k with respect to r_2 (see equation 6.9), with the virtual positronium term included. See caption to figure 6.3 for legend.

Without the ϕ_{vps} term included in the scattering wave function, the expectation values of the potentials show simple wells at 3 a.u. and 4 a.u. in the positronium and positron coordinates respectively, but since ϕ_{vps} has such a dramatic effect on the resonance shape and position, the interaction potential is likely to have the more complicated structure. Figure 6.5 does not show any minimum, since one is not expected in the electron coordinate because it is already bound to the core by the model potential V_1^- but at the resonance, the potential is much more attractive. At energies away from the resonance these potential wells do not appear.

6.5 Behaviour of the Phase Shift in passing through Resonance

A resonant feature is characterized by a rapid jump in the phase shift through π as an extra node is added to the scattering wave function. This cannot be seen directly in the plot of the s-wave phase shift against k since the Kohn method directly calculates the tangent of the phase shift and the subsequent inverse tangent operation yields a modular value of the phase shift with the limits $\frac{\pi}{2} < \eta < \frac{\pi}{2}$. The feature is analogous to *Levinson's theorem.* Levinson's theorem is usually presented in terms of the number of bound states, n_l, supported by an interaction potential in a particular partial wave, such that

$$\lim_{k \to 0} \eta_l = n_l \pi. \tag{6.10}$$

With a potential just unable to support an $(n+1)^{\text{th}}$ bound state, the phase shift reaches a maximum value of

$$\lim_{k \to 0} \eta_l = \left(n_l + \frac{1}{2} \right) \pi. \tag{6.11}$$

Although the resonance discussed above occurs at a non-zero energy, the reasons for the phase shift passing through π close to the resonance are similar to those involved in Levinson's theorem in the limit of zero energy.

Further evidence of this can be seen with the *eigenphase sum* above the positronium formation threshold. In two-channel scattering there is no such thing as a single phase

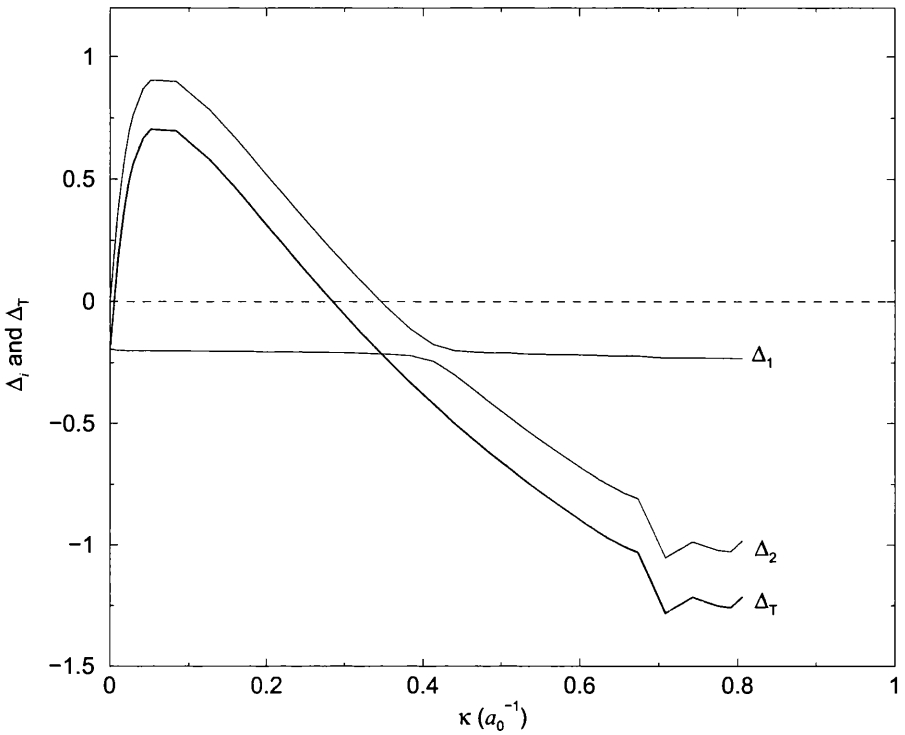

Figure 6.6: Variation of the eigenphase shifts, Δ_i, and the sum of the eigenphase shifts, $\Delta_T = \Delta_1 + \Delta_2$ with positronium wavenumber, above the the positronium formation threshold for model V_3.

shift; instead, the corresponding quantity above E_{th} is the eigenphase sum. The eigenphase shifts are found by diagonalizing the $\boldsymbol{S}$ matrix described in Chapter 2 (see equation 2.66) and the diagonalized matrix, $\overline{\boldsymbol{S}}$, has the elements

$$\overline{\boldsymbol{S}}_{ij} = \delta_{ij} e^{2i\Delta_i} \tag{6.12}$$

where Δ_i are the eigenphase shifts.

Figure 6.6 shows how the eigenphases and the eigenphase sum, $\Delta_T = \Delta_1 + \Delta_2$, vary with positronium momentum for model V_3, with no resonance.

The plot in figure 6.7 shows the eigenphase and eigenphase sum for the model V_1 with the resonance just below the positronium formation threshold, and there is a very distinct jump in the eigenphase sum from $\sim -\frac{\pi}{2}$ up to $\sim \frac{\pi}{2}$. This occurs in exactly the same energy region as the resonances in the individual $\boldsymbol{K}$ matrix elements. It is believed that this jump in Δ_T is due to the fact that $\Delta_T = \pi$ at $\kappa = 0$, and therefore a more appropriate plot of the eigenphases, Δ_i, and their sum, Δ_T, is as indicated by the dotted lines. This

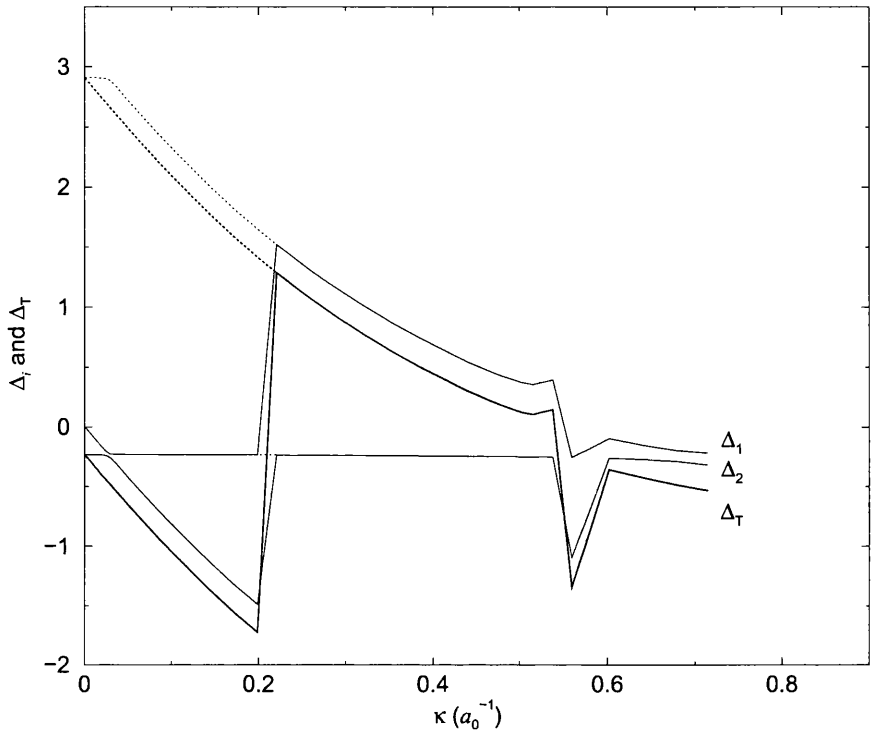

Figure 6.7: Variation of the eigenphase shifts, Δ_i, and the eigenphase sum, Δ_T with positronium wavenumber, above the the positronium formation threshold for model V_1. The dotted lines indicate the more appropriate interpretation of what happens to the eigenphases and their sum.

is analogous to with Levinson's theorem that the phase shift should start at π if there is one bound state. That is why the resonance feature in the individual $\boldsymbol{K}$ matrix elements shown in figures 4.11 and 4.12 do not yield a resonance feature in the two-channel cross sections.

6.6 Annihilation Rate at the Resonance

The plot in figure 5.1 shows a dramatic feature in Z_{eff} for model V_1 at the position of the resonance. This occurs with or without the virtual positronium included, although the position of the resonance converges more slowly without it (see Section 6.3). This feature is shown in greater detail, together with the elastic scattering cross section, in figure 6.8, with the virtual positronium term included. The resonance feature in Z_{eff} is narrower and much more sharply peaked than is the elastic scattering cross section, with $Z_{\text{eff}} > 10^{11}$!,

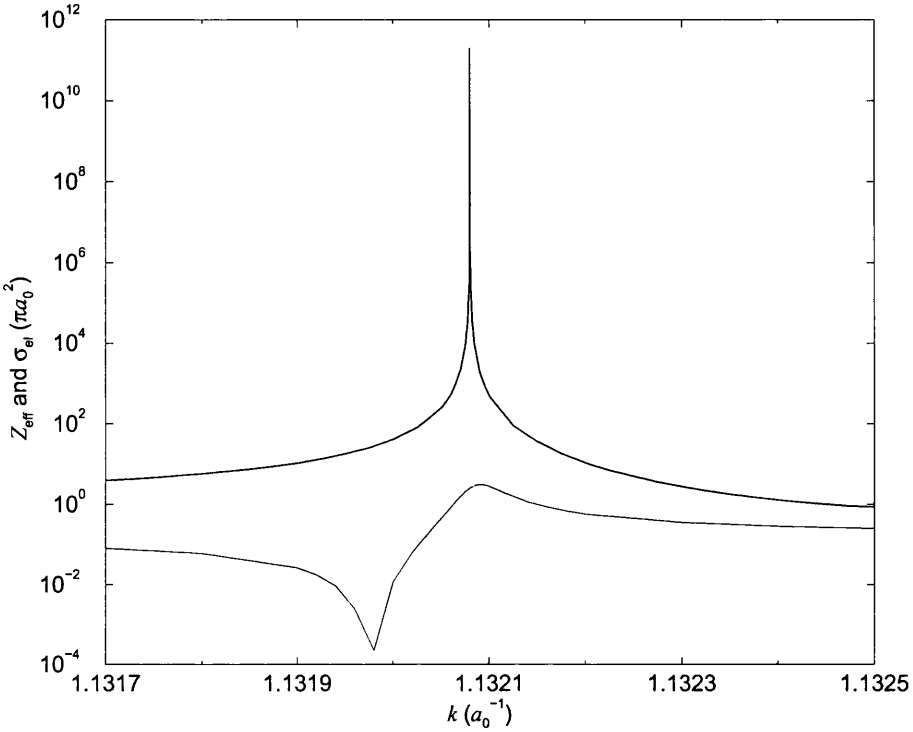

Figure 6.8: Variation of the s-wave contribution to Z_{eff} (thick line) and σ_{el} (thin line) with k at the resonance, with the ϕ_{vps} term included for model V_1.

although σ_{el} peaks at the same energy as does Z_{eff}.

Larger noble gas atoms and some molecules can have $Z_{\text{eff}} \gg Z$, for example positron-xenon scattering yields $Z_{\text{eff}} > 300$ (e. g. Iwata *et al* 1995, Wright *et al* 1985), and these high values are believed to be caused by the positron forming a weakly bound state with the target. The work of Gribakin (2001) has shown that the large values of Z_{eff} ($Z_{\text{eff}} = 1.2 \times 10^5$ for positron-hexane collisions) which arise in many positron-molecule collisions can be explained qualitatively by positron capture into vibrationally-excited states of the positron-molecule system. Although no such mechanism can occur with helium, the evidence discussed above suggests that the positron is nevertheless trapped for much longer than the usual collision time in a resonant state with the model atom.

Although the real positron-helium system has no resonances below E_{th}, the evidence presented above suggests that such a feature is a real feature of the model. We have shown that the resonance feature in model V_1 arises from a virtually bound state, where, in the semi-classical picture, the positron can be trapped for a relatively long period of time on

the model atom.

This unphysical feature is found in some other model potentials (see Peach 1982) which can cause problems in calculations of, for example, the elastic scattering and positronium formation cross sections in the Ore gap.

Chapter 7

Conclusions from the Positron-Helium Collision Study

In Chapters 4, 5 and 6 we have investigated the low energy collision processes involved in positron-atom scattering using one-electron models of the helium atom. The success of these one-electron models has been varied and some very accurate results from other low energy positron-helium collision studies have been reproduced comparatively well, both qualitatively and quantitatively.

The three model atoms used to represent the helium atom showed a mixed rate of success. Initially, from examining the elastic scattering phase shifts for the first model potential, V_1, provided by Peach (1998), the results compare excellently with the results of Van Reeth and Humberston (1999). However, the presence of a resonance just below E_{th}, and across it for the $l \geq 1$ partial waves, unfortunately creates inaccurate results for the two-channel scattering cross sections, both qualitatively as well as quantitatively. Model V_2, also provided by Peach (1998), despite reproducing the same ground state energy, first excited state energy and dipole polarizability of the real helium atom does not reproduce the elastic phase shifts as well as model V_1, although the qualitative agreement was good. However, this model does not support a resonance,and the energy dependence of the elastic scattering and positronium formation cross sections is similar to that of

the accurate results of Van Reeth and Humberston (1999) above $E_{\rm th}$. The third model potential, V_3, represents a simple comparative model, and although the ground state energy, the first excited state energy and the dipole polarizability of the model atom are not the same as those of the real helium atom, the model yields reasonably qualitatively accurate results compared with the crude nature of the model, for both elastic scattering below $E_{\rm th}$ (for this model) and for the positronium formation cross section above. The two channel elastic scattering cross sections are significantly too low, although this is expected from looking at the elastic scattering phase shifts, η, just below $E_{\rm th}$. The elastic cross section, $\sigma_{\rm el}$ is proportional to $\sin^2\eta$, and it can be seen from figures 4.6, 4.13 and 4.14, that the results using model V_3 have phase shifts significantly lower in magnitude at the higher energies resulting in lower elastic cross sections just above $E_{\rm th}$, assuming that the elastic cross section is continuous across the positronium formation threshold. Figure 4.7 shows that when virtual positronium formation is not included in the trial wave function the apparent discontinuity at this threshold is small.

The study of the annihilation processes reveals some problems which may be associated with the nature of one-electron models as a whole. Only direct annihilation was studied here. Although the cross section for direct annihilation was assumed to be too small for this process to be considered as an open channel, the annihilation cross section was examined as a function of the value $Z_{\rm eff}$, the effective number of electrons in the vicinity of the positron. We saw, in the results in Section 5.3, that the results provided by the one-electron models do not fit the accurate results of Van Reeth *et al* (1996) which agreed very well with the experimental results. The value obtained for $Z_{\rm eff}$ at zero energy is $Z_{\rm eff} = 2.56$ (for model V_1), compared with the accurate value $Z_{\rm eff} = 3.93$, but the energy dependence of $Z_{\rm eff}$ is similar to that obtained by Van Reeth *et al* (1996). The Doppler shifts in the energies of the annihilation γ-rays were also calculated but model V_3 provided the best agreement with the results of Van Reeth *et al* (1996). The success of model V_3 in reproducing the Doppler shift in the γ-ray energies and the positronium formation cross section calculated by Van Reeth *et al* (1996) and Van Reeth and Humberston (1999) may

be attributed to the close agreement between the electron density functions of model V_3 and that of Van Reeth and Humberston.

Overall the three models have provided varied degrees of success in reproducing the accurate results of the *ab initio* calculations of Van Reeth and Humberston (1999). No single model represents both the elastic and inelastic collision process accurately but each has its advantages. Model V_3, especially, despite its comparatively crude nature, represents elements of the collisions processes rather well, and it is therefore believed that a one-electron model of helium may be found which can reproduce the elastic scattering and positronium formation cross sections, the Doppler shifts in the energies of the annihilation γ-rays, and the one-electron density function reasonably accurately without supporting a resonance.

Chapter 8

Zero E_{th} Model Atom

8.1 Introduction

The work described in this chapter is related to a correlation found in positron-atom scattering by Humberston and Van Reeth (2000) between the positronium formation cross section, σ_{Ps}, and the positronium formation threshold, E_{th}, of that atom. At a given incident positron energy in excess of E_{th}, a log-linear plot (see figure 8.1) of σ_{Ps} against E_{th} for noble gas targets, yields a straight line implying a relationship between these quantities of the form

$$\sigma_{\mathrm{Ps}} = A\, e^{-BE_{\mathrm{th}}}, \tag{8.1}$$

where A and B are atom-independent parameters which are functions of the excess energy of the positron. The parameter A can therefore be interpreted as the positronium formation cross section for an atom with a zero positronium formation threshold energy. No such atom exists, but considering the qualitative successes of the helium models discussed in the previous chapters, it is possible to create a model atom with $E_{\mathrm{th}} = 0$. The only real 'atom' which has an ionization energy of 6.8 eV is positronium itself, and electron- and positron-positronium scattering has been studied previously (Ward *et al* 1987), so useful information about the energy dependence of A may possibly be obtained from these investigations.

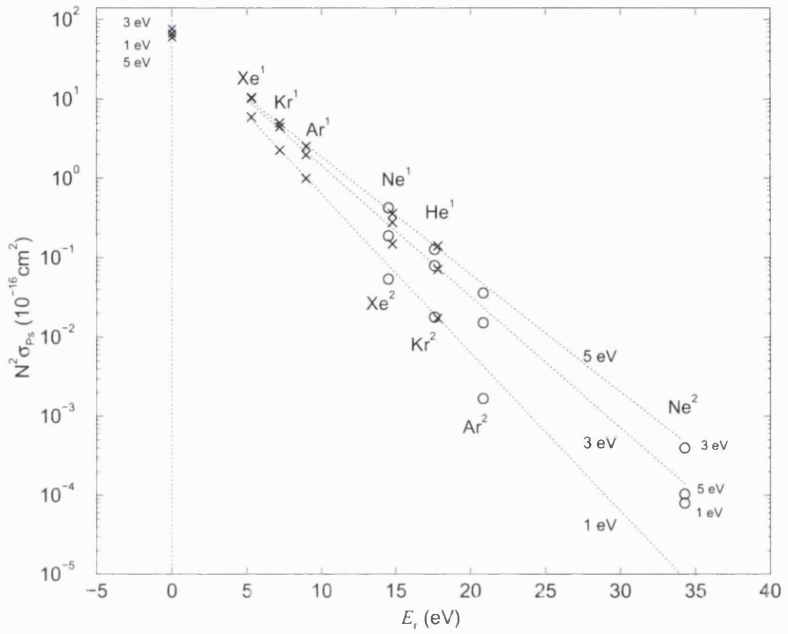

Figure 8.1: Variation of the positronium formation cross sections in single and double ionization of the noble gases with respect to E_r (see text for definition) for three incident positron energies. ×, single ionization; ○, double ionization; superscripts and N refer to degree of ionization. × at $E_r = 0$ are extrapolated points of the single ionization data, ignoring neon.

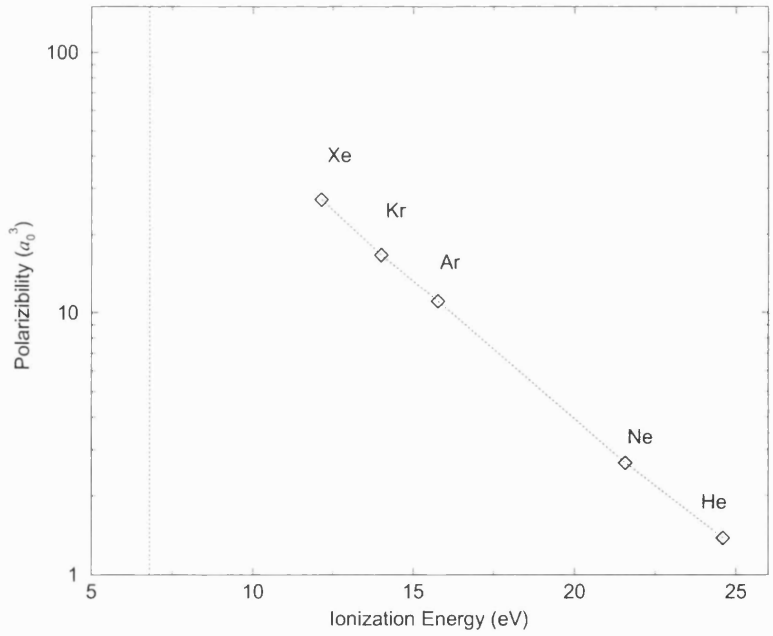

Figure 8.2: Variation of the dipole polarizability of noble gas atoms with respect to the ionization energies. Dotted line parallel to the ordinate marks the ionization energy of positronium.

8.2 Correlations between $\sigma_{\rm Ps}$ and $E_{\rm th}$

The correlations referred to above were first discovered whilst considering the phenomenon of the suppression of positronium formation in the double ionization of atoms by positron impact, i.e. the process

$$e^+ + A \longrightarrow Ps + A^{2+} + e^-. \tag{8.2}$$

Experimental studies by Bluhme *et al* (1998) of positron-impact double ionization of helium and neon atoms showed an almost complete suppression of positronium formation in the 6.8 eV wide energy interval below the threshold for double ionization, where double ionization can only occur in conjunction with positronium formation. This interval is known as the *second Ore gap*. The initial explanation for this suppression was a process called the electron recapture model. Within the second Ore gap, when the positronium is formed and the other electron is ejected, the positronium will be moving slowly in the field of a doubly charged ion. This makes it likely that the electron in the positronium will be recaptured by the ion, resulting in the highly exothermic reaction

$$Ps + He^{2+} \longrightarrow He^+ + e^+. \tag{8.3}$$

The positron will emerge with a kinetic energy close to $\Delta E = (E_{\rm i}^{2+} - E_{\rm i}^{+} - 6.8$ eV), where $E_{\rm i}^{2+}$ and $E_{\rm i}^{+}$ are the double and single ionization energy thresholds respectively. For increasingly heavier noble gases, the value of ΔE becomes smaller, and since this represents the strength of the electrostatic forces responsible for electron recapture, the probability of electron recapture become smaller and $\sigma_{\rm Ps}$ increases.

A similar relation between the energy liberated to the positron, $E_{\rm r}$, and $\sigma_{\rm Ps}$ is expected for positronium formation in single ionization. The relationship for both single and double ionization has the form

$$\sigma_{\rm Ps}^{N} = \frac{A}{N^2}\, e^{-BE_{\rm r}}, \tag{8.4}$$

where $E_{\rm r} = (E_{\rm i}^{+} - 6.8$ eV$) = E_{\rm th}$ and $N = 1$ for single ionization and $E_{\rm r} = (E_{\rm i}^{2+} - E_{\rm i}^{+} - 6.8$ eV$) = \Delta E$ and $N = 2$ for double ionization. N is an *ad hoc* parameter but the values

given above give the best fit to the experimental data. Figure 8.1 shows a good correlation between σ_{Ps} and E_{r} for different atoms.

The coefficients A and B are dependent on the excess energy of the positron but are atom-independent. This pattern also holds for the alkali atoms as well, with a different set of coefficients A and B and the modulus of E_{r} being substituted in the exponent, so that the lighter alkalis (e.g. lithium and sodium) have the higher σ_{Ps} than the heavier alkalis. Because of the fit to the alkali atoms, it seems that the mechanism behind this σ_{Ps} suppression is due to the kinematics of the positron in the field of the atom.

Positronium formation in noble gas atoms is an endothermic process, that is, the incoming positron loses energy by capturing the electron and forming positronium. The outgoing positronium moves away from the atomic ion with less energy than the incoming positron, which must therefore be slowed enough to form positronium. This is less likely in the tightly bound light noble gas atoms, resulting in lower positronium formation cross sections, but is more likely in the heavier gas targets with more extended electron clouds.

Conversely, positronium formation in the alkali atoms is exothermic, so the incoming positron must gain energy and speed up to form positronium which is ejected from the atomic ion. This is more likely in relatively tightly bound light alkali atoms where the positron can interact strongly with the positive atomic core, resulting in higher positronium formation cross sections than for the heavier alkalis with better shielded nuclei.

This is a semi-classical qualitative argument with no explanation for the form of equation (8.4). More studies need to be made, but similar relationships also hold surprisingly well between ionization cross sections and ionization threshold energies in electron-, proton- and antiproton-atom collisions above the ionization thresholds, with a different set of A and B coefficients for each projectile and target atom group (Van Reeth *et al* (2001).

The work that follows is the construction of a model atom with a binding energy equal to that of positronium for which σ_{Ps} should approximate to the parameter A in equation (8.1). The positronium formation process is then neither endothermic nor exothermic. We

will also discuss the electron- and positron-positronium scattering calculations made by Ward *et al* (1987).

8.3 Model Atom with $E_{\text{th}} = 0$

When creating the model atom we have to recognize the limitations in the model itself. We only have two pieces of data with which to fit this model atom, the ground state energy, E_0, and the dipole polarizability, α. Figure 8.2 shows how the dipole polarizability increases as the single ionization energy of the atom approaches 6.8 eV. Extrapolating the points to fit an atom with an ionization energy of 6.8 eV gives an estimated dipole polarizability $\alpha \approx 100\ a_0^3$. It seems appropriate, therefore, to construct a model atom with a ground state energy $E_0 = -0.25$ a.u. and a dipole polarizability of approximately $\alpha = 100\ a_0^3$.

In order to provide a comparison of the positronium formation cross section for this model atom with the energy dependence of A derived from the experimental noble gas data, calculations must be carried out up to an incident positron energy of a few electron-volts. Therefore the lowest inelastic threshold of this model atom, the first excitation threshold with energy E_1, must be high enough above the ground state to provide a sufficient energy range.

Since the model is not representing any real atom we can start with a potential similar to the first two terms in the one-electron model potential used in Chapter 3, equation (3.4). It seems justifiable to start with an electron-core potential of the form

$$V^-(r) = -\frac{1}{r} - \left(\frac{1}{r} + \delta + \delta' r\right) e^{-\gamma r}, \tag{8.5}$$

or an even simpler model,

$$V^-(r) = -\frac{1}{r} - \delta e^{-\gamma r}, \tag{8.6}$$

which, by comparison, might be helpful in determining the validity of any other model.

Using the Rayleigh-Ritz variational method, described in Chapter 3, the parameters δ, δ' and γ can be varied to fit the required ground state energy and the dipole polarizability.

We must now consider the choice of a positron-core potential. The easiest choice will be to use the negative of the electron-core,

$$V^{+}(r_1) = -V^{-}(r_1) = \frac{1}{r_1} + \left(\frac{1}{r_1} + \delta + \delta' r_1\right) e^{-\gamma r_1}, \tag{8.7}$$

and the electron-positron potential is

$$V^{e^-e^+} = -\frac{1}{r_{12}}. \tag{8.8}$$

The limitations mentioned above mean that any results obtained with these models cannot accurately represent the limiting case of an increasingly massive noble gas atom for which E_0 would approach -0.25 a.u., but the comparison of a few models may at least provide adequate data to compare with the data derived from the correlation plots.

The positronium formation cross-section is calculated in the same way as has been described in Chapters 2 and 4, using the Kohn variational method with a similar form of the two-channel wave function to that used in Chapter 4.

Three model potentials have been created, split into two types. The first type, which uses the electron-core potential from equation (8.5), are models V_1^M and V_2^M, and the second, which uses the electron core potential given in equation (8.6), is model V_3^M. All the model potentials reproduce a ground state energy of $E_0 = -0.25$ a.u. to 4 decimal places. Only model atoms of the first type, equation (8.5), contain enough parameters to fit both the ground state energy and the required dipole polarizability, $\alpha = 100.0\ a_0^3$. The properties of the three models are given in table 8.1 and the potential parameters, δ, δ' and γ, are given in appendix A.

8.4 Electron- and Positron-Positronium Scattering

Detailed *ab initio* studies of the elastic scattering of electrons and positrons from positronium were made by Ward *et al* (1987). Because positronium, by definition, has a positronium formation threshold at $k = 0$, the results from this work may be used to provide some data comparable to those obtained from the model atom described above. Although

Table 8.1: Properties of three model atoms with $E_0 = -0.25$ a.u.: ground state energy (E_0), first excited state (E_1), the wavenumber of the incident positron at the first excitation threshold k (a_0^{-1}), full dipole polarizability of the model atom (α).

Model	E_0(a.u.)	E_1(a.u.)	$k(a_0^{-1})$	$\alpha(a_0^3)$
V_1^M	-0.2499993	-0.07715	0.597	100
V_2^M	-0.2499861	-0.05778	0.620	100
V_3^M	-0.2499943	-0.08987	0.566	43

there are similarities which make the work of Ward *et al* (1987) useful for this study, there are also some important differences which need to be taken into account.

The first obvious difference is the mass of the target 'atom'. The lepton-positronium system has no particle at its centre of mass whereas in the positron-atom scattering system, the centre of mass is taken to be at the position of the target atom core. The second difference is that the incident particle has an indistinguishable partner in the target, which means that exchange between the incoming particle and the identical particle in the target needs to be taken into consideration. Because of charge conjugation symmetry, electron-positronium scattering has exactly the same cross section as positron-positronium scattering.

The work of Ward *et al* (1987) provided the singlet and the triplet phase shifts for elastic scattering, using the Kohn method, with s-, p-, d- and f-partial waves contributions being evaluated. The asymptotic forms of the s-wave singlet and triplet trial wave functions, for example, are

$$\Psi_t^{\pm}(\rho, r) \underset{\rho\to\infty}{\sim} Y_{0,0}\sqrt{k}\frac{1}{\sqrt{2}}(1 \pm P_{12})\left[\frac{\sin k\rho}{k\rho} + \tan\eta_t^{\pm}\frac{\cos k\rho}{k\rho}\right]\Phi_{\mathrm{Ps}}(r), \tag{8.9}$$

where P_{12} is the space exchange operator, ρ is the coordinate between the centre of mass of the positronium and the incoming lepton and η^+ and η^- are the singlet and triplet

trial phase shifts respectively. The positronium wave function is known exactly, $\Phi_{\rm Ps} = \frac{1}{\sqrt{8\pi}} e^{-\frac{1}{2}r_{12}}$.

These wave functions can be manipulated into the form we require, where we need no exchange contribution, since all the particles are assumed to be distinguishable, but a rearrangement channel (positronium formation) is required. If we define our system to be an incoming positron scattering from a positronium target where the particles are distinguishable, then the required trial wave function Ψ^t is related to Ψ^+ and Ψ^- by

$$\Psi_t^{\pm}(\rho, r) = (1 \pm P_{12})\, \Psi^t, \tag{8.10}$$

so

$$\Psi^t = \left(\Psi^+ + \Psi^-\right), \tag{8.11}$$

In order to calculate the elastic and rearrangement channel cross-sections, we need a two component wave function where the first component is as above, i. e. $\Psi_1^t = \Psi^t$, and the second component represents the time reverse situation. So the two-component wave function has the asymptotic forms

$$\begin{aligned} \Psi_1^t &\underset{\rho\to\infty}{\sim} Y_{0,0}\left[\frac{\sin k\rho}{k\rho} + \left(\tan\eta_t^+ + \tan\eta_t^-\right)\frac{\cos k\rho}{k\rho}\right]\Phi_{\rm Ps}(r) \\ &\underset{\rho'\to\infty}{\sim} Y_{0,0}\left(\tan\eta_t^+ - \tan\eta_t^-\right)\frac{\cos k\rho'}{k\rho'}\,\Phi_{\rm Ps}(r'), \end{aligned} \tag{8.12}$$

$$\begin{aligned} \Psi_2^t &\underset{\rho'\to\infty}{\sim} Y_{0,0}\left[\frac{\sin k\rho'}{k\rho'} + \left(\tan\eta_t^+ + \tan\eta_t^-\right)\frac{\cos k\rho'}{k\rho'}\right]\Phi_{\rm Ps}(r') \\ &\underset{\rho\to\infty}{\sim} Y_{0,0}\left(\tan\eta_t^+ - \tan\eta_t^-\right)\frac{\cos k\rho}{k\rho}\,\Phi_{\rm Ps}(r), \end{aligned} \tag{8.13}$$

where ρ' is the coordinate between the outgoing lepton and centre of mass of the positronium in the rearrangement channel, and r' is the coordinate between the positronium leptons in the rearrangement channel.

Now we have a trial wave function comparable to the two channel wave function described in the derivation of the Kohn method in equation (2.65), where the new variational $\boldsymbol{K}$ matrix elements are simply related to the singlet and triplet variational phase shifts calculated by Ward *et al* (1987) in such a way that

$$K_{11} = K_{22} = \tan\eta^+ + \tan\eta^- \tag{8.14}$$

$$K_{21} = K_{12} = \tan\eta^{+} - \tan\eta^{-} \quad , \tag{8.15}$$

and the elastic (σ_{11}) and rearrangement (σ_{12}) cross sections are given by

$$\sigma_{pq} = \frac{4\pi(2l+1)}{k^2}\left|\left(\frac{\boldsymbol{K}}{\mathbf{1}-i\boldsymbol{K}}\right)_{pq}\right|^2 . \tag{8.16}$$

8.5 Results

The positronium formation cross sections obtained from the various positron-model atom scattering calculations, and also from the modified positron-positronium scattering results of Ward *et al* (1987) are shown in figures 8.3-8.9. The main features of the cross sections are the differences close to $k = 0$ and the convergence pattern of the results for the different potentials at higher energies, $k > 0.2\ a_0^{-1}$. At these energies the results within each model are well converged within the accuracy required to fit to the data fit shown in figure 8.1. The low energy discrepancies are believed to arise from the high polarizability of the models.

At low energies the model atom is most susceptible to distortion by the incident positron, so extra intermediate-range terms which account for the p-type distortions of the atomic target or the positronium should be included in the trial wave function. The new terms called *polarized orbital* terms (see Temkin and Lamkin 1961) are of the form

$$\Phi^1_{\rm pol} = Y_{l,0}\left(\theta_1,\phi_1\right)\cos\theta_{12}\left(r_2+\frac{r_2^2}{2}\right)\frac{g_1(kr_1)}{r_1^q}\phi_{\rm He}(r_2) \tag{8.17}$$

$$\Phi^2_{\rm pol} = Y_{l,0}\left(\theta_\rho,\phi_\rho\right)\cos\theta_{\rm Ps}\left(2r_{12}+\frac{r_{12}^2}{2}\right)\frac{g_2(\kappa\rho)}{\rho^q}\phi_{\rm Ps}(r_{12}), \tag{8.18}$$

where the functions g_i $(i = 1,2)$ represent either the Bessel or Neumann functions in the appropriate coordinates, i. e. $g_1(kr_1) = j_l(kr_1)$ or $n_l(kr_1)f_{sh}$ (f_{sh} is the appropriate shielding function for the Neumann function) and $g_2(\kappa\rho) = j_l(\kappa\rho)$ or $n_l(\kappa\rho)f_{sh}$. The effect of these terms on the convergence of the positronium formation cross sections can be seen in figure 8.10. Notice that the polarized orbital terms do not greatly affect the results at higher impact energies.

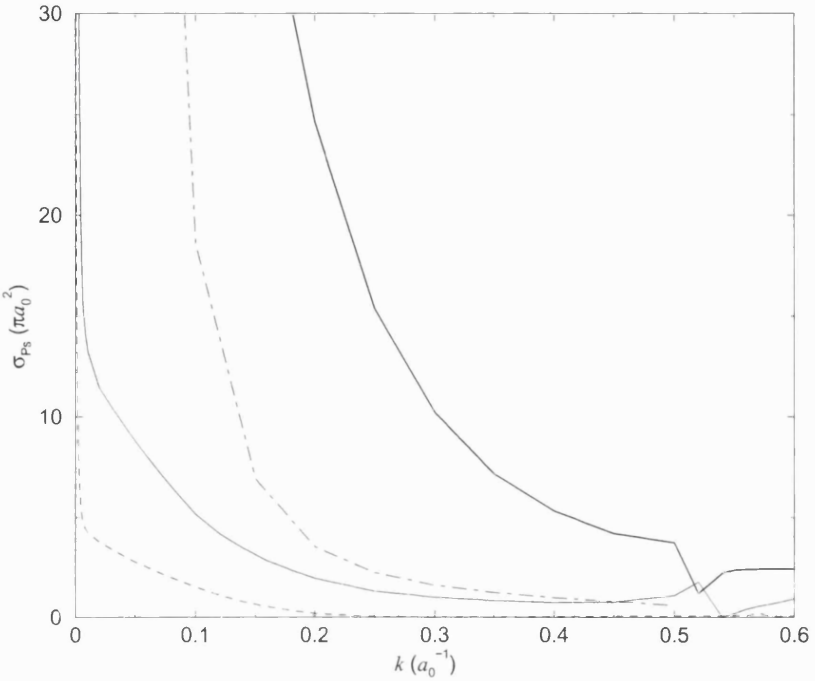

Figure 8.3: Variation of the s-wave positronium formation cross section $\sigma_{\rm Ps}$ with respect to the positron wavenumber k for various model atoms with $E_0 = E_{\rm Ps}$ with $\omega = 8$. Thick line, V_1^M; thin line, V_2^M; dashed line; V_3^M; chain curve, results obtained using data of Ward *et al* (1987) for positron-positronium scattering (see Section 8.4).

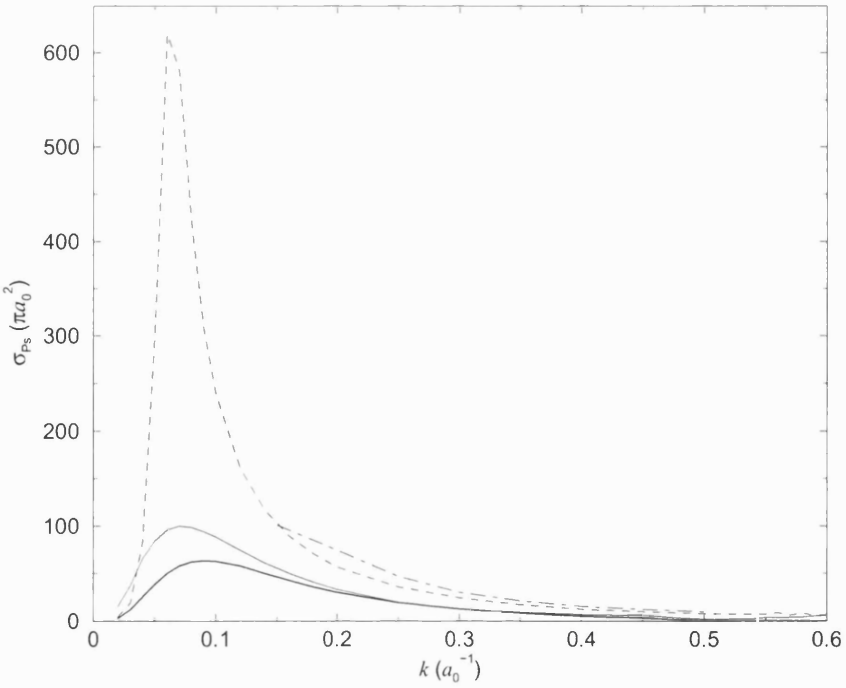

Figure 8.4: Variation of the p-wave $\sigma_{\rm Ps}$, with respect to k for model atoms with $E_0 = E_{\rm Ps}$ with $\omega = 8$. See caption to figure 8.3 for legend.

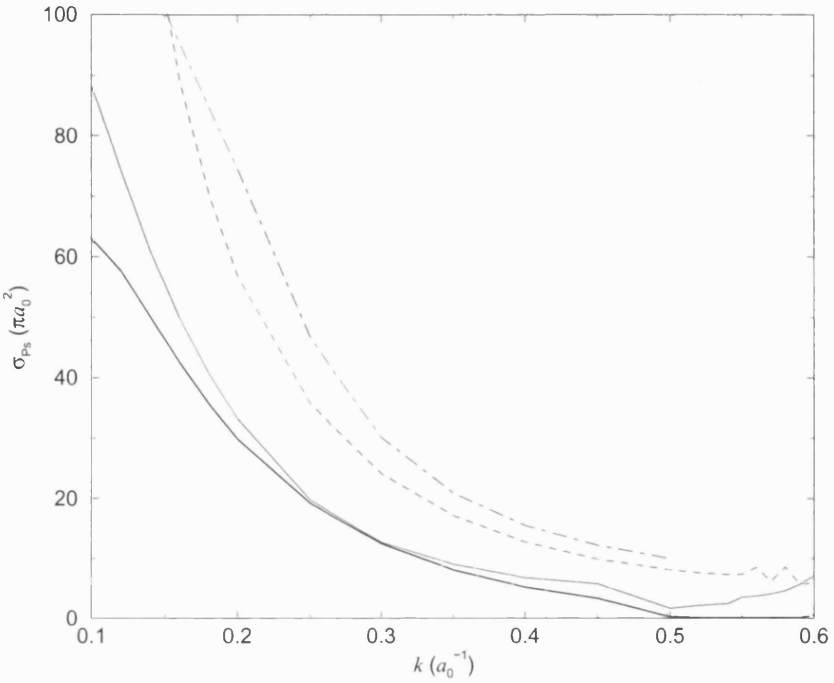

Figure 8.5: Variation of the p-wave σ_{Ps}, with respect to k for model atoms with $E_0 = E_{\mathrm{Ps}}$ with $\omega = 8$. See caption to figure 8.3 for legend.

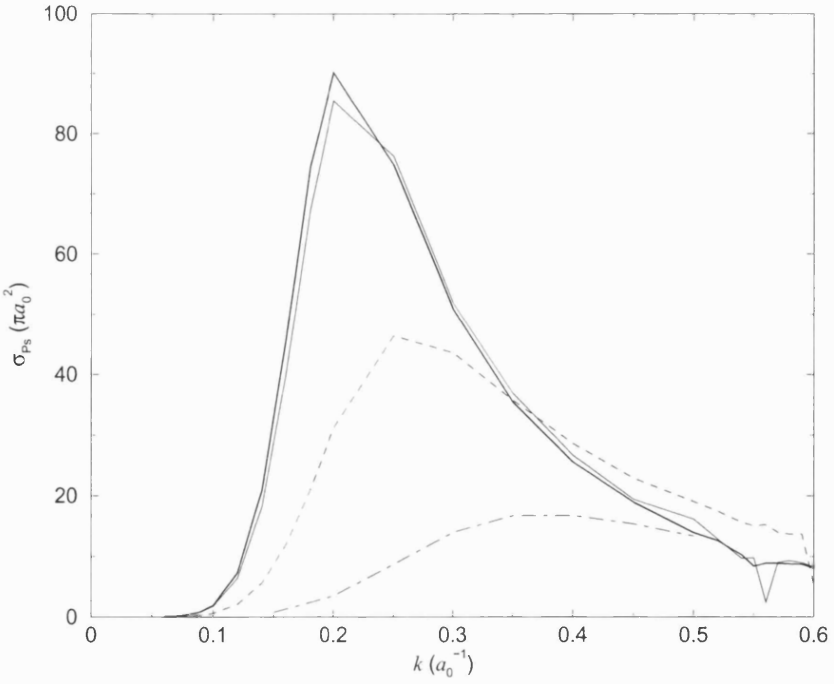

Figure 8.6: Variation of d-wave σ_{Ps}, with respect to k for model atoms with $E_0 = E_{\mathrm{Ps}}$ with $\omega = 8$. See caption to figure 8.3 for legend.

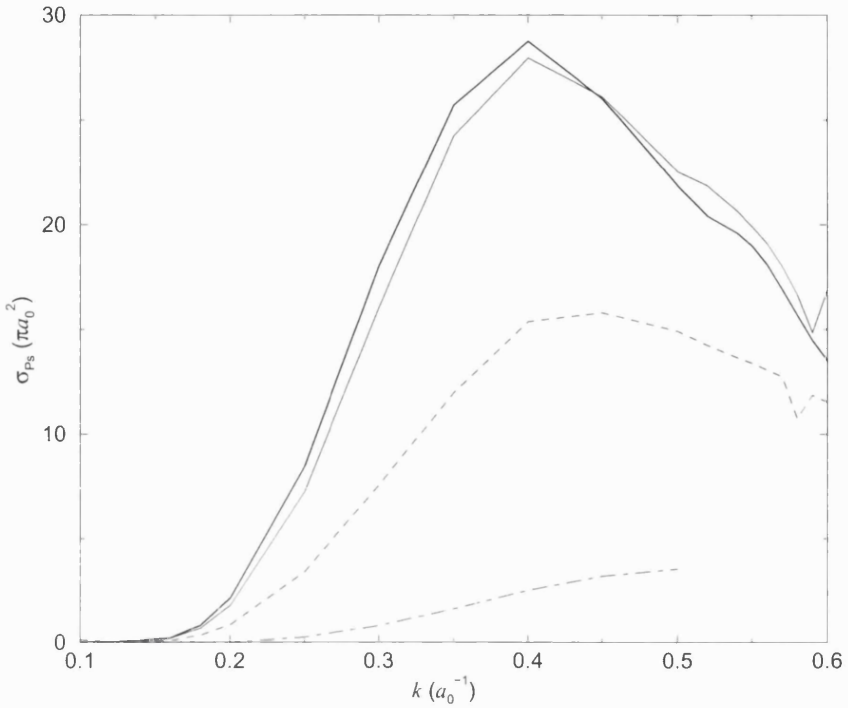

Figure 8.7: Variation of f-wave $\sigma_{\rm Ps}$, with respect to k for model atoms with $E_0 = E_{\rm Ps}$ with $\omega = 8$. See caption to figure 8.3 for legend.

The behaviour of the s-wave contribution to $\sigma_{\rm Ps}$ close to $k = 0$ should be sensitive to the precise value of the ground state energy of the model atom. Wigner's threshold theory (see equations 4.62-4.66) predicts the energy dependence of $\sigma_{\rm Ps}$ for endothermic processes, however a more appropriate method of finding the threshold energy dependence for $\sigma_{\rm Ps}$ for this system is using the fact that the energy dependence for inelastic processes is given by the first Born approximation (see for example Bardsley and Nesbet 1973) where

$$K_{12} \propto k^{1/2}\kappa^{1/2}. \tag{8.19}$$

Therefore, since $\sigma_{\rm Ps} \propto \mid K_{12} \mid^2 /k^2$, then $\sigma_{\rm Ps} \propto \kappa/k$. In exothermic reactions, such as positronium formation from positron-lithium scattering, $k \rightarrow 0$ as κ tends to a finite constant and the threshold energy dependence is $\sigma_{\rm Ps} \propto 1/k$. In this system, with a target atom with a ground state energy equal to that of positronium, k is directly proportional to κ and hence as $k \rightarrow 0$, $\sigma_{\rm Ps}$ tends to a finite constant.

The results plotted in figure 8.3 indicate that $\sigma_{\rm Ps}$ tends to infinity as $k \rightarrow 0$ and are consistent with the values of the ground state energies of the models in 8.1 which show that

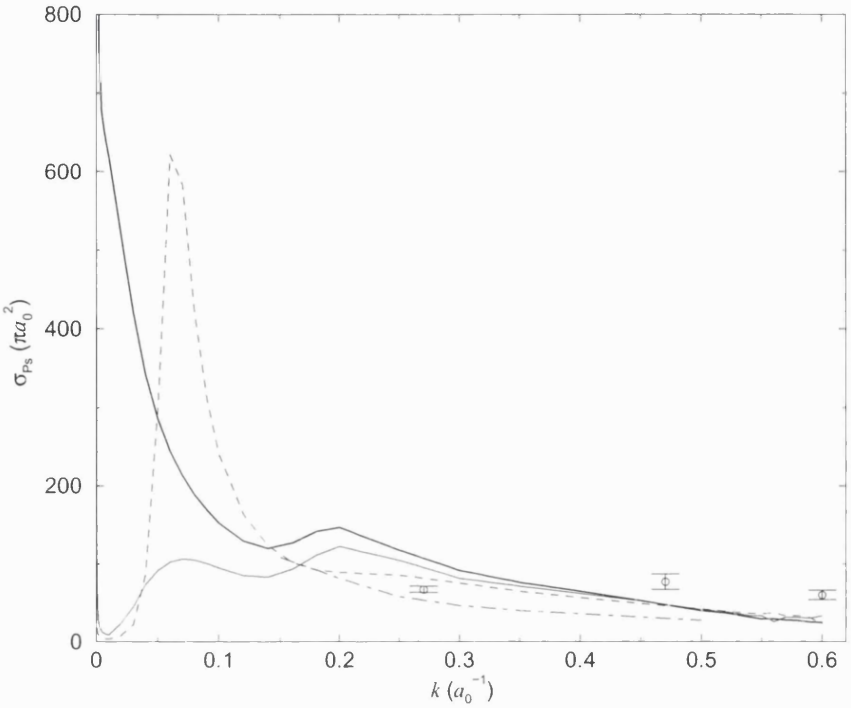

Figure 8.8: Variation of the sum the of s-, p-, d- and f-partial wave positronium formation cross section contributions, $\sigma_{\rm Ps}$, with respect to the positron wavenumber k for model atoms with $E_0 = E_{\rm Ps}$ with $\omega = 8$. Thick line, V_1^M; thin line, V_2^M; dashed line; V_3^M; chain curve, results for calculations using data of Ward *et al* (1987) (see Section 8.4); ∘, extrapolation from experimental data (see parameter A in equation 8.1 and $\overline{\sigma_{\rm Ps}}$ in table 8.2).

positronium formation from these model atoms is a slightly exothermic reaction. However, these threshold effects occur over a narrow energy range.

Another feature of all three of these models is the existence of a bound state of the positron-atom system lying below the ground state energy, which provides another close analogy with positron-positronium scattering. Figure 8.11 shows the eigenvalues for model V_1^M (see Section 6.2), and it can be seen that there is a bound state with an energy between -0.26 a.u. and -0.28 a.u. This state draws a parallel with the bound state of a positron or electron with positronium called the positronium ion. The most recent calculations of Ho (1993) and Frolov and Yeremin (1989) provide a binding energy of the positron to the positronium of 0.012 a.u., so the positronium ion has a ground state energy of -0.262 a.u.

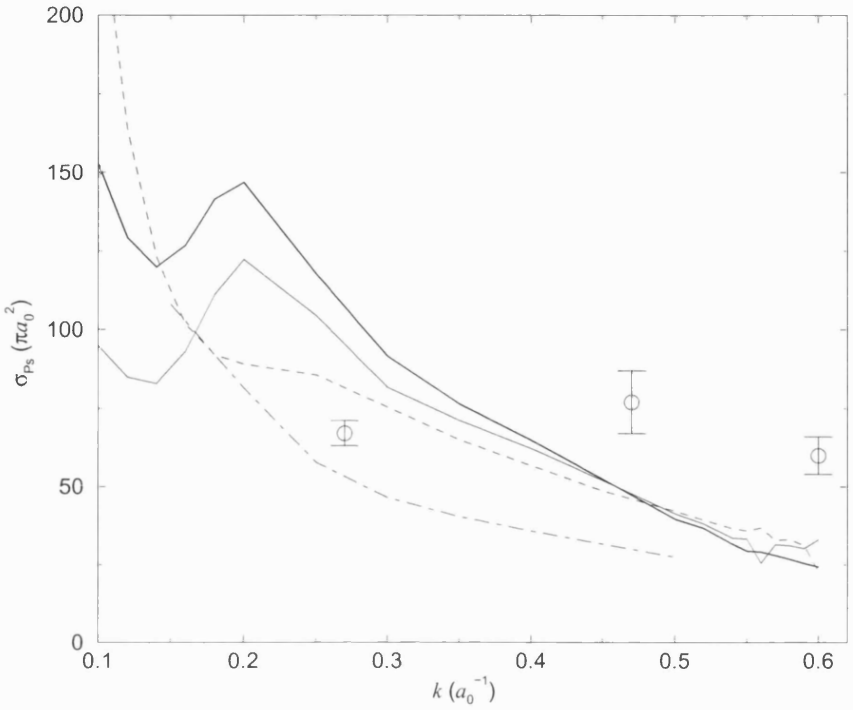

Figure 8.9: Variation of sum of s-, p-, d- and f-partial wave positronium formation cross section contributions, σ_{Ps}, with respect to the positron wavenumber k for model atoms with $E_0 = E_{\mathrm{Ps}}$ with $\omega = 8$. See caption to 8.8 for legend.

The bound state of the positron and the model atoms has an energy comparable to this and, as with the positronium ion, there are no excited bound states of the positronium ion system.

These states do not seem to affect the cross sections noticeably but the $\boldsymbol{K}$-matrix elements do pass through zero due to the eigenphase sum starting at π when $k = 0$ and passing through $\pi/2$ at higher energies (see the discussion in Section 6.5).

The results gained from the data of Ward *et al* (1987), show a very similar energy dependence in each of the partial wave contributions to σ_{Ps} to those of our model atoms. In order to compare the results more precisely a scaling factor would need to be introduced to account for the difference in the masses of the particles and the dipole polarizability of the targets involved in positron-positronium scattering, and positron-atom scattering.

The sum of the s-, p-, d- and f-wave contributions to σ_{Ps} plotted in figures 8.8 and 8.9 provide a reasonably good fit to the energy dependence of the parameter A in equation

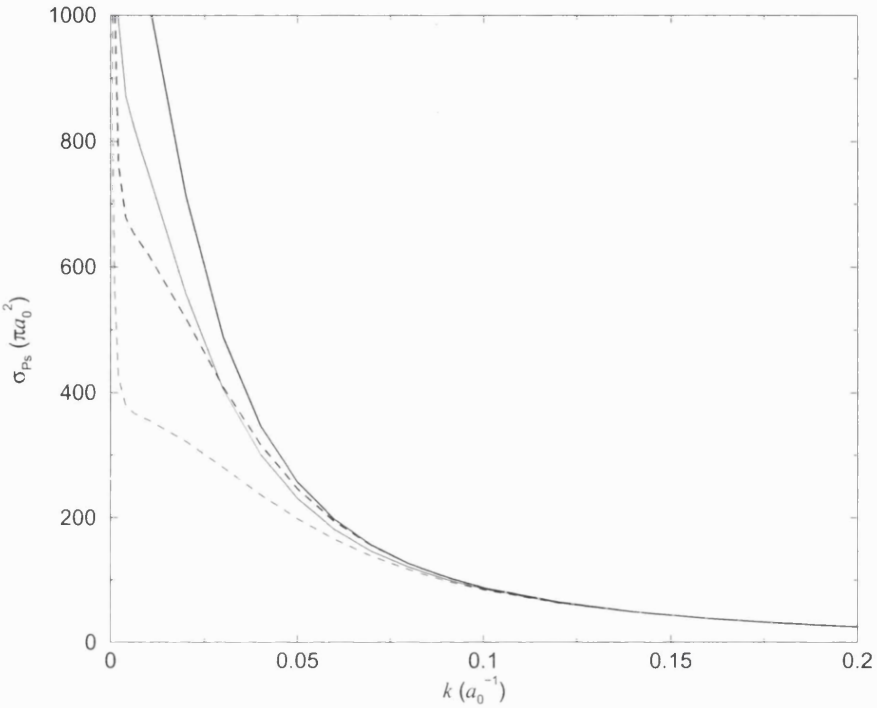

Figure 8.10: Variation of the s-wave positronium formation cross section, $\sigma_{\rm Ps}$, with respect to the positron wavenumber, k for model V_1^M. Thick solid line, four $\Phi_{\rm pol}$ terms included, $\omega = 8$; thin solid line, four $\Phi_{\rm pol}$ terms included, $\omega = 6$; thick dashed line, no $\Phi_{\rm pol}$ terms included, $\omega = 8$; thin dashed line, no $\Phi_{\rm pol}$ terms included, $\omega = 6$.

(8.1), this being the extrapolation to $E_{\rm th} = 0$ of the experimental data shown in figure 8.1 and in table 8.2. An average value of $\sigma_{\rm Ps}$ between the three models are taken, $\overline{\sigma_{\rm Ps}^M}$, and compared with the extrapolated experimental points, $\overline{\sigma_{\rm Ps}}$. The agreement between the results for the model atom and the extrapolated experimental results is not all that good quantitatively, but there is satisfactory qualitative agreement. Note that the f-wave contributes significantly, hence so may higher partial waves. This could explain the differences with the experimental results.

8.6 Conclusion

The positronium formation cross sections obtained using models to represent the atoms with a zero energy positronium formation threshold, $E_{\rm th} = 0$, are reasonably consistent with the observed correlation of the positronium formation cross sections, $\sigma_{\rm Ps}$, at different

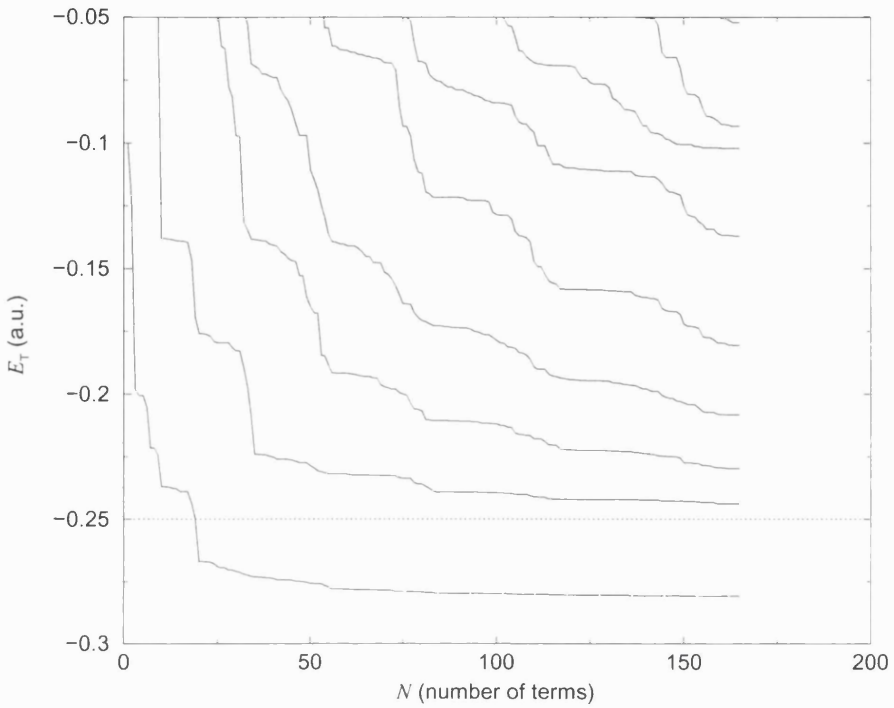

Figure 8.11: Variation of the lowest eigenvalues of the Hamiltonian matrix for the positron-model atom system with $E_0 = E_{\mathrm{Ps}}$ for model V_1^M with respect to increasing N, the number of short-range correlation functions in the basis. The ground state energy of the model atom is $E = -0.25$ a.u., but the lowest eigenvalue of the positron-atom system converges to a value below this, establishing the existence of a bound state of the positron-model atom system.

energies for different noble atoms with the value of E_{th} for each of the these atoms. Despite the limits of the one-electron models discussed in Chapter 7, the relatively simple nature of the models used, and the crude assumptions made about them, regarding positron-core interactions, dipole polarizability, the angular momenta and number of the actual orbiting electrons represented by the model, these models have proved to be reasonably successful. Each of the three models studied in this work have different forms of σ_{Ps} at or near zero incident positron energy but all merge to similar values at higher energies (see figure 8.8). The results yielded by the models at the threshold all fit the threshold law for an exothermic reaction, described in equation (8.19), but have forms which are dependent on the detailed structure of the potentials and the precise value of the ground

Table 8.2: Comparison of the sum of the s-, p-, d- and f-wave positronium formation cross sections at different energies, labelled in electron-volts (E), and positron wavenumbers (k). $\overline{\sigma_{\rm Ps}^M}$ is the mean of the positronium formation cross section for the three model atoms; $\overline{\sigma_{\rm Ps}}$ is the extrapolated value of $\sigma_{\rm Ps}$ from the experimental data for the noble gases for an atom with $E_0 = E_{\rm Ps}$ (see figure 8.1).

E(eV)	k (a_0^{-1})	$\overline{\sigma_{\rm Ps}^M}$ (10^{-16}cm^2)	$\overline{\sigma_{\rm Ps}}$ (10^{-16}cm^2)
1	0.27	94±10	67±4
3	0.47	47±1	77±10
5	0.60	27±5	60±6

state energy for the model. We also investigated three other models which did not violate any threshold laws but the expected threshold behaviour was over such a narrow energy range that the necessary behaviour would not be noticeable compared to the range and structure of $\sigma_{\rm Ps}$ for the other models. An interesting feature of all these models was a bound state of the positron-model atom system at an energy just below the ground state of the model atom, revealed by the stabilization method (see figure 8.11). This bound state lies at a similar energy to that of a positron bound to positronium forming Ps^+. Analogies were made between the nature of these model atoms and the positronium atom. Indeed, the structure of our approximations to $\sigma_{\rm Ps}$ obtained from the phase shifts calculated by Ward *et al* (1987) for positron-positronium scattering, show a similar energy dependence to those calculated using the model atoms, with an expected energy rescaling related to the differences in the relative masses of the two systems.

It can be seen in table 8.2 that, although the agreement between the results for the models and the extrapolated experimental results is not all that good quantitatively, there is nevertheless satisfactory qualitative agreement. The results from our calculations of the

positronium formation cross section for an atom with a binding energy equal to that of positronium itself can therefore be considered as providing support for the interpretation of the parameter A in equation (8.1) as the positronium formation cross section for an atom with a zero threshold energy for this process.

Chapter 9

Hydrogen-Antihydrogen Collisions

9.1 Introduction

Dirac's (1928) prediction of the positron, and subsequent discovery, lead also to the postulation that for every particle in nature there is a corresponding antiparticle. The ATHENA project at CERN aims to create the simplest antimatter atom - antihydrogen consisting of a positron orbiting an antiproton. The production of antihydrogen should enable the most rigorous tests to be made so far of CPT symmetry and the WEP (see Chapter 1). Antihydrogen atoms have been made at very high energies (moving close to the speed of light) but they have not yet been trapped and subjected to detailed investigation. However, with the ability to cool antiprotons to very low energies, it should soon be possible to form, and trap, cold antihydrogen. It is therefore important to understand how antihydrogen will react with ordinary matter within the experimental apparatus at very low temperatures (< 1 K). The main cause of loss of antihydrogen from the trap is expected to be collisions with molecular hydrogen (H_2) and atomic helium, so it is of interest to study the collisions with these atoms. It has also been proposed that elastic collisions with hydrogen may be used to cool the antihydrogen (Jonsell *et al* 2001).

The theoretical study of hydrogen-antihydrogen collisions is far from comprehensive or complete, though this system has been studied in reasonable detail. The purpose of the present work is to investigate the viability of using techniques developed by Van

Reeth and Humberston (1999), and used successfully by them for investigating the four-body positron-helium scattering problem, to investigate the four-body system of hydrogen-antihydrogen scattering. Similar techniques might then be used to investigate helium-antihydrogen scattering using a one-electron model of helium.

9.2 Theory

Hydrogen-antihydrogen scattering is a four body system, but there is no particle at the centre of mass of the system. There have been several previous studies of the hydrogen-antihydrogen system, most notably by Kolos *et al* (1975), Armour *et al* (1998) and Jonsell *et al* (2001). All these studies have used the Born-Oppenheimer approximation, and the molecular-like interaction energy of the hydrogen-antihydrogen system has been calculated using the Rayleigh-Ritz variational method (described in Chapter 3). An accurate interaction potential energy curve between the two atoms can be found and one-dimensional elastic scattering calculations can be made. However, in these previous works the configuration of the system was expressed in spherical prolate coordinates, which tend to provide a somewhat less transparent representation of the system than do the interparticle coordinates.

If we consider the hydrogen-antihydrogen system when the proton and antiproton are very close together, i. e. the internuclear coordinate $R \simeq 0$, it is obvious that the electron and positron are no longer bound to the nuclei and are free to form positronium. This process of rearrangement is energetically favourable when R is less than a critical distance, R_c. The hydrogen-antihydrogen system can then rearrange itself in to positronium and a bound proton-antiproton system called protonium (Pn), so

$$\mathrm{H} + \overline{\mathrm{H}} \longrightarrow \mathrm{Pn} + \mathrm{Ps}. \tag{9.1}$$

At very low temperatures the positronium is formed in its ground state and the protonium, to conserve energy, is formed in the Rydberg state of $n = 24$. Previous studies of hydrogen-antiproton and proton-antihydrogen (e.g. see Fermi and Teller 1947, Armour and Brown

1993) systems suggest that $0.639\ a_0 < R_c < 0.8\ a_0$. For values of $Rc < 0.639\ a_0$ the two leptons can certainly not bind to the proton and antiproton.

The results presented here have been obtained only from preliminary work, so the inelastic rearrangement channel is not included, although below a certain temperature the rate of inelastic collisions is expected to be greater than the elastic collision rate, and consequently annihilation will ultimately be the dominant collision process. With the method described below we can calculate a bound on the critical distance, R_c, below which positronium will be formed, and also calculate the variation of the electron-positron annihilation rate with internucleon separation R. This should provide a basis on which to comment on the success and the limitations of the model.

In order to simplify the model we have used the adiabatic Born-Oppenheimer approximation. This is a valid approximation because the mass of the electron is so much less than that of the proton and therefore the speeds at which the leptons are moving are much greater than those of the nucleons. All the interparticle interactions are taken into consideration but the nuclei are set at a fixed distance R from each other and the total energy of the system is calculated using the Rayleigh-Ritz variational method. The nuclei are fixed at different values of R and an adiabatic approximation to the atom-antiatom interaction potential can then be calculated.

9.2.1 Interaction Energy

The total interaction potential, V_{T}, is the sum of the six interparticle Coulomb potentials, so that, using the nomenclature of figure 9.1

$$V_{\mathrm{T}} = -\frac{1}{r_1} + \frac{1}{r_2} - \frac{1}{r_3} - \frac{1}{r_{12}} + \frac{1}{r_{13}} - \frac{1}{r_{23}}, \tag{9.2}$$

and, since we are working in the adiabatic approximation, the total Hamiltonian can be expressed as

$$H = -\frac{1}{2}\nabla^2_{\boldsymbol{r}_2} - \frac{1}{2}\nabla^2_{\boldsymbol{r}_3} + V_{\mathrm{T}}. \tag{9.3}$$

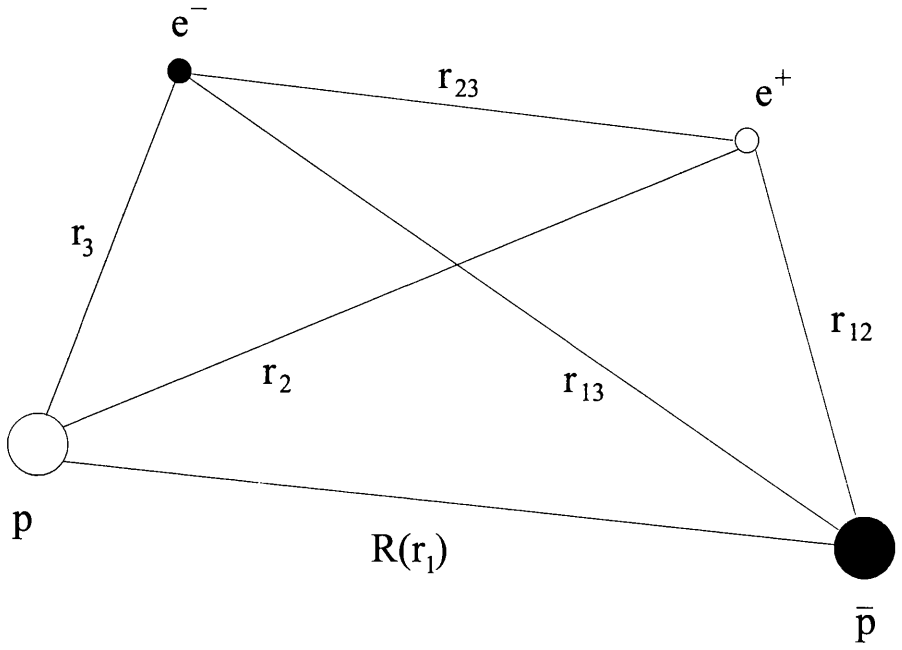

Figure 9.1: Coordinates of the hydrogen-antihydrogen system

The total energy of the system at a given proton-antiproton separation R, $E(R)$, is given by

$$E(R) = \frac{\langle \mathbf{\Phi} \,|H|\, \mathbf{\Phi} \rangle}{\langle \mathbf{\Phi} \mid \mathbf{\Phi} \rangle}, \tag{9.4}$$

where $\mathbf{\Phi}$ is the wave function of the system. The interaction potential $V(R)$ between the hydrogen and antihydrogen is trivially related to $E(R)$ by

$$V(R) = E(R) - E_{\mathrm{H}} - E_{\overline{\mathrm{H}}} = E(R) + 1, \tag{9.5}$$

where $E_{\mathrm{H}}(= -0.5 \text{ a.u.})$ and $E_{\overline{\mathrm{H}}}(= -0.5 \text{ a.u.})$ are the ground state energies of the hydrogen and antihydrogen atoms, respectively. Consequently, $V(R) \to 0$ as $R \to \infty$.

The trial wave function, $\mathbf{\Phi}^t$, is chosen to be of Hylleraas form,

$$\mathbf{\Phi}^t = \sum_{i=0}^{N} c_i \phi_i, \tag{9.6}$$

where

$$\phi_i = e^{-\alpha r_3}\, e^{-\gamma r_{12}}\, r_2^{k_i}\, r_3^{l_i}\, r_{12}^{m_i}\, r_{13}^{p_i}\, r_{23}^{q_i} \tag{9.7}$$

and the non-negative integer indices, k, l, m, p and q, are chosen such that the sum is

equal to or less than the positive integer ω, i.e.

$$k_i + l_i + m_i + p_i + q_i \leq \omega. \tag{9.8}$$

The variational energy of the system at a particular value of R is found by solving the matrix eigenvalue equation,

$$(\boldsymbol{H} - E_0^v \boldsymbol{A})\, \boldsymbol{c} = 0 \tag{9.9}$$

where the matrix elements of $\boldsymbol{H}$ and $\boldsymbol{A}$ are given by

$$H_{ij} = \langle \phi_i \mid H \mid \phi_j \rangle\,, \tag{9.10}$$

$$A_{ij} = \langle \phi_i \mid \phi_j \rangle\,, \tag{9.11}$$

and $\boldsymbol{c}$ is a column matrix listing the optimum values of the linear coefficients in the variational wave function. Since the system under study is symmetric between the hydrogen and antihydrogen atoms, we can establish a symmetry to reduce the number of terms which need to be calculated, and the new variational trial wave function is extended as follows;

$$\phi_i \rightarrow \phi_i + \overline{\phi}_i, \tag{9.12}$$

where $\overline{\phi}_i = P_{(3,12)}\phi_i$, and $P_{(3,12)}$ is an exchange operator which exchanges the coordinates of the hydrogen with those of the antihydrogen. We therefore have symmetry under the interchanges

$$r_3 \leftrightarrow r_{12}, \tag{9.13}$$

$$r_2 \leftrightarrow r_{13}. \tag{9.14}$$

In addition, since there is no explicit difference between the two atoms, it is reasonable to set the two non-linear variational parameters α and γ in the correlation functions, equation (9.7), to be equal, i.e. $\alpha = \gamma$.

9.2.2 Integration Techniques

The evaluation of all the matrix elements H_{ij} and A_{ij} requires integration over the five interparticle coordinates, r_2, r_3, r_{12}, r_{13} and r_{23} for fixed R. The volume element $d\tau$ for

integration over the vectors $\boldsymbol{r}_2$ and $\boldsymbol{r}_3$ for fixed R is

$$d\tau = d\boldsymbol{r}_2 d\boldsymbol{r}_3, \tag{9.15}$$

$$= 2\pi r_2^2 dr_2 \sin\theta_{12} d\theta_{12} r_3^2 dr_3 \sin\theta_{13} d\theta_{13} d\phi_{23}, \tag{9.16}$$

where ϕ_{23} is the angle between the two planes defined by r_1, r_3 and r_{13} and r_1, r_2 and r_{12}. But

$$r_{12}^2 = R^2 + r_2^2 - 2Rr_2\cos\theta_{12}, \tag{9.17}$$

so

$$r_{12} dr_{12} = Rr_2 \sin\theta_{12} d\theta_{12}, \tag{9.18}$$

and similarly $r_{13}dr_{13} = Rr_3\sin\theta_{13}d\theta_{13}$, so the volume element can also be expressed as

$$d\tau = \left(\frac{2\pi}{R^2}\right) r_2 dr_2 r_{12} dr_{12} r_3 dr_3 r_{13} dr_{13} d\phi_{23}. \tag{9.19}$$

The $\boldsymbol{H}$-matrix elements, for example, have the form

$$H_{ij} = \frac{2\pi}{R^2}\int_0^\infty r_2 dr_2 \int_{|r_1-r_2|}^{r_1+r_2} r_{12} dr_{12} \int_0^\infty r_3 dr_3 \int_{|r_1-r_3|}^{r_1+r_3} r_{13} dr_{13} \int_0^{2\pi} \phi_i H \phi_j d\phi_{23}. \tag{9.20}$$

The integrations over the coordinates r_2 and r_3 are performed using the Gauss-Laguerre numerical procedure (see equation 4.38), and those over the coordinates r_{12} and r_{13} are performed using the Gauss-Legendre procedure,

$$\int_a^b F(x)dx \approx \sum_{i=1}^{M} w_i F(x_i), \tag{9.21}$$

where the limits a and b are mapped on to the range -1 and $+1$ to match the formula given in equation (6.7). The integral over the planar angle ϕ_{23} is also performed using a form of Gauss-Legendre quadrature procedure,

$$\int_0^{2\pi} D(\cos\theta)d\theta = \frac{2\pi}{n}\sum_{i=1}^{n} D\left(\cos\frac{(2i-1)\pi}{2n}\right), \tag{9.22}$$

which is exact if D is a polynomial of degree $(2n-1)$ or less. The minimum and maximum values of r_{23} with $\phi_{23} = 0$ and $\phi_{23} = \pi$ respectively can be calculated from the relationships

$$r_{23\min}^2 = r_2^2 + r_3^2 - 2r_2r_3\left(\sin\theta_{12}\sin\theta_{13} + \cos\theta_{12}\cos\theta_{13}\right), \tag{9.23}$$

$$r_{23\max}^2 = r_2^2 + r_3^2 - 2r_2r_3\left(-\sin\theta_{12}\sin\theta_{13} + \cos\theta_{12}\cos\theta_{13}\right). \tag{9.24}$$

The integration over the angle ϕ_{23} is only exact when calculating even powers of r_{23}, but if enough integration points are used then integrals of odd integer powers of r_{23} can also be evaluated to a sufficient degree of accuracy.

This procedure is not sufficiently accurate when evaluating the matrix elements which include the $1/r_{23}$ term in the Hamiltonian. For these integrals, the planar description of the interparticle coordinates are shifted such that the two planes are now defined by r_2, r_1 and r_{12} and r_2, r_3 and r_{23} and the angle between them is ϕ_{13}. Then,

$$d\tau = \left(\frac{2\pi}{R^2}\right) r_2 dr_2 r_{12} dr_{12} r_3 dr_3 r_{23} dr_{23} d\phi_{13}, \tag{9.25}$$

and the integrations are modified accordingly.

9.3 Results

9.3.1 Interaction Energy, $E(R)$

We have calculated the total interaction energy at various interbaryonic distances R down to the lowest bound on the critical distance. The results given in table 9.1 reveal that there is a significant improvement in the upper bound on $E(R)$ when the odd powers of r_{23} are included in the trial wave function. This is also noticeable in the convergence of $E(R)$ as the number of terms in the wave function is increased. The critical distance, R_c, can be found by finding the distance at which the total interaction energy, neglecting the Coulomb attraction between the baryons, is equal to the binding energy of positronium, i.e.

$$E'(R_c) = E(R_c) + \frac{1}{R_c} = E_{\mathrm{Ps}}, \tag{9.26}$$

$$= -0.25 \text{ a.u.} \tag{9.27}$$

where the function $E'(R)$ represents the leptonic energy of the system.

Figure 9.2 shows how $E'(R)$ becomes more negative as the number of terms in the wave function is increased. As with the scattering phase shifts and the $\boldsymbol{K}$ matrix elements

Table 9.1: Comparison of hydrogen-antihydrogen interaction energies, $E(R)$, at R = 1.0 a.u. for different values of ω and numbers of terms, N in the trial wave function. Superscript a refers to both even and odd powers of r_{23} included in the wave function, and superscript b refers to only even powers of r_{23} included.The estimates of the converged values are shown as "$N = \infty$".

ω	N^a	N^b	E^a	E^b
0	1	1	-1.156200	-1.156200
1	4	3	-1.238685	-1.215525
2	13	10	-1.263628	-1.235083
3	32	22	-1.271341	-1.241927
4	70	48	-1.273505	-1.247981
5	136	88	-1.274130	-1.251835
Extrapolated	∞	∞	-1.278323	-1.275071

calculated in Chapters 4 and 8, there is an empirical regular pattern in the convergence of the value of R_c as ω is increased (see figure 9.4).

The values of $E(R)$ were determined by solving equation (9.9), but the calculations were not as straightforward as those described in Chapter 3 for the ground state energy of helium. The solutions of the matrix eigenvalue equations for the hydrogen-antihydrogen system were subject to numerical errors which resulted in two problems; for large matrices (i.e. $\omega \geq 4$) and for values of R close to R_c. Firstly, the results output by the numerical routines used to solve the matrix eigenvalue equations sometimes yielded eigenvalues which were too negative to compare with the results of previous studies. These spurious results are believed to arise from numerical inaccuracies in solving the large matrix eigenvalue equations because numerical anomalies arise when the eigenvalues are recalculated using

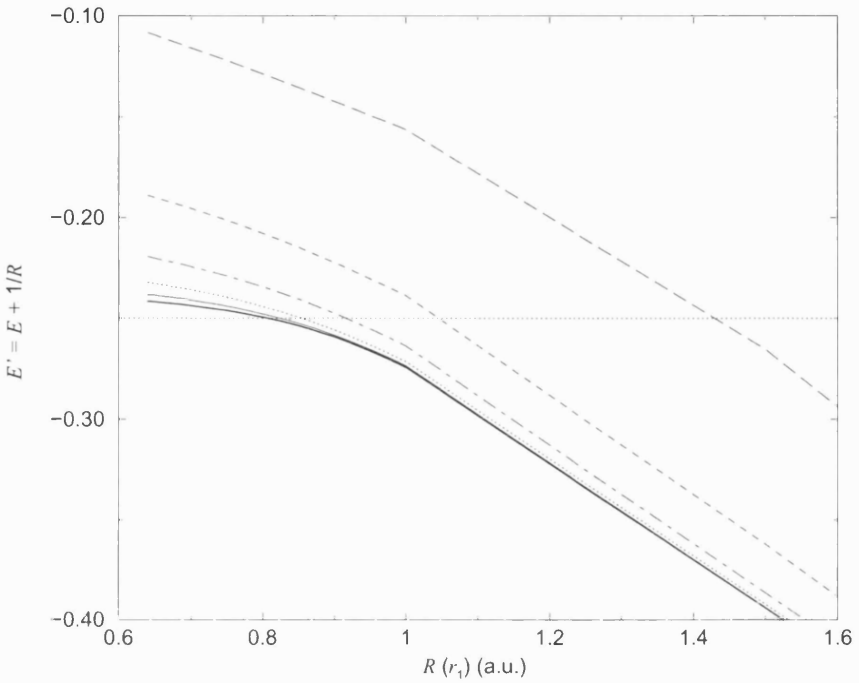

Figure 9.2: Variation of E' with respect to R for different numbers of terms in the wave function, with both even and odd powers of r_{23} included. Thick line, $\omega = 5$, thin line, $\omega = 4$; dotted line, $\omega = 3$; dot-dashed line, $\omega = 2$; short dashed line, $\omega = 1$; long dashed line, $\omega = 0$.

the eigenvector of the coefficients. The equation

$$E^* = \boldsymbol{c}^T \boldsymbol{H} \boldsymbol{A}^{-1} \boldsymbol{c} \tag{9.28}$$

where E^* is the eigenvalue recalculated from the calculated coefficients, $\boldsymbol{c}$, should be satisfied exactly, i.e. $E^* = E$. However, for the lowest few eigenvalues, $E^* \simeq E$ only to the order of only 1 part in 10^2. The values of the interaction potential, $E(R)$, which we have quoted in this work may actually be the fifth or sixth eigenvalue, but then $E^* = E$ to 1 part in 10^5 or better.

The second numerical problem which arises is that the eigenvalues and eigenvectors obtained are sometimes complex, even though the matrices $\boldsymbol{H}$ and $\boldsymbol{A}$ are real and symmetric. This can occur because the matrices are not positive-definite. These problems should not arise in an exact calculation, but we are using numerical techniques which are subject to errors.

Table 9.2: Comparison of the $H - \overline{H}$ potentials, $E(R)$, given by this work with $\omega = 5$, the results of Armour *et al* (1998), Jonsell *et al* (2001), Kolos *et al* (1975) and Chamberlain and Armour (2000).

R(a.u.)	This Work	Armour	Jonsell	Kolos	Chamberlain
0.80	-1.499230	-1.5006	-	-	-1.500376
0.85	-1.430018	-1.4289	-1.428121	-	-1.430612
0.90	-1.370210	-1.3682	-1.368924	-	-1.370514
0.95	-1.318604	-1.3174	-1.317803	-1.314522	-1.318835
1.00	-1.274130	-1.2723	-1.273695	-1.271095	-1.274369

Table 9.2 shows the most accurate results of the present work compared with the results of Kolos *et al* (1975), Armour *et al* (1998), Jonsell *et al* (2001) and the most recent accurate results of Chamberlain and Armour (2000). Kolos *et al* used a total of 77 basis functions containing all integer powers of the interlepton coordinates (r_{23} in this work) between 0 and 2. Armour *et al* used 32 basis functions of effectively the same form as those of Kolos *et al* but they included a term in the wave function representing virtual positronium, in a very similar manner to that used in the positron-helium scattering described in Section 4.4.1. The results in table 9.2 show how effective this term is. Even with less than half the basis functions, the results of Armour *et al* provide a lower value of the interaction energy than do those of Kolos *et al*, which is especially noticeable at values of R close to R_c. Jonsell *et al* (2001) have used a more restricted form of basis function with only two non-linear variational parameters instead of the four used in the two previous references, but 908 basis functions were used containing all integer powers between 0 and 3 of the interlepton coordinates. Although no explicit virtual positronium term was included in the wave function, the addition of the extra power of r_{23} more than makes up for it, providing even lower values of the energy at higher values of R. The work of Chamberlain

and Armour (2000) has built on the work of Armour *et al* (1998) but 426 basis functions have been used, with all integer powers of the interleptonic coordinates between 0 and 6 included. This has provided the lowest bounds on the interaction energy yet obtained for values of $R > R_c$.

In this work we have used up to 136 terms, with all integer powers of r_{23} between 0 and 5 included, and this has yielded a value of the interaction energy somewhere between the results of Jonsell *et al* (2001) and those of Chamberlain and Armour (2000). It can be seen in table 9.2 that the results of this work provide lower values of $E(R)$ compared to Jonsell *et al* (2001) and Kolos *et al*, and that this improvement gets better at lower values of R, indicating that in our methods the higher powers of r_{23} represent virtual positronium reasonably well close to R_c.

Using the empirical extrapolation method described in Section 4.3, we can see how $E(R)$ converges for a particular value of R and estimate the values of $E(R)$ for an infinite number of terms in the trial wave function, i.e. $\omega = \infty$. Above the known upper limits of R_c (< 0.8 a.u.) the convergence seems reasonable (see table 9.1), particularly when the odd powers of r_{23} are included in the wave function.

There is, however, a problem when using this extrapolation method to estimate the value of E' for $R \simeq R_c$. Equation (9.27) shows that, for values of $R < R_c$, then $E'(R) > -0.25$ a.u. As R is decreased to values below $R = 0.8$ a.u., the calculated values of $E'(R)$ for finite ω are all above -0.25 a.u., but their extrapolated values remain below, even for $R = 0.639$ a.u. which is known to be the lower bound on R_c. The extrapolated values of E' for $R < 0.8$ a.u. imply that the positronium is not quite free from the proton and antiproton even when $R = 0.639$ a.u. The Rayleigh-Ritz variational method provides upper bounds on the energy eigenvalues and cannot be violated, that is, for any given wave function the calculated value of $E'(R)$ cannot be below the exact value of $E'(R)$ for the model. This leads to one of two conclusions; either the critical distance R_c is even lower than the lower bound of $R = 0.639$ a.u., or the extrapolation method is not valid in the region where the system is more appropriately described as a free positronium-protonium

system. Since the trial wave function used here is really only suitable to describe the hydrogen-antihydrogen system, we to assume that it is the extrapolation method which is not valid, for $R \simeq R_c$

In order to represent the system close to (and just above) R_c accurately, a representation of virtual positronium must be explicitly included. This is described in greater detail below in Section 9.4.

9.3.2 Annihilation

The rate for direct annihilation of the positron and electron has been evaluated as a function of R. Annihilation occurs at the point when $r_{23} = 0$, so that $r_3 = r_2$ and $r_{12} = r_{13}$, and the annihilation rate, is

$$\Gamma(R) = 2\pi\alpha^4 \left(\frac{c}{a_0}\right) \left[1 - \alpha\left(\frac{17}{\pi} - \frac{19\pi}{12}\right)\right] Z_{\text{eff}} = 100.617\, Z_{\text{eff}}, \tag{9.29}$$

where

$$Z_{\text{eff}}(R) = \frac{\langle \mathbf{\Phi} \,|\delta\,(\boldsymbol{r}_3 - \boldsymbol{r}_2)|\, \mathbf{\Phi}\rangle}{\langle \mathbf{\Phi} \mid \mathbf{\Phi}\rangle} \tag{9.30}$$

and $\mathbf{\Phi}$ is the total wave function for a given value of R. The results of the Z_{eff} calculations in this work have been plotted in figure 9.3. In this system it is not appropriate to interpret Z_{eff} as the effective number of electrons in the vicinity of the electron, as described in Chapter 5. Instead, it is the probability of the positron and electron being at the same position in space. However, we will continue to describe the annihilation using the parameter Z_{eff} since it has an analogous mathematical form (compare with equation 5.3), and $\Gamma(R)$ and Z_{eff} are trivially related by equation (9.29).

When the hydrogen and antihydrogen atoms are quite far apart the overlap of the electron and positron wave functions is small, and the value of $Z_{\text{eff}}(R)$ is therefore very small. As the atoms come closer together Z_{eff} increases, but as R approaches $R_c \simeq$0.8 a.u. Z_{eff} starts to decrease. This is not what would be expected for the system, but there is no variational bound on the calculated value of Z_{eff} although in practice the value of $Z_{\text{eff}}(R)$ usually increases as ω increases, as can be seen in figure 9.3. The decrease in the value of

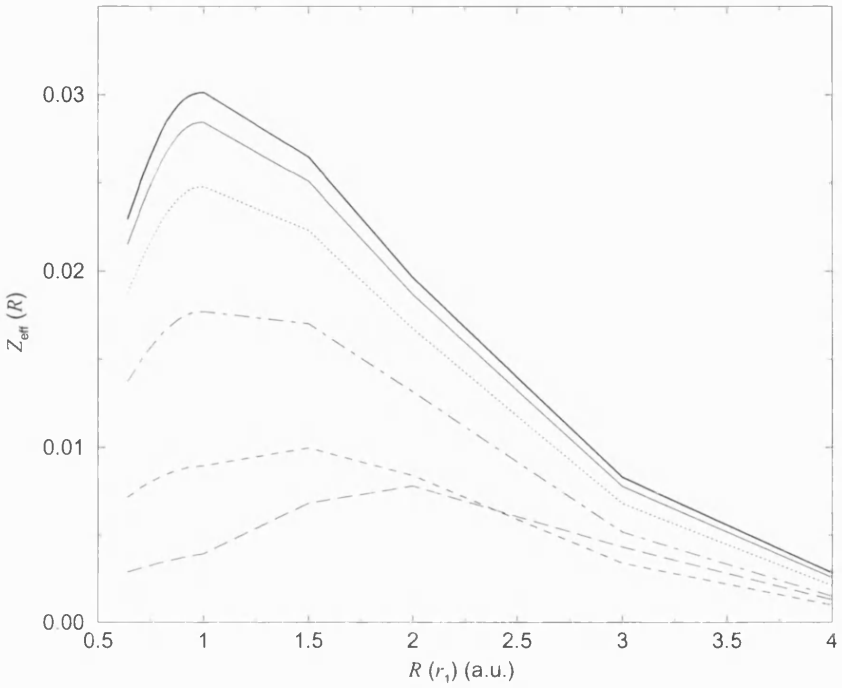

Figure 9.3: Variation of Z_{eff} with respect to R for different numbers of terms in the wave function, with both even and odd powers of r_{23} included. See caption to figure 9.2 for legend.

Z_{eff} could arise because of the inexact wave function of the total system used in evaluating the interaction energy. As the system rearranges to form positronium-protonium, Z_{eff} would be expected to become infinite near R_c since all positronium that is formed eventually annihilates. A similar argument has been used by Van Reeth *et al* (1996) to explain the sharp increase in Z_{eff} just below the positronium formation threshold in positron-atom scattering (see Section 5.3). However, the wave function used here makes no allowance for the formation of real positronium and the representation of virtual positronium by the usual short-range correlation functions may not be very efficient. In our system, where no positronium is allowed to be formed, the repulsion of the electron by the antiproton and the positron by the proton may be enough to keep the leptons further apart from each other than they should be when $R \simeq R_c$. This limitation in the form of the wave function is expected to have a significantly larger effect on Z_{eff} than on the energy because the error in Z_{eff} is of first order in the error in the wave function whereas the error in the energy is of second order. Recent results obtained by Chamberlain (2002) do not show

this decrease in $Z_{\text{eff}}(R)$ close to R_c.

In the ATHENA experiments, the hydrogen and antihydrogen will be kept in magnetic traps, and the spins of the leptons will be aligned parallel to each other. Consequently all annihilation of electrons and positrons should be via three photon decay which, as explained in Chapter 5, occurs at a rate approximately 400 times slower than two photon decay. Jonsell *et al* (2001) have concluded that the rate for annihilation in flight of the proton and antiproton is faster than the estimated direct lepton annihilation via three photons, which cannot be taken into account in the Born-Oppenheimer approximation used here.

9.3.3 The Critical Distance R_c

Chamberlain and Armour (2000) have calculated the value of R_c directly by solving the energy eigenvalue equation for a range of values of R, searching for the specific value of $E'(R) = E(R) + 1/R = -0.25$ a.u.. What is probably a more accurate estimate of the critical distance has been obtained in the present work by looking at the convergence of the values of the energy at a given value of R for wave functions with particular ω and using a similar pattern of convergence to that described previously (see Sections 4.3 and 9.3.1). Although the extrapolated values of $E(R)$ for a given R seem to be lower than expected, the values of R for which $E'(R) = -0.25$ a.u. used to calculate the convergence of R_c are not. Extrapolation to infinite ω should then give a lower, and more accurate, value of R_c, as can be seen in figure 9.2, so the extrapolated value of $R_c(\omega = \infty)$ could be a reasonable approximation. The convergence of R_c with respect to ω is found to be well represented by

$$R_c(\omega) = R_c(\infty) + \frac{A}{\omega^{1.15}}, \tag{9.31}$$

as can be seen in figure 9.4, and the converged value of this work gives $R_c = 0.7519$ a.u. A similar calculation has been carried out by the author on the data of Chamberlain and Armour (2000), yielding a value of $R_c = 0.7724$ a.u. compared with their best direct result of $R_c = 0.7937$ a.u.

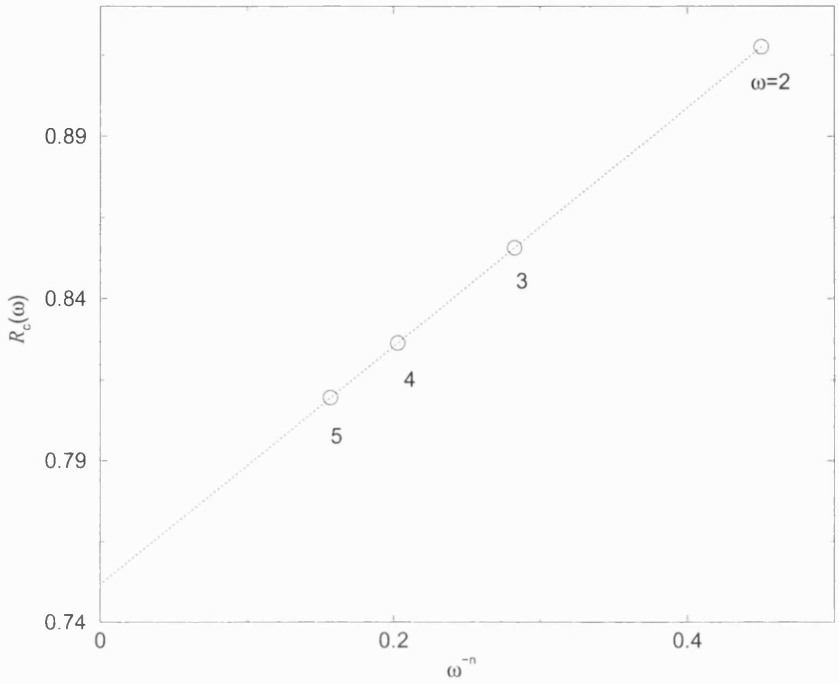

Figure 9.4: Convergence of the critical distance R_c for increasing ω. The straight line is the line of best fit when $n = 1.15$ (see equation 9.31)

9.4 Further Studies and Conclusions

The objective of the work reported in this chapter has been to investigate the feasibility of applying similar techniques to those developed for investigating the full four-body positron-helium scattering system to the four-body system of hydrogen-antihydrogen scattering. Here, the trial wave function has been expressed directly in terms of the five interparticle coordinates (for a given fixed value of R) instead of the somewhat less intuitive spheroidal coordinates employed by other workers (e. g. Kolos *et al* (1975), Armour *et al* (1998) and Jonsell *et al* (2001)). It has therefore been easier to construct terms in the wave function which represent specific configurations of the system such as virtual positronium, which becomes progressively more important as the value of R approaches the critical separation R_c when positronium can be formed and escape from the vicinity of the residual protonium. The present results obtained for the hydrogen-antihydrogen interaction potential within the Born-Oppenheimer approximation compare well with previous results.

9.4.1 Rearrangement Cross Section

A complete treatment of low energy hydrogen-antihydrogen scattering should include the open channel of rearrangement into positronium and protonium, but this is a more substantial task than we had time to complete. This rearrangement channel is likely to have a profound effect on the possibility of trapping antihydrogen for any reasonable time interval because once positronium is formed it will certainly undergo annihilation with a lifetime of at most 142 ns (for ortho-positronium), followed by annihilation of the protonium, resulting in the complete destruction of the antihydrogen atom. Estimates have previously been made by Jonsell *et al* (2001) of the cross section for positronium formation by calculating the $\boldsymbol{T}$-matrix element for the rearrangement. The $\boldsymbol{T}$-matrix is related to the $\boldsymbol{S}$- and $\boldsymbol{K}$-matrices (see equation 2.66), so that

$$\boldsymbol{T} = \frac{i}{2}(\mathbf{1} - \boldsymbol{S}) = \frac{\boldsymbol{K}}{\mathbf{1} - i\boldsymbol{K}}, \tag{9.32}$$

and hence, by equation (2.68), the partial cross section σ_{pq} is directly proportional to $|T_{pq}|^2$.

The $\boldsymbol{T}$-matrix is usually represented as a function of final and initial states, denoted by subscripts f and i respectively. So, for instance, a system in the initial state Ψ_i and final state Φ_f, with an interaction potential V has the $\boldsymbol{T}$-matrix element T_{fi} given by

$$T_{fi} = \langle \Phi_f | V | \Psi_i \rangle, \tag{9.33}$$

where $V = V(R)$, is the atomic interaction potential as calculated above (see equation 9.5). To calculate the $\boldsymbol{T}$-matrix element representing the rearrangement channel in the hydrogen-antihydrogen system, Φ_f is the wave function representing the outgoing plane waves of positronium and protonium, and Ψ_i should be the full wave function representing both incoming hydrogen-antihydrogen plane waves *and* outgoing hydrogen-antihydrogen and outgoing positronium-protonium plane waves.

However, in the work of Jonsell *et al* (2001), instead of using the full wave function Ψ_i, representing elastic and rearrangement channels, an approximate form of Ψ_i was used

which represented only elastic hydrogen-antihydrogen scattering. This function was obtained by solving the one-dimensional Schrödinger equation for the baryonic wave function (as a function of R) representing scattering by the adiabatic potential $V(R)$ i.e.

$$-\frac{\hbar^2}{M}\frac{d^2}{dR^2}f(R) + V(R)f(R) = E_{\rm x}f(R), \tag{9.34}$$

where M is the mass of the proton and $E_{\rm x}$ is the total energy supported by the baryonic system and then multiplying the function $f(R)$ by the previously determined function $\Phi_f(\boldsymbol{r}_2, \boldsymbol{r}_3; R)$ involving the leptonic coordinates. Given that the rearrangement channel is exothermic, and therefore the cross-section for the rearrangement process tends to infinity at zero incident energy, its neglect in the wave function Ψ_i may have a significant effect on the cross section for rearrangement, and therefore on the probability of annihilation in a collision between hydrogen and antihydrogen.

What is required is a full two-channel formulation of hydrogen -antihydrogen scattering, with the elastic scattering and rearrangement channels included in a similar manner to that employed in the determination of positronium formation in positron-helium collisions (see Chapter 4).

Using the $\boldsymbol{K}$-matrix formulation, in which we deal with a real two-component wave function similar to that described in Chapter 4, the asymptotic forms of the two components of the wave function are

$$\Psi_1 \underset{r_1\to\infty}{\sim} \text{elastic H} - \overline{\text{H}} \text{ scattering} \tag{9.35}$$

$$\underset{\rho\to\infty}{\sim} \text{Ps} - \text{formation} \tag{9.36}$$

$$\Psi_2 \underset{r_1\to\infty}{\sim} \text{elastic Ps} - \text{Pn scattering} \tag{9.37}$$

$$\underset{\rho\to\infty}{\sim} \text{H} - \overline{\text{H}} \text{ formation.} \tag{9.38}$$

9.4.2 Helium-Antihydrogen Scattering

The residual gases in the trap in which the antihydrogen atoms are confined are likely to be molecular hydrogen and helium rather than atomic hydrogen, and so investigations need

to be made of antihydrogen collisions with these targets, both of which are substantially more difficult to consider than atomic hydrogen.

As a first attempt at considering collisions of antihydrogen with helium, it is probably appropriate to consider the one-electron model of helium which has been employed in previous chapters of this thesis. Clearly there are similarities with hydrogen-antihydrogen collisions, although there is now no symmetry between the two atoms. Considering the single channel process for atom-antiatom collisions as we have described above, the forms of the basis functions in of the trial wave function do not have to be modified since a flexible trial wave function may adequately represent the distorted helium and antihydrogen target wave functions. However, since there is no node in the models of the helium wave function described in Chapter 3, equation (9.7) may be multiplied by the helium target wave function in order to more adequately represent the helium-antihydrogen system. An appropriate form of basis function is therefore

$$\phi_i = \Phi_{\rm He}(r_3) e^{-\alpha r_3}\, e^{-\gamma r_{12}}\, r_2^{k_i}\, r_3^{l_i}\, r_{12}^{m_i}\, r_{13}^{p_i}\, r_{23}^{q_i}. \tag{9.39}$$

Now there is no symmetry between the two atoms, so generally $\alpha \neq \gamma$, and there is no exchange operation between any of the coordinates (see equations 9.12-9.14).

The total interaction potential, $V_{\rm T}$ needs to be modified to include the electron-helium core model potentials, V^-, described in Chapter 3. The electron-positron interaction is the pure Coulomb attraction and the positron-helium core potential , V^+, is the hydrogenic static plus the dipole polarizability terms as used in the positron-helium scattering calculation (also described in Chapter 3). We presently have no two-body potential to represent the interaction of an antiproton with a helium ion core, but since the proton and antiproton are stationary in the adiabatic calculation of $E(R)$, initial calculations may use V^+ as the antiproton-helium ion core potential. However, this potential term is constant for a particular value of R and can therefore be neglected when calculating a value of R_c for the helium-antihydrogen scattering system.

As with the positron-helium scattering calculation, we also have to consider a potential term which represents the polarization of the helium ion core by the positive and negative

leptons. In this case, in analogy with equation (3.41) we have a four-body term, V_θ, which takes into account the polarization of the helium core by the electron, positron and also the antiproton, even though there is no overall helium core-antiproton interaction included in the total potential, $V_{\rm T}$. The total potential function, apart from the dependence on R, is therefore

$$V_{\rm T} = V^-(r_3) + V^+(r_2) - \frac{1}{r_{12}} + \frac{1}{r_{13}} - \frac{1}{r_{23}} + V_\theta(R, r_2, r_3, \theta_{12}, \theta_{13}, \theta_{23}), \tag{9.40}$$

where

$$V_\theta = \alpha_d \left(\frac{\cos\theta_{12}}{R^2 r_2^2} f_1 - \frac{\cos\theta_{13}}{R^2 r_3^2} f_2 + \frac{\cos\theta_{23}}{r_2^2 r_3^2} f_3 \right), \tag{9.41}$$

and f_1, f_2 and f_3 are functions which appropriately shield V_θ as r_2 and r_3 approach zero.

It may be necessary to add a virtual positronium type term to the wave function to represent the electron and positron weakly bound to the proton-antiproton system. Armour *et al* (1998) used a function which was similar to the form used in positron-helium scattering close to the positronium formation threshold (see Section 4.4.1 and equation 4.60). A suitable form of virtual positronium term for this system is

$$\phi_{\rm vps} = \phi_{\rm Ps}(r_{23}) \frac{e^{-\kappa\rho}}{\rho} \left(1 - e^{-\delta\rho}\right)^3, \tag{9.42}$$

where $\phi_{\rm Ps}$ is the exact positronium wave function and the coordinate ρ is the distance between the centre of mass of the atom-antiatom system and the centre of mass of the weakly bound positronium, so that the vector $\boldsymbol{\rho}$ is defined generally as

$$\boldsymbol{\rho} = \frac{(M_1 - M_2)}{2(M_1 + M_2)} \boldsymbol{R} + \frac{1}{2} (\boldsymbol{r}_3 + \boldsymbol{r}_{12}), \tag{9.43}$$

where M_1 and M_2 are the masses of the two nuclei and $\boldsymbol{R}$ is the vector from M_1 to M_2. In our method we have not needed to define the position of the centre of mass, but if the interbaryonic separation is small enough it may be sufficient to approximate the coordinate ρ as

$$\rho = \frac{1}{2} (r_3 + r_{12}). \tag{9.44}$$

Chapter 10

Summary and Conclusions

In this work we have investigated various low energy collision processes associated with positron-atom scattering using one-electron models of atoms and a simplified model of hydrogen-antihydrogen scattering. The success of these one-electron models has been varied and some results from other positron-atom studies have been reproduced comparatively well both qualitatively and quantitatively.

To study low energy positron-helium collisions we used three one-electron models and compared the results with those of Van Reeth and Humberston (1999) who provided accurate results from *ab initio* calculations. At energies below the positronium formation threshold, $E_{\rm th}$, all three models yielded reasonably accurate elastic scattering cross-sections, and one in particular, V_1, reproduced the results of Van Reeth and Humberston to an excellent degree. This model has shown the remarkable accuracy which can be obtained from using these models, but also some adverse side effects (see Chapter 4 and Chapter 6). Model V_1 supports a resonant state at an energy just below $E_{\rm th}$ which affects the elastic scattering and positronium formation cross-sections above $E_{\rm th}$. The other two models reproduced the energy dependence of the results calculated by Van Reeth and Humberston (1999) reasonably well as well as the cusp-like feature in the positronium formation cross-section just above $E_{\rm th}$. Although no one of the models studied here can accurately reproduce all the features of the scattering cross sections, these results have

provided evidence that a single one-electron model of helium can be found which might provide reasonably accurate scattering results.

The study of positron-electron annihilation in this system, however, did not yield such satisfactory results (see Chapter 5). Although the energy dependence of Z_{eff} calculated here was similar to that calculated by Van Reeth *et al* (1996), the results are too low. This is considered to be a limitation of one-electron models generally, since this particular process is heavily dependent of the interaction between the single electron and the positron, although the model attempts to reproduce the effect of a two electron atom.

Despite the poor results from the Z_{eff} calculations, the study of the Doppler shift in the energy of the γ-rays produced in the electron-positron annihilation revealed mixed success. Despite the comparatively crude nature of model V_3, which effectively neglected any electron exchange contributions to the potential, it was this model which reproduced the results of Van Reeth *et al* (1996) most accurately. It is believed that this can be attributed to the form of the electron density function (see figure 3.8), where that for model V_3 agrees most closely with that calculated from the two-electron helium wavefunction of Van Reeth and Humberston (1999). This correlation may be useful in finding a one-electron model of helium with greater overall reliability.

If a model helium atom can be found with the correct positronium formation threshold energy, and which does not support a positron-helium resonant state, then it may be possible to study helium-antihydrogen collisions using the method described in this work, and reasonably accurate results could be expected.

In Chapter 8, use of the one-electron models was extended to create an entirely artificial model atom with a binding energy of 6.8 eV and a dipole polarizability compatible with the observed correlation between dipole polarizability and binding energy for the noble gases. Positronium formation cross sections were then calculated to test the hypothesis proposed in the correlation study of Humberston and Van Reeth (2000), that the coefficient A in equation (8.1) was the positronium formation cross section for an atom with a zero positronium formation threshold. The calculated cross-sections did not provide an exact

fit to the energy dependence of the parameter A derived from the experimental data, but the three models provided results of the same order as the cross sections extrapolated from the experimental results. This, again, shows how useful the one-electron models of noble gases can be.

An adiabatic approximation was used in studies of hydrogen-antihydrogen collisions using a basis set of Hylleraas type functions somewhat similar to those employed in the positron-helium scattering calculations. Using the Rayleigh-Ritz variational method, which provides a rigorous upper bound on the interaction energy between the hydrogen and the antihydrogen, $E(R)$, this study yielded values of the atom-antiatom interaction potential which are improvements on three of the main studies previously undertaken (Kolos *et al*, 1975, Armour *et al* (1998) and Jonsell *et al*, 2001). Recently more accurate studies have been undertaken which have provided even better values of this potential function using more terms and a virtual positronium term (Chamberlain and Armour 2000), but our investigations have shown that the technique used here is rather good. From this point it should be feasible, without too many complications, to use our one-electron models of helium to provide information about low energy helium-antihydrogen system collisions.

There are complications arising from the method, however, which relate to the representation of the open channel of the positronium and protonium formation below the critical distance, R_c, as well as the limitations of the one-electron models of helium described above. But an initial investigation, at least into upper bounds on R_c and the form of the interaction potential at large values of R, is certainly possible.

The models studied here have shown that representing a noble gas atom as a one-electron atom can sometimes provide accurate results. Considering the mixed quality of the results of the scattering cross sections and annihilation spectra from the positron-helium collision study, we believe it is possible to create a model which represents the helium atom rather well in positron-helium scattering for the one and two open channel scattering processes. A one-electron model atom has been devised for neon, although it is not trivial to calculate neon-positron scattering cross sections since a positron-neon

ion core potential needs to be designed, even if just based on a hydrogenic static type of potential with an additional dipole polarizability interaction term. Also, in neon, the "outer" electron would be in a 2p state so there is an additional complication regarding the coupling of the angular momentum of the positron to that of the electron.

Given the measure of success achieved in this work using one-electron models to represent both real and non-existent atoms, and the promising prospects for successful further studies, it is apparent that such models can be useful in providing at least preliminary results to back up early studies of low energy collisions or correlations theories. More accurate results may then be achieved by other methods.

Appendix A

Potential Parameters

A.1 One-Electron Models of Helium

The model interaction potential, V, between the electron and the helium ion core is a function of r, the distance between them, and is described by equations (3.4-3.6) in Chapter 3;

$$V(r) = -\frac{1}{r} - \frac{1}{r}\left(1 + \delta r + \delta' r^2\right) e^{-\gamma r} - \frac{\alpha_d}{2r^4}\omega_2(\beta r) - \frac{\alpha_q}{2r^6}\chi_3(\beta' r)\,\chi_4(\beta' r) + \frac{3\beta_d}{r^6}\omega_2(\beta_1 r) + \frac{24\gamma_d}{r^6} f(E_\mathrm{i})\,\omega_2(\beta_2 r), \tag{A.1}$$

where the functions ω_n and χ_n shield the singularities as $r \to 0$, and are such that

$$\omega_n(x) = [\chi_n(x)]^2 \tag{A.2}$$

and

$$\chi_n(x) = 1 - e^{-x} \sum_{m=0}^{\infty} \frac{x^m}{m!}, \tag{A.3}$$

and the function

$$f(E_\mathrm{i}) = \frac{\gamma_E}{\pi} \tan^{-1}\left(-\frac{\pi}{\gamma_E} E_\mathrm{i}\right). \tag{A.4}$$

The parameters α_d, α_q, β_d, γ_d and E_i are known exactly because they represent measurable physical properties of the positively charged helium ion. The parameter β is the same in V_1^-, V_2^-, V_3^- and V^+. The parameter β_3 in the shielding function of the "three-body" potential, V_θ (see equation 3.41), also takes this value when V_1^- is used, but $\beta_3 = 2.2012848$

Table A.1: Parameters in the three model electron-helium ion core potentials.

Parameter	V_1^-	V_2^-	V_3^-
δ	-1.787276	-39.76972	2.0
δ'	1.627833	99.52617	0
γ	1.238589	4.5605785	4.0
α_d	0.28125	0.28125	0.28125
β	2.967346	2.967346	2.967346
α_q	0.234375	-	-
β'	2.317501	-	-
β_d	0.0839844	-	-
β_1	2.16761	-	-
γ_d	0.02596029	-	-
γ_1	2.540849	-	-
β_2	1.560583	-	-
E_i	0.90369424	-	-

when using the other models. The parameters in all three model potentials are shown in table A.1.

A.2 Potentials for the Zero E_{th} Model Atom

The general forms of these model potentials are similar to those described above in equation (A.1) but with only the long-range Coulomb attraction and a term representing the static interaction between the electron and the ion core. The electron-core potentials V_1^M and V_2^M have the form

$$V(r) = -\frac{1}{r} - \left(\frac{1}{r} + \delta + \delta' r\right) e^{-\gamma r}, \tag{A.5}$$

Table A.2: Parameters of the three one-electron model atom core potentials for an atom with a zero positronium formation threshold energy.

Parameter	V_1^M	V_2^M	V_3^M
δ	-10.3	-88.46098	-1.99
δ'	4.69321	48.0	-
γ	1.24	2.0	1.5

and model V_3^M has an even simpler form,

$$V(r) = -\frac{1}{r} - \delta e^{-\gamma r}. \tag{A.6}$$

All the parameters are found empirically by fitting the properties of the model atoms described to the value of the ground state energy and the dipole polarizability if possible (see Section 8.3). The values of these parameters are shown in table A.2.

Bibliography

Anderson C D (1932) *Science* **76** 238

Armour E A G and Humberston J W (1991) *Phys. Reports* **204** 165

Armour E A G and Brown W B (1993) *Acc. Chem. Res.* **26** 168

Armour E A G, Carr J M and Zeeman V (1998) *J. Phys. B* **31** L679

Bardsley J N and Nesbet R K (1973) *Phys. Rev. A* **8** 203

Baur G, Boero G, Brauksiepe S, Buzzo A, Eyrich W, Geyer R, Grzonka D, Hauffe J, Kilian K, LoVetere M, Macri M, Moosburger M, Nellen R, Oelert W, Passagio S, Pozzo A, Röhrich K, Sachs K, Schepers G, Sefzick T, Simon R S, Stratmann R, Stinzing F and Wolke M 1996 *Phys. Lett. B* **368** 251

Bhatia A K and Drachman R J (1990) *Annihilation in Gases and Galaxies* ed. Drachman R J (NASA Conf. Pub. 3058) p 257

Bhatia A K and Drachman R J (1997) *Can. J. Phys.* **75** 11

Blanford G, Christian D C, Gollwitzer K, Mandelkern M, Munger C T, Schultz J and Zioulas G (1998) *Phys. Lett. B* **80** 3037

Bluhme H, Knudsen H, Merrison J O and Poulsen M R (1998) *Phys. Rev. Lett.* **81** 73

Chamberlain C W and Armour E A G (2000) *Private Communication*

Chamberlain C W (2002) *Private Communication*

Charlton M and Humberston J (2001) *Positron Physics* (Cambridge University Press)

Coleman P G, Griffith T C, Heyland G R, and Killeen T L (1975) *J. Phys. B* **8** 1734

Davies S A, Charlton M and Griffith T C (1989) *J. Phys B* **22** 327

Dirac P A M (1928) *Proc. Roy. Soc. A* **117** 610

Fermi E and Teller E (1947) *Phys. Rev.* **72** 399

Frolov A M and Yeremin A Y (1989) *J.Phys. B* **22** 1263

Gilbert S J, Barnes L D, Sullivan J P and Surko C M (2002) *Phys. Rev. Lett.* **88** 043201

Greaves R G, Tinkle M D and Surko C M (1994) *Phys. Plasma* **1** 1439

Gribakin G (2001) *New Directions in Antimatter Chemistry and Physics* ed. Surko, C M and Gianturco F A (Kluwer Acad. Pub.)

Hartree D R (1928) *Proc. Cambridge. Phil. Soc.* **24** 89

Hewitt R N, Noble C J and Bransden B H (1992) *J.Phys. B* **25** 557

Ho Y K (1993) *Phys. Rev. A* **48** 4780

Humberston J W, Van Reeth P, Watts M S T and Meyerhof W E (1997) *J. Phys. B* **30** 2477

Humberston J W and Van Reeth P (2000) *J. Phys. B.* **33** L97

Hylleraas (1929) *Z. f. Physik* **54** 347

Iwata K, Greaves R G, Murphy T J, Tinkle M D and Surko C M (1995) *Phys. Rev. A* **51** 473

Jonsell S, Saenz A, Froelich P, Zygelman B and Dalgarno A (2001) *Phys. Rev. A* 052712

Kahn P and Gosh A (1983) *Phys. Rev. A* **28** 2181

Kauppila W E, Stein T S, Smart J H, Dababneh M S, HO Y K, Downing J P and Pol V (1981) *Phys. Rev. A* **24** 725

Kolos W, Morgan Jr. D L, Schrader D M and Wolniewicz L (1975) *Phys. Rev. A* **11** 1792

Lucchese R R (1989) *Phys. Rev. A* **40** 6879

Martin W C (1960) *J. Research of the Nat. Bur. Stand.* **64** 19

McCurdy C W, Rescigno T N and Schneider B I (1987) *Phys. Rev. A* **36** 2061

Mills Jr. A P (1981) *Phys. Rev. Lett.* **46** 717

Mohorovičić S (1934) *Astron. Nachr.* **253** 93

Moore C E (1970) *Ionization Potentials and Ionization Limits Derived from the Analyses of Optical Spectra* **34** (Nat. Stand. Ref. Data Ser., Nat. Bur. Stand.)

Nesbet R K (1980) *Variational Methods in Electron-Atom Scattering* (Plenum)

O'Malley T F, Rosenberg L and Spruch L (1962) *Phys. Rev.* **125** 1300

Osman P E (1965) *Phys. Rev.* A **140** 8

Peach G (1982) *Comments At. Mol. Phys.* **11** 101

Peach G (1998) *Private Communication*

Ruark A E (1945) *Phys. Rev.* **68** 278

Ryzhikh G and Mitroy J (1997) *Phys. Rev. Lett.* **79** 4124

Schwartz C (1961a) *Phys. Rev.* **124** 1468

Schwartz C (1961b) *Phys. Rev.* **123** 1700

Surko C M, Leventhal M and Passner A (1989) *Phys. Rev. Lett.* **62** 901

Temkin A and Lamkin J C (1961) *Phys. Rev.* **121** 788

Van Dyck Jr R S, Schwinbuerg P B and Dehmelt H G (1987) *Phys. Rev. Lett.* **59** 26

Van Reeth P, Humberston J W, Iwata K, Greaves R G and Surko C M (1996) *J.Phys. B* **29** L465

Van Reeth P and Humberston J W (1998) *J. Phys. B* **31** L621

Van Reeth P and Humberston J W (1999) *J. Phys. B* **32** 3651

Van Reeth P, Humberston J W and Laricchia G (2001) *J. Phys. B* **34** L271

Ward S J, Humberston J W and McDowell M R C (1987) *J.Phys. B* **20 127** 127

Watts M S T (1994) *Ph. D. Thesis, Univ. London*

Watts M S T and Humberston J W (1994) *Hyp. Int.* **89** 47

Wheeler J A (1946) *Ann. N.Y. Acad. Sci.* **48** 219

Wigner E P (1948) *Phys. Rev.* **73** 1002

Wright G L, Charlton M, Griffith T C and Heyland G R (1987) *J.Phys. B* **20** 1865

J. Phys. B: At. Mol. Opt. Phys. **33** (2000) 2589–2603. Printed in the UK PII: S0953-4075(00)50441-6

Positron scattering by equivalent one-electron models of helium

J T Dunn, P Van Reeth, J W Humberston and G Peach

Department of Physics and Astronomy, University College London, Gower Street, London WC1E 6BT, UK

Received 30 March 2000

Abstract. Low-energy positron–helium scattering is investigated using three different one-electron models of helium in order to find out if such a model is capable of yielding accurate results for elastic scattering, positronium formation and positron–electron annihilation. Comparisons are made with the accurate results obtained from *ab initio* variational calculations of Van Reeth and Humberston (Van Reeth P and Humberston J W 1999 *J. Phys. B: At. Mol. Opt. Phys.* **32** 3651). The most elaborate helium model used here gives accurate values for the elastic scattering phase shifts throughout most of the energy range up to the positronium formation threshold. However, near-threshold resonances associated with this model have substantial effects on all the partial wave contributions to the positronium formation cross section that have been investigated. The other two helium models yield rather less accurate elastic scattering phase shifts but the positronium formation cross sections are in good qualitative, and even reasonably good quantitative, agreement with the accurate results. None of the models yields very accurate results for the annihilation cross section.

1. Introduction

Due to the complex nature of many-body collision processes, very detailed *ab initio* studies of positron scattering by atoms have been made only for hydrogen and helium. In positron–hydrogen scattering there are three particles to consider, and hence only three inter-particle coordinates, whereas in positron–helium scattering there are four particles, and therefore six inter-particle coordinates. Also, the wavefunction of the helium target is not known exactly. These factors complicate the calculations by several orders of magnitude in comparison with those for positron–hydrogen scattering and it would therefore be desirable to find out if accurate results can be obtained for positron–helium scattering using a one-electron model of helium. If such a model can be found, it may be possible to generate similar one-electron models for heavier atoms, for which *ab initio* studies are even more difficult, greatly simplifying the task of calculating positron scattering parameters.

One-electron models of helium have been used previously to study positron–helium scattering (Hewitt *et al* 1991), but these studies were mainly at intermediate energies. In the present work we are interested in low-energy positron scattering up to the threshold for the first excited state of the target atom (in positron–helium scattering this is the $2\ ^1S$ state, with a threshold energy of 20.61 eV), and we consider elastic scattering, positronium formation and electron–positron annihilation. Below the positronium formation threshold, the energy of which is

$$E_{\mathrm{th}} = E_{\mathrm{i}} - E_{\mathrm{Ps}}, \tag{1}$$

0953-4075/00/132589+15$30.00

where E_i and E_{Ps} are the single ionization energy of the atom and the binding energy of the ground state positronium respectively, only elastic scattering and annihilation are considered. In the Ore gap, the energy interval between E_{th} and E_{2^1S}, the two channels of positronium formation and elastic scattering are studied. Accurate variationally determined results have recently been obtained by Van Reeth and Humberston (1999), hereafter referred to as VRH, for the parameters describing elastic scattering, annihilation and positronium formation in low-energy positron–helium collisions, and these provide the standard by which we judge the quality of the results obtained using the various one-electron models of helium under investigation.

Previous equivalent one-electron models of helium have been of a simple form and have not provided particularly accurate results for positron–helium scattering (Hewitt *et al* 1991). Here, we are attempting to find a model which is capable of yielding accurate results and reproducing some of the detailed features found in the more accurate *ab initio* investigations. Equivalent one-electron models for other atoms have been used in other positron scattering calculations, but most successfully for alkali atoms (e.g., Watts and Humberston (1992)) which consist of a valence electron weakly bound to a compact core. In contrast, helium is perhaps the most inappropriate atom to consider in this way since the two electrons are in completely equivalent 1s orbitals, and neither electron can be considered as being more tightly bound to the nucleus than the other. Nevertheless, such a model would be very useful if it could be found.

2. Electron–core and positron–core potentials

In this work we consider three model electron–core potentials;

$$V_1^-(r_2) = -\left(\frac{1}{r_2} + \delta + \delta' r_2\right) e^{-\gamma r_2} - \frac{1}{r_2} - \frac{\alpha_d}{2r_2^4}\omega_2(\beta_0 r_2) - \frac{\alpha_q}{2r_2^6}\chi_3(\beta' r_2)\chi_4(\beta' r_2) + \frac{3\beta_d}{r_2^6}\omega_2(\beta_1 r_2) + \frac{24\gamma_d}{r_2^6} f(E_i)\omega_2(\beta_2 r_2), \tag{2}$$

$$V_2^-(r_2) = -\left(\frac{1}{r_2} + \delta + \delta' r_2\right) e^{-\gamma r_2} - \frac{1}{r_2} - \frac{\alpha_d}{2r_2^4}\omega_2(\beta_0 r_2), \tag{3}$$

$$V_3^-(r_2) = -\left(\frac{1}{r_2} + \delta\right) e^{-\gamma r_2} - \frac{1}{r_2} - \frac{\alpha_d}{2r_2^4}\omega_2(\beta_0 r_2), \tag{4}$$

where the coordinate r_2 is defined in figure 1, and α_d is the dipole polarizability of the core. The functions ω_2, χ_3 and χ_4 shield the singularities at $r_2 = 0$ in the various components of the potential function, and are defined by

$$\omega_n(y) = [\chi_n(y)]^2; \qquad \chi_n(y) = 1 - e^{-y}\sum_{i=0}^{n}\frac{y^i}{i!}; \tag{5}$$

$$f(E_i) = \frac{\gamma_1}{\pi}\tan^{-1}\left(-\frac{\pi}{\gamma_1}E_i\right). \tag{6}$$

The potentials V_1^- and V_2^-, which have been provided by Peach (1982), have been generated by fitting the general forms of the potentials to spectroscopic data, and they give very accurate values of the ground state energy and dipole polarizability of the helium atom. The potential V_2^- is a simplified version of V_1^- but with the range of the 'static' component more similar to the range of the hydrogenic static potential. However, the electron–core potentials V_1^- and V_2^- both give stable and very accurate values of the ground state energy, E_0, and the dipole

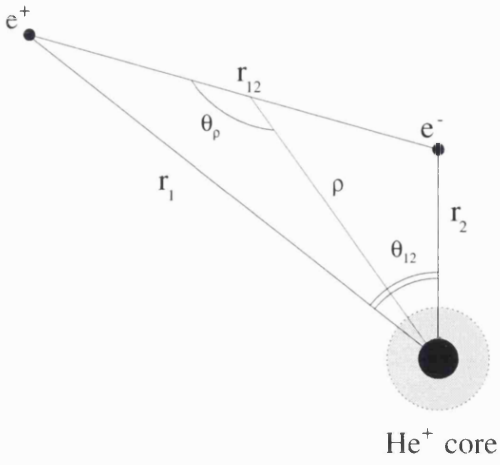

Figure 1. The coordinates of the model positron–helium system.

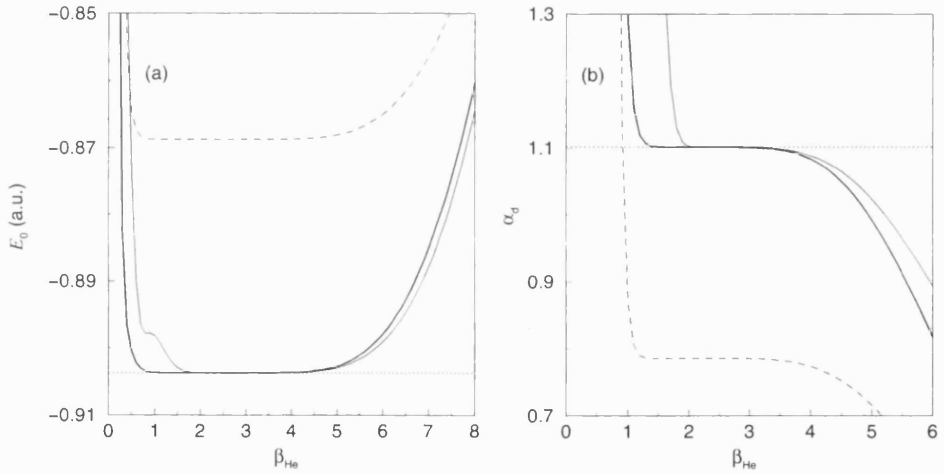

Figure 2. Variation with respect to the nonlinear parameter β_{He} in the helium atom wavefunction (see equation (7)) of (*a*) the ground state energy; (*b*) the dipole polarizability. Note that the full dipole polarizability of the atom has the core value, $\alpha_c = 0.281\,25\ a_0^3$, added to it. The number of terms in each helium wavefunction is ten. Thick curves, V_1^-; thin curves, V_2^-; dashed curves, V_3^-; dotted lines parallel to the abscissa are the exact data.

polarizability, α_{He}, as shown in figure 2 and tabulated in table 1. The electron–core potential V_3^- with $\delta = 2$ and $\gamma = 4$ is simply the hydrogenic static potential for the He^+ ion, added to which is the core dipole polarization potential. This potential gives significantly less accurate values of the energies of the bound states and the dipole polarizability. It may be noted that only δ, δ', γ, and γ_1 are free parameters. The values of the parameters in these potentials are listed in the appendix.

Before scattering calculations can be carried out, a target electron–core 'helium' wavefunction is required and so a variational Rayleigh–Ritz calculation was performed using

Table 1. Properties of the model atoms (minimum or stabilized values): ground state energy (E_0), first excited state (E_1), full dipole polarizability of the model atom (α_{He}), dipole polarizability of the model neglecting the core dipole polarizability (α). Note that the total dipole polarizability of the model helium atom is the sum of the polarizability of the single electron and the core polarizability. Also note that $E_i = |E_0|$ in equation (1).

Model	E_0 (au)	E_1 (au)	α_{He} (a_0^3)	α (a_0^3)
V_1^-	−0.903 694 24	−0.187 85	1.383 27	1.102 02
V_2^-	−0.903 693 22	−0.146 58	1.383 75	1.102 50
V_3^-	−0.868 736 48	−0.155 99	1.066 59	0.785 34
Exact	−0.903 694 24[a]	−0.145 97[b]	1.383 24[c]	—

[a] Moore (1970).
[b] Martin (1960).
[c] Bhatia *et al* (1997).

a very flexible trial wavefunction of the form,

$$\Phi_{He}(r_2) = e^{-\beta_{He} r_2} \sum_{i=0}^{n} c_i r_2^i. \tag{7}$$

The dipole polarizability of the target system was calculated by perturbing the system with a very small electric field. There is no bound on the value of the polarizability but a stable region with respect to varying the nonlinear parameter β_{He} in the one-electron helium wavefunction implies a suitable choice of β_{He}. A detailed description of this method for determining the dipole polarizability has been given by Thomas and Humberston (1972). The full polarizability of the model atom is defined as the polarizability of the single electron plus that of the hydrogenic core, 0.281 25 a_0^3.

The positron–core potential, V^+, is assumed to be the exact hydrogenic static potential, together with a core dipole polarization term, so that

$$V^+(r_1) = \frac{1}{r_1} + \left(\frac{1}{r_1} + 2\right) e^{-4r_1} - \frac{\alpha_d}{2r_1^4} \omega_2(\beta_0 r_1). \tag{8}$$

The total potential function of the three-body system, V_T, also contains the positron–electron interaction, V_{12}, and a 'three-body' potential term, V_θ, which exactly cancels the polarization potentials when the positron and electron are at the same position (see Peach (1983)), so that

$$V_T = V^-(r_2) + V^+(r_1) + V_{12}(r_{12}) + V_\theta(r_1, r_2, \theta_{12}), \tag{9}$$

where

$$V_{12}(r_{12}) = -\frac{1}{r_{12}}, \tag{10}$$

$$V_\theta(r_1, r_2, \theta_{12}) = \frac{\alpha_d}{r_1^2 r_2^2} \cos\theta_{12} \chi_2(\beta_0 r_1) \chi_2(\beta_0 r_2). \tag{11}$$

3. Scattering calculations

Above the positronium formation threshold, only two processes are considered as open channels: elastic scattering and positronium formation. The positron–electron annihilation channel is also open, but the cross section for this process is negligible in comparison to the

cross sections for the two other processes. The total Hamiltonian, H_T, and the total energy, E_T, are given by

$$H_T = -\tfrac{1}{2}\nabla_{r_1}^2 - \tfrac{1}{2}\nabla_{r_2}^2 + V_T, \tag{12}$$

$$= -\tfrac{1}{4}\nabla_{\rho}^2 - \nabla_{r_{12}}^2 + V_T, \tag{13}$$

$$E_T = \tfrac{1}{2}k^2 + E_0 = \tfrac{1}{4}\kappa^2 + E_{Ps}, \tag{14}$$

where ρ is the coordinate from the core to the centre of mass of the positronium (see figure 1) and k and κ are the positron and positronium wavenumbers respectively.

We use the Kohn variational method (see VRH) which provides a variational $\boldsymbol{K}$ matrix, described by the stationary functional,

$$\boldsymbol{K}_{mn}^{v} = \boldsymbol{K}_{mn}^{t} - \langle \Psi_m^t | 2(H_T - E_T) | \Psi_n^t \rangle \qquad (m, n = 1, 2). \tag{15}$$

The trial wavefunction has two components to represent fully the two scattering channels, and they have the form

$$\Psi_1 = S_1 + K_{11}^t C_1 + K_{21}^t C_2 + \sum_{i=1}^{N} c_i \phi_i \tag{16}$$

$$\Psi_2 = S_2 + K_{22}^t C_2 + K_{12}^t C_1 + \sum_{j=1}^{N} d_j \phi_j, \tag{17}$$

where

$$S_1 = Y_{l,0}(\hat{r}_1)\sqrt{k}\Phi_{He}(r_2) j_l(kr_1) \tag{18}$$

$$C_1 = -Y_{l,0}(\hat{r}_1)\sqrt{k}\Phi_{He}(r_2) n_l(kr_1) f_{sh}(r_1) \tag{19}$$

$$S_2 = Y_{l,0}(\hat{\rho})\sqrt{2\kappa}\Phi_{Ps}(r_{12}) j_l(\kappa\rho) \tag{20}$$

$$C_2 = -Y_{l,0}(\hat{\rho})\sqrt{2\kappa}\Phi_{Ps}(r_{12}) n_l(\kappa\rho) f'_{sh}(\rho), \tag{21}$$

$$\phi_i = y_{l,0}(\hat{r}_1, \hat{r}_2) e^{-(\alpha r_1 + \beta r_2 + \gamma r_{12})} r_1^{k_i} r_2^{l_i} r_{12}^{m_i}, \tag{22}$$

where $y_{l,0}$ is an appropriate rotational harmonic (see equations (30)–(32)). The functions f_{sh} and f'_{sh} shield the Neumann functions at the origins ($r_1 = 0, \rho = 0$), $\Phi_{Ps}(r_{12})$ is the positronium wavefunction, and the short-range distortions represented by ϕ_i are summed over all terms with non-negative powers of r_1, r_2 and r_{12} such that

$$k_i + l_i + m_i \leqslant \omega, \tag{23}$$

where ω is a positive integer. Increasing the value of ω then provides a convenient means of systematically improving the trial function. Exploiting the stationary properties of the elements of the Kohn functional with respect to variations of the linear parameters, $\boldsymbol{K}_{ij}^t (i, j = 1, 2)$, $c_i (i = 1, \ldots, N)$, $d_j (j = 1, \ldots, N)$, a set of linear simultaneous equations is obtained which, when solved, ultimately yields $\boldsymbol{K}^v$ and hence the two-channel partial wave cross sections which are given by

$$\sigma_{mn}^{l} = \frac{4\pi(2l+1)}{k_m^2} \left| \left(\frac{\boldsymbol{K}^v}{\boldsymbol{I} - \mathrm{i}\boldsymbol{K}^v} \right)_{mn} \right|^2, \tag{24}$$

where $\boldsymbol{I}$ is the unit matrix, σ_{11} and σ_{12} are σ_l and σ_{Ps} respectively and $k_1 = k$ and $k_2 = \kappa$.

Below the positronium formation threshold, the trial wavefunction is reduced to a single component representing a single channel, i.e. all terms relating to positronium are dropped.

The Kohn method does not provide a rigorous bound but there is an empirical lower bound on the diagonal $\boldsymbol{K}$-matrix elements, $\boldsymbol{K}_{11}^v$ and $\boldsymbol{K}_{22}^v$, so that they usually increase and converge toward the exact values, as ω is increased (see table 2). However, for particular values of the

Table 2. Convergence of the s-wave positron–helium scattering phase shifts with respect to the number of short-range correlation terms in the scattering wavefunction, N, at $k = 1.0\,a_0^{-1}$. These are to be compared with the accurate value of $\eta_0 = -0.189$ from VRH.

N (ω)	V_1^-	V_2^-	V_3^-
84 (6)	−0.1910	−0.1792	−0.1719
120 (7)	−0.1907	−0.1786	−0.1717
165 (8)	−0.1905	−0.1785	−0.1716
220 (9)	−0.1903	−0.1783	−0.1714
286 (10)	−0.1903	−0.1782	−0.1714

nonlinear parameters, $\boldsymbol{K}^v$ can become singular (Schwartz 1961a). Using the 'inverse Kohn method', a variant of the Kohn method, singularities can be shown to be either Schwartz singularities or actual features of the model, since a Schwartz singularity is very unlikely to be obtained with both methods. The complex Kohn method is also used in order to reduce further the possibility of confusion between Schwartz singularities and actual singularities of the models (Miller and Jansen op de Haar 1987, Rescigno *et al* 1995).

4. Single channel elastic scattering

4.1. S-wave phase shifts

Below the positronium formation threshold the calculated phase shifts were compared with the accurate results of VRH. The most accurate s-wave scattering phase shifts for all three models are shown in figure 3. The data shown are for $\omega = 10$, which provides very well converged phase shifts for each model. The results for model 1 compare favourably with those of VRH, especially at low energies. However, just below the positronium formation threshold a resonance-like structure appears. This feature appears in the results obtained using all three variations of the Kohn method and is therefore not considered to be a Schwartz singularity. Its existence has been confirmed using the 'stabilization method' described by Drachman and Houston (1975) and Bhatia and Drachman (1989). This feature is therefore considered to be a 'true' resonance within the model potential being used.

The principle behind the stabilization method is that a scattering resonance will manifest itself as a stabilized eigenvalue of the matrix eigenvalue equation

$$\langle \phi_i | (H - E_T) | \phi_j \rangle = 0, \tag{25}$$

in a square integrable basis of functions ϕ_i ($i = 1, \ldots, N$). Provided the basis is large enough, one of the eigenvalues will be found close to the position of the resonance. As the size of the basis is increased the position of a resonance can usually be easily identified as a series of avoided crossings of the lines joining corresponding eigenvalues, as shown in figure 4. These eigenvalues were obtained using the basis functions

$$\phi_i = \mathrm{e}^{-(\alpha r_1 + \beta r_2 + \gamma r_{12})} r_1^{k_i} r_2^{l_i} r_{12}^{m_i}. \tag{26}$$

An avoided crossing of successive eigenvalues is observed in figure 4 just below the positronium formation threshold, $E_T = E_{th} = -0.25$ au.

In order to understand better the mechanism responsible for the resonance, we plotted the potential function ($V_T - V_{12}$) as a function of r_1 when $r_1 = r_2$, and therefore $r_{12} = 0$. The potential function for a coalescent positronium, with $r_{12} = 0$, interacting with any other system should be zero for all r_1, but this is not the case here. Instead, a shallow but rather wide minimum is found which arises because, in our model, the static interaction between the positron and

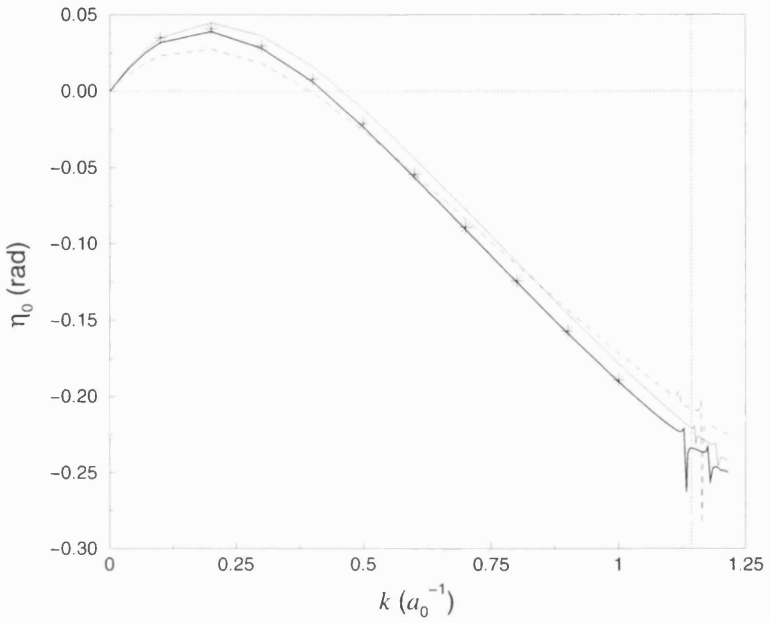

Figure 3. The variation of the s-wave elastic scattering phase shift with respect to the positron wavenumber, k for $\omega = 10$. Thick curve, V_1^-; thin curve, V_2^-; dashed curve, V_3^-; $*$, accurate results of VRH; dotted line parallel to the ordinate marks the exact positronium formation threshold, k_{th}. Note: the resonance in model 3 which lies below the exact positronium formation threshold is not a true resonance because it lies above the positronium formation threshold for this model.

helium ion core does not exactly balance the electron–core static interaction. The positron–core static potential was chosen to be that for a hydrogenic core, whereas the electron–core static potential has a rather different functional form, and is of longer range, because it incorporates some allowance for exchange between the two electrons. Consequently, the structure of the resonance appears to arise from positronium temporarily weakly bound to the helium ion core. The expectation values of the interaction potentials of either the electron, positron or 'positronium' near the resonant energies also shed light on the nature of the resonance. By calculating

$$\overline{V}_k(\rho) = \int \Psi(\rho, r_{12}, \theta_\rho)(V^+ + V^-)\Psi(\rho, r_{12}, \theta_\rho) r_{12}^2 \, \mathrm{d}r_{12} \sin\theta_\rho \, \mathrm{d}\theta_\rho, \tag{27}$$

$$\overline{V}_k(r_1) = \int \Psi(\rho, r_{12}, \theta_\rho)(V^+ + V_{12})\Psi(\rho, r_{12}, \theta_\rho) r_{12}^2 \, \mathrm{d}r_{12} \sin\theta_\rho \, \mathrm{d}\theta_\rho, \tag{28}$$

$$\overline{V}_k(r_2) = \int \Psi(\rho, r_{12}, \theta_\rho)(V^- + V_{12})\Psi(\rho, r_{12}, \theta_\rho) r_{12}^2 \, \mathrm{d}r_{12} \sin\theta_\rho \, \mathrm{d}\theta_\rho, \tag{29}$$

it can be shown that at energies very close to the resonance, deep potential wells are apparent which have minima approximately 2, 3 and 4 au from the core, when expressed in the electron, positronium and positron coordinates, respectively. Away from the resonance these potential wells do not appear.

Despite this model supporting a resonant state which is not found in the real system, there is very favourable agreement between the results for model 1 and those of VRH. The other two models do not support resonant states below their respective positronium formation thresholds, but they provide less accurate s-wave phase shifts.

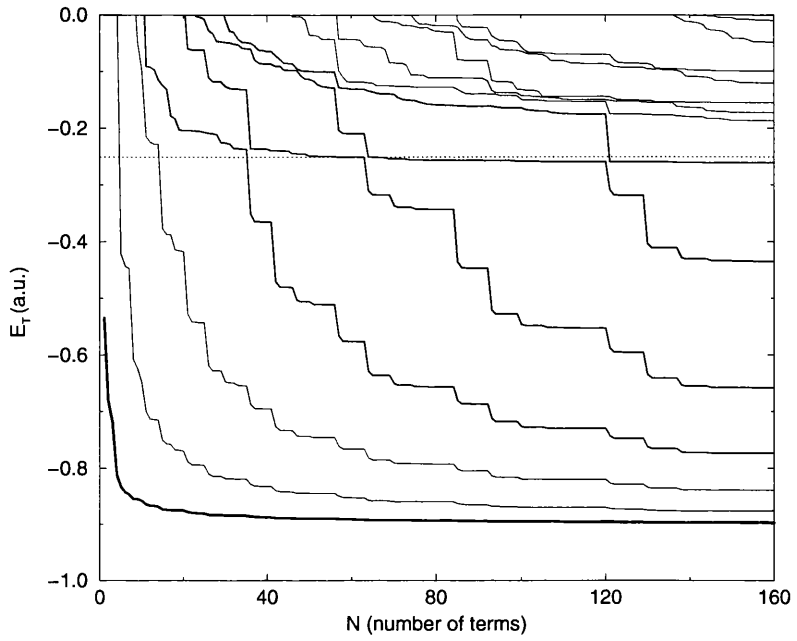

Figure 4. Variation of the lowest eigenvalues of the Hamiltonian of the model positron–helium system with respect to increasing N, the number of short-range correlation functions in the basis. Thick line, E_0; medium lines, E_3, E_4, E_5 and E_6; dotted line parallel to the abscissa is at the exact positronium formation threshold: $E_T = -0.25$ au $= -6.8$ eV.

4.2. Higher partial waves

At large distances from the target system only the positron has non-zero angular momentum, and the long-range parts of the trial wavefunction involve the appropriate spherical Bessel functions and spherical harmonics. At short range, however, the total angular momentum can be 'shared' with the electron, so the sum of the short-range correlation functions in the trial wavefunction, $\Phi(l)$, is modified from the s-wave form to become a set of Hylleraas trial functions multiplied by appropriate harmonic functions (Schwartz 1961b); thus,

$$\Phi(l=1) = Y_{10}(\hat{r}_1) r_1 \sum_{i=1}^{N} a_i \phi_i + Y_{10}(\hat{r}_2) r_2 \sum_{j=1}^{N} b_j \phi_j, \tag{30}$$

$$\Phi(l=2) = Y_{20}(\hat{r}_1) r_1^2 \sum_{i=1}^{N} a_i \phi_i + \psi(1,1,2,0) r_1 r_2 \sum_{j=1}^{N} b_j \phi_j + Y_{20}(\hat{r}_2) r_2^2 \sum_{k=1}^{N} c_k \phi_k, \tag{31}$$

where

$$\psi(1,1,2,0) = \sum_{m=-1}^{+1} Y_{1,m}(\hat{r}_1) Y_{1,-m}(\hat{r}_2) \langle 1, m; 1, -m | 2, 0 \rangle. \tag{32}$$

As with the s-wave calculations, the results for the model potential V_1^- agree well with the results of VRH, except near the positronium formation threshold (see figure 5). Although a resonance now appears in the p-wave just above the threshold (possibly due to the effect of the centrifugal barrier) the phase shift is affected below, as the resonance is noticeably broader than the s-wave resonance. As for the s-wave, model V_2^- gives phase shifts which are slightly too positive in both the p- and d-waves. However, the values of the low-energy phase shifts

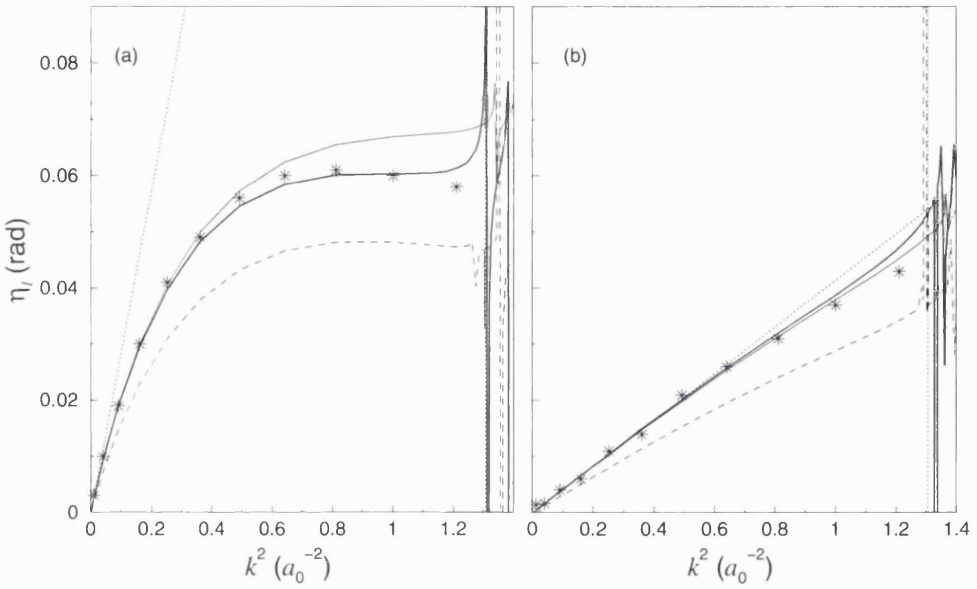

Figure 5. The variation of: (*a*) the p-wave; (*b*) the d-wave elastic scattering phase shifts with respect to k^2 for $\omega = 10$. Thick line, V_1^-; thin curve, V_2^-; dashed curve, V_3^-; $*$, accurate results of VRH; dotted curve, formula of O'Malley *et al* (1962) (equation (33)); dotted line parallel to the ordinate is at the exact k_{th}^2.

for $l > 0$ should be related to the dipole polarizability of the target atom, α_{He}, by the formula (O'Malley *et al* 1962)

$$\eta_l \approx \frac{\pi \alpha_{He} k^2}{(2l-1)(2l+1)(2l+3)}. \tag{33}$$

The results for models 1 and 2, both of which provide accurate values of α_{He}, fit this low-energy approximation very well, at least for sufficiently low positron energies (see figure 5). Note that α_{He} is the full dipole polarizability of the atom because the core polarization potential is included in the total potential.

4.3. Annihilation

An additional process in positron–atom scattering, which has no counterpart in electron–atom scattering, is positron–electron annihilation. This channel is open at all incident positron energies, but the cross section for annihilation is usually very small compared to the cross sections for all other processes, although annihilation is the ultimate fate of all positrons. Below the positronium formation threshold the annihilation cross section can be expressed as

$$\sigma_{an} = \pi r_0^2 c Z_{eff}/v, \tag{34}$$

where r_0 is the classical radius of the electron ($=e^2/m_e c^2$), v is the speed of the positrons, and Z_{eff} is an energy-dependent effective number of electrons per atom with which the positron can annihilate. This is defined for an atom with Z electrons by

$$Z_{eff} = \sum_{i=2}^{Z+1} \int |\Psi(r_1, r_2, \ldots, r_{Z+1})|^2 \delta(r_1 - r_i)\, dr_1\, dr_2 \ldots dr_{Z+1}, \tag{35}$$

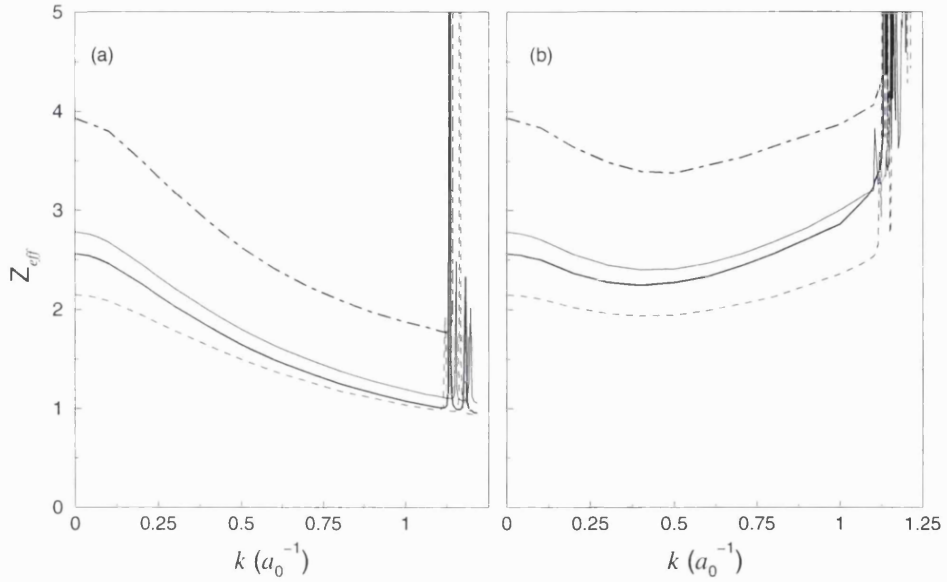

Figure 6. The variation of $Z_{\rm eff}$ with respect to positron wavenumber: (*a*) s-wave contribution; (*b*) sum of s-, p- and d-wave contributions. Chain curve, results of Van Reeth *et al* (1996); thick curve, V_1^-; thin curve, V_2^-; dashed line, V_3^-.

where $\boldsymbol{r}_1$ is the positron coordinate and $\boldsymbol{r}_i$ $(i = 2, \ldots, Z+1)$ are the coordinates of the Z electrons in the target atom. The total elastic scattering wavefunction must now be normalized to unit positron density at infinity. In the Born approximation, in which there is assumed to be no distortion of the wavefunctions of either the incident positron or the target atom, $Z_{\rm eff} = Z$, independent of the incident positron energy. In reality, however, the total wavefunction is distorted so that the value of $Z_{\rm eff}$ is usually enhanced, sometimes by a substantial factor.

The determination of $Z_{\rm eff}$ provides a stringent test of the accuracy of the total wavefunction because the error in the expression for $Z_{\rm eff}$, equation (35), is of first order in the error in the wavefunction, whereas the error in the Kohn phase shift is of second order. It is of interest to compare the values of $Z_{\rm eff}$ obtained using the wavefunctions for the present one-electron model of helium with the accurate values obtained by VRH. One immediate difference is that in the Born approximation the present calculations yield $Z_{\rm eff}^B = 1$, compared with the Born value of two for the real system. One might therefore think that the calculated result for $Z_{\rm eff}$ should be multiplied by two before comparing with the accurate value. However, because two of the one-electron models of helium used here have the correct value of the dipole polarizability, $\alpha_{\rm He} = 1.383\ a_0^3$, and there is known to be a fairly good correlation between the dipole polarizability of a target atom and the value of $Z_{\rm eff}$ at low positron energies (Osman 1965, Davies *et al* 1989), one might expect a reasonably accurate value of $Z_{\rm eff}$ to be obtained without multiplication by a factor of two. Using the most accurate elastic scattering wavefunction generated here, the value obtained for $Z_{\rm eff}$ at essentially zero energy (1.4×10^{-7} eV) is 2.56 (for model 1), which is significantly smaller than the accurate value of 3.88 obtained by Van Reeth *et al* (1996) at the same energy; however, multiplying by two gives $Z_{\rm eff} = 5.12$ which is significantly larger than the accurate value. It would therefore seem that we are not justified in multiplying by two, and we must accept that the one-electron models used here do not provide as accurate a representation of annihilation as they do of elastic scattering. Part of the

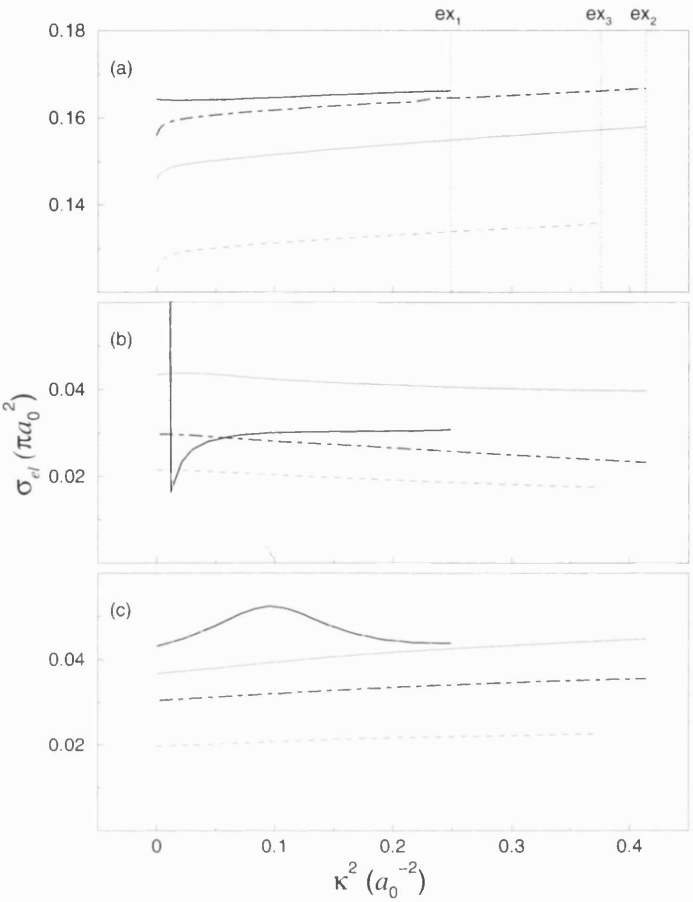

Figure 7. Variation of the partial wave elastic cross sections with respect to κ^2, the positronium wavenumber squared: (*a*) s-wave; (*b*) p-wave; (*c*) d-wave. Thick curve, V_1^-; thin curve, V_2^-; dashed curve, V_3^-; chain curve, accurate results of VRH; dotted lines parallel to the ordinate are the first excitation thresholds for the three models; ex_1 for V_1^-; ex_2 for V_2^- (and exact threshold); ex_3 for V_3^-. Note: $\kappa^2 = 0$ is offset slightly in order that threshold structure may be seen.

discrepancy may be due to the fact that the polarizability of our single-electron model differs from the exact value by the polarizability of the helium ion core, 0.281 25 a_0^3. Accordingly, because of the above-mentioned correlation between Z_{eff} and the dipole polarizability, we should probably expect the calculated value of Z_{eff} to be approximately 20% smaller than the correct total value, i.e. $Z_{\text{eff}} \sim 3.1$. On this basis the present value is only 18% smaller than it might be expected to be. Furthermore, in the real two-electron helium atom the total Z_{eff} is the sum of two (equal) contributions, each one corresponding to positron annihilation with a single electron (see equation (35)). In our one-electron model of helium the 'second' electron is in a sense in the core, and therefore we should perhaps add a contribution arising from positron 'annihilation' with the core, i.e.,

$$Z_{\text{eff}}^{+} = 4\pi \int |\Psi(r_1 = 0, r_2, r_{12} = r_2)|^2 r_2^2 \, \mathrm{d}r_2. \tag{36}$$

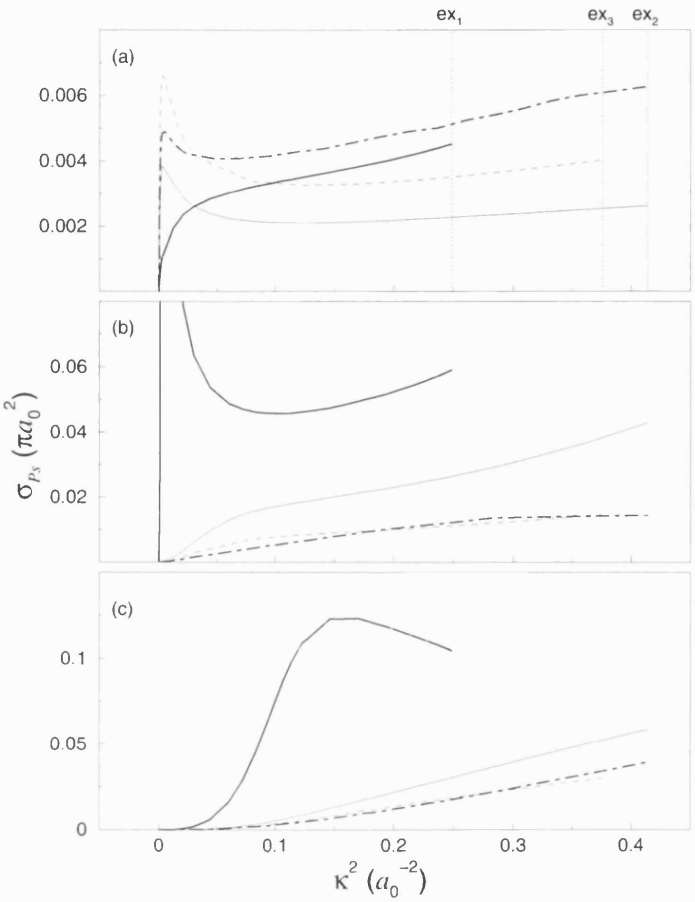

Figure 8. Variation of the partial wave positronium formation cross sections with respect to κ^2, the positronium wavenumber squared: (*a*) s-wave; (*b*) p-wave; (*c*) d-wave. See caption to figure 7 for legend.

This contribution to Z_{eff} is, however, zero at zero incident positron energy, and is small at all energies, having a maximum value of 0.12. It therefore has an negligible effect on the results. The dependence of the s-wave contribution to Z_{eff} (neglecting Z^{+}_{eff}), and the sum of the first three partial wave contributions to Z_{eff}, on the incident positron wavenumber is plotted in figure 6 for each of the three models.

5. Results above the positronium formation threshold

Above the positronium formation threshold results have been obtained for the s-, p- and d-wave contributions to the elastic scattering and positronium formation cross sections for a range of energies up to, and even exceeding, the lowest positron-impact excitation threshold of the target atom for each of the potential models defined previously. The most accurate s-wave results, obtained with $\omega = 6$, are plotted in figures 7 and 8 as functions of κ^2; i.e., four times the kinetic energy of the positron in excess of the threshold energy for positronium formation. In this way we ensure that the position of this threshold is the same on all the plots. Note

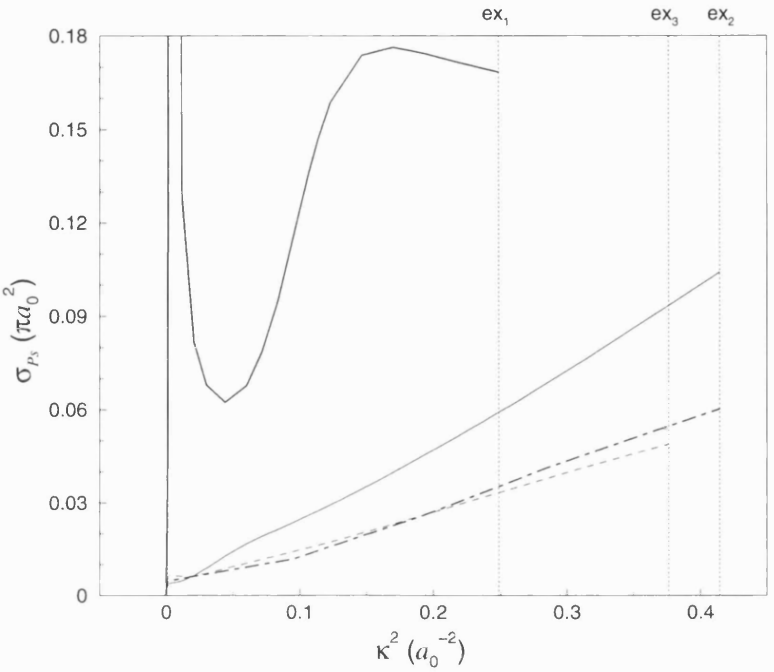

Figure 9. The variation of the sum of the s-, p-, and d-wave positronium formation cross sections with respect to κ^2. See caption to figure 7 for legend.

that the data shown are terminated at the first excitation threshold for each model, since higher energy results do not take all the open channels into account. Also plotted in figures 7 and 8 are the accurate s-wave results of VRH. Although the differences between the model 1 results and those of VRH for elastic scattering are rather larger above the threshold than below, the overall level of agreement is nevertheless reasonably good, except very close to the threshold where the influence of the near-threshold resonance is still felt. The values of $\sigma_{el}(l = 0)$ for the other two models are significantly smaller, although both display a rather flat energy dependence similar to that for model 1.

In the case of the positronium formation cross section, the values of $\sigma_{Ps}(l = 0)$ for model 1 are significantly different from those of VRH just above the threshold, where the accurate results display an abrupt rise to quite a pronounced peak. In contrast, the model 1 results, although having the infinite slope at the threshold required by Wigner's threshold law, rise smoothly to a gently rising plateau of similar magnitude to the corresponding feature in the results of VRH. The absence of a near-threshold peak in $\sigma_{Ps}(l = 0)$ for this model may be due to the influence of the resonance below the threshold, since the corresponding results obtained with the other two models, neither of which supports a below-threshold resonance, display near-threshold peak structure in $\sigma_{Ps}(l = 0)$ rather similar to that of VRH, and similar energy dependence thereafter, although somewhat lower in magnitude.

The p- and d-wave contributions to σ_{Ps} obtained using model 1 are both in poor agreement with the corresponding accurate results because of the influence of resonances within the Ore gap. A very narrow p-wave resonance just above the positronium formation threshold causes $\sigma_{Ps}(l = 1)$ to have a large peak in its vicinity. The d-wave contribution to σ_{Ps} is affected by a much broader resonance whose influence extends throughout the Ore gap. Therefore, the sum

of the first few partial wave contributions to σ_{Ps} calculated with model 1 is very different from the accurate results of VRH, as may be seen in figure 9. The other two models do not support p- or d-wave resonances in the positron–atom system at energies within or below the Ore gap, and the results display a similar energy dependence to that of the accurate results. Indeed, the results for the simplest model, model 3, are in reasonably good agreement with the accurate values of VRH.

6. Comments and conclusions

We have investigated low-energy positron scattering by three one-electron models of helium with a view to finding out if any of them is capable of providing reasonably accurate cross sections for elastic scattering, annihilation and positronium formation. None of the three models considered here provides good agreement with all the accurate theoretical data, although model 1 gives an excellent fit to the elastic scattering data below the positronium formation threshold. However, the quality of the positronium formation data is much less good because of resonances close to the positronium formation threshold in this particular model of the positronium–helium system. The other models, which do not support resonances, yield rather less accurate elastic cross sections but reasonably good positronium formation cross sections, particularly in respect of the energy dependence. Indeed, the comparatively crude model 3 yields very good results for σ_{Ps}. In an attempt to obtain more accurate results for the scattering parameters we have modified the parameters in model 3 from their exact static values, but there is no significant improvement overall. Nevertheless it might be possible to construct a one-electron model of helium incorporating some of the features in model 1, but without the resonances, which would yield accurate results for low-energy elastic scattering and positronium formation. It is doubtful, however, whether the elastic scattering wavefunction for such a system would give a correspondingly accurate value of the annihilation rate parameter Z_{eff}.

Equivalent one-electron models have been devised for other atoms, including other noble gases (Leo *et al* 1995, 2000), and we are currently investigating low-energy positron scattering from these. Unfortunately, unlike for helium, no very accurate results of *ab initio* calculations are available with which to compare, although theoretical results of moderate accuracy do exist. (A comprehensive review of positron–atom scattering, together with an extensive list of references, has been written by Walters *et al* (1997).) These, and available experimental data, will hopefully provide reasonably stringent tests of the qualities of various one-electron models.

Acknowledgments

One of us (JD) is in receipt of an ESPRC Research Studentship. This work was also supported by the ESPRC on grant GR/L38431.

Appendix

The parameters α_d, α_q, β_d and γ_d are known exactly because He^+ is hydrogenic. The parameter β_0 is the same in V_1^-, V_2^-, V_3^- and V^+. The parameter β_0 in the shielding function of the 'three-body' potential, V_θ, also takes this value when V_1^- is used, but

$$\beta_0 = 2.201\,2848$$

when using the other models. The parameters of all three model potentials are shown in table A.1.

Table A.1. Parameters of the three model potentials.

Parameter	V_1^-	V_2^-	V_3^-
δ	−1.787 276	−39.769 72	2.0
δ'	1.627 833	99.526 17	0
γ	1.238 589	4.560 5785	4.0
α_d	0.281 25	0.281 25	0.281 25
β_0	2.967 346	2.967 346	2.967 346
α_q	0.234 375	—	—
β'	2.317 501	—	—
β_d	0.083 984 4	—	—
β_1	2.167 61	—	—
γ_d	0.025 960 29	—	—
γ_1	2.540 849	—	—
β_2	1.560 583	—	—

References

Bhatia A K and Drachman R J 1990 *Annihilation in Gases and Galaxies (NASA Conf. Pub. vol 3058)* ed R J Drachman p 257

——1997 *Can. J. Phys.* **75** 11

Davies S A, Charlton M and Griffith T C 1989 *J. Phys. B: At. Mol. Opt. Phys.* **22** 327

Drachman R J and Houston S K 1975 *Phys. Rev.* A **12** 885

Hewitt R N, Noble C J and Bransden B H 1991 *J. Phys. B: At. Mol. Opt. Phys.* **25** 557

Leo P J, Mullamphy D F T, Peach G and Whittingham I B 1995 *J. Phys. B: At. Mol. Opt. Phys.* **28** 4449

——2000 Private communication

Martin W C 1960 *J. Res. NBS* **64** 19

Miller W H and Jansen op de Haar B M 1987 *J. Chem. Phys.* **86** 6213

Moore C E 1970 *Ionization Potentials and Ionization Limits Derived from the Analyses of Optical Spectra* vol 34 *(National Standards Reference Data Series)* (Washington, DC: National Bureau of Standards)

O'Malley T F, Rosenberg L and Spruch L 1962 *Phys. Rev.* **125** 1300

Osman P E 1965 *Phys. Rev.* A **140** 8

Peach G 1982 *Comment. At. Mol. Phys.* **11** 101

——1983 *Atoms in Astrophysics* ed Burke, Eissner, Hummer and Percival (New York: Plenum) p 115

Rescigno T N, McCurdy C W, Orel A E and Lengsfield B H 1995 *Computational Methods for Electron–Molecule Collisions* ed W M Huo and F A Gianturco (New York: Plenum)

Schwartz C 1961a *Phys. Rev.* **124** 1468

——1961b *Phys. Rev.* **123** 1700

Thomas M A and Humberston J W 1972 *J. Phys. B: At. Mol. Phys.* **5** L229

Van Reeth P, Humberston J W, Iwata K, Greaves R G and Surko C M 1996 *J. Phys. B: At. Mol. Opt. Phys.* **29** L465

Van Reeth P and Humberston J W 1999 *J. Phys. B: At. Mol. Opt. Phys.* **32** 3651

Walters H R J, Kernoghan A A, McAlinden M T and Campbell C P 1997 *Photon and Electron Collisions with Atoms and Molecules* ed Burke and Joachain (New York: Plenum) p 313

Watts M S T and Humberston J W 1992 *J. Phys. B: At. Mol. Opt. Phys.* **25** L491

J. Phys. B: At. Mol. Opt. Phys. **33** (2000) L669–L676. Printed in the UK PII: S0953-4075(00)15801-8

LETTER TO THE EDITOR

Correlations between cross sections and threshold energies for positronium formation

P Van Reeth, J W Humberston, G Laricchia and J T Dunn

Department of Physics and Astronomy, University College London, Gower Street, London WC1E 6BT, UK

Received 26 July 2000

Abstract. Strong correlations between the cross sections and threshold energies for positronium formation in positron-impact single ionization of noble gases are shown to exist over a wide energy range. These correlations also extend to higher degrees of ionization, and they can be used as an empirical tool for predicting such cross sections within the relevant Ore gaps. Similar correlations are shown to exist for the exothermic positronium formation process in positron-impact single ionization of the alkali atoms. All the single ionization data are consistent with the hypothesis that the magnitude of the positronium formation cross section is determined by the modulus of the difference between the kinetic energies of the incident positron and the emerging positronium. An explanation is given for the qualitative difference between the alkali atoms and the noble gases in the magnitude of the ratio of the cross sections for positronium formation into the ground and first excited states.

In a recent letter, Humberston and Van Reeth [1] proposed a model of positronium (Ps) formation in positron–atom collisions in which the initial formation process is followed by the possible recapture of the electron in the Ps by the residual ion. This two-stage process, which was initially devised to explain the suppression of Ps formation in the double ionization of helium and neon [2, 3], predicts a correlation between the Ps formation cross section, σ_{Ps}, and E_r, the energy liberated to the positron when the electron is recaptured. At a given energy slightly in excess of the relevant Ps formation threshold, the experimental values of σ_{Ps} for both double and single ionization of the noble gases were found to be highly correlated with E_r, the relationship being of the form,

$$\sigma_{Ps}^{N} = \frac{A}{N^2}\exp(-BE_r), \tag{1}$$

where $E_r = (E_i^2 - E_i^1 - 6.8)$ eV and $N = 2$ for double ionization, $E_r = (E_i^1 - 6.8)$ eV and $N = 1$ for single ionization (E_i^N is the Nth ionization threshold of the atom), and A and B are energy dependent parameters, the same for all noble gases. The value of E_r for single ionization is also the threshold energy for Ps formation, E_{Ps}. In this letter we present further data which reveal a similar correlation between σ_{Ps}^1 and E_r for the alkali atoms, and also for the noble gases at high energies.

In figure 1 we present a log–linear plot of the cross sections for Ps formation in single ionization of the noble gases at five different positron energies in excess of the Ps formation threshold, each incident energy being less than the ionization energy, E_i^1. The correlation can be seen to hold over nearly two orders of magnitude, although the data for neon are somewhat out of line. The slope of the fit to equation (1), the parameter $-B$, becomes less negative as the excess energy of the incident positron increases, which corresponds to the fact that the peak in σ_{Ps}^1 is closer to the threshold for the heavier noble gases (see [4]).

0953-4075/00/200669+08$30.00

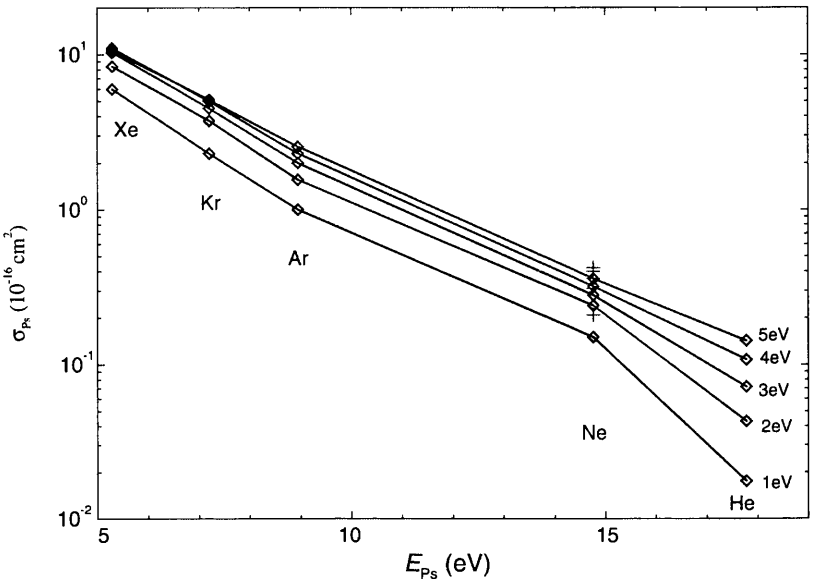

Figure 1. Ps formation cross sections in positron-impact single ionization of the noble gases plotted against E_{Ps} at five excess positron energies within the Ore gap. He, [5]; Ne, [6]; Ar, Kr and Xe, [4] (◇) and Ne, [4] (+).

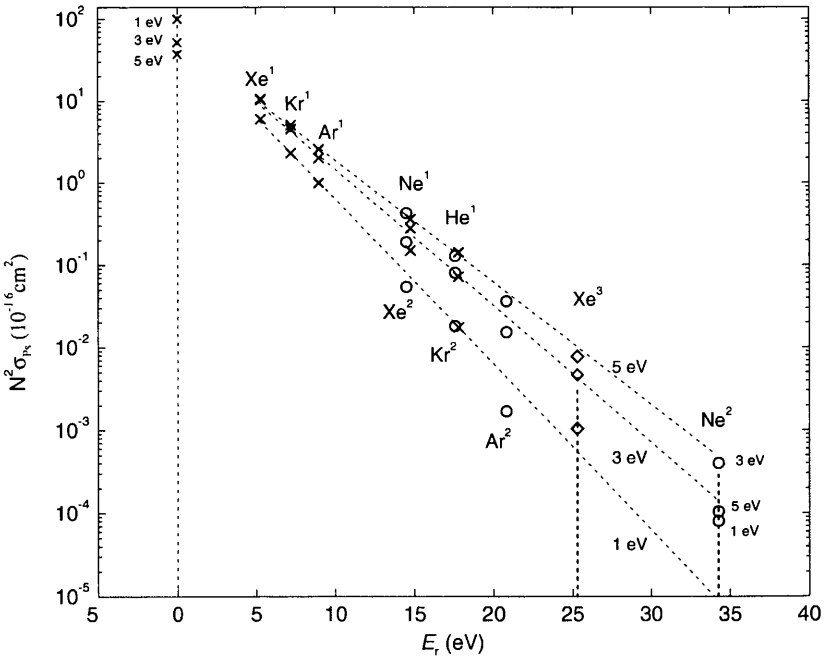

Figure 2. Ps formation cross sections in positron-impact single, double and triple ionization of the noble gases plotted against E_r (see text for references; superscripts indicate degrees of ionization). The results at $E_r = 0$ are for Ps formation in single ionization of a model one-electron atom.

In figure 2 we present the scaled cross sections, i.e. $N^2 \times \sigma_{Ps}^N$, for the noble gases in both single and double ionization [3]. The data for double ionization are found to fit equation (1) very well, indicating a strong correlation between σ_{Ps}^N and E_r and also the validity of the N^2 factor. The double ionization data for Ne again do not fit quite so well but one should note that the magnitude of σ_{Ps}^2 is very small for this atom and the fractional error is large, the absolute error being of the same order of magnitude as the data points (for clarity, only the error bar at one energy is shown). Equation (1) can be used to predict σ_{Ps}^N at energies within the so-called Ore gap (for a definition see [1]) for degrees of ionization which have not yet been measured, or to confirm the validity of experimental results. As an example, recent measurements by Moxom [7] of the positronium formation cross section in the triple ionization of Xe within the third Ore gap have been found to be in very satisfactory agreement with our predicted values, as may be seen in figure 2.

An interesting feature of the form of equation (1) is that the only atom-dependent term is the parameter E_r in the exponent. The equation can be interpreted as the coefficient A, which gives σ_{Ps}^1 for an atom with $E_{Ps} = 0$, i.e. 6.8 eV ionization energy, multiplied by a term $\exp(-BE_r)$, which specifies by how much this cross section is reduced in an actual atom. There is no real atom with $E_{Ps} = 0$ except for Ps itself, but we have developed a model atom with this energy, based on a one-electron model of He, which has been shown to give quite accurate results for positron–helium scattering [8]. The preliminary results of a Kohn variational calculation of σ_{Ps}^1 for this model are included in figure 2 and they agree very well with the extrapolation to $E_{Ps} = 0$ of the data for the noble gases. Further details of the model will be discussed in a future paper, where we will also consider the mechanisms of Ps formation and the energy dependence of the coefficients A and B in equation (1).

In the previous letter [1] we mentioned that an extrapolation of the noble gas data at 4 eV excess energy fitted well with the experimental data for magnesium obtained by Stein *et al* [9]. This choice of energy was somewhat fortuitous, however, since at higher energies the magnesium and noble gas data are less consistent with each other. Instead of a single universal curve for all atoms, it is more probable that there is a curve for each group of atoms with similar shell structure. Therefore one might expect atoms belonging to a given column of the periodic table to fit a relationship similar to that in equation (1) but with different values for the A and B coefficients. Unfortunately, there are not sufficient experimental or theoretical data to verify the correlation for the alkalines.

The alkali atoms, however, have been studied in some detail, both theoretically [10–14] and experimentally [9]. An important difference between these atoms and the noble gases is that in the former case the ionization energy is less than 6.8 eV, so that $E_{Ps} < 0$, and therefore ground state Ps formation is an exothermic process. A naive assumption that equation (1) might apply for negative E_{Ps} without any modification would imply that the cross section for ground-state Ps formation, σ_{Ps}^1 (1S), should be smaller for Li than for Rb, which is contrary to the data. In figure 3(*b*) we see that σ_{Ps}^1 (1S) decreases as E_r (= E_{Ps}) becomes more negative (i.e. as the process becomes more exothermic). An endothermic process which is more closely related to Ps formation in the noble gases is the formation of neutral alkali atoms in collisions of Ps with alkali positive ions. The cross section for this process, σ_A, is simply related to σ_{Ps}^1 (1S) by (see [15])

$$\sigma_A = \frac{k^2}{\kappa^2}\sigma_{Ps}^1(1S), \tag{2}$$

where the wavenumber of the Ps atom, κ, is related to that of the positron, k, by $\kappa = 2(0.5k^2 + 0.25 - E_i^1)^{1/2}$ (au) and the threshold energy for atom formation is $E_{Th} = 0.25 - E_i^1$ (au).

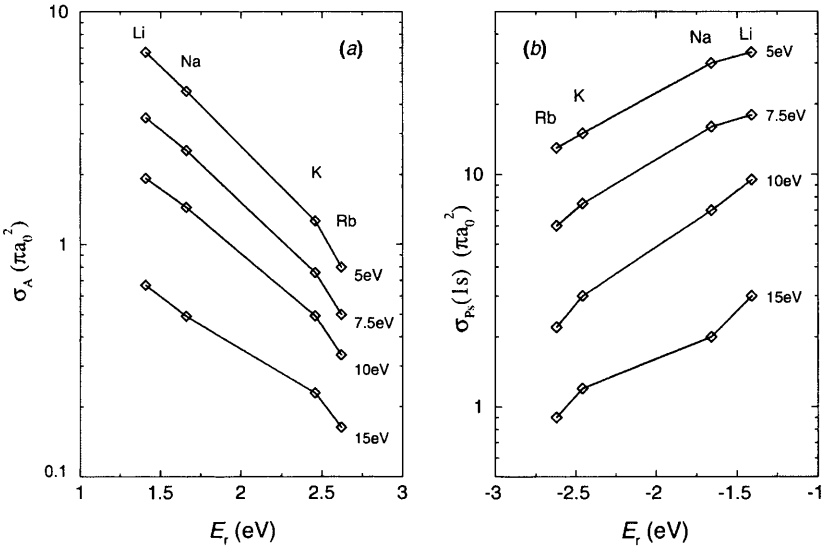

Figure 3. (*a*) Cross sections for atom formation in Ps collisions with singly ionized alkali atoms. (*b*) Ground state Ps formation cross sections in positron collisions with alkali atoms, for Rb and Cs [10], for Na [11], for K [12] and for Li [13]. $\sigma_{Ps}(1s)$ is not plotted for Cs as it is very small and the relative error is large.

Figure 3(*a*) clearly shows the correlation between σ_A and the positive threshold energy (here $E_r = E_{Th}$) for atom formation. The behaviour is similar to that found for σ_{Ps}^{I} (1S) in the noble gases, i.e. σ_A decreases exponentially as the threshold energy increases.

The results shown in figure 3(*b*) for Ps formation in single ionization of the alkali atoms also reveal a strong correlation between σ_{Ps} and E_r, the relationship being of the form

$$\sigma_{Ps}^{I} = A \exp(-B|E_r|). \tag{3}$$

This equation therefore applies equally to both endothermic and exothermic Ps formation processes in single ionization, albeit with rather different values of A and B from those appropriate for the noble gases data.

The energy E_r, which we have previously considered to be the energy liberated to the positron when the electron in the Ps atom is recaptured, is also, for single ionization, the difference, whether positive or negative, between the kinetic energies of the incoming positron and the outgoing Ps. The fit of so many data to equation (3) leads us to formulate the hypothesis that, at a given incident positron energy above the Ps formation threshold, the larger the difference between the kinetic energies of the incoming positron and the outgoing Ps atom, the smaller is the Ps formation cross section. A large energy difference implies a large change in the speed of the positron and therefore a large impulse on the positron during the collision. For Ps to be formed the positron must change its average speed so as to match that of the outgoing Ps. An atom with a large value of E_{Ps}, such as He, has a relatively compact electron cloud surrounding the nucleus. Consequently, a close encounter between the positron and the nucleus, as is required if the positron is to be slowed down sufficiently for Ps formation to occur, is relatively improbable. In contrast, an atom with a smaller value of E_{Ps} has a more extended electron cloud and the positron may more easily penetrate sufficiently close to the nucleus to achieve the required reduction in speed, thereby increasing the probability of Ps formation.

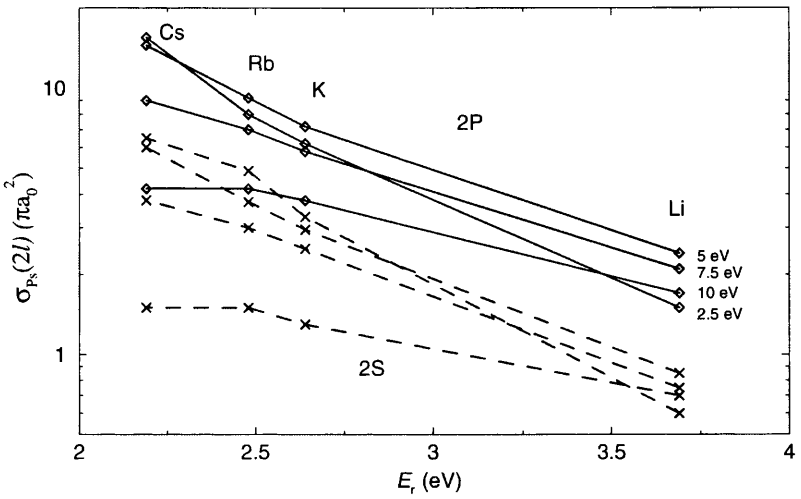

Figure 4. Cross sections for Ps formation into the 2S and 2P excited states in positron collisions with alkali atoms at four different excess energies, the same for both sets (see figure 3 for references). There are no available data for $\sigma_{Ps}(2, l)$ for Na.

For the alkali atoms, however, the situation is reversed. Now the average speed of the positron must be increased during the collision if Ps is to be formed, and the positron must therefore interact more strongly with the attractive electron cloud than with the nucleus. But if the atom has a very low ionization energy, e.g. Rb, the positron may easily penetrate close to the nucleus and be slowed down, the opposite of what is required for Ps formation to take place. Therefore, according to this model we would expect the cross section for Ps formation in single ionization to be smaller for He than for Xe, and to be larger for Li than for Rb, as is indeed the case.

An advantage of the above hypothesis over the previously described electron recapture model is that it provides qualitative agreement with observed results for Ps formation in single ionization of the alkali atoms directly, without requiring the atom formation process in positronium–ion collisions to be considered first. Also, the emphasis is now more on the initial Ps formation process rather than on the subsequent destruction of Ps by electron recapture.

The cross sections for Ps formation into the 2S and 2P states in positron collisions with alkali atoms are shown in figure 4 and they too are found to be correlated with the threshold energy for excited state Ps formation, $E_i - 1.7$ eV, in a similar way to that given in equation (3). Also, as was shown by Campbell *et al* [16], the sum of the cross sections for positronium formation into excited states is a larger fraction of the total Ps formation cross section for alkali atoms with lower E_i^1, while the ground state positronium formation cross section is a larger fraction of the total for alkali atoms with higher E_i^1. These features are entirely consistent with the form of equation (3), although possibly with different values of the parameters A and B for the ground and the excited states. Thus Li, with $E_i^1 = 5.392$ eV and therefore $|E_r^1| = |E_i^1 - 6.8|$ eV = 1.402 eV, would be expected to have a larger ground state Ps formation cross section, σ_{Ps}^1 (1S), than does Rb with $E_i^1 = 4.177$ eV; and this is so. However, $\sigma_{Ps}^1(n = 2)$ is smaller for Li than for Rb because E_r^2 ($= E_i^1 - 1.7$ eV for the $n = 2$ excited states) has the value 3.692 eV for Li and 2.477 eV for Rb. These threshold energies for ground state and excited state Ps formation, E_r^1 and E_r^2, are presented in a schematic manner in figure 5, together

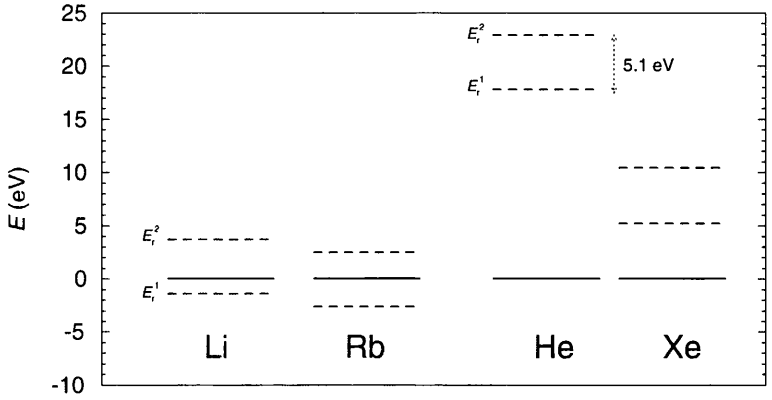

Figure 5. Threshold energies; E_r^1 for Ps formation into the $n = 1$ state and E_r^2 for Ps formation into the $n = 2$ state for Li, Rb, He and Xe.

with the corresponding values for He and Xe. Stein *et al* [9] had previously speculated that the magnitudes of the cross sections for Ps formation into the ground and excited states might be correlated with the proximities of the corresponding Ps formation threshold energies to zero, but here we have a more quantitative explanation of this phenomenon in the form of equation (3).

A significant difference between the positronium formation cross sections for the alkalis and the noble gases is that the relative contributions of the cross sections for formation into excited states are substantially greater for the alkali atoms than for the noble gases. In the results for the noble gases presented above we have considered the formation of Ps into all states because there are almost no data available for formation into individual Ps states. Only for He are such data available [16], which indicate that the sum of $\sigma_{Ps}^1(n)$ $(n > 1)$ contributes at most 20% to the total σ_{Ps}^1 at energies close to, or greater than, the peak in σ_{Ps}^1. We believe that it is possible, using equation (3), to estimate the relative contributions of $\sigma_{Ps}^1(n)$ $(n > 1)$ for the heavier noble gases by considering the ratio, $R = \sigma_{Ps}^1(n = 2)/\sigma_{Ps}^1(n = 1)$. For a given atom, X, this ratio will be $R(X) = (A_2/A_1)\exp(-B_2|E_r^2| + B_1|E_r^1|)$, where the superscripts 1 and 2 on E_r refer to formation into the ground state and the $n = 2$ excited states respectively. Using this result, it is now possible to find the ratio of the ratios for two different atoms. We first consider two alkali atoms, Li and Rb for instance, and find

$$R(\text{Li, Rb}) = \frac{R(\text{Li})}{R(\text{Rb})} = \exp(-[E_i^1(\text{Li}) - E_i^1(\text{Rb})][B_2 + B_1]), \tag{4}$$

where $E_i^1(\text{Li})$ and $E_i^1(\text{Rb})$ are the single ionization energies of Li and Rb. The ionization energy of Li is larger than that of Rb and B_1 and B_2 are always positive, so that $R(\text{Li, Rb}) < 1$ and the ratio of σ_{Ps}^1 $(n = 2)$ to σ_{Ps}^1 $(n = 1)$ is therefore expected to be smaller for Li than for Rb. This is indeed the case; at 5 eV excess energy $R(\text{Li}) \approx 0.1$ and $R(\text{Rb}) \approx 1$, and at 10 eV excess energy $R(\text{Li}) \approx 0.25$ and $R(\text{Rb}) \approx 2.5$.

For the noble gases, e.g. He and Xe,

$$R(\text{He,Xe}) = \exp(-[E_i^1(\text{He}) - E_i^1(\text{Xe})][B_2 - B_1]). \tag{5}$$

Unfortunately, we do not have any data from which to extract the individual values of B_1 and B_2, and we cannot therefore make a precise prediction of the value of $R(\text{He, Xe})$. However, the data for the alkali atoms seem to indicate that at the higher energies $B_1 \approx B_2$. If we assume a similar pattern for the noble gases we could conclude from equation (5) that $R(\text{He, Xe}) \approx 1$,

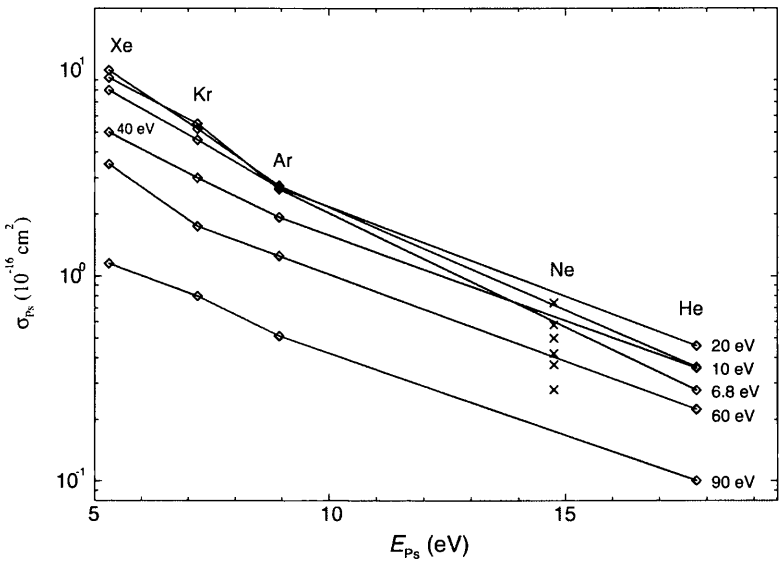

Figure 6. Ps formation cross sections in positron-impact single ionization of the noble gases plotted against E_{Ps} at six excess positron energies beyond the Ore gap. He, [16]; Ne, [17]; Ar, Kr and Xe, [9].

so that the ratio of $\sigma_{Ps}^{1}(n = 2)$ to $\sigma_{Ps}^{1}(n = 1)$ is approximately the same for all the noble gases, with a value of approximately 20% obtained from the data of Campbell *et al* [16] for He.

The usefulness of equation (3) in predicting Ps formation cross sections would be greatly enhanced if it were shown to be valid at positron energies significantly higher than the top of the Ore gap. At energies more than 6.8 eV in excess of the threshold energy for ground state Ps formation, direct ionization of the target is also possible, and the opening of another channel for ionization might be expected to result in σ_{Ps}^{1} being less well correlated with E_{Ps}. However, this is not so, at least in single ionization of the noble gases, as can be seen in figure 6, where values of σ_{Ps}^{1} at excess energies of up to 90 eV are plotted against E_{Ps}. With increasing excess positron energy between 6.8 eV and 30 eV, the slope of the best straight line fit to the data changes as the Ps formation cross sections for the various atoms reach their peak values; but above approximately 40 eV the slope becomes fairly constant. Although the correlation extends over only one order of magnitude, and the uncertainties in the data are estimated to be on average at least 25%, these results, and similar ones for σ_{Ps}^{1} for the alkali atoms (see figure 4), suggest that the mechanism responsible for the correlation between σ_{Ps}^{1} and E_{Ps} at low excess energies also acts at higher energies. As no reliable data are yet available for Ps formation in double ionization above the second Ore gap, we have not been able to investigate the correlation of these cross sections with E_r.

In this letter we have presented several examples which suggest that the correlations between σ_{Ps} and E_r given by equations (1) and (3) are of fundamental importance. The correlations are shown to hold for a wide energy range and different degrees of ionization, and the equations are found to be useful empirical tools for predicting Ps formation cross sections which have not yet been measured or calculated. Further investigations are being undertaken and hopefully these will help us to obtain a better understanding of these interesting phenomena.

We would like to thank Dr J Moxom for supplying us with the results for the triple ionization of Xe before publication. This work was supported by the UK EPSRC on grants GR/L38431 and GR/L96837.

References

[1] Humberston J W and Van Reeth P 2000 *J. Phys. B: At. Mol. Opt. Phys.* **33** L97
[2] Bluhme H, Knudsen H, Merrison J P and Poulsen M R 1998 *Phys. Rev. Lett.* **81** 73
[3] Moxom J, Schrader D M, Laricchia G, Xu J and Hulett L D 1999 *Phys. Rev.* A **60** 2940
[4] Meyerhof W E and Laricchia G 1997 *J. Phys. B: At. Mol. Opt. Phys.* **30** 2221
[5] Van Reeth P and Humberston J W 1999 *J. Phys. B: At. Mol. Opt. Phys.* **32** 3651
[6] Jin B, Miyamoto S, Sueoka O and Hamada H 1994 *At. Coll. Res. Japan* **20** 9
[7] Moxom J 2000 *J. Phys. B: At. Mol. Opt. Phys.* **33** L481
[8] Dunn J T, Van Reeth P, Humberston J W and Peach G 2000 *J. Phys. B: At. Mol. Opt. Phys.* **33** 2589
[9] Stein T S, Harte M, Jiang J, Kauppila W E, Kwan C K, Li H and Zhou S 1998 *Nucl. Instrum. Methods* B **143** 68
[10] Kernoghan A A, McAlinden M T and Walters H R J 1996 *J. Phys. B: At. Mol. Opt. Phys.* **29** 3971
[11] Kernoghan A A 1996 *PhD Thesis* The Queen's University of Belfast
[12] McAlinden M T, Kernoghan A A and Walters H R J 1996 *J. Phys. B: At. Mol. Opt. Phys.* **29** 555
[13] McAlinden M T, Kernoghan A A and Walters H R J 1997 *J. Phys. B: At. Mol. Opt. Phys.* **30** 1543
[14] Watts M S T and Humberston J W 1992 *J. Phys. B: At. Mol. Opt. Phys.* **25** L491
[15] Humberston J W, Charlton M, Jacobsen F M and Deutch B I 1987 *J. Phys. B: At. Mol. Phys.* **20** L25
[16] Campbell C P, McAlinden M T, Kernoghan A A and Walters H R J 1998 *Nucl. Instrum. Methods* B **143** 41
[17] Diana L M, Sharma S C, Fornari L S, Coleman P G, Pendleton P K, Brookes D L and Seay B E 1985 *Proc. 7th Int. Conf. on Positron Annihilation* ed P C Jain, R M Singru and K P Gopinathan (Singapore: World Scientific) p 428